The Journal of Weather Modification

Vincent J. Schaefer (1906-1993)

Volume 26 Number 1 April 1994

Weather Modification Association

- THE JOURNAL OF WEATHER MODIFICATION -

COVER: *Cover photo of Vincent J. Schaefer was provided by T. J. Henderson, Atmospherics Incorporated.*

EDITED BY:

James R. Miller, Editor
Joie L. Robinson, Editorial Assistant
Institute of Atmospheric Sciences
South Dakota School of Mines and Technology
501 E. St. Joseph Street
Rapid City, South Dakota 57701-3995 U.S.A.
Phone: (605) 394-2293
FAX: (605) 394-6061

PUBLISHED BY:

The Weather Modification Association
P. O. Box 8116
Fresno, California 93747 U.S.A.
Phone: (209) 434-3486

Additional copies of the Journal of Weather Modification are available for U.S. $25.00 each (members) and U.S. $50.00 each (non-members). U.S. $525.00 for complete set of all 26 volumes/28 issues (members and non-members).

PRINTED BY:

Fenske Printing
Rapid City, South Dakota U.S.A.

Membership information is available by contacting the WMA Association at the Fresno, California, address shown above.

Appreciation to the South Dakota Community Foundation for partial support for the production of Volume 26 is gratefully acknowledged.

ISBN: 0739-1781

- THE JOURNAL OF WEATHER MODIFICATION -
WEATHER MODIFICATION ASSOCIATION

VOLUME 26 NUMBER 1 APRIL 1994

TABLE OF CONTENTS: PAGE

- NON-REVIEWED SECTION -

- WEATHER MODIFICATION ASSOCIATION - GENERAL INFORMATION -

DR. VINCENT J. SCHAEFER -- A REMEMBRANCE

Thomas J. Henderson, President

Atmospherics Incorporated
Fresno, California

It is with a deep sense of humility and honor that I can share a few thoughts about a person who clearly in many ways influenced more people in the field of weather modification than any other person in the world. The Journal of Weather Modification would probably not exist in its present form if it were not for the historic inputs from Dr. Vincent J. Schaefer. Through a classic serendipitous observation nearly 48 years ago, Vince Schaefer opened a world that has provided an area of interest beyond measure. I had the privilege of knowing Vince Schaefer for more than 40 years. During those years it was a delight to be with him on some 15 field research expeditions.

Serendipity forms a major cornerstone of science and Vince Schaefer believed in the chance encounter. It's influence can be found in almost every major scientific discovery. From this, can we then conclude that anyone who makes an important chance observation will necessarily move on to a major discovery? Of course not! Serendipity requires something much more than merely a chance encounter. It requires someone who can recognize that such a chance encounter has meaning, may also apply to another subject not directly associated with the initial observation, and it may be put to practical use. As Nobel Laureate Irving Langmuir once said....., **"The unexpected occurrence is not enough. You must know how to profit from it"**. Louis Pasteur put it another way.....**"In the field of observation, chance favors only the prepared mind"**. Vince Schaefer had this strong ability to focus on a physical process, but more importantly, to extract meaning from an observation or measurement and recognize its value. Only a select few possess that ability.

What followed the formation of ice crystals in Schaefer's classic cold box experiment, strongly illustrates this talent. On the afternoon of November 13, 1946, just four months after the cold box experiment, Vince Schaefer was in a single engine airplane with Curtis Talbot, a pilot for the interesting experiment about to unfold. Schaefer's laboratory notebook provides the best insight to what followed over the Mt. Greylock area in Massachusetts.

> *"Curt flew into the cloud and I started the dispenser in operation. I dropped about three pounds of dry ice and then we swung around and headed south. About this time I looked toward the rear and was thrilled to see long streamers of snow falling from the base of the stratus cloud through which we had just passed. I shouted to Curt to swing around, and as we did so, we passed through a mass of glistening snow crystals! We made another run through a dense portion of the unseeded cloud, during which time I dispensed about three more pounds of crushed dry ice. We then swung west of the cloud and observed draperies of snow which seemed to hang for 2,000-3,000 feet below us, very similar to what we observe in the cold box in the laboratory. While still in the cloud as we saw the glinting crystals all over, I turned to Curt and we shook hands as I said 'we did it'". Needless to say, we were quite excited."*

That simple cloud seeding experiment was the first successful demonstration that a natural supercooled cloud could be converted at will into a cloud of ice crystals. The modern science of cloud physics and experimental meteorology had begun.

In the years that followed, the large number of people who have been involved in this area of atmospheric science and technology.....many of you reading this present volume of the JWM.....provides strong testimony to Vince Schaefer and his ability to make an important observation, move quickly forward to a classic discovery, and soon provide an actual example of its value.

Vince Schaefer was born in Schenectady, New York and attended school in that city, eventually leaving high school at age 17 to work and help support his family. His career began as a tool and dye maker at General Electric in 1922, becoming a Journeyman tool maker in 1926. That opened the door for him to work with Dr. Irving Langmuir, the Nobel Laureate research scientist. His association with Langmuir was a rich 20-year experience. Some of Vince Schaefer's memoirs at that time were titled, "Twenty Years at Langmuir University".

As a pioneering member of the Langmuir-Schaefer-Vonnegut research team, he was present when the ice nucleation property of silver iodide was noted by Dr. Bernard Vonnegut shortly after the dry ice experiments. However, supercooled clouds and ice crystals were not the only areas of interest pursued by these researchers while at General Electric. This team invented several important devices, including gas mask filters, submarine detectors, and a machine for generating clouds of smoke to conceal military maneuvers. Their military research also focused on the problems of ice on aircraft wings, precipitation static causing radio interference, and a broad range of weather projects. Vince Schaefer developed various instruments, including a meter to measure the moisture in clouds. One of his most famous discoveries was the original method for capturing ice crystals and preserving the delicate impressions in a plastic film for subsequent microscopic

applications, studies and permanent files. Throughout his rich career, Vince Schaefer published more than 300 scientific papers and books.

Probably the most important project to evolve during the years of General Electric's interest in weather modification was Project Cirrus. Although weather modification and experimental meteorology were remote from traditional research work at General Electric, it was clear to the company that the basic discoveries of Vince Schaefer were possibly of great significance to the country. Accordingly, a joint laboratory and field research effort was organized between the group at General Electric and the U.S. Army Signal Corps, the Office of Naval Research, and the U.S. Air Force. The name of "Project Cirrus" given to this research program was conceived by Vince Schaefer, since the act of cloud seeding transforms cloud droplets to clouds of tiny ice crystals, which also form the cirrus classification.

Project Cirrus was active from 1947 through 1952 and, in retrospect, it is clear that Project Cirrus activities stirred the imagination of scientists throughout the world. In those short few years the laboratory and field work accomplished by that small group of researchers must be acknowledged as astounding. Essentially all of the weather modification research and operations of today can find roots in the enormous number of papers and technical reports from Project Cirrus. Vince Schaefer was a strong team member of that program.

Vince left General Electric in 1954 to become Director of Research for the Munitalp Foundation, a chance to continue his interest in weather modification and cloud physics. In 1960 he founded the Atmospheric Sciences Research Center at the State University of New York at Albany. He was the Director of ASRC from 1966 through 1974 and was Director Emeritus and a Research Consultant until his death in 1993. Vince Schaefer was awarded an Honorary Doctor of Science degree in 1948 from Notre Dame University, also receiving Honorary Doctorate from Siena College in 1975 and York College in Toronto, Canada in 1983. In 1976 he was the first recipient of the Vincent Schaefer Award for Weather Modification presented by the Weather Modification Association. The University Foundation at Albany awarded him its Citizen's Laureate Award in 1980.

During his career Vince Schaefer was elected a Fellow of the American Meteorological Society, the American Geophysical Union, and the American Association for the Advancement of Science. His broad range of interests led him to organize the Mohawk Valley Hiking Club in 1929, the Vann Epps-Hartley Archeological Chapter in 1931, and the Schenectady Wintersports Club in 1932. In 1933, he proposed the Long Path of New York which ultimately ran from New York City to Whiteface Mt. in the Adirondacks. Along these same lines of outdoor interests, he was a Trustee of the Mohonk Preserve, an Honorary Director of both the Huyke Preserve and the Rensselaerville Institute, all in New York. In the middle of all this, he was also a Director in the Dutch Barn Preservation Society, helping preserve several historic structures in the upstate New York area during the last decade.

Vince Schaefer recognized the importance of education to young men and women. He generously devoted much of his time to these subjects. For example, he developed the Natural Sciences Institute which provided in the 1960's an opportunity for some 500 high school students from all over the United States to discover the world around them through observations in the field and hands-on experiments in the laboratory. Education of young people was not his only input to the general field of learning. His organization of the Yellowstone Field Research Expedition was a ten-year landmark program from 1960 to 1970. During the winter months deep within Yellowstone National Park, he invited small groups of established researchers with different disciplines to come and observe the wonders of some unique natural phenomena and conduct their individual research efforts in one of the world's most spectacular environments. A total of some 250 scientists eventually attended one or more of the Yellowstone Research Expeditions and most were astounded at the unusual learning experiences.

One cannot comment on the remarkable life of Dr. Vincent Schaefer without mentioning his wife, Lois Perret Schaefer, whom he married July 27, 1935. Lois was a remarkable lady who had an unusual insight to people. Along with this she was an absolute joy, providing much substance to conversations, knowledge about people and things, and adding a great sense of humor to nearly any situation. Above all, as a mother, she supplied the right sense of values to the three children she and Vince raised in upstate New York. Lois passed away in 1992.

The survivors of Vince and Lois Schaefer include two daughters, Susan Sullivan of Sudbury, Massachusetts, and Katherine Miller of Golden, Colorado; a son, Dr. James M. Schaefer now living in the Schaefer home in Schenectady, New York; two brothers, Paul and Karl both of Niskayuna; two sisters, Gertrude Fogarty and Margaret Allen, both of Albany, seven grandchildren and one great-grandchild.

Throughout his life, this incredible genius of meaningful observations and discoveries, developed a strong sense of humility and humor. Sharing was another of his marvelous attributes, passing along bits of information, ideas and suggestions. For this reason, there is a lot of Vince in many of us who knew him and loved him. I only hope that some of us take the time to keep those ideas moving along the chain of knowledge. He would smile if this happens, probably having many a good laugh at some of our misconceptions, mistakes and wrong turns, at the same time appreciating the things we accomplish which were at one time a part of his work.

The simplest answer to the remarkable life of Dr. Vincent Schaefer may be found in his response to a question I posed about three weeks before his death. "Do you have any idea why you have pursued so many different areas of interest and have been so successful in lending insight to all these subjects?". His reply was simply,

"Sure, because it was fun!"

Dr. Vincent J. Schaefer was born on the 4th of July 1906. He passed away July 25, 1993 at Ellis Hospital in Schenectady, New York. He was 87.

VINCENT J. SCHAEFER IN RETROSPECT

The following photographs are a few samples of those taken by Tom Henderson during his forty years of friendship with Vince. Most were obtained at various scientific meetings and during field trips when,

> ***"I was trying to keep up with the observations, measurement instruments, thought processes and specific conversation. Often it was more than a little embarrassing in the field to find myself stepping on something that Vince had just noted was an important subject for further observation".***

A FRIEND.....

The Vince Schaefer "discovery experiment".

Breathing into a cold box to form a supercooled cloud, then introducing a substance to act as ice nuclei (dry ice, liquid nitrogen, silver iodide, etc.), and finally observing the mini-snowstorm which follows. This simple yet classic experiment, repeated many thousands of times throughout the world has served as the cornerstone for all subsequent programs of research and technology.

TYPICAL "SCHAEFER EFFECT" -- COLD CLOUD SEEDING

SEEDING HALF A CLOUD WITH DRY ICE
RAIN FROM THE RIGHT HALF, NONE FROM THE LEFT.

COLD FOG CLEARING -- DRY ICE

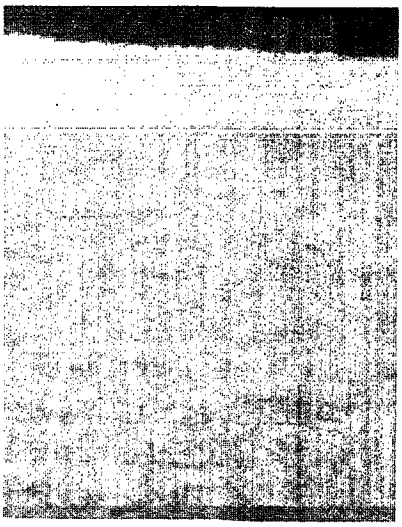

FOG DECK.....

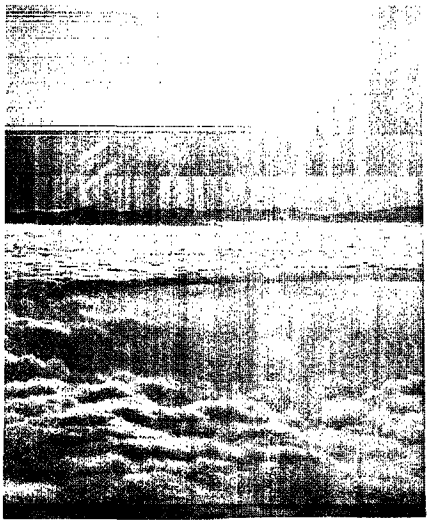

.....CLEARING

.....CLEARED

AWARDS.....FIRST RECIPIENT OF THE WMA VINCENT J. SCHAEFER AWARD

ADVENTURE.....YELLOWSTONE FIELD RESEARCH EXPEDITION

GREEN RIVER EXPEDITION

THE THOUGHT PROCESS.....

A BETTER UNDERSTANDING.....

IT'S RIGHT OVER THERE.....

O.K. LET'S GO DOCUMENT IT!

SCHAEFER AND STUDENTS

CAMPFIRE TALK

UNCOMPAGHRE
NATIONAL FOREST

SAN JUAN WATERSHED

SCHAEFER AND SCIENTISTS

LOIS AND VINCE
WITH PAUL McCREADY

C. MOGONO, SCHAEFER

SCHAEFER, WEICKMANN, PODZIMEK

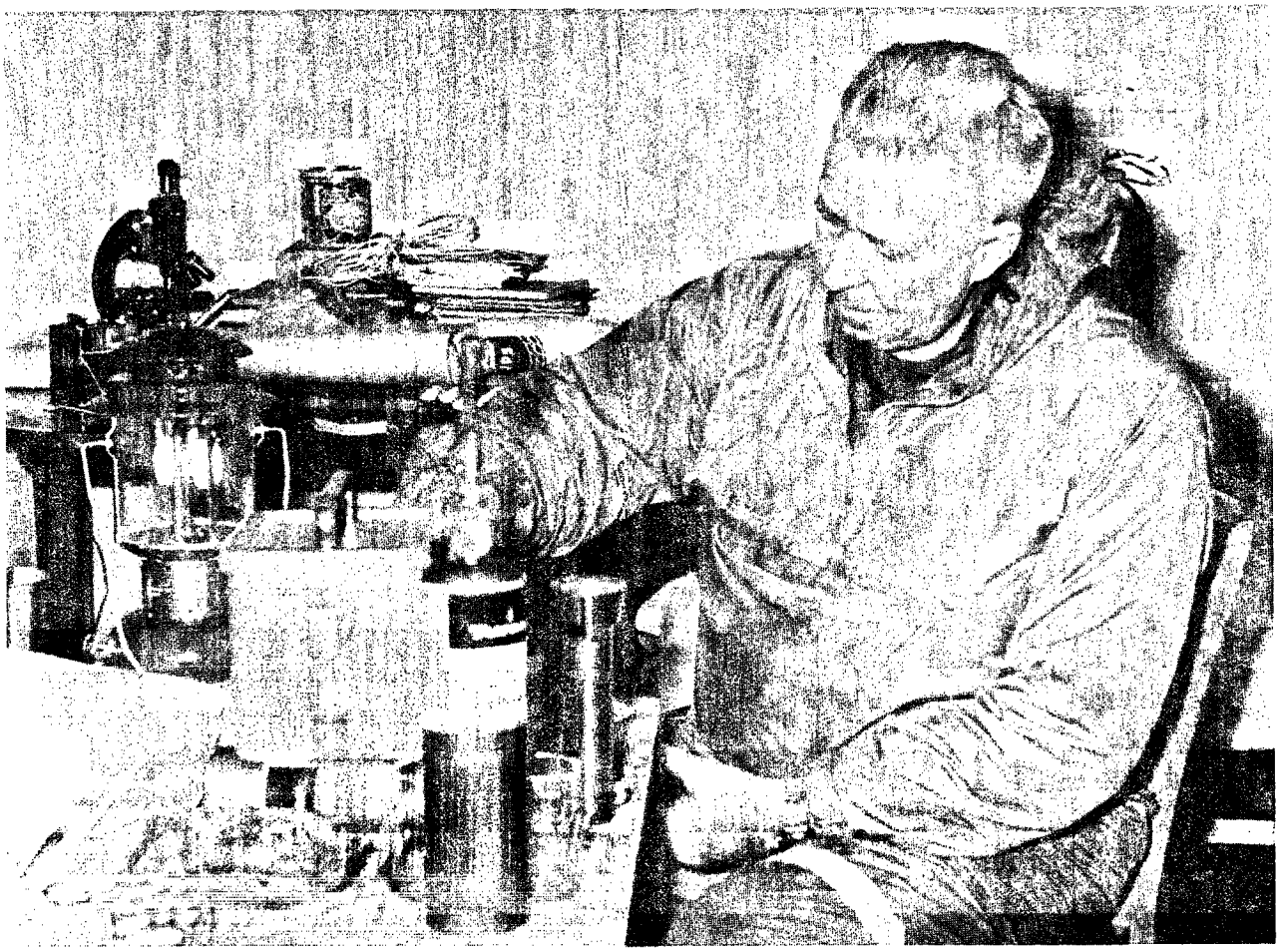

INDOOR FIELD LABORATORY

OUTDOOR MEASUREMENTS

MICROSCOPES.....

.....AND MONOLAYERS

THE PIONEERS
Vince Schaefer - Bernie Vonnegut

28 June 1993

THE MONDAY LUNCH BUNCH
Ray Falconer
Vince Schaefer
Duncan Blanchard
Bernie Vonnegut

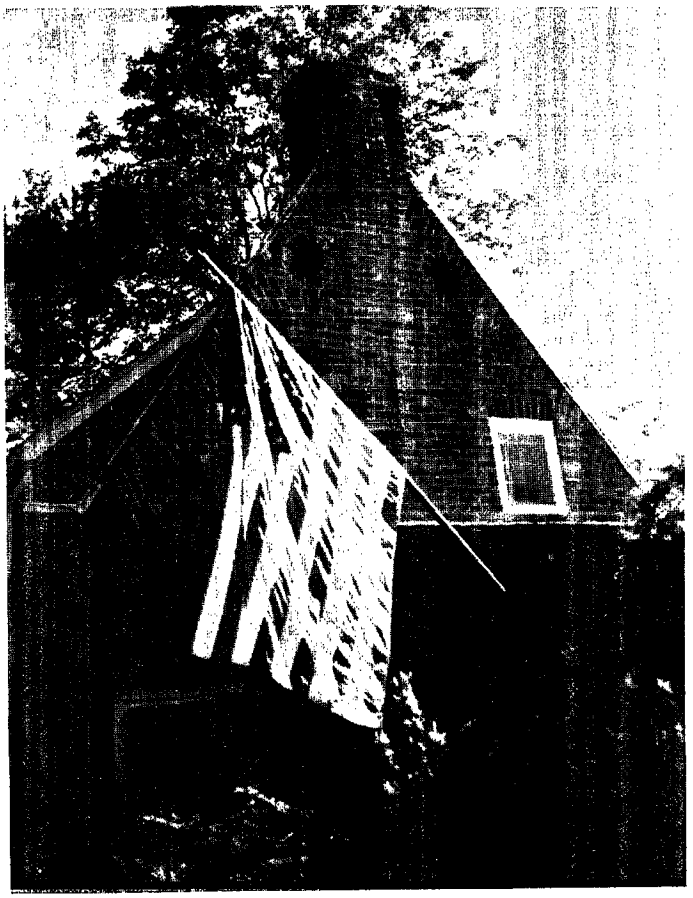

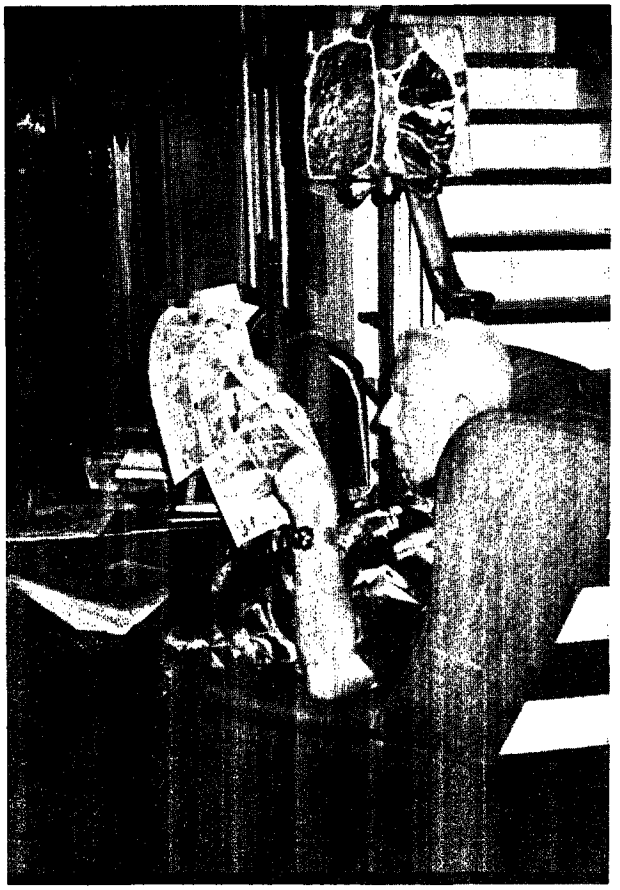

VINCE SCHAEFER'S HOME,
Schenectady, NY - appropriate scene for someone born on the 4th of July.

RESTING.....
but still sharing ideas

"REVIEWED"

APPLICATIONS OF THE CLARK MODEL TO WINTER STORMS OVER THE WASATCH PLATEAU

James A. Heimbach, Jr
University of North Carolina
Asheville, NC 28804

and

William D. Hall
National Center for Atmospheric Research
Boulder, CO 80307

Abstract. The configuration of the Clark mesoscale model to a field experiment conducted over the central Utah Wasatch Plateau experimental area is briefly described. Its application is demonstrated using one case from the early winter 1991 Utah/NOAA Cooperative Atmospheric Modification Research Program. Observations of sulfur hexaflouride and ice nuclei were used to test the model. The results were in reasonable agreement with field measurements of plume positions; however, plume concentrations were underpredicted. The model was run with a Kessler warm rain parameterization to examine the characteristics of liquid condensate. Patterns of liquid water predicted by the model suggest that depletion of liquid water to the lee of the crest could be due to subsidence warming. This complicates the estimation of liquid water depletion through precipitation processes.

1. INTRODUCTION

Although measuring technology has increased the amount, variety and quality of data available from weather modification programs, there remain temporal and spatial limitations. Numerical modeling offers the opportunity to supplement the measurements, provided the models earn the confidence of the user. Modeling can also aid in operational planning and serve as a platform to test seeding strategies. Modeling has been applied to winter orographic cloud seeding programs for both operations and research. One example is described by Reynolds *et al.* (1989) who applied the GUIDE model to SCPP to estimate targeting of supercooled liquid water (LW) content and fallout during winter California orographic storms. The Clark model has been applied to the Arizona project (Bruintjes, 1992), which, like the experiment described herein, is part of the NOAA/state cooperative program. For this, the Clark model was used to predict transport and dispersion, as well as cloud parameters. The purpose of this paper is to describe the application of the Clark mesoscale model to the winter orographic weather modification activities in the Wasatch Plateau of central Utah, and to give an example of its use.

The principal goal of modeling the Utah project has been to examine the transport and diffusion of seeding material. Targeting of seeding material has been cited as a significant problem in winter orographic weather modification projects (Reynolds *et al.*, 1989; Super, 1990; Super and Huggins, 1992). This issue was listed as the second goal of the research program designed for the cooperative program (Utah Dept. of Nat. Res., 1991), which was "piggy-backed" on the Utah operational program.

2. DATA

The data applied to this modeling were collected during the Utah/NOAA Cooperative Atmospheric Modification Program run from mid-January to mid-March 1991. The experimental area was the Wasatch Plateau located in central Utah. Figure 1 shows the experimental area and the locations of some of the instrumentation. Surface meteorological parameters were monitored at the Department of Transportation (DOT) site. At this point, a dual-channel microwave radiometer (Hogg *et al.*, 1983) provided by the U.S. Bureau of Reclamation recorded vertically integrated LW amounts. A network of 5 precipitation gauges was maintained across the Plateau. Each gauge was in a sheltered location to minimize wind-induced undercatch. Wind velocity and air temperature were monitored by 3 PROBE automatic weather stations in addition to the DOT observatory. One PROBE weather station was at the High Altitude Site (HAS), one was in the entrance to Cottonwood Canyon, 3 km NE of the town of Fairview, and one was 3.3 km further up that canyon. An instrumented van sampled along a 7 km stretch called the "Skyline Drive." This is where Highway 31 parallels the west edge of the Plateau, 1 km north to 6 km south of the DOT site.

An instrumented Beechcraft King Air C-90 aircraft (N46RF) was provided by USDC/NOAA/ARC. Its configuration and scientific direction were by the NOAA/ERL/ARS in Boulder, CO. The designated flight tracks are indicated in Fig. 1 as the two S-N lines roughly on the upwind and downwind edges of the Plateau. The aircraft recorded state parameters, LW content (King/CSIRO and FSSP), ice crystal imagery (2D-C), and horizontal winds. The aircraft's position was monitored with LORAN and GPS.

Silver iodide was released by 8 valley generators established by North American Weather Consultants (hereafter NAWC) for the operational project. Ice nuclei concentrations were monitored by three acoustical counters (Langer, 1973); one in the aircraft, one at the DOT site and one in the van. For portions of the case study, sulfur hexaflouride (SF_6) was released within the mouth of Birch Creek Canyon. The SF_6 tracer gas was measured by a fast-response detector (Benner and Lamb, 1985) on the aircraft.

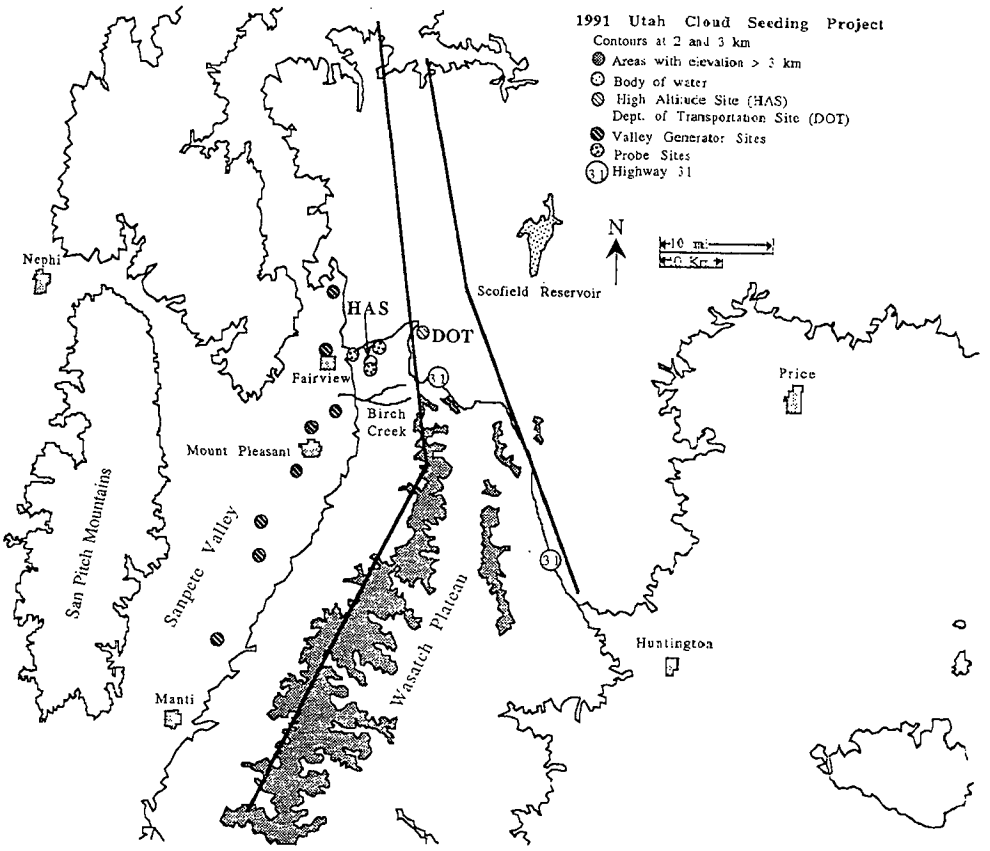

Fig. 1. The early winter 1991 Wasatch Plateau experimental area.

This was a Scientech LBF-3 instrument which has a detection limit of 10 ppt or less in normal ambient conditions.

3. MODEL DESCRIPTION AND SETUP

The three-dimensional, time dependent numerical model by Clark and associates of the National Center for Atmospheric Research (hereafter NCAR) was selected for application to the Utah program (Clark, 1977; Clark and Farley, 1984; Clark and Hall, 1991). The model is nonhydrostatic and anelastic which allows vertical acceleration but eliminates acoustic-scale waves. The model uses geo-spherical nonorthogonal coordinates with terrain following vertical coordinates such that the lowest grid points of the model are aligned with the terrain, and the top is at a constant level.

A description of the theory used to simulate the boundary layer is presented by Clark *et al.* (1994). At the surface there is an imposed stress which uses a drag law to represent surface friction. Above the surface, stress is a function of the eddy mixing coefficient, K, and the velocity field. Within the surface boundary layer, K is a function of deformation. Above the surface boundary layer, K is also a function of the eddy Prandtl number which is set to unity and the Richardson number.

The model includes a two-way interactive grid nesting procedure. This enables finer temporal and spatial resolutions to be defined within the inner domain, and a broader upwind fetch can be economically input to the model while applying the fine resolution only to the innermost areas of interest. For the applications described herein, a three-domain setup was applied. The outermost domain had a 9 km horizontal resolution; the middle, a 3 km resolution; and the innermost domain had a 1 km resolution. The vertical resolution was "stretched" with Δz being 100 m at the surface increasing to 1000 m at and above 18 km (all elevations in MSL).

3.1 Topography

The source of topography data was a file available at NCAR with a resolution of 30 sec (approx. 0.8 km) for the continental U.S. In the topography generation mode, the model determined the latitudes/longitudes for each grid point and elevations were interpolated to these points. The resulting terrain was run through a two-dimensional nine-point smoother twice to insure stability within the model. An overly rough terrain can generate noise in the model when the pressure solver is applied. Three-dimensional depictions of the three domains and their relative positions are shown in Fig. 2. The vertical scales of Fig. 2 are exaggerated. The innermost domain shows good detail of the terrain; however, the

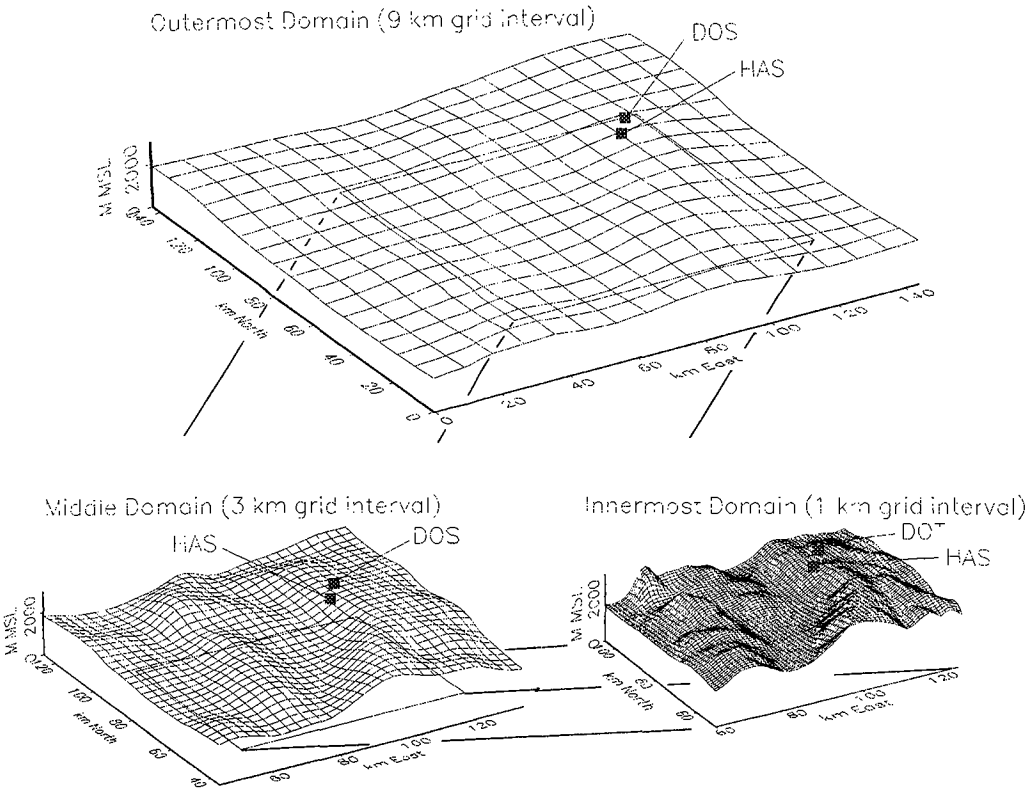

Fig. 2. Topography for the three nested models.

canyons on the west slope of the Plateau, more specifically, Birch Creek and Cottonwood canyons, are not well-defined.

Only analyses for the innermost domain are illustrated in this paper. The coordinates for these (Figs. 5, 6, 7, 9, 10 and 11) are in km from the southwest corner of the outermost domain. The coordinates for the figures illustrating airborne plume encounters (Figs. 4 and 8) are km from the DOT site. The areas and scales of the horizontal figures are identical allowing overlaying for comparative purposes.

3.2 The Initializing Sounding

The model was initialized from a single sounding. The sounding was applied homogeneously over all domains and the outermost boundary had the equation of continuity relaxed to provide zero net mass flux into the model for the variable terrain. Initially a single sounding was input to the model; however, a majority of the soundings had one or more nuances to which the model was sensitive, e.g., a shallow inversion layer or a superadiabatic zone. A composite sounding was derived by overlaying timely balloon-borne and aircraft-derived soundings. In so-doing the irregularities could be discerned. The sounding input to the model was hand-drawn and represented a somewhat smoothed profile for the time of the case study. For the 6 March case, the Ely sounding was included. This is approximately 290 km to the west of the target area. To insure computational stability, the highest available level from the composite sounding was repeated to 5 mb.

3.3 Modeling Tracer Releases

The model allows the release of tracer material from one or more locations. For the Utah application, the tracer is input to the innermost mesh as $Q = \partial M/\partial t$ (gm hr^{-1}) and is initially distributed over an entire grid bin of volume $\Delta x \Delta y \Delta z = 0.1$ km^3. The advective transport scheme of Smolarkiewicz (1983, 1984) is used in the model which requires the manipulation of a mixing ratio by mass, q, rather than a concentration (mass per volume). Following Bruintjes (1992),

$$\frac{\partial q}{\partial t} \approx \frac{\Delta q}{\Delta t} = \frac{Q}{\tilde{\rho}\Delta x \Delta y \Delta z},$$

where $\tilde{\rho}$ represents the base state of density upon which the model imposes perturbations. Since all the releases were on the surface, $\Delta z = 100$ m. The equation of conservation of tracer is

$$\tilde{\rho}\frac{dq}{dt} = \tilde{\rho}\frac{\partial q}{\partial t} + \nabla\cdot(\tilde{\rho} K \nabla q)$$

where K is the eddy mixing coefficient. For the runs described herein, the tracer releases were turned on after the model had been integrated for one hour. In the generator portion of the model, the tracer material was kept as a mixing ratio. This was converted to picograms per cubic meter (10^{-12} gm m^{-3}, hereafter

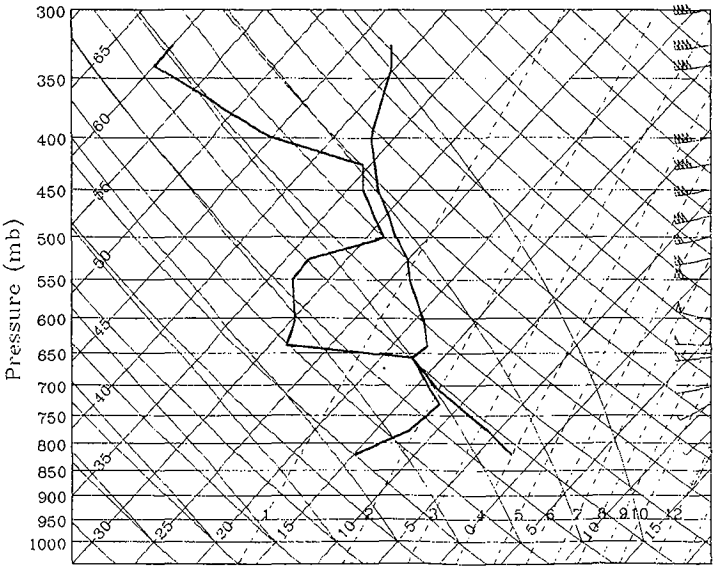

Fig. 3. Composite sounding used to initialize model for 6 March 1991.

pgm m^{-3}) in the analysis portion.

3.4 Warm Rain Parameterization

The Clark model has an option which simulates warm rain production. The term "warm rain" implies liquid condensate which can be supercooled. A modified form of the Kessler (1969) parameterization is used. A detailed description of the warm rain application within the model is given by Clark (1979). The Kessler parameterization assumes there are two forms of condensed water: cloud water and rain water. Drop-size distributions, fall velocities and conversion from cloud to rain water are calculated from empirical arguments. This so-called "bulk-parameterization" simplifies the calculation of liquid condensation by assuming a given shape or characteristic spectrum for each class of hydrometeor. The alternative is a detailed approach where the spectrum of each hydrometeor class is subdivided into many independent variables and the microphysical calculations can be formally treated. This latter approach is far more expensive in terms of computer time and memory, though probably more accurate. The ice phase option of the model was not applied to the case described in this paper.

3.5 Logistics of Running Model

The model was run on the NCAR CRAY YMP located in Boulder, CO. The model's run parameters were input by making changes to the FORTRAN code stored on the CRAY, then compiling the program. The changes were made by submission of JCL (job control language) which is used by the CRAY system to make insertions, substitutions and deletions to the code in a temporary file. Graphics output was sent to the machine of choice through the use of the UNIX rcp command and processed locally using NCARGraphics software. For each hour of simulated time, approx. 10 Mbytes of graphics were produced and approx. two hours of CRAY CPU time were required.

4. ANALYTICAL TECHNIQUES

4.1 Sulfur Hexaflouride Data

The aircraft SF_6 data used in this report were the post-season processed data provided by NAWC, whose technicians were responsible for the airborne detector. False signals, such as those induced by sudden changes in cabin pressure, were found by visual inspection of the data and flight notes. Ice nuclei concentrations resulting from co-released AgI and SF_6 can be inferred if the dilution factor for SF_6 is assumed to be the same as for AgI from collocated sources. This assumes that scavenging and sedimentation processes are negligible or similar for the two substances. Equation (2) below was used to estimate concentrations of AgI (gm m^{-3}).

$$\chi_{AgI}=1.7567X10^{-9}\frac{Q_{AgI}}{Q_{SF6}}\frac{fp}{T}. \qquad (1)$$

The source strengths of AgI and SF_6 are Q_{AgI} and Q_{SF6} (mass per time). The concentration of SF_6 is f which is expressed in ppt by volume. The ambient pressure, p, is in mb and T is °K.

4.2 Calculating Airborne AgI Plume Positions

The IN detector's response is lagged due to delays caused by plumbing and the time needed to grow acoustically-detectable crystals (≥ 20 μm). The response is also smoothed because of mixing within the cloud chamber. The response of the detector was calibrated in a series of ground tests and airborne sampling of co-released AgI and SF_6 plumes. The most precise response parameter was found to be the AgI plume entry delay determined from the time of first response. Since the flights consisted of pairs of passes in opposite directions, approximations of horizontal extent of IN could be made using pairs of plume edges.

Previous work by Super *et al.* (1988) suggests that the lag time to plume edge is a power function of the sum of IN counts for the entire plume penetration. The AgI plume edge times used in this paper are defined by the first second of seven seconds having ≥ 3 IN counts. This method was appropriate for the small concentrations typically detected by the aircraft. The power curve fit is

$$lag(\text{sec})=96.7\left(\sum cnts\right)^{0.228}-0.5. \qquad (2)$$

The range of measured lag times for small IN

sums was approximately ± 20 s, which corresponds to approximately 1.8 km flight distance. For Σ cnts < 15, the three counts in 7 s criteria could usually not be met. In this case, a coarse estimate of the mean lag for all IN detected in a given pass was used to approximate the plume position. This was found to average 89 s. For the 6 March case, Eq. (2)'s minimal sum of counts criterium was met for all aircraft passes.

5. MODELING THE 6 MARCH CASE

5.1 Weather and Data Collection

The case discussed in this paper occurred on 6 March 1991. This was a cold storm with little liquid water and no imbedded convection. On this date, a short wave passed the target area between 1730 and 1740. Preceding the wave was a small area of moisture as well as cold air advection. At the DOT site, the winds were Wly prior to frontal passage, veering to WNWly by 1900. Behind the wave there was some drying and diurnal warming. The Mount Pleasant and the 1600 Ely soundings indicated winds of less than 7 m s^{-1} below 700 mb.

At the DOT site, the wind direction trends were similar to the soundings'. During the experimental period, the DOT site's speeds were 4 to 6 m s^{-1}, declining to 2 to 4 m s^{-1} after 1930, then becoming nearly calm by midnight. At the two Cottonwood Canyon PROBE sites, both up-canyon and down-canyon winds were recorded. The down-canyon winds, presumably katabatic, occurred between approximately 0600 and 0915, and after 2115. The speeds at both sites were 3 to 4 m s^{-1} until 0425, and 0 to 2 m s^{-1} thereafter. The relative humidities and temperatures at the Cottonwood Canyon sites followed a diurnal trend with low humidities and high temperatures occurring during the daylight hours. The percent relative humidities ranged from the low 40's to the mid 80's, and the temperatures from -12.9 to -3.3°C at both sites.

For the 6 March case, the aircraft was over the experimental area from 1615 to 1915. During this time, 14 N-S passes were made, of which two were on the east track. The first nine passes were made at the minimum IFR elevation, as shown on Figs. 6, 7 and 10. Thereafter, all passes were made at a constant 3.7 km. Average temperatures and pressures at flight level ranged from -19 to -15 °C and 655 to 687 mb respectively during plume encounters.

Precipitation was recorded on the Plateau in the early morning, and during the experimental period. The DOT site received the largest amount of precipitation of the Plateau gauges, both in terms of duration and quantity.

The radiometer at the DOT site indicated a small amount of vertically integrated LW in the early morning and again after 1000 (Huggins *et al.*, 1992). The peak hourly-averaged LW depth recorded was 0.04 mm during the hour ending 1400. Satellite-derived cloud-top temperatures were between -20 and -15 °C except from 1200 to 1800 when the cloud-top temperatures ranged from -31 to -27 °C.

Defining the initial conditions for the model was not straightforward because there were two distinct sounding types. Prior to the short wave passage there was a subsidence inversion based at 650 mb. As the wave approached, this changed to lapse conditions with little variation in the profile below 650 mb. The initializing sounding was a compromise between the two regimes which had a small inversion at 650 mb. This profile is shown in Fig. 3.

5.2 Modeling the Birch Creek SF_6 Release of 6 March 1991

Sulfur Hexaflouride was released from 1605 to 1915 on 6 March at a rate of 22.7 kg hr^{-1} from the mouth of Birch Creek Canyon. Figure 4 is a composite of all airborne plume penetrations for this date. The peak SF_6 value detected was 903 ppt at 1847 on the west track. After this, there were two passes by the aircraft on the west track, during which no SF_6 was detected, presumably due to the cessation of SF_6 release. Of the 13 passes excluding the last two, the lowest peak value was 41 ppt.

If a Montana State University generator dispensing 30 gm hr^{-1} was collocated at the SF_6 site, then the range of inferred peak AgI concentrations found by the application of Eq. 1 would be $2.5X10^2$ to $5.5X10^3$ pgm m^{-3}. Applying the calibration of this generator (Super and Heimbach,1983) to the inferred AgI concentrations gives peak effective IN concentrations ranging from 150 to 3300 IN L^{-1} effective at flight-level temperatures. Use of mean SF_6 concentrations would produce smaller concentrations of IN by up to an order of magnitude (Griffith *et al.*,1992).

A 30 gm hr^{-1} AgI release from the Birch Creek surface site was modeled. Fig. 5 shows the modeled plume at 2.9 km after a 2 hr release. No contours were present on the next higher analysis level. The model predicted the general W-E transport and meander of the plume measured at higher levels by the aircraft. At the 2.9 km level there is one small element which moved to the NE. There are three west-to-east zones of higher concentrations. The westernmost is due to the proximity of the source to the vertical motion forced by the windward edge of the plateau. The others result from the vertical motion caused by gravity waves; the higher concentrations being in areas of upward motion. The surface plume (not shown) had a northward drift in the valley and lateral spreading, which was induced by low-level directional shear. Observations by the aircraft and surface wind observations suggest the plume was transported up the Birch Creek Canyon; however, the model's 1 km topography did not have enough

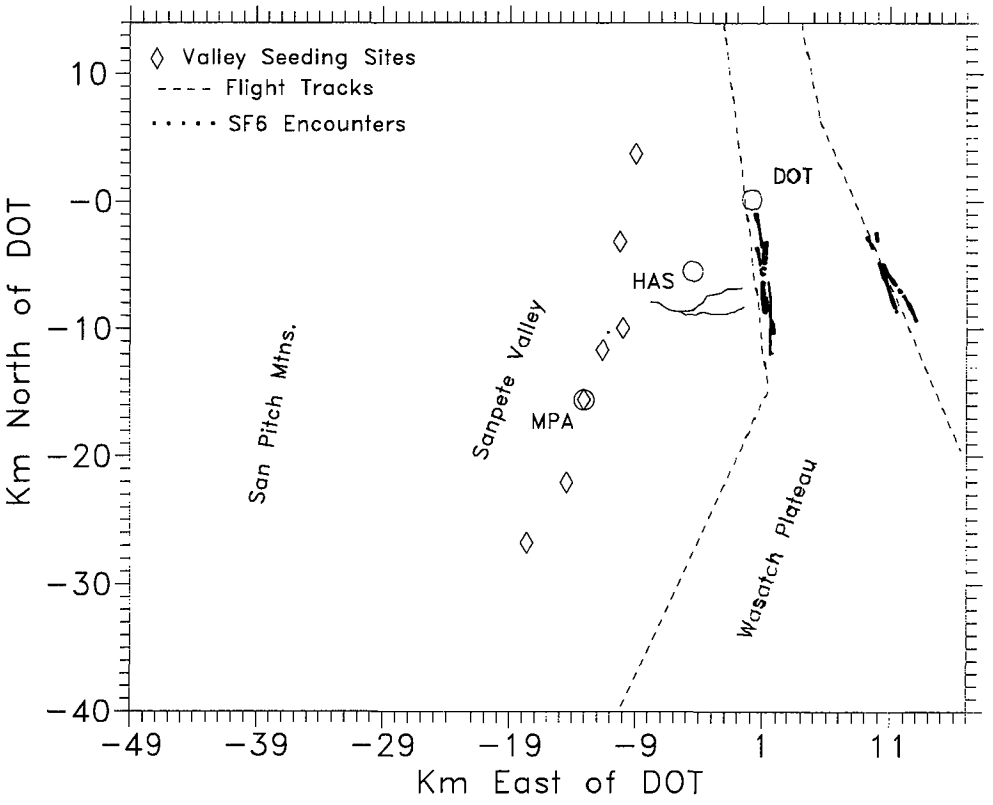

Fig. 4. Composite airborne SF_6 encounters from 6 March 1991 flight.

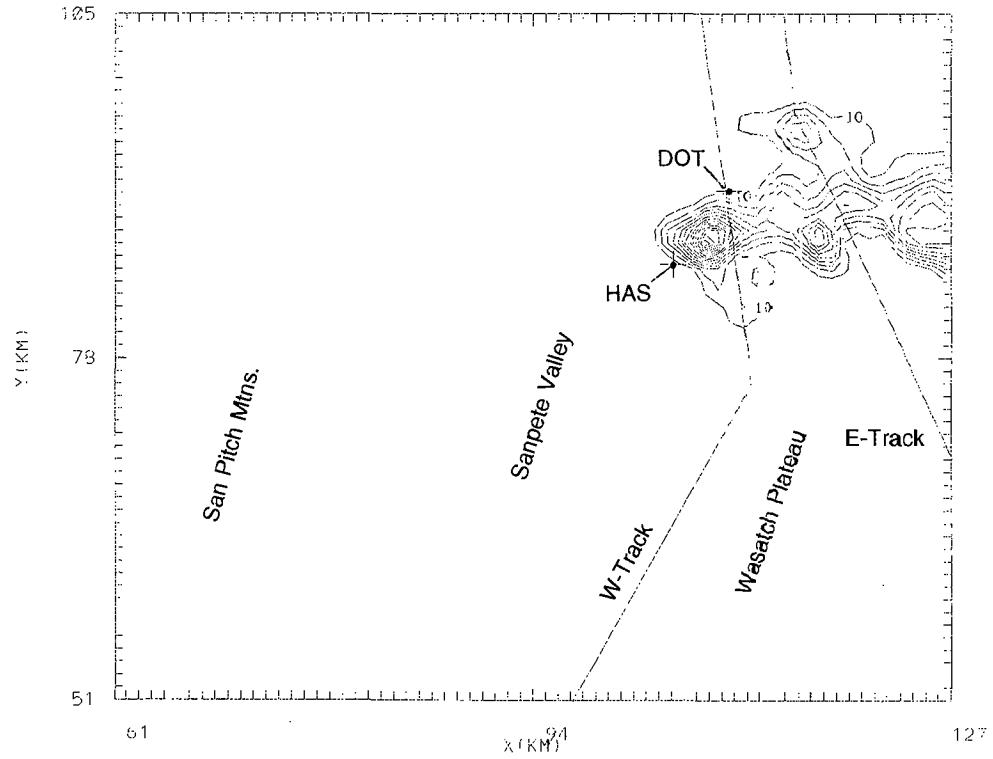

Fig. 5. Contours of modeled AgI at 2.9 km for 6 March 1991 simulated release from Birch Creek. The release time was 2 hr after an initial 1 hr integration. In this and the other figures showing AgI concentrations, the minimum contour and contour interval are 10 picograms per cubic meter (pgm m^{-3}).

resolution to mimic this situation on this day.

A S-N vertical cross section of modeled AgI through the DOT site is shown in Fig. 6 which is for the same time as Fig. 5. This figure also depicts the west flight track which has its minimum IFR elevation decrease to the north of the DOT site. The model indicates less than 10 pgm m^{-3} at minimum IFR level, predicting lower concentrations than suggested by the SF_6 monitoring. The differences may be due to the use of peak SF_6 concentrations and the initial spread of the modeled tracer material through one grid bin. The model properly predicted a rapid decrease in concentration with elevation, but more rapidly than the aircraft sampling of SF_6 suggests. Figure 7 is a S-N cross section 5 km to the west of Fig. 6. This figure demonstrates the effect of vertical motion over the Plateau. In the western cross section, the simulated AgI plume has more than double the elevation above ground level than the other; however, the minimum contour has about the same elevation MSL. Both highlight the plume's transport over lower topography of the plateau.

5.3 Valley AgI Releases for 6 March 1991

Silver Iodide was released from each of the operational valley sites on 6 March using the NAWC generators which dispensed 8 gm AgI hr^{-1}. The releases started after 1215 and ended at or before 2135. The plume edges from this flight are shown in Fig. 8. All the plume penetrations had sufficient numbers of IN to meet the criteria for edge determination. There is a preponderance of edges in the vicinity of Birch Creek Canyon. Three edges, including two on the east flight track suggest a transport through the vicinity of the DOT site. There are several edges east of Mount Pleasant. Overall, effluent from the northern 6 valley sites appears to have been detected by aircraft sampling. The total number of IN registered per plume penetration ranged from 30 to 353, with the maximum being the first pass

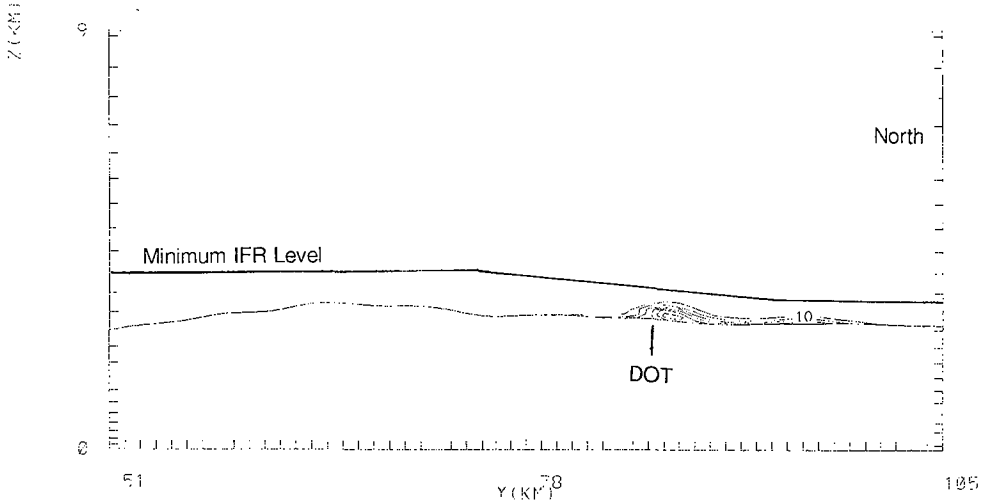

Fig. 6. North-south vertical cross section showing contours of AgI for simulated release from Birch Creek Canyon for 6 March 1991. This cross section is through the DOT site. In this and the other north - south cross sections, the minimum IFR elevation of the west flight track is drawn.

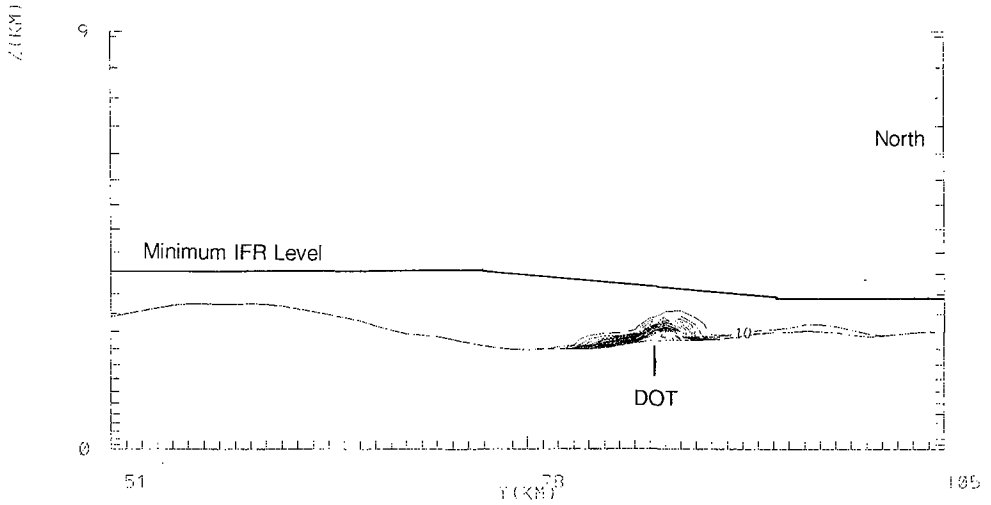

Fig. 7. Same as Fig. 6 but 5 km to west.

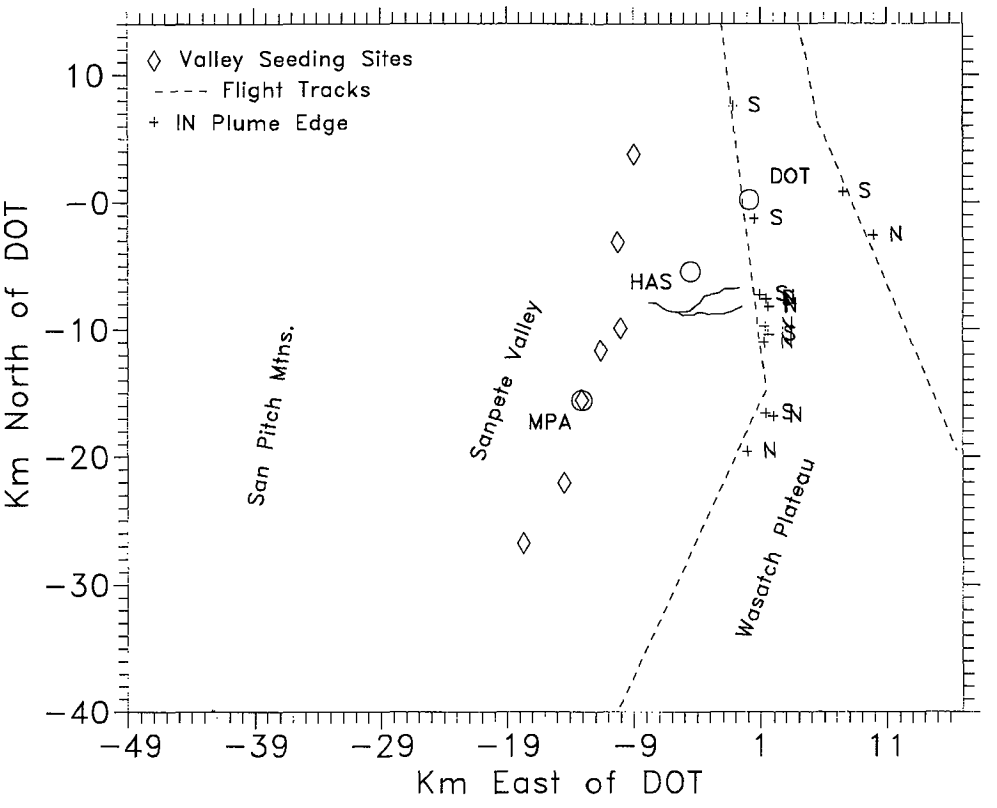

Fig. 8. Ice nuclei plume edges from flight of 6 March 1991. Crosses indicate estimated plume entry points, and "N" and "S" show the direction of flight.

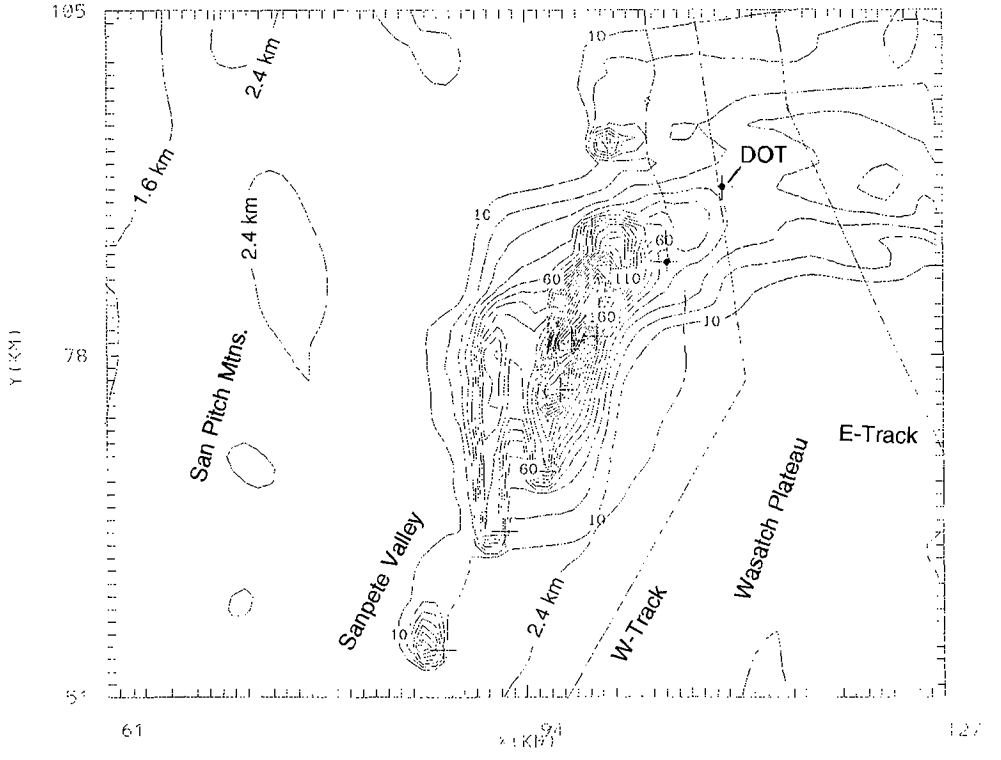

Fig. 9. Surface concentrations of AgI from simulated release of 8 gms hr^{-1} from each of eight valley sites for 6 March 1991. The contours are for 2 hr release after an initial 1 hr integration of the model. Undotted crosses indicate AgI release points.

which was farthest to the north.

A simulated release of eight gms AgI hr^{-1} from each of the 8 valley sites was modeled. The release started as the others, one hour after the initialization of the model and continued for two hours. By the end of the run, the model showed transport of AgI over the Plateau but limited to the northern portion of the experimental area, which has the lower elevation (Fig. 9). The surface plot shows a pooling of AgI in the valley and some spread to the west due to a shallow easterly flow modeled in some portions of the valley. The pooling was confirmed by surface measurements of IN taken by the van after 2100. The van sampled through Cottonwood Canyon to Fairview. No IN were detected at or above 2.0 km. Concentrations increased to 5500 L^{-1} effective at -20 C at Fairview which has an elevation of 1.8 km.

Figure 10 is a S-N vertical cross section of AgI through the DOT site. This is for the same time as Fig. 9. Ice nuclei were sampled by the van along Skyline drive from 1524 to 2036. The plume was found throughout the length of the surface traverses which were from 1 km north of the DOT site to 6 km south. This occurrence was matched by the model, but surface verification was not possible to the north. The average surface concentrations found by the van were 400 to 800 IN L^{-1}, effective at -20 C. Also, ten-minute averaged IN measurements at the DOT site ranged from several hundred to over 1500 L^{-1} during the experimental period. The model showed surface concentrations of 10 to 50 pgm m^{-3} in this area (see Fig. 10). This corresponds to 100 to 500 IN L^{-1} assuming natural draft conditions over the NAWC generator and effectiveness for -20 C (Super and Huggins, 1992). Though less than the van measurements, this is in better agreement than the elevated model results which applied IN concentrations inferred by SF_6 discussed above. The somewhat better surface results suggest that vertical transport was underestimated by the model for this case.

The underprediction is also due to the minimum dimensions of an innermost grid bin being 1. X 1. X 0.1 km^3, which forces an initial plume dilution. The aircraft traveled one grid interval in approximately 10 s, therefore a more appropriate comparative value would be an average over 10 s which would lower the maximum value of SF_6 by up to an order of magnitude. Another cause for underprediction may be caused by the model's smoothed terrain providing less topographic forcing than reality. Both of these limitations could be reduced by increasing the spatial resolution of the model; however, this requires increased computer resources.

5.4 Modeling Liquid Water for 6 March 1991 Case

The 6th of March case had cloud tops at about 3.8 km (aircraft observation) and trace icing was observed. Throughout the flight there was hazy ground contact except during a FROPA at approximately 1709 to 1730. The maximum 1 min average LW content measured by the aircraft was 0.06 gm m^{-3}.

Figure 11 shows a W-E vertical cross section of liquid cloud water (q_c) after 4 hr of model integration for the 6th. The influence of a gravity wave is indicated just east of the San Pitch Mountains, where subsidence eliminated condensation. Further to the east over the San Pete Valley, a large vertical zone of condensation occurs in the ascending air. The wave's influence continues over the Plateau, showing decreasing cloud depth and q_c several km downwind of the windward edge. Aircraft observations indicated decreasing cloud heights and clear ground contact over the eastern portions of the plateau, giving credence to the model's predictions. The clouds obscured the high elevations throughout the simulation

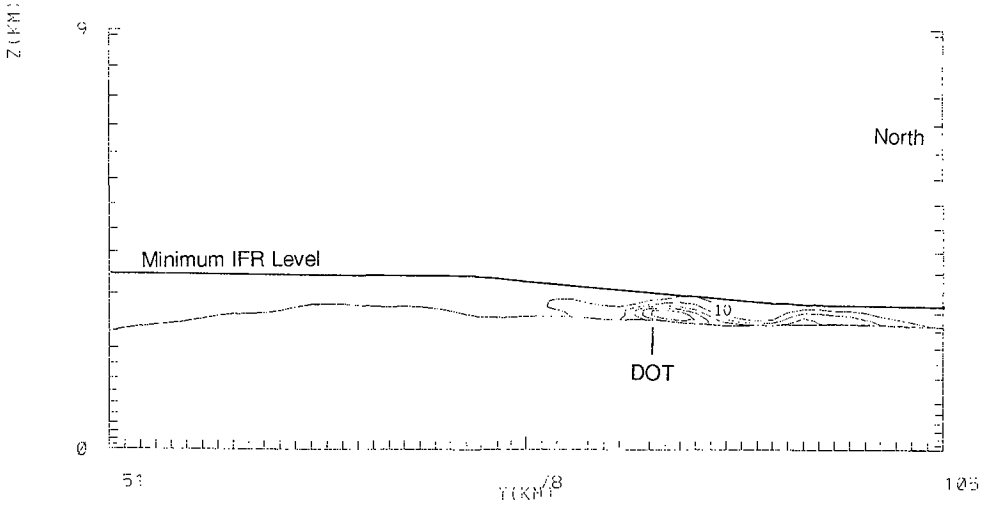

Fig. 10. North - south vertical cross section through DOT site depicting AgI concentrations resulting from 2 hr simulated release of AgI from the eight valley operational sites.

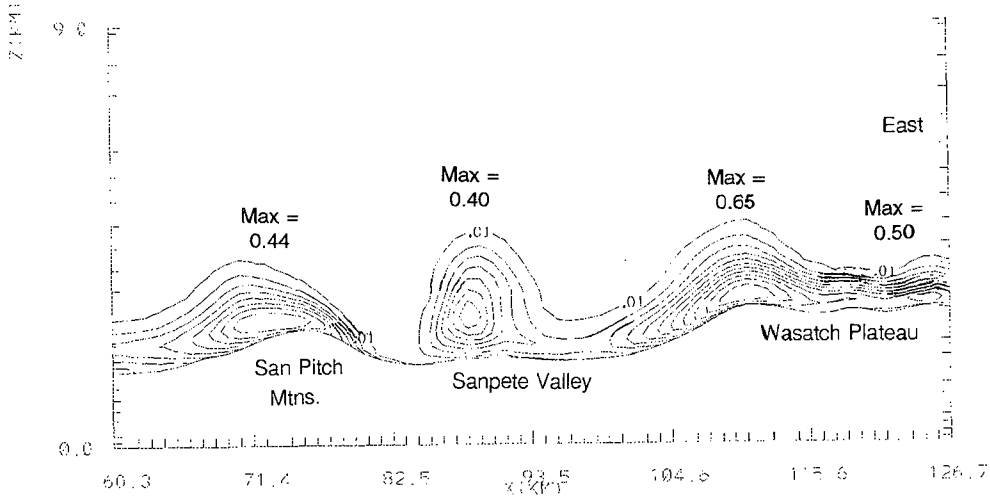

Fig. 11. West - east vertical cross section of modeled liquid water for the 6 March 1991 case after 4 hr integration. The contour interval is .06 gm kg^{-1}. A minimum contour of 0.01 gm m^{-3} is included.

and the q_c values found by the model are quite high in some areas. This may be artificially high because the ice phase was not implemented, whereas in reality, this date was one of the coldest sampled and cloud ice was observed. Over time the modeled q_c indicated a decreasing vertical thickness of condensation.

The model demonstrated a sensitivity of cloud water content to gravity waves. One of the goals of the Utah research program is to understand the effect of seeding on q_c depletion over the Plateau. Subsidence produced by gravity waves could complicate this issue.

6. DISCUSSION

The model results were in reasonable agreement with observations of plume positioning. The observed meandering of plumes, transport over lower terrain and shallow vertical dispersion were predicted by the model. The model's elevated concentrations were smaller than those inferred by SF_6 observations. This is likely for three reasons: 1) the tracer was given an instantaneous dispersal throughout one grid bin upon release; 2) the model predicted less vertical transport than reality; and 3) comparisons were done using peak SF_6 observations; however, the use of average SF_6 concentrations, though somewhat ambiguous, could not explain all the difference.

The model illustrated several points which should be considered in planning future winter orographic weather modification operations which employ surface sources.

- Seeding material can be confined to a depth of several hundred meters over the terrain.
- The horizontal and vertical positions of the release point are critical. In this study, the best release points were on the windward slopes of the barrier to take advantage of terrain-forced vertical motions.
- Pooling of seeding material can occur in the valley areas, and its transport can be guided by the character of lower terrain.

The most critical factor in ground-based targeting is placing the source in an area having positive vertical velocity near the surface. Typically, this is windward of the crest. Areas at the crest or just downwind showed small or negative vertical velocities in simulations. Valley sites can be poor locations because the vertical motion fields may not reach low enough and the valley surface winds are too poorly organized to provide consistent transport.

The use of an upwind seeding site, e.g., the San Pitch Mountains, was modeled (not illustrated in this paper) and found to have some possibility of success. An upwind release site has the advantages of providing a broader plume, earlier nucleation and opportunity for greater vertical transport. The drawbacks include targeting inconsistencies, increased lead time and dilution. It would be worthwhile to try one or more test releases from the San Pitch Mountains using a mobile source of AgI. SF_6 is not the tracer of choice for this because of the large dilutions anticipated while crossing the Sanpete Valley.

It would be useful to model transport and diffusion using a Lagrangian transport scheme. The Lagrangian treatment uses a coordinate system which follows effluent particles rather than remaining stationary. This eliminates the effect of the initial dispersion of tracer material and would give a better visual display of plume characteristics. A finer innermost mesh is needed to better simulate the effects of flow around the terrain of the experimental area. In particular, the canyons, which are important in the transport of low elevation seeding material, are not well-represented in the model. Finally, the model

is being implemented on workstation environments. Though not possible to run the model with a fine resolution on a workstation, it does offer the ability to utilize the model in a field environment, enabling an operational application in a field environment.

Acknowledgements. A. Super is acknowledged for his encouragement in the modeling effort and many fruitful discussions which helped in producing this paper. T. Clark is acknowledged for his patient and skilled tutoring in the application of the model. There are many who participated in the field work and later analysis which provided data used in this paper. C. Ogden was the operations director of the program. His organizational abilities were key to the successful conduct of the 1991 experiment. A. Huggins provided surface, sounding and satellite data summaries used in this report. G. Wilkerson provided processed SF_6 data and informative notes on the SF_6 instrumentation. J. Boatman, D. Wellman, S. Wilkerson, L. Gunter and Y. Kim of the NOAA/ERL/ARS group are cited for their part in producing an excellent data set from the 1991 flight operations. Funding for this work was through Contract No. 93-0874 between UNCA and the Utah Department of Natural Resources, Division of Water Resources as part of the Utah/NOAA Cooperative Atmospheric Modification Research Program.

7. REFERENCES

Benner, R.L. and B. Lamb, 1985: A fast response continuous analyzer for halogenated atmospheric tracers. *J. Atmos. Oceanic Tech.*, 2, 582-589.

Bruintjes, R.T., 1992: Observational and Numerical Studies of Cloud and Precipitation Development with a View to Rainfall Enhancement. Doctoral dissertation, Univ. of S. Africa. 193 pp.

Clark, T.L., 1977: A small scale dynamic model using terrain following coordinate transformation. *J. Comp. Physics*, **24**, 186-215.

_____, 1979: Numerical simulations with a three-dimensional cloud model: lateral boundary condition experiments and multi-cellular severe storm simulations. *J. Atmos. Sci.*, **36**, 2191-2215.

_____ and R.D. Farley, 1984: Severe downslope windstorm calculations in two and three spatial dimensions using anelastic interactive grid nesting: a possible mechanism for gustiness. *J. Atmos. Sci.*, **41**, 329-350.

_____ and W.D. Hall, 1991: Multi-domain simulations of the time dependent Navier Stokes equations: Benchmark error analyses of nesting procedures. *J. Comp. Phys.*, **92**, 456-481.

_____, _____ and R.M. Banta, 1994: Two- and three-dimensional simulations of the 9 January 1989 severe Boulder windstorm: Comparison with observations. [Accepted for publication in *J. Atmos. Sci.*]

Griffith, D.A., G.W. Wilkerson, W.J. Hauze and D.A. Risch, 1992: Observations of ground released sulfur hexaflouride tracer gas plumes in two winter storms. *J. Weather Mod.*, **24**, 49-65.

Hogg, D.C., F.O. Guiraud, J.B. Snider, M.T. Decker and E.R. Westwater, 1983: A steerable dual-channel microwave radiometer for measurement of water vapor and liquid in the troposphere. *J. Climate Appl. Meteor.*, **22**, 789-806.

Huggins, A.W., M.A. Wetzel and O.A. Walsh, 1992: Investigations of Winter Storms over the Wasatch Plateau During the 1991 Utah/NOAA Field Program. Final Report for the Utah Dept. of Nat. Res. Desert Research Institute, Reno Nev. 252 pp.

Kessler, E., 1969: On the distribution and continuity of water substance in atmospheric circulations. *Meteor. Monogr.*, **No. 32**, Amer. Meteor. Soc. 84 pp.

Langer, G., 1973: Evaluation of NCAR ice nuclei counter. Part I: Basic operations. *J. Appl. Meteor.*, **10**, 1000-1011.

Reynolds, D.A., J.A. Humphries and R.H. Stone, 1989: Evaluation of a 2-month cooperative ground-based silver iodide seeding program. *J. Weather Mod.*, **21**, 14-28.

Smolarkiewicz, P.K., 1983: A simple positive definite advection scheme with small implicit diffusion. *Mon. Wea. Rev.*, **111**, 479-486.

Smolarkiewicz, P.K., 1984: A fully multidimensional definite advection transport algorithm with small implicit diffusion. *J. Comp. Phys.*, **54**, 325-362.

Super, A.B., 1990: Winter orographic cloud seeding status in the intermountain west. *J. Weather Mod.*, **22**, 106-116.

_____ and J.A. Heimbach, Jr., 1983: Evaluation of the Bridger Range winter cloud seeding experiment using control gauges. *J. Climate Appl. Meteor.*, **22**, 1989-2011.

_____ and A.W. Huggins, 1992: Investigations of the targeting of ground-released silver iodide in Utah. Part II: Aircraft observations. *J. Weather Mod.*, **24**, 35-48.

_____, B.A. Boe, E.W. Holroyd, III, and J.A. Heimbach, Jr., 1988: Microphysical effects of wintertime cloud seeding with silver iodide over the Rocky Mountains. Part I: Experimental design and Instrumentation. *J. Appl. Meteor.*, **27**, 1145-1151.

Utah Department of Natural Resources, Division of Water Resources, 1991: 1991 Field Operations Plan, Utah/NOAA Cooperative Atmospheric Modification Research Program. Salt Lake City, 27 pp.

FURTHER ANALYSIS OF A SNOWPACK AUGMENTATION PROGRAM USING LIQUID PROPANE

by

David W. Reynolds
U.S. Department of the Interior
Bureau of Reclamation
Sacramento, California

Abstract. The California Department of Water Resources, with technical assistance from the Bureau of Reclamation, is continuing to pursue the use of liquid propane as a viable agent for seeding winter clouds. The tracer SF_6, sulfur hexafluoride, is used to simulate the transport and dispersion of propane-generated ice crystals. Sulfur hexafluoride was released from two separate high-altitude propane dispenser sites as a proxy for seeded ice crystals. Aircraft measurements of SF_6 indicated that at the normal flight altitudes of 2500 m over the valley and 2680 m over the downwind ridge, the aircraft was flying near the top of the plumes. When the aircraft was able to fly below cloud base near the release altitude of 2200 m, substantial SF_6 was observed. A portion of the plume was observed to rise to elevations about 500 m above the release altitude. The lower portion of the plume was also observed to descend into the valley some 600 m below the release altitude. Comparison of aircraft measurements with model predictions of plume (Gaussian) horizontal dispersion compare favorably. The model verifies that the vertical dispersion of the plume is limited to only 300 to 500 m above the dispenser altitudes. Gravity waves are shown to have a significant impact on the transport of tracer/seeded crystals across the target area. The aircraft intersected 35 seeded plumes on 4 separate days. Only 11 of the 35 plumes indicated seeding effects. The lack of liquid water was considered the main reason why most plumes did not indicate seeding effects. On February 17, distinct seeding effects were noted on five of six plumes intersected from one of the sites. Apparent dynamic seeding effects were also noted on several of these passes. Precipitation at a gauge directly in line with the aircraft-observed seeding plume showed a factor of five increase in precipitation over surrounding gauges for the hour in which seeding effects would have been expected. Seeding effects were also noted on March 16, a day when the temperature at the dispenser was near or slightly above freezing.

1. INTRODUCTION

The LOREP (Lake Oroville Runoff Enhancement Project) is a 5-year randomized seeding experiment being conducted by the California DWR (Department of Water Resources). The long-term goal of the project is to increase runoff to Oroville Reservoir, the main reservoir of the State Water Project located in northern California. Both physical and statistical analyses are being conducted in the hope of documenting the increases in the winter snowpack obtainable by seeding winter storms with liquid propane. Reynolds (1989, 1991, 1992) describes the original design, and development and testing, of a remote propane dispenser. The present paper summarizes follow-on field studies using both aerial and ground-based tracer and microphysics observations to further document seeding efficacy using ground-based liquid propane.

During mid-January to mid-March 1993, an intensive field program was conducted within the LOREP target area, Figure 1. Emphasis was placed on documenting the transport and dispersion of a tracer and/or seeding-induced ice crystals from the dispensers to the downwind edge of the target area. Sulfur hexafluoride was released at approximately 22 kg h^{-1} from two separate high-altitude propane dispenser sites. Site 7 was located on the crest of the Sierra and site 9 was positioned some 5 km west of the crest. Two different locations were used to identify which site transports seeded crystals more reliably into supercooled clouds. Only limited propane seeding could be performed due to an excessively wet early winter.

Measurement systems included a highly instrumented research aircraft provided by the National Oceanic and Atmospheric Administration. A high-altitude mountaintop observatory was established within the target area (JCC in Fig. 1). The aircraft and the observatory were equipped with continuous SF_6 analyzers and optical ice crystal probes. The analyzer is capable of detecting SF_6 concentrations to 5 ppt (parts per trillion). A dual-channel radiometer was located at the mountaintop observatory to measure the integrated liquid water and vapor within passing clouds. Four time sequential syringe samplers were used to collect 15-min air samples at specified locations within the valley to monitor SF_6. Locations of weighing precipitation gauges with .25-mm resolution are shown in Figure 1. In addition, three mountaintop weather stations provided measurements of supercooled liquid water through use of an icing rate meter.

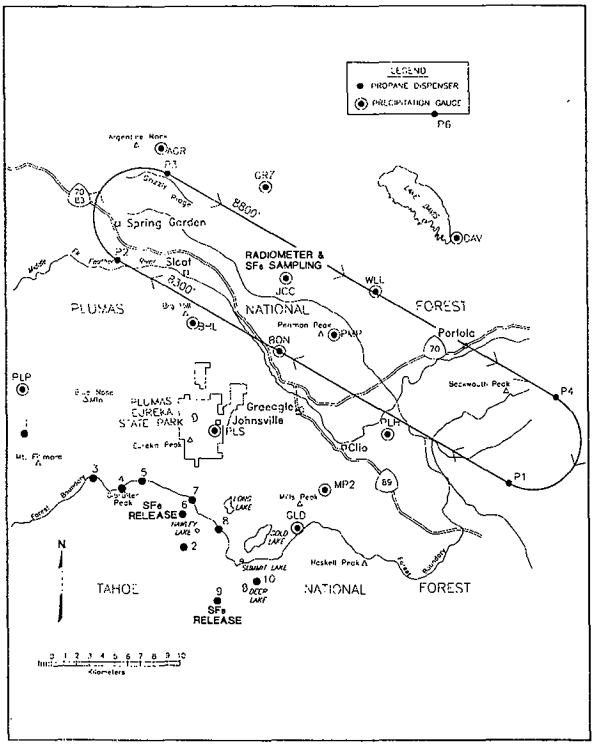

Fig. 1. Lake Oroville Runoff Enhancement Project instrumentation locations for the 1992-1993 field season. Aircraft flight tracks and way points annotated.

2. SULFUR HEXAFLUORIDE TRACER STUDIES

Previous tracer studies conducted for this program showed that subsidence (possibly gravity waves) to the lee of the Sierra Nevada may, at times, force some of the artificially produced ice crystals down into the valley before enough growth takes place (Reynolds, 1992). It is thus important to document the plume centerline and not just the lower portion of the plume.

The aircraft flight pattern used during research missions is shown in Figure 1. The flight leg flown between P1 and P2 was the valley track flown at 2500 m. The flight leg between P3 and P4 was the ridge track flown at 2680 m. During VFR (Visual Flight Rules) flights, these same tracks were flown but at flight levels down to 2100 m. At times the aircraft would fly short legs further downwind between P3 and P6, and from P6 to P4. During IFR (Instrument Flight Rules) conditions, these legs were flown at 2600 m.

Nine separate experiments were conducted this past season. Of these, four had both SF_6 and propane released, while five had SF_6 only.

Briefly, aircraft intersections of SF_6 plumes from sites 7 and 9 indicated the following. At flight altitudes of 2500 m over the valley and 2680 m over the ridge, the aircraft was generally near the tops of the SF_6 plume. At least half of the valley and ridge passes found no SF_6 when it was expected. Plume widths over the valley averaged 3 km from site 7 (15 min downwind) and 5 km from site 9 (23 min downwind). This equates to a 3- and 3.6-m s^{-1} horizontal dispersion for sites 7 and 9, respectively. At flight altitudes near 2200 m, plume widths increased along with SF_6 concentrations. This indicated the plume centerline was remaining near the release altitude. For the ridge tracks, the site 7 average plume width was 3.8 km, and the site 9 width averaged 6.6 km. At a nominal 36 min and 44 min downwind from the release, this equates to a 1.7- and 2.5-m s^{-1} dispersion. On 1 of 3 days in which passes were made downwind of the ridge track, SF_6 was detected with consistency. These intersections were about 1 h downwind. Plume horizontal dimensions of 14 and 15 km were observed for sites 7 and 9, respectively, equating to a 4-m s^{-1} spread rate. In general, the plume from site 9, initiated further west from the crest, experienced more horizontal and vertical dispersion and thus appears to be a better location for releasing seeding material.

2.1 GUIDE Model Verification

The GUIDE model is a simple two-dimensional kinematic model incorporating Gaussian plume dispersion (Rauber et al., 1988). The model is used operationally to predict the area of effect from seeding. The model has 5-km horizontal resolution and 100-m vertical resolution. Horizontal winds are derived by simply extrapolating winds measured from the Johnsville rawinsonde (Fig. 1). Vertical motions are derived by multiplying the component of the wind normal to the model terrain by the slope of the terrain between model grid points. This method of calculating vertical velocities generally overestimates the magnitude of the vertical motions, in the absence of gravity waves. It will be shown later that gravity waves are frequently present over the target area.

For each of the 9 days having SF_6 releases and aircraft sampling, the model was initialized using the sounding closest in time to the release. This was within 1 h of release time. The model-predicted plume was plotted over the target area topography. An example of this is described below.

On March 9, detailed vertical and horizontal measurements of plumes from both sites were documented in VFR conditions. Figure 2 shows the predicted plumes (dotted lines) from both sites based on the 0900 PST Johnsville sounding. Aircraft-observed SF_6 concentrations above 10 ppt are noted by symbols. [Box, 10-15 ppt; plus, 15-50 ppt; X, 50-100 ppt; asterisk, 100-150 ppt; shaded star, 150-200 ppt; sun, 200-250 ppt; open star, >250 ppt]. The maximum concentration observed was over 300 ppt. The predicted plumes are in line with observed SF_6 intersections over the valley. However, over the ridge, the tracer is to the right of the predicted plumes. This indicates that the plumes may be going around the highest terrain to the right. Average aircraft wind directions measured over the ridge were 5 to 8 degrees more westerly than observed over the valley.

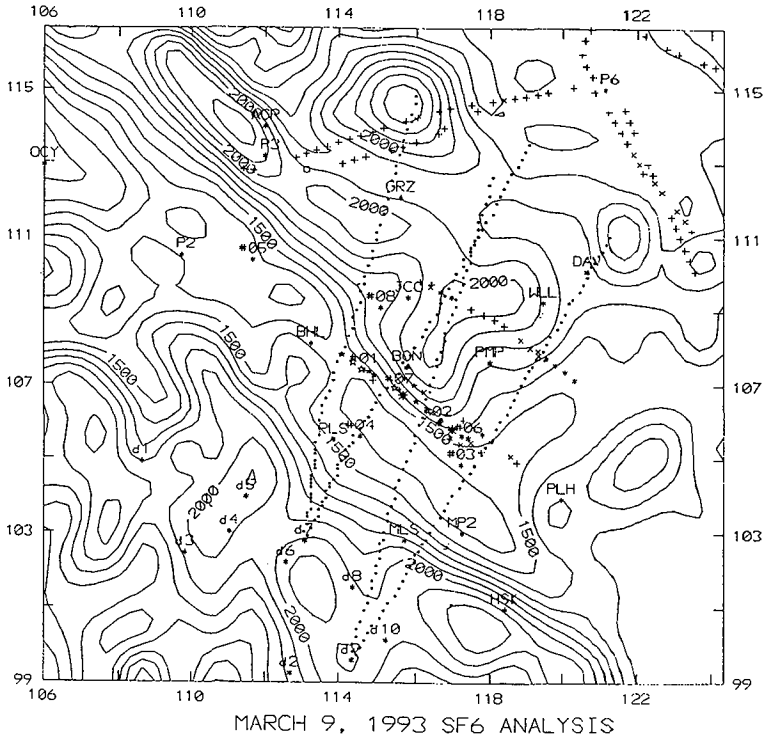

Fig. 2. GUIDE-model-predicted plumes (dotted lines) from sites 7 and 9 overlaid onto terrain contours for 9 March, 0900 PST. Aircraft- observed SF_6 concentrations above 10 ppt noted by symbols.

Downwind of the ridge, the observed plumes are wider than model predictions. Substantial mixing downwind of the second ridge is causing rapid diffusion of the plumes. A vertical cross section of SF_6 concentrations for March 9 is shown in Figure 3. The plume centerline appears to be moving almost horizontally over the valley, then displaced vertically a few hundred meters over the second ridge. Some SF_6 was observed in the valley and at JCC. The discussion in Section 2.2 is relevant to this observation.

Of the nine experiments conducted with aircraft sampling of SF_6, all but one had model-predicted horizontal plume locations within 1 to 2 km of observed locations. The model-predicted vertical plume displacement is usually within a few hundred meters of the maximum height of plume rise.

2.2 Influence of Gravity Waves on the Transport of Seeding Material

It is well known that downwind of the Sierra crest, mountain lee waves are observed during stable atmospheric conditions (Holmboe and Klieforth, 1957). It has also been shown that the ascent rate of rawinsonde balloons can be used to identify the presence of these lee waves (gravity waves) (Lalas and Einaudi, 1980, Reid, 1972, and Shutts et al., 1993). These authors show that the ascent rate can be measured to within .2 m s^{-1} using 20- to 40-s pressure increments. The data from the Johnsville rawinsonde are recorded every 2 s and the ascent rate can be calculated every 20 s. Based on the free lift of the balloon and the payload, a nominal ascent rate of 5 m s^{-1} is assumed. This was subtracted from the observed ascent rate to estimate free air vertical velocity. This was then plotted with respect to distance from Johnsville to observe any trends in vertical motions. An example of this is shown in Figure 4 for the March 9 case. A generalized streamline analysis is shown based on the computed vertical velocities and approximating a single lee wave. This lee wave motion is obviously restricting the vertical transport of the tracer until the air traverses almost completely past the valley. The tracer is then transported vertically up and over the second ridge. The aircraft sampling locations for March 9 are shown to be in a location where the tracer would be transported to these sampling levels. If seeding had occurred on this day, little growth would have occurred during downward transport. Subsequent growth on the windward side of the second ridge may not be fast enough to allow the crystals to fall out before being transported over the gauge network.

Analysis of soundings taken during SF_6 releases both this year and from previous years indicates that this lee wave is almost always present. It is the reason why at least some SF_6 has been observed in the valley in 23 of 25 tracer experiments conducted. The amplitude and phase of the wave varies considerably. In certain cases, it can rapidly transport the tracer down into the valley. In other cases, it can rapidly transport the tracer/crystals upward over

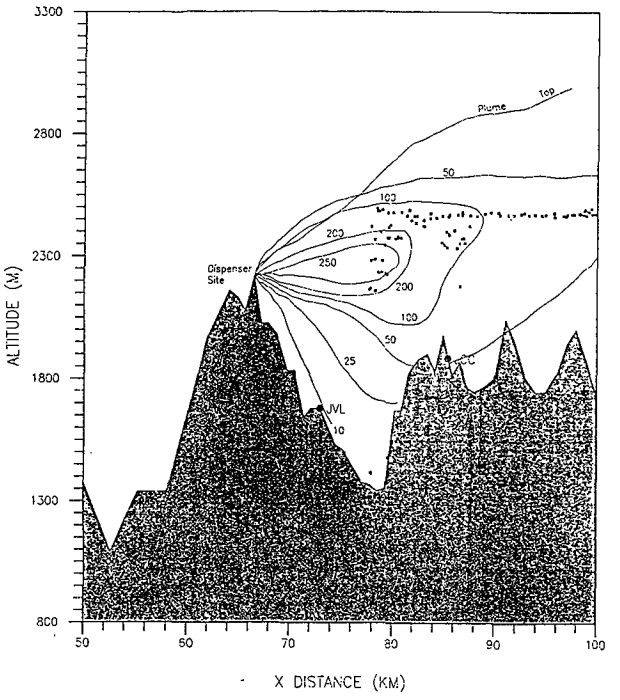

Fig. 3. Cross section from Sierra Crest to Grizzly Ridge showing contoured SF_6 concentrations observed by aircraft and ground based sequential samplers for 9 March. Asterisks denote sampling locations. Model-predicted plume top shown.

the center of the valley and well over the second ridge.

In an attempt to better document this lee wave and its effects on vertical transports, a 915-MHz wind profiler (Rodgers et al., 1993) was installed this winter near Graeagle (see Fig. 1). A statistical consensus of profiler winds is produced each hour. Ground clutter can seriously affect these winds in the absence of precipitation. Figure 5 shows a comparison of profiler 1-h consensus winds compared to the instantaneous winds from the rawinsonde for February 10, 1994, at 1700 GMT. The profiler vertical velocities shown are overwhelmed by particle fall speeds in this example. This day is fairly typical in showing that the profiler winds and rawinsonde winds agree quite well. It is assumed that the profiler is about a quarter to half wavelength further downwind than JVL and thus in the bottom or rising portion of the wave. Notice in the descending air experienced by the balloon near the crest (2200 m) and in the rising air between 2500 and 4000 m the profiler winds underestimate the rawinsonde-measured wind speeds. This may indicate the variable nature of the wave during 1 h.

The profiler-observed vertical velocities do not indicate the strong rising motion observed by the balloon from 2500 m to 4000 m, even though the balloon passed within the sampling volume of the profiler. This may indicate particle fall speeds are cancelling out the free air vertical motions. An analysis of the profiler spectra may help address this question.

Figure 6 shows the vertical motions calculated from the GUIDE model for February 10, using the 1700 GMT sounding. Although crude, it does simulate the general trend observed from the balloon ascent rates. A more detailed three-dimensional, nonhydrostatic model is needed to better predict the phase and amplitude of the wave and its relationship to stability, wind speed, and wind direction.

2.3 Direct Detection of Seeding Effects

Of the 4 days having both SF_6 and propane releases, February 17 provided the best documented case of seeding effects. On February 17, seeding was conducted (13 L h^{-1} propane) from site 7 from 0830 to 0930 PST and from site 9 from 0930 to 1030 PST. Temperatures at the dispensers were near -5 °C. Radiometric liquid water averaged .1 mm. Mountaintop icing data showed liquid water contents of .1 g m^{-3}.

Of the eight aircraft intersections of the site 7 SF_6 plume (four valley and four ridge), no definitive seeding effects were observed. Data from both aircraft liquid water probes indicated liquid water contents averaged less than .02 g m^{-3} and cloud droplet concentrations averaged less than 25 per cc within the eight plumes.

The plume from site 9 was intersected six times (three valley and three ridge). Four had distinct seeding signatures. An increase in cloud water was noted within site 9 plumes. Pass 13, along the valley, shows the most distinct seeding signature observed. Figure 7 shows a well defined SF_6 plume (vertical lines denote 11-s lag) centered on a region of enhanced, but rather small ice crystals (dashed line in 2D panel are crystals < 250 microns). A distinct habit change from hexagonal to needle crystals occurred at this location. The liquid water at this location is also the highest observed on this flight. This is contradictory to the glaciogenic seeding hypothesis in that seeding should reduce cloud water by growth of the enhanced ice crystals. An explanation is that seeding rates with propane are much higher than normally used for silver iodide, 6000 g h^{-1} vs 30 g h^{-1}, respectively. Because of homogenous nucleation, propane produces very rapid condensation and subsequent freezing of billions of ice crystals releasing latent heat which can increase the clouds buoyancy by several tenths of degrees centigrade. These results are consistent with numerical model results simulating seeding of orographic clouds (Orville et al., 1984). Similar, but not as impressive signatures were seen on the other three passes. One pass on February 9 indicated results very similar to this case.

One minute averages (about 4.8 km of flight) of crystal concentrations and calculated precipitation rates within and outside the site 9 seeding plumes showed a 33% increase in ice crystal concentrations and an 18% increase in calculated precipitation rate.

The tracer SF_6 was on a trajectory passing over the Jackson Creek Observatory (JCC) and directed at the GRZ gauge. The SF_6 sequential

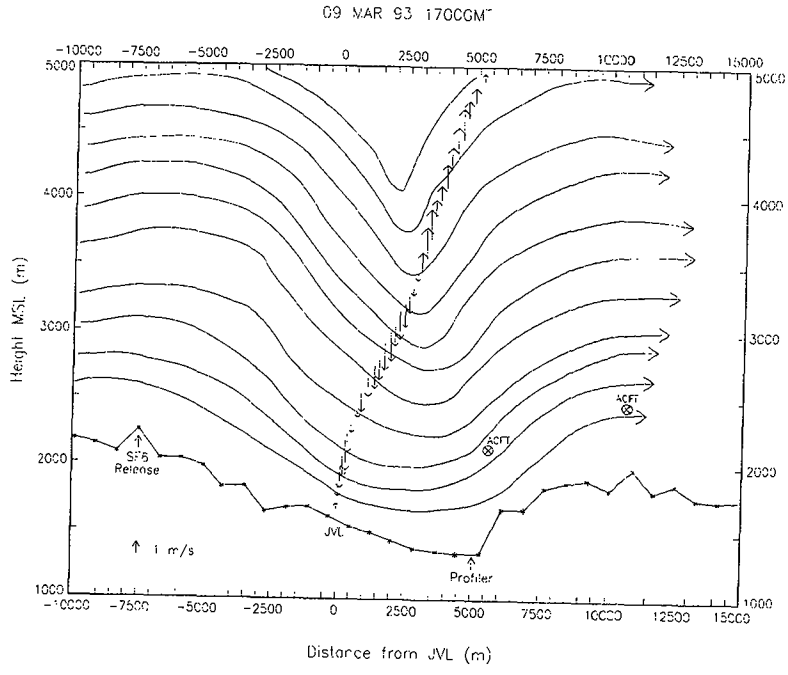

Fig. 4. Cross section of terrain relief along 205 degrees with the balloon-observed free air vertical velocities denoted by up or down arrows. The magnitude of the vertical velocity is scaled by arrow length. The location of aircraft sampling, SF_6 release, and the location of the wind profiler used in 1994 are shown.

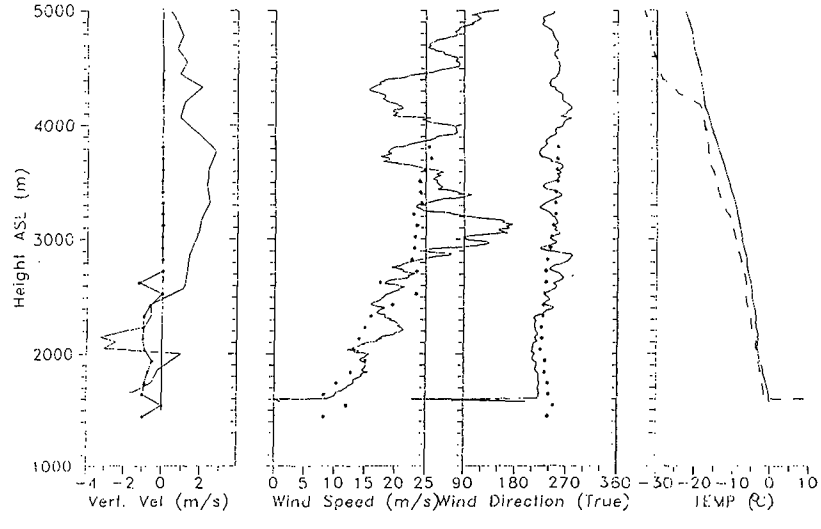

Fig. 5. Comparison of rawinsonde-observed horizontal and vertical winds (solid line) and profiler 1-h consensus winds (asterisks) for February 10, 1994. The rawinsonde-measured temperature and dewpoint vertical profiles are also shown.

3400.	.68	.68	.68	-2.03	1.69	1.02	.34	-1.02	.34	-.68	.34	.6
3300.	.89	.89	.89	-2.68	2.24	1.34	.45	-1.34	.45	-.89	.45	.8
3200.	1.11	1.11	1.11	-3.34	2.78	1.67	.56	-1.67	.56	-1.11	.56	1.1
3100.	1.19	1.19	1.19	-3.56	2.96	1.78	.59	-1.78	.59	-1.19	.59	1.1
3000.	1.44	1.44	1.44	-4.33	3.61	2.17	.72	-2.17	.72	-1.44	.72	1.4
2900.	1.56	1.56	1.56	-4.68	3.90	2.34	.78	-2.34	.78	-1.56	.78	1.5
2800.	1.45	1.45	1.45	-4.35	3.63	2.18	.73	-2.18	.73	-1.45	.73	1.4
2700.	1.17	1.17	1.17	-3.50	2.91	1.75	.58	-1.75	.58	-1.17	.58	1.1
2600.	1.02	1.02	1.02	-3.05	2.54	1.52	.51	-1.52	.51	-1.02	.51	1.0
2500.	.82	.82	.82	-2.45	2.04	1.23	.41	-1.23	.41	-.82	.41	.8
2400.	.59	.59	.59	-1.76	1.47	.88	.29	-.88	.29	-.59	.29	.5
2300.	.63	.63	.63	-1.88	1.57	.94	.31	-.94	.31	-.63	.31	.6
2200.	.71	.71******		-2.12	1.76	1.06	.35	-1.06	.35	-.71	.35	.7
2100.	.74	.74******		-2.21	1.84	1.10******		-1.10	.37	-.74	.37	.7
2000.	.65**********			-1.95	1.62**********			-.97	.32	-.65	.32*****	
1900.	.53**********			-1.59	1.32**********			-.79******		-.53	.26*****	
1800.**********				-1.14	.95**********					-.38**********		
1700.**********				-.69**********								
1600.**********												
1500.**********												
1400.**********												
1300.**********												
1200.**********												

Fig. 6. GUIDE-model-calculated vertical velocities over the project terrain (asterisks). Horizontal grid spacing is 5 km. Vertical grid spacing is 100 meters. These data should be compared to the rawinsonde-observed vertical velocities shown in Figures 4 and 5. Vertical velocities need to be considered only up to 2800 m since SF_6 is almost always observed below this altitude.

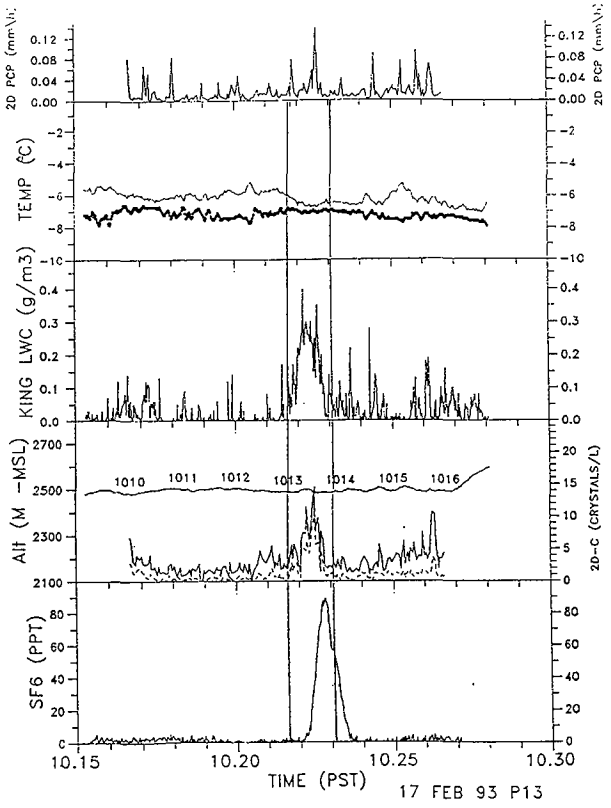

Fig. 7: Variables observed or calculated from aircraft observations during plume tracing experiment of February 17. From top to bottom: calculated precipitation rate from 2D ice probe; temperature (thin) and dew point (heavy); cloud liquid water; cloud ice concentration (solid) and particles classified as tiny (dashed); SF_6 concentration. Vertical lines denote true position of SF_6 plume accounting for 11 s lag.

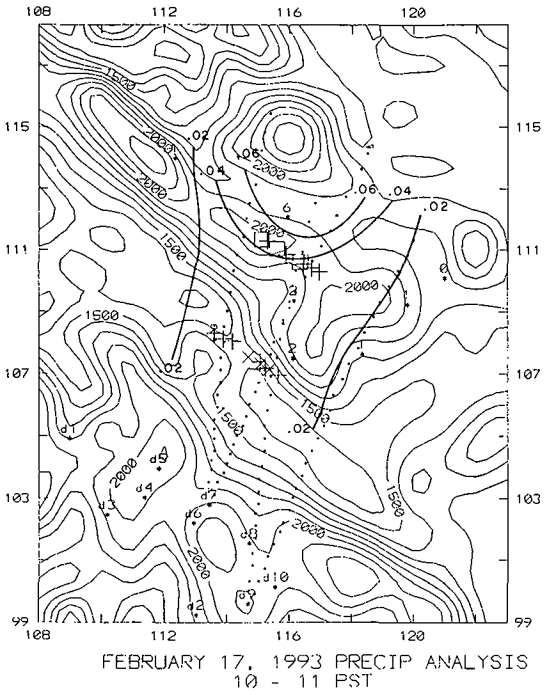

Fig. 8. Isohyets for 1000 to 1100 PST 17 February with aircraft-observed SF_6 locations and GUIDE model plumes noted.

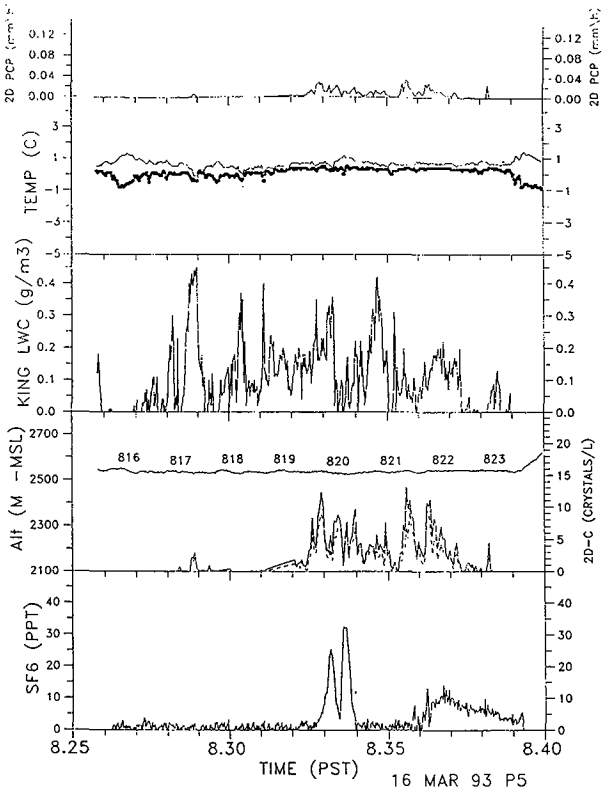

Fig. 9. Same as Fig. 7 but for 16 March pass 5 along valley track. Site 9 then site 7 plumes sampled.

sampler, about a kilometer west of JCC, indicated SF_6 from both site 7 (0930 to 1000 PST) and site 9 releases (1015 to 1045 PST). There were indications of ice crystal concentration increases on the 2D probe at JCC during the period from 0900 to 1015 PST of up to 30 L^{-1} above a background of 15 L^{-1}. Precipitation increases were also noted for those gauges within the fallout trajectory. Figure 8 is an isohyetal map of 1-h precipitation totals in the gauge network between 1000 and 1100 PST. Here we see more precipitation in the gauge at GRZ (.06 in), directly in line with the tracer trajectory.

March 16 provided documentation of seeding effects when ambient air temperatures were near 0 °C. Seeding was conducted for 1 h from both sites 7 and 9. Aircraft observations showed temperatures just above freezing at 2500 m. Liquid water contents were near the highest observed on any flight. Of the five SF_6 plumes observed by aircraft from site 7, three indicated apparent seeding effects. This is notable in that seeding was performed near 0 °C.

Figure 9 shows the aircraft data for pass 5 along the valley. The site 9 plume is intersected first at 0820 PST followed by site 7 at 0822 PST. Liquid water is observed along the entire pass. The ice crystal probe detects ice crystals near and during plume intersections. Almost all crystals are less than 250 microns (dotted line). Images (not shown) indicated the crystals to be hexagonal plates, consistent with fog seeding done near 0 °C with dry ice (Deshler et al., 1987). It has been observed that propane seeding in fog at temperatures near +1 to +2 °C has caused precipitation (Gerdel, 1968). Gerdel suggests that a propane hydrate or clathrate is formed by the inclusion of gas molecules in the ice crystal. Such crystals have a melting, or dissociation, between +1 and +6 °C. This is dependent on the number of molecules of propane included in the clathrate. It is clear that more study is needed to verify this hypothesis.

3. CONCLUSIONS

Aircraft measurements of SF_6 released from two separate high-altitude propane dispenser sites indicate the plumes rarely rise above 2700 m or 500 m above the release altitude. Comparison of aircraft measurements with GUIDE model predictions of plume horizontal and vertical dispersion compare favorably. However, it is apparent that commonly observed lee waves have a significant impact on the transport of seeded crystals over the target area.

The aircraft intersected 35 seeded plumes on four separate days. Only 11 of the 35 plumes indicated seeding effects. The lack of liquid water minimized seeding effects. On February 17, distinct seeding effects were noted on five of six plumes intersected from one of the sites. Apparent dynamic seeding effects were noted on several of these passes. Precipitation at a gauge directly in line with the aircraft-observed seeding plume showed a factor of five increase in precipitation over surrounding gauges. Seeding effects using liquid propane were noted 1 day when the temperature at the dispenser was near or slightly above freezing.

Acknowledgements. The LOREP is managed by the California Department of Water Resources and funded by the State Water Project. The Bureau of Reclamation provided technical direction.

4. REFERENCES

Benner, R.L., and R. Lamb, 1985: A fast response continuous analyzer for halogenated atmospheric tracers. *J. Atmos. and Ocean. Tech.*, 2, 582-589.

Deshler, T., D.W. Reynolds and J.H. Humphries, 1987: Observations of snow crystal concentration, habit, riming and aggregation collected at the ground during six fog seeding experiments. *Proc. 11th Conf. Wea. Modif.*, Edmonton, Canada, Amer. Meteor. Soc., 118-121.

Gerdel, R.W., 1968: Note on the use of liquified propane for fog dispersal at the Medford-Jackson Airport, Oregon. *J. Appl. Meteor.*, 7, 1039-1040.

Holmboe, J., and H. Klieforth, 1957: Investigations of Mountain Lee Waves and the Air Flow Over the Sierra Nevada. Final Report, Contract No. AF19(604)-728, Dept. of Meteor., UCLA. 299 pp.

Lalas, D.P., and F. Einuadi, 1980: Tropospheric gravity waves: their detection by and influence on rawinsonde balloon data. *Quart. J. R. Meteor.* Soc, **106**, 885-864.

Orville, H.D., R.D. Farley and J.H. Hirsch, 1984: Some surprising results from simulated seeding of stratiform-type clouds. *J. Climate Appl. Meteor.*, **23**, 1585-1600.

Rauber, R.M., R.D. Elliott, J.O. Rhea, A.W. Huggins and D.W. Reynolds, 1988: A diagnostic technique for targeting during airborne seeding experiments in wintertime storms over the Sierra Nevada. *J. Appl. Meteor.*, **27**, 811-828.

Reid, S.J., 1972: An observational study of lee waves using radiosonde data. *Tellus*, **24**, 93-596.

Reynolds, D.W., 1989: Design of a ground based snowpack enhancement program using liquid propane. *J. Wea. Mod.*, **21**, 29-34.

Reynolds, D.W., 1991: Design and field testing of a remote liquid propane dispenser. *J. Wea. Mod.*, **23**, 49-53.

Reynolds, D.W., 1992: A snowpack augmentation program using liquid propane. Preprints, AMS Symposium on Planned and Inadvertent Weather Modification. Atlanta, GA. 88-95.

Rodgers, R.R., W.L. Ecklund, D.A. Carter, K.S. Gage and S.A. Ethier, 1993: Research applications of a boundary-layer wind profiler. *Bull. A. M. S.*, **74**, 567-580.

Shutts, G.J., P. Healy and S.D. Mobbs, 1993: A multiple sounding technique for the study of gravity waves. *Quart. J. R. Meteor. Soc.*, **120**, 59-77.

IMPLICATIONS OF EARLY 1991 OBSERVATIONS OF SUPERCOOLED LIQUID WATER, PRECIPITATION AND SILVER IODIDE ON UTAH'S WASATCH PLATEAU

Arlin B. Super
Bureau of Reclamation
Denver CO 80225

Abstract. The Utah/NOAA Atmospheric Modification Program conducted an observational program in early 1991, with additional support from the Bureau of Reclamation. A summary is presented of observations obtained on the Wasatch Plateau of central Utah which includes SLW (supercooled liquid water), precipitation, AgI (silver iodide ice nuclei), air and dewpoint temperature, and wind velocity. With the exception of AgI ice nuclei, measurements were made on 20 days with storm conditions. Silver iodide was monitored during part or all of a subset of 12 days when valley AgI generators were being operated.

It is shown that abundant SLW existed during many hours, and a large fraction of these hours did not have precipitation observed on top the Plateau. The SLW flux over the Plateau-top's windward edge exceeded the average precipitation on top the Plateau. These findings suggest significant seeding potential may exist.

Acoustical ice nucleus counter observations were adjusted to temperatures typical of AgI plume tops. Aircraft measurements showed the plume tops were usually less than 1 km above the Plateau. The adjusted ice nucleus observations suggest effective AgI ice nuclei concentrations were too low for productive seeding much of the time when SLW was present. The main problem appears to be the warm temperatures of the SLW during most storm periods. Effective concentrations of AgI ice nuclei are not expected at such temperatures with the generators and release rates used in the Utah operational seeding program. However, these estimates were based on a 1981 generator calibration in a cloud simulation laboratory which may not be totally representative of winter orographic clouds. Direct observations are needed of ice particle concentrations caused by seeding orographic clouds for the range of conditions typical of winter storms.

The challenge is to develop means of routinely targeting the SLW zone with adequate concentrations of seeding-caused ice crystals which can start the precipitation formation processes in naturally inefficient clouds. A number of approaches are suggested which could make the Utah operational seeding program more effective.

1. INTRODUCTION

Observations of SLW (supercooled liquid water), precipitation, AgI (silver iodide) IN (ice nuclei), wind velocity, and air and dewpoint temperature were made on the Plateau (Wasatch Plateau) of central Utah between mid-January and mid-March 1991. This observational program was part of the Utah/NOAA (National Oceanic and Atmospheric Administration) Atmospheric Modification Program.

Overall purposes of the Utah/NOAA Atmospheric Modification Program are:

(1) To physically evaluate the effectiveness of the Utah operational cloud seeding program in enhancing the mountain snowpack.
(2) To suggest means of improving operational program effectiveness.

The project design of the operational program and the general seeding hypothesis are discussed by Griffith et al. (1991). Briefly, the program uses a widespread network of manual AgI generators operated upwind (west) of major mountain barriers. The generators are located mostly at valley sites with some generators near canyon mouths. The seeding hypothesis states that SLW is present in Utah storms which can be reached by the AgI, and that growth times and trajectories of augmented precipitation can impact the intended target areas. Special weather forecasts are made to determine whether storms meet stated seeding criteria and which, if any, generators should be operated in attempts to affect particular target areas.

The early 1991 Utah/NOAA observational program emphasized the transport and dispersion of ground-released AgI over the Plateau. Most AgI releases were made from valley and canyon mouth locations, but some were made from a high altitude site on the Plateau's windward slope as discussed further by Super and Holroyd (1994). Other discussion of the transport and dispersion of AgI over the Plateau includes Griffith et al. (1992), Heimbach and Super (1992) and Super and Huggins (1992).

This paper does not directly address the transport and dispersion of ground-released AgI except as monitored at a single Plateau-top observatory. Rather, this paper's purpose is to consider and relate particular variables of interest to winter orographic cloud seeding in an "overview" sense for the period of measurements. The SLW observations were summarized by Huggins et al. (1992). This paper expands upon their work in that precipitation observations are considered in more detail, and Plateau-top observations of AgI are discussed for periods of valley generator operation. Estimates of per-storm SLW flux over the Plateau during early 1991 have been presented by Super and Huggins (1993). Sassen and Zhao (1993) discuss the cloud seeding implications of a related data set collected over the Tushar Mountains of southern Utah.

2. OBSERVATIONS

Twenty days were selected for analysis of SLW and precipitation. Seeding was conducted during some of these days but any effects of seeding on SLW and precipitation measurements are not known. These 20 days (midnight to midnight - all times are LST) had almost complete measurements of the types noted above as well as significant SLW and/or precipitation. Amounts of SLW and precipitation outside these days were very limited during the late January to mid-March 1991 period. A few periods with significant SLW and precipitation occurred during the period January 14-27, but some precipitation data are missing.

Observations of IN were made on top the Plateau during part or all of a subset of 12 of the 20 days when valley seeding was being conducted from a network of 8 AgI generators (shown on Fig. 1 of Super and Holroyd, 1994). A total of about 164 h of seeding was carried out during these 12 days.

The days selected for analysis are listed below. Underlined dates had valley seeding and IN observations during at least part of the day.

January: 28
February: 3,12,13,14,16,17,18,19,28
March: 1,2,3,4,5,6,7,10,11,14

Vertically-integrated SLW measurements were available from the Bureau of Reclamation's microwave radiometer. This type of instrument and its data retrieval have been discussed by Hogg et al. (1983). It was located at 2700 m (all elevations above mean sea level) near the Plateau-top's west edge at the head of a major canyon (the DOT site on Fig. 1 of Super and Holroyd, 1994).

Ambient temperatures at the radiometer were less than 0 °C for the large majority of hours with detectable liquid water, so all liquid was supercooled during such periods. A blower continuously directed a large volume of air over the outside reflector to keep it clear of snow and, to a lesser extent, occasional melted precipitation. The latter is not believed to have significantly affected measurements because melted precipitation was rare during above freezing hours, and the reflector was periodically checked and wiped dry if needed.

Twenty-five hours of radiometer data are missing from the 20 selected days, 6 of which are after 1800 on March 14 because of termination of the field program.

Wind speed and direction were measured by heated sensors (to prevent rime ice accumulation) which were located 7.5 m above ground level on a tower at the radiometer site. Air and dewpoint temperatures were measured on the same tower using an aspirated, chilled-mirror device and calibrated thermistors. These observations are complete for all 20 days with the exception of the last 6 h of March 14.

Ice nuclei concentrations were measured with a semiquantitative NCAR acoustical IN counter (Langer 1973, Super and Holroyd 1994) at the radiometer site. The unit was reconditioned by the system's inventor (G. Langer) just prior to the field program.

The NCAR IN counter rarely indicated a concentration as high as 1 IN L^{-1} unless seeding was being conducted. This is not meant to suggest what the natural IN concentration was because the accuracy of the NCAR IN counter in measuring natural IN is not well known, as is true of most IN monitoring devices. However, experience with the counter indicated that IN concentrations above about 1 IN L^{-1} at -20 °C, the cloud chamber temperature, were effectively AgI IN concentrations.

The NCAR IN counter was routinely checked for proper operation. Filtered air was periodically sampled to insure that IN count rates would decrease to very low levels. Flow checks insured against system air leaks. Several comparisons were made with a similar truck-mounted NCAR IN counter parked nearby when AgI was present. The two counters produced similar IN concentration values. Few problems were encountered with the radiometer site NCAR IN counter during the course of the field season.

Precipitation was measured by three shielded, weighing Belfort gauges on top of the Plateau. These gauges were located in protected clearings in the conifer forest just west of the radiometer site, near the center of the Plateau top, and near the Plateau-top's east edge (see Fig. 1 of Super and Holroyd, 1994). These measurements are complete for all 20 days.

3. PRECIPITATION AND SLW DISTRIBUTIONS

3.1 General

A sorting program counted and listed the hours with measurements between any specified minimum and maximum hourly average values of SLW, wind speed and direction, air temperature and dewpoint temperature, and hourly precipitation averaged for the three gauges. Hours with missing SLW measurements were ignored. A total of 455 h with complete data exists, which was used in the analysis to be presented. An

exception is that a separate shorter data file was used for periods with IN measurements discussed in Sec. 8. No attempt was made to examine these data on a storm-by-storm basis. Rather, all data were considered together as a single set in a first step toward a "climatology." Of course, 20 days with storm activity from about 1.5 mo of a single winter do not begin to approach a climatology. However, because such observations are limited, in particular of SLW and AgI, it is of interest to consider an overview of the Plateau observations that do exist.

To place the observations in perspective, 179 h (39 pct) of the available 455 h had detectable precipitation, meaning at least one of the three gauges recorded at least 0.01 in. of precipitation. A total of 333 h (73 pct) had an hourly average SLW amount of 0.01 mm or greater. The radiometer's slight baseline drift was conservatively adjusted so that it is highly likely that all 333 h had SLW present, even when the hourly average was only 0.01 mm. A total of 169 h (37 pct) had simultaneously detectable SLW and precipitation. Only 10 h had measurable precipitation with no SLW observed. These 10 h were cold (average -11 °C at 2700 m), and were mostly associated with postfrontal, northwesterly flow.

3.2 Distribution of Precipitation

Hourly precipitation and SLW amounts are both known to have highly skewed frequency distributions in winter orographic storms. Table 1 lists the precipitation frequency distribution for the 179 h with detectable amounts in any of the gauges. (All precipitation observations were made in English units and are so reported.) The median hourly precipitation rate (snow liquid water equivalent) was about 0.015 in. Ninety pct of all hours had 0.06 in. or less. But 4 h exceeded 0.10 in. and the maximum observed hourly rate was 0.177 in.

Table 1 shows that the 41 pct of precipitation hours which received an average of 0.01 in. or less contributed only 10 pct to the total precipitation for all hours. Conversely, the 2 pct of precipitating hours with amounts exceeding 0.10 in. accounted for 11 pct of the total precipitation. About half the total precipitation fell during the 83 pct of the precipitating hours with average rates of 0.05 in. h^{-1} or less. The 17 pct of hours with higher rates produced the other half of the total precipitation.

3.3 Distribution of SLW

The hourly frequency distribution of SLW amounts listed in Table 2 is also highly skewed. The median of all hours with SLW of 0.01 mm or greater was 0.06 mm. Almost 90 pct of all hours had 0.30 mm or less average SLW. However, 20 h exceeded 0.50 mm and 7 h exceeded 1.00 mm. The maximum recorded hourly mean was 1.50 mm.

Nineteen of the 20 h in excess of 0.50 mm occurred during a single storm event between the evening of March 3 and noon of March 5. All 7 h above 1.00 mm occurred between 1900 on March 4 and 0800 on March 5, an unusually warm and windy period.

The surface temperature at the radiometer was between 0 and +2 °C during portions of the 7 h with above 1.0 mm SLW. This raises the possibility of measurement errors caused by melting snow on the outside reflector. However, such errors are believed minor because of air blown across the reflector and periodic manual checks. Moreover, precipitation rates were light during the above freezing, high SLW periods, and much of the precipitation consisted of graupel which bounced off the reflector. Similar amounts were recorded by the nearby Desert Research Institute radiometer which effectively shed water drops with a spinning reflector. It is possible that some presumed liquid cloud water observations were elevated by a liquid film on falling ice particles above the radiometer. However, SLW hourly mean values continued to exceed 1.0 mm after the surface temperature reached and fell below 0 °C.

4. PRECIPITATION RATES EQUIVALENT TO SLW AMOUNTS

Based on aircraft observations and upwind rawinsonde measurements during winter storms, a westerly component of 10 m s^{-1} is typical for the

Table 1. - Frequency distribution of 179 h with observed precipitation.

Hourly Precip. (inches)	Percent	Cumulative Percent of hours	Cumulative Percent of total Precip.
0.003-0.010	41	41	10
0.011-0.020	20	61	22
0.021-0.030	12	73	34
0.031-0.040	5	78	41
0.041-0.050	5	83	49
0.051-0.060	7	90	66
0.061-0.070	5	95	79
0.071-0.080	2	97	85
0.081-0.090	1	98	89
0.091-0.100	0	98	89
0.101-0.177*	2	100	100

* change in interval size

Table 2. - Frequency distribution of 333 h with observed SLW.

Hourly SLW (mm)	Percent	Cumulative Percent
0.01-0.05	47	47
0.06-0.10	18	65
0.11-0.15	10	75
0.16-0.20	7	82
0.21-0.25	4	86
0.26-0.30	3	89
0.31-0.40*	2	91
0.41-0.50	3	94
0.51-1.00*	4	98
1.01-1.50	2	100

* change in interval size

lowest 600 m above the Plateau, believed to contain most of the SLW. Let it be assumed that the layer containing the SLW had a wind speed component normal to the Plateau of 10 m s^{-1}. The vertically integrated SLW, multiplied by the representative wind speed for the layer containing the SLW, provides a first approximation estimate of the SLW flux. The flux represents the upper limit for cloud seeding potential. While it is impractical for seeding to convert all available SLW to precipitation, total downwind precipitation caused by seeding cannot exceed the SLW flux.

To put the SLW flux values into perspective, their equivalent precipitation amounts were calculated by assuming the flux was totally converted to precipitation which fell uniformly over a 10-km distance, approximately the width of the Plateau top. A precipitation rate equivalent to this data set's observed median rate of 0.015 in. h^{-1} would require a SLW value in excess of 0.10 mm for these assumptions. Table 2 shows that 65 pct of all hours with SLW had amounts of 0.10 mm or less above the west (windward) edge of the Plateau top. Some of this SLW flux was naturally converted to precipitation farther downwind. Therefore, even if seeding was capable of converting all the remaining "excess" SLW flux to additional precipitation, hourly rates would be quite limited for the majority of SLW hours. On the other hand, this 65 pct represents a large number of hours (216) with SLW amounts of 0.10 mm or less. If seeding could provide, on average, even an additional rate of 0.002 in. h^{-1} during these many hours, the resulting precipitation accumulation would be 0.43 in. This figure represents 9 pct of the total which fell on the Plateau top during the 20 storm days comprising this data set. Therefore, beneficial precipitation could result from even minor seeded precipitation rates if the seeding was effective for many hours over the course of a winter.

Table 3 lists the precipitation rate equivalent to the midpoint of each SLW range in Table 2 with the assumptions that the SLW-layer wind speed normal to the barrier was 10 m s^{-1} and all SLW flux was converted to precipitation of uniform intensity over a 10-km distance. The frequency of each range listed in Table 2 was used to estimate the percent of the total SLW flux (or equivalent precipitation) contributed by that range. The cumulative frequency of SLW flux is also listed.

Table 3 indicates that the many hours with SLW amounts less than or equal to the median of 0.06 mm have limited precipitation production potential. For example, approximately half of all hours with SLW (169 h) had amounts ranging from 0.01 through 0.06 mm with an average SLW value of 0.026 mm. Multiplying this average SLW value with an assumed representative wind speed of 10 m s^{-1} provides an estimated total SLW flux for the 169 h. If this estimated flux was converted to uniform precipitation over the approximate 10-km width of the Plateau top, the equivalent precipitation would be about 0.6 in. For comparison, the total precipitation for the 20 days in question averaged 4.7 in. on top of the Plateau, a figure 8 times as large.

In contrast, the average SLW amount was 0.267 mm for the 164 h with values of 0.07 mm or greater. For the same assumptions, that is equivalent to 6.2 in. of precipitation. Therefore, to a first approximation and ignoring other factors, the wetter half of all SLW hours had the potential to contribute ten times as much precipitation as the drier half.

The estimated contributions of SLW flux listed in Table 3 suggest that one-third of all flux occurred with SLW amounts less than about 0.18 mm, one-third with amounts between 0.18 and about 0.55 mm, and one-third with higher amounts. Table 3 underestimates the importance of the higher SLW amounts because they tend to be associated with stronger winds resulting in greater fluxes than estimated with a constant 10 m s^{-1} wind speed.

Tables 2 and 3 show the potential importance for seeding of the relatively few hours with high SLW amounts. Although only 6 pct of all SLW hours exceeded 0.50 mm, their SLW flux is estimated at 37 pct of the total. Seeding operations obviously should make every effort to successfully seed the wetter hours. But it may be difficult to convert a large fraction of this

Table 3. - Precipitation rates equivalent to the midpoints of the listed SLW ranges if the mean wind speed normal to the barrier was 10 m s^{-1} in the layer containing the SLW, and the SLW flux was converted to uniform precipitation over a 10-km distance. The contribution of SLW flux (or equivalent precipitation) is expressed as a percent of the total flux for all cases. The cumulative frequency is also listed.

Hourly SLW (mm)	Hourly precip. (mm)	(in)	Percent of total SLW flux	Cumulative percent of total SLW flux
0.01-0.05	0.11	0.004	10	10
0.06-0.10	0.29	0.011	10	20
0.11-0.15	0.47	0.019	9	29
0.16-0.20	0.65	0.026	8	37
0.21-0.25	0.83	0.033	6	43
0.26-0.30	1.01	0.040	6	49
0.31-0.40*	1.28	0.050	5	54
0.41-0.50	1.64	0.065	9	63
0.51-1.00*	2.74	0.108	20	83
1.01-1.50	4.54	0.179	17	100

* change in interval size

abundant flux to precipitation, at least with common seeding approaches. The high flux hours are characterized by stronger winds and higher temperatures. Strong winds provide limited time for ice crystal formation, growth to snowflake or graupel sizes, and fallout to the surface. Ice crystal mass growth rates tend to be slower at higher temperatures (Redder and Fukuta 1989). Moreover, temperatures nearer freezing may make it impractical to create significant IN concentrations with AgI (see Sec. 9).

5. COMPARISON OF DRIER AND WETTER SLW HOURS

The wetter and drier SLW hours are further compared in the following tables. Table 4 lists them according to whether or not precipitation was detected. Tables 5 and 6 list a number of variables of interest for the wetter and drier hours, respectively.

Table 4 shows that for the drier half of the SLW hours, precipitation occurred during 70 h but was not detected during 99 h. The frequency was reversed for the wetter hours, which had precipitation during 99 h and no precipitation during 65 h. In either category, a large fraction of hours with SLW present had no precipitation. It is particularly encouraging that 40 pct of the wetter hours were not precipitating (at least not at detectable rates at the three Plateau-top gauges). Economically important cloud seeding potential may exist during some similar periods. Of course, cloud seeding potential also may exist when natural precipitation is occurring but is insufficient to convert all SLW to precipitation.

The 65 wetter hours without precipitation had significantly less SLW on the average than the 99 wetter hours with precipitation (0.150 vs 0.344 mm). The nonprecipitating hours were slightly warmer and noticeably drier (larger temperature-dewpoint spread) on the Plateau top, and had lighter wind speeds. Lighter winds and a drier atmosphere at mountain-top altitudes would be expected to result in less condensate production and is consistent with the lower SLW. These conditions would be expected to be associated with less dynamic storm phases, unlikely to produce as much precipitation. Nevertheless, the average of 0.15 mm SLW for the wetter nonprecipitating hours could represent significant seeding potential, if sufficient ice crystal concentrations can be created by seeding and if adequate time (distance) exists for ice crystal growth and fallout. These nonprecipitating hours have the advantage that more time is available with the lighter wind speeds.

As might be expected, the 99 drier hours without precipitation were warmer, drier, and less windy than the 70 drier hours with precipitation. The hours with precipitation had an average Plateau-top wind direction of 265°; all other categories had average winds near 245°. This observation suggests the precipitating hours with limited SLW were more likely to be postfrontal. Winds aloft generally shift to northwesterly after frontal passage while Plateau-top winds shift from southwesterly to westerly or northwesterly.

The 164 h with SLW of 0.07 mm or greater (wetter hours) occurred within a narrow range of wind direction as shown in Table 5 and the lower panel of Fig. 1. It can be seen that 75 pct of these hours had Plateau-top winds between 210 and 270°. Moreover, the average SLW amounts and wind speeds associated with this wind direction range were significantly higher than for other directions, which should result in greater SLW flux. Most of the precipitation was associated with the same 60° sector, likely as a consequence of the higher frequency of SLW occurrence and presumed higher flux amounts. An additional 11 pct of the SLW hours had winds between 270 and 300°. Limited SLW and precipitation occurred outside the 90° sector between 210-300°.

Table 6 is similar to Table 5 but lists observations for the 169 h which had average SLW values between 0.01 and 0.06 mm inclusive. Most of these drier SLW hours were also associated with westerly flow, but were somewhat less

Table 4. - Summary of average wind, temperature, moisture, and total precipitation partitioned by median SLW amount and whether precipitating or not.

SLW range (mm)	Precip.	Hours	SLW (mm)	Temp (°C)	Dewpt. (°C)	Speed (m/s)	Dir. (deg)	Precip. (inch)
0.01-0.06	Yes	70	.028	-6.9	-7.6	4.4	265	1.56
0.01-0.06	No	99	.025	-4.0	-8.6	3.1	242	0.00
0.07-1.50	Yes	99	.344	-2.5	-3.2	6.4	246	3.08
0.07-1.50	No	65	.150	-1.9	-6.1	4.3	243	0.00

Table 5. - Distribution of 164 h with SLW values of 0.07 mm or greater vs wind direction. The average SLW, air temperature, dewpoint temperature, wind speed, and average total precipitation on top the Plateau are given for indicated wind direction sectors.

Wind Direction (degrees true)	Pct of hours	SLW (mm)	Temp. (°C)	Dewpt. (°C)	Wind Speed ($m\ s^{-1}$)	Total Precip. (inch)
150-179	5	.13	-2.6	-8.2	3.0	0.05
180-209	4	.19	-0.7	-5.0	4.6	0.06
210-239	30	.30	-0.7	-3.2	6.6	0.97
240-269	45	.31	-2.7	-4.4	5.6	1.56
270-299	11	.15	-3.0	-3.6	4.0	0.34
300-329	5	.11	-6.8	-7.5	5.3	0.10
330-149	0	N/A	N/A	N/A	N/A	N/A

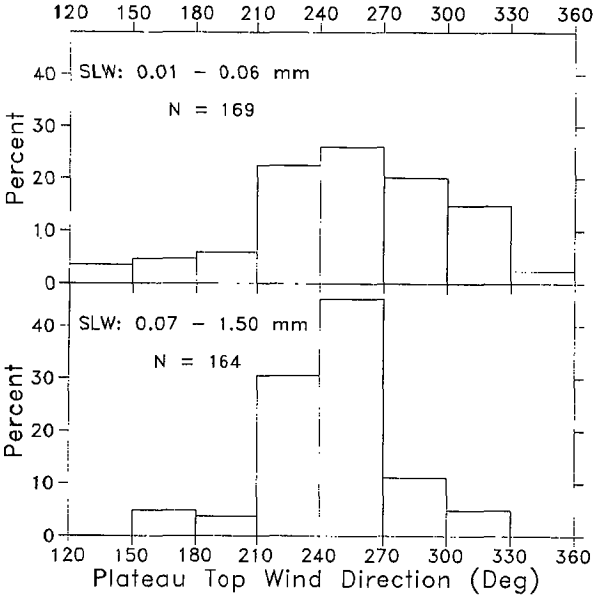

Fig. 1. Distribution of wind direction at the 2700-m microwave radiometer site for 169 drier hours (upper panel) and 164 wetter hours (lower panel).

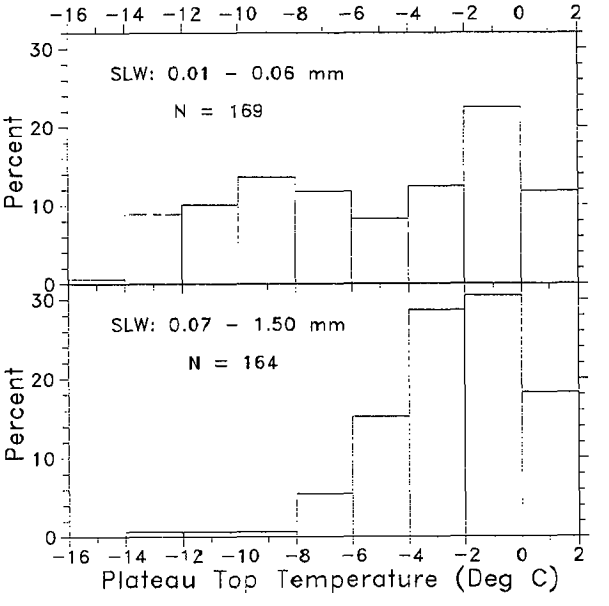

Fig. 2. Distribution of temperature at the 2700-m microwave radiometer site for 169 drier hours (upper panel) and 164 wetter hours (lower panel).

Table 6. - Distribution of 169 h with SLW values from 0.01 to 0.06 mm vs wind direction. The average SLW, air temperature, dewpoint temperature, wind speed, and average total precipitation on top the Plateau are given for indicated wind direction sectors.

Wind Direction (degrees true)	Pct of hours	SLW (mm)	Temp. (°C)	Dewpt. (°C)	Wind Speed ($m\ s^{-1}$)	Total Precip. (inch)
120-149	4	.01	-6.8	-8.2	1.1	0.00
150-179	5	.03	-2.9	-7.2	3.1	0.15
180-209	6	.02	-3.6	-10.7	3.1	0.02
210-239	22	.03	-1.0	-6.3	4.8	0.41
240-269	26	.03	-5.4	-8.0	3.7	0.59
270-299	20	.03	-7.8	-8.7	3.5	0.25
300-329	15	.02	-8.2	-9.4	3.5	0.13
330-359	2	.01	-9.7	-10.7	1.8	0.01
000-119	0	N/A	N/A	N/A	N/A	N/A

concentrated than the wetter hours as shown on the upper panel of Fig. 1. For example, although 86 pct of the wetter hours were in a 90° sector (210 to 300°) in Table 5, 83 pct of all hours of Table 6 were in a wider 120° sector (210 to 330°). The many cases between 270 and 360° are likely postfrontal because Plateau-top winds generally shift to the northwest quadrant after cold frontal passage.

Wind speeds with the drier SLW hours were lighter for all wind direction ranges with a westerly component than for the wetter SLW hours of Table 5. The strongest winds of Table 6 were associated with wind directions between 210 and 270°, similar to Table 5. The SLW amounts in this range were as high as found with any other wind direction range so it is presumed that the greater SLW fluxes occurred with southwest to westerly flow.

The drier hours tended to be colder and had greater temperature-dewpoint differences, indicating less atmospheric moisture at Plateau-top levels. The average air temperature and dewpoint temperature for the 164 wetter hours of Table 5 was -2.2 and -4.3 °C; the averages for the 169 drier hours of Table 6 were -5.2 and -8.2 °C.

Figure 2 shows hourly frequency distributions of air temperature measured at the 2700-m microwave radiometer site during the wetter and drier SLW hours. The drier hours, shown in the upper panel, did not have a marked temperature dependence for temperatures above -14 °C. In contrast, the wetter hours were concentrated between -6 and +2 °C, with almost 60 pct of all hours between -4 and 0 °C. Aircraft observations from early 1991 suggest that most of the SLW was within 1000 m of the Plateau top, and limited ground-released AgI reached that altitude. If it is assumed that the top of the SLW zone was always 1000 m above the surface with a typical moist adiabatic lapse rate, only about 1 in 5 of the wetter hours had any SLW colder than -11 °C. Most of the SLW was at lower altitudes with warmer temperatures. The implications for cloud seeding are discussed in Sec. 9.

Finally, the airflow was examined in the canyon leading from the valley west of the Plateau to the radiometer site. Hourly mean wind velocity observations were made about 3 km above the canyon mouth at an elevation of 2230 m. Wind speeds were usually between 1 and 3 $m\ s^{-1}$ during storms, and either upcanyon or downcanyon in direction.

The airflow was approximately evenly divided for the drier hours between 91 h with upcanyon flow and 78 h with downcanyon flow. When the wetter hours were considered, upcanyon flow existed for 125 h, and downcanyon flow for 39 h. This suggests a higher likelihood of valley-released AgI being transported to cloud levels during wetter episodes.

6. RELATIONSHIPS BETWEEN SLW AND OTHER PARAMETERS

The 333 h with SLW values of 0.01 mm or greater were used to calculate the amount of the SLW variance explained by various other parameters. A number of curve-fitting routines were attempted, but none explained more variance than simple linear least-squares regression. No single parameter was highly associated with SLW amounts; however, some definite trends and limits did exist.

Table 7 shows the percent of SLW variance explained by simple linear regression with each of several variables. As previously discussed, Fig. 1 showed a strong association of higher SLW values with southwesterly and westerly winds. However, the relationship is not well expressed by a simple linear regression equation. The variance explained by the absolute departure of the wind direction from 240° (near the SLW highest values) is only 9 pct. The highest amounts of SLW variance were explained by wind speed (27 pct) and dewpoint temperature (24 pct). Other relationships were quite weak.

Figure 3 plots SLW amounts for all 333 h with detectable SLW against wind speed. As discussed by Huggins et al. (1992), radiometer site winds were markedly slower than free atmosphere winds near the same altitude. (However, they showed that the radiometer wind direction was a reasonable approximation of free atmosphere flow). Figure 3 shows considerable scatter but a general trend; higher SLW amounts

Table 7. - Percent of SLW variance explained by linear least-squares regression with indicated variables. All but precipitation were measured at the 2700 m-radiometer site.

Variable	Percent Variance
Wind direction departure from 240° (absolute value)	9
Wind speed	27
Air temperature	14
Dewpoint temperature	24
Temperature minus dewpoint	1
Average precipitation	12

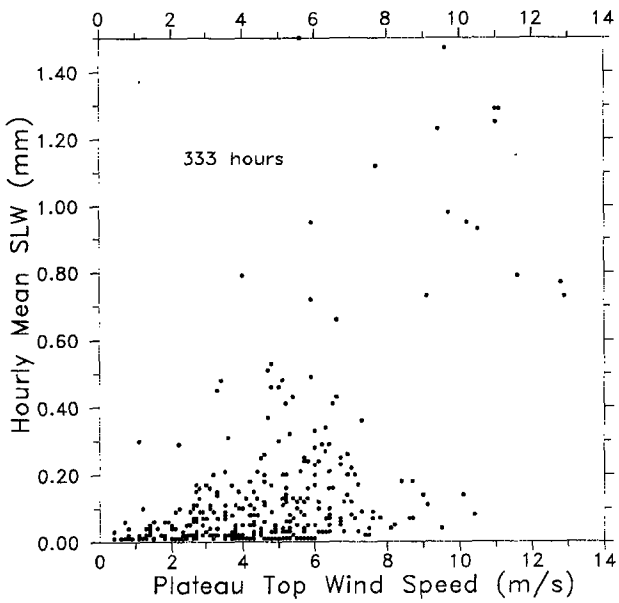

Fig. 3. Plot of hourly mean SLW amounts vs wind speed at the 2700-m microwave radiometer site for hours with detectable SLW.

tended to be associated with higher wind speeds. It might be expected that stronger winds would result in higher forced ascent rates up the windward slopes of the Plateau, resulting in greater liquid condensate production (more SLW). Although 35 pct of the 164 wetter SLW hours had wind speeds in excess of 6 m s^{-1}, only 9 pct of the drier 169 h had wind speeds that strong.

Table 7 shows little linear relationship between SLW and air temperature. However, only 2 pct of the 164 wetter SLW hours had temperatures less than -7 °C, whereas 37 pct of the 169 drier SLW hours were that cold. No hour with an average SLW amount exceeding 0.20 mm was colder than -5 °C on the Plateau top.

7. RELATIONSHIPS BETWEEN PRECIPITATION AND OTHER PARAMETERS

The distribution of the 179 h with measurable precipitation is given vs wind direction in Table 8. Again, a strong dependence between frequency of precipitation and wind direction is evident. The 90° sector between 210-299° contains 80 pct of all hours with precipitation and 88 pct of the total precipitation. Expanding the sector to 120° by adding the 300-329° range accounts for 92 pct of all precipitation hours and 94 pct of the total precipitation. Little precipitation fell on the Plateau during the 20-day study period unless the Plateau-top wind had a westerly component, orthogonal to the north-south oriented barrier.

Table 9 is similar to Table 7 but for the 179 h with detectable precipitation. It shows that little variance was explained by linear regression with any of the indicated variables. The dewpoint temperature was the best predictor, explaining 18 pct of the variance in precipitation.

Finally, both ordinary (Pearson product-moment) and tie-adjusted rank (Spearman) correlation coefficients were calculated between precipitation and SLW for the 169 h with both detected. The ordinary coefficient was 0.23, and the rank coefficient was 0.40. The latter is more appropriate because the highly skewed distributions of both precipitation and SLW violate the assumption of a normal distribution. Although a relationship exists, significant at the 1-pct level, the association between precipitation and SLW is weak.

The weak but significant relationship between SLW and precipitation is positive, with higher precipitation rates tending to be associated with higher SLW amounts. This relationship, based on hourly data, is similar to that found by Super and Huggins (1993) between SLW flux and precipitation for entire storm episodes. The hourly relationship further discredits the view that winter storm periods tend to be either efficient, with abundant precipitation and little or no SLW, or inefficient, with little precipitation but abundant SLW. Instead, the tendency is for higher precipitation rates to accompany periods with greater SLW. But the SLW was measured above the Plateau-top's windward edge while precipitation was averaged across the entire Plateau top. Therefore, the hourly relationship may simply follow from the natural conversion of SLW into precipitation.

8. MEASUREMENTS OF AgI ICE NUCLEI REACHING THE PLATEAU TOP

8.1 Summary of AgI Observations

As previously noted, an NCAR IN counter was operated at the 2700-m radiometer site during part or all of 12 days that were seeded with 8

Table 8. - Distribution of 179 h with detectable precipitation at one or more of the three gauges on top of the Wasatch Plateau. Average SLW, air temperature, dewpoint temperature and average total precipitation on top of the Plateau are given for indicated wind direction sectors.

Wind Direction (degrees true)	Percent of hours	Ave. SLW (mm)	Ave. temp. (°C)	Ave dewpt. (°C)	Total precip. (inch)
150-179	4	.10	-3.0	-4.3	0.20
180-209	2	.07	-5.4	-6.8	0.07
210-239	26	.29	-1.1	-2.1	1.38
240-269	36	.29	-3.7	-4.3	2.16
270-299	18	.06	-8.5	-8.8	0.61
300-329	12	.04	-8.8	-9.1	0.26
330-359	2	.01	-11.1	-11.8	0.03
000-149	0	N/A	N/A	N/A	0.00

Table 9. - Percent of precipitation variance explained by linear least-squares regression with indicated variables, all measured at the 2700-m radiometer site.

Variable	Percent variance
Wind direction departure from 240° (absolute value)	11
Wind Speed	6
Air temperature	13
Dewpoint temperature	18
Temperature minus dewpoint	2
Average SLW	7

AgI generators located along the valley floor west of the Plateau. The generators were sited along a 38 km north-south distance, and each released about 8 g h^{-1} AgI (Griffith et al. 1992).

In order to take a "first look" at the targeting of valley-released AgI, a computer file was developed which contained hourly mean values of vertically integrated SLW and AgI concentration. Observations were included in the hourly summary file only if the 8 valley AgI generators had been on for 2 h or more to allow for transport time to the Plateau top, hourly mean SLW values were 0.01 mm or greater, and the NCAR IN counter log did not indicate any problems with the instrument's operation. Hours with suspect data were rejected. Hours after AgI generators were turned off were not included. These criteria resulted in 144 h of valid data from 7 storm episodes from January 28 through March 11, 1991.

The NCAR IN counter was operated at a cloud chamber temperature near -20 °C with a sampling volume of about 10 L min^{-1}. Raw "counts" were multiplied by a factor of ten to account for known ice crystal losses to the counter's glycol-covered walls and bottom cone (Langer 1973). Resulting IN L^{-1} were estimated at two additional temperatures, -10 and -15 °C, using a 1981 Colorado State University CSL (Cloud Simulation Laboratory) calibration of the Utah operational seeding generators presented by Griffith et al (1991). This procedure assumes that NCAR IN counter observations of AgI concentration at -20 °C are reasonably accurate. Super and Holroyd (1994) present some evidence and refer to other evidence that suggest this may be a reasonable assumption for a properly maintained and operated NCAR IN counter and AgI from a different type of generator. However, the accuracy of NCAR IN counter observations of the particular AgI seeding agent used in the Utah operational program is not known.

The procedure further assumes that CSL observations of the temperature dependence of effective AgI IN are reasonably accurate for the Utah operational AgI seeding agent in winter orographic cloud. The validity of this assumption is not known.

It would be desirable to obtain a new AgI generator calibration because of improvements in the simulation laboratory over the years. But even with a new calibration, there would be the concern about how representative any laboratory test is for AgI nucleation in orographic clouds. These uncertainties should be borne in mind in the discussion to follow, and conclusions to be drawn should be considered tentative. However, placing winter orographic cloud seeding on a firmer scientific footing requires use of the best measurements and knowledge at hand, even when they are known to have limitations.

The 1981 NAWC (North American Weather Consultants) AgI generator effectiveness values (ice crystals per gram of AgI) at -10 and -15 °C were approximately 1 and 25 pct of those at -20 °C for natural tunnel draft conditions. These values will be used because winds near the valley generators were light during most 1991 storms. (Percentage values were similar for maximum tunnel flow conditions). The stated percentage values were used to develop Figs. 4 and 5 which summarize estimated AgI IN concentrations at temperatures more typical of the SLW zone top than the NCAR IN counter's -20 °C.

Figure 4 shows IN L^{-1} at -10 °C estimated from the NCAR IN counter observations for the

available 145 h. The top panel is for the drier 59 h between 0.01 and 0.06 mm, while the lower panel is for the wetter 85 h between 0.07 and 1.5 mm. It is seen that for a temperature of -10 °C about half of the wetter hours had less than 2 IN L^{-1} while 73 pct of the drier hours were in that range. The tendency for wetter hours to have somewhat higher IN concentrations is presumed to be caused by stronger dynamics (higher wind speeds up the Plateau's windward slopes) and more frequent embedded convection. Both processes can enhance the vertical transport of valley-released AgI to Plateau-top levels.

Figure 5 shows that about half the wetter hours had estimated concentrations less than 50 IN L^{-1} at a temperature of -15 °C. The distributions are more skewed than indicated by Figs. 4 and 5. For -10 °C half the hours in the 0-2 IN L^{-1} range were below 0.3 IN L^{-1} in each panel of Fig. 4. The corresponding value is 7.5 IN L^{-1} for -15 °C shown in Fig. 5. None of the drier hours exceeded 10 IN L^{-1} in Fig. 4 (250 IN L^{-1} in Fig. 5) and only 6 pct of the wetter hours were between 10-20 IN L^{-1} (250-500 IN L^{-1} in Fig. 5).

8.2 Artificial IN Concentration for Effective Seeding

The appropriate IN concentration for effective cloud seeding has received limited discussion in the scientific literature, perhaps because of the uncertainties involved. There is, of course, no single "correct" IN concentration because cloud conditions and growth processes vary widely. But cloud seeding operators and experimenters must choose AgI release rates and these should be based on physical reasoning. The following discussion attempts to provide an order-of-magnitude estimate of the appropriate AgI IN concentration for effective precipitation enhancement in winter orographic clouds in the intermountain West.

Observations of natural precipitation reveal highly skewed distributions with most ice particles having limited mass and only a "fortunate" fraction encountering a growth environment which allows them to become relatively large. Ice crystals nucleated by AgI might be expected to result in similar skewed distributions under most circumstances. Even when heavy riming produces graupel (snow pellets), masses are typically 0.1-0.2 mg with 150 cm s^{-1} fall speeds (Locatelli and Hobbs 1974).

For the sake of illustration, let it be assumed that 10 pct of effective AgI IN produce graupel of mass 0.15 mg and 150 cm s^{-1} fall speed. Because contact nucleation proceeds slowly, and the IPC (ice particle concentration) during most graupel showers is low, we will assume that the remaining AgI IN produces relatively small crystals or does not nucleate ice. Then for 10 AgI IN L^{-1} the resulting snowfall rate is approximated by one graupel particle L^{-1}. The liter volume can be imagined to be a vertical cylinder of 150 cm height and 6.67 cm^2 cross-sectional area with one particle falling through the cylinder each second. The resulting snowfall rate is 0.15 mg per 6.67 cm^2 per second,

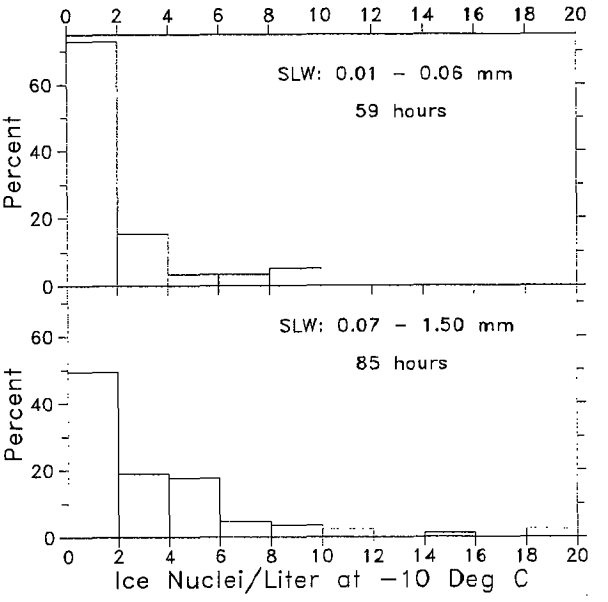

Fig. 4. Distribution of ice nuclei per liter, effective at -10 °C, based on NCAR counter measurements at the 2700-m microwave radiometer site. The upper panel is for 59 h with SLW between 0.01 - 0.06 mm while the lower panel is for 85 h with SLW between 0.07 - 1.50 mm.

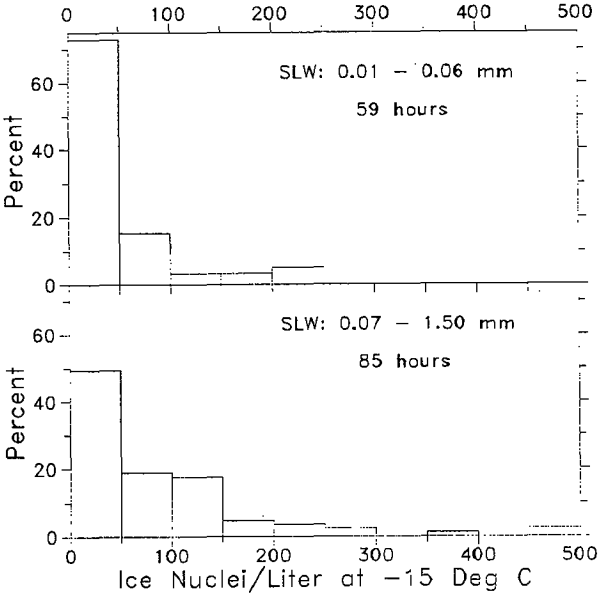

Fig. 5. Distribution of ice nuclei per liter, effective at -15 °C, based on NCAR counter measurements at the 2700-m microwave radiometer site. The upper panel is for 59 h with SLW between 0.01 - 0.06 mm, while the lower panel is for 85 h with SLW between 0.07 - 1.50 mm.

equivalent to 0.8 mm h^{-1} (0.03 in. h^{-1}). Table 1 shows that 73 pct of the observed Plateau-top precipitation was at this rate or less, which contributed about one-third of the total precipitation. Therefore, this rate can be considered typical. However, early 1991 observations suggested that most Plateau-top precipitation does not result from graupel but rather from snowflakes with riming ranging from none to moderate.

Fukuta et al. (1988) presented average ice particle masses observed during winter storms in the Tushar Mountains of southern Utah. These were calculated from the mass precipitation rate and the photographically-determined number flux. Both single crystals and aggregates were counted in determining the number flux. Mass calculations were presented for 18 time segments, each several hours in length. Average masses for these segments ranged between about 0.02-0.30 mg. The median of all averages was about 0.05 mg which should represent a "typical" snowflake. However, since many of the snowflakes were aggregates of individual crystals, typical crystal mass must be significantly less. A typical value for individual crystals appears to be less than 0.02 mg from the Tushar Mountain observations and other investigations cited by Super and Huggins (1992). Seeded ice crystals might be anticipated to have less average mass than naturally-nucleated crystals under most conditions because the latter often have longer growth times.

Using an average ice crystal mass of 0.02 mg, a fall velocity of 75 cm s^{-1} and an effective AgI IN concentration of 10 L^{-1} results in a precipitation rate of 0.5 mm h^{-1} (0.02 in. h^{-1}). This example optimistically assumes that each potential AgI IN actually nucleated an ice crystal.

Both the calculations based on graupel and those based on typical individual crystals result in relatively low precipitation rates of 0.5 to 0.8 mm h^{-1} (0.02 to 0.03 in. h^{-1}). It can be argued that seeding should produce at least 10 ice crystals L^{-1} in order to result in noticeable precipitation increases. For example, if seeding produced only 1 ice particle L^{-1}, the seeding would need to be effective for a large number of hours each winter to significantly affect the seasonal snowfall. At 1 seeded ice crystal L^{-1}, the precipitation rate corresponding to the above examples would be about 0.065 mm h^{-1} (0.0026 in. h^{-1}). It would take almost 1000 h of such seeding to provide a 10 pct increase in the normal Wasatch Plateau April 1 snowpack water equivalent. But the operational program usually seeds no more than a few hundred hours per winter and it is unlikely that seeding is effective for more than some fraction of those hours. Therefore, a precipitation rate corresponding to 1 ice crystal L^{-1} in the above example would provide limited additional snowpack.

Further evidence that 10 IN L^{-1} generally may be a marginal rate for effective seeding exists from observations within seeded clouds. Super and Heimbach (1988) presented measurements from aircraft ice particle imaging probes indicating mean seeded IPCs near 10 L^{-1} over the Bridger Range of Montana (see their Tables 1 and 2). Natural IPCs were 1 L^{-1} or less. Calculated precipitation rates at aircraft levels were less than 0.1 mm h^{-1} (no ground measurements were available). Super and Boe (1988) presented similar observations of 5-20 L^{-1} IPC within seeded cloud over the Grand Mesa, Colorado, where natural IPCs were 0.2-2.6 L^{-1} (see their Table 2). The mean estimated precipitation rates at aircraft levels were somewhat higher over the Grand Mesa, between 0.1-0.4 mm h^{-1}. Ground precipitation observations were available which showed mean precipitation rates similar to aircraft level estimates, and peak precipitation rates of about 1 mm h^{-1}. These limited examples suggest that IPCs of about 10 L^{-1} usually corresponded to less than 0.25 mm h^{-1} (0.01 in.h^{-1}) precipitation production for the sampled conditions. Table 1 shows that such low rates accounted for little of the total precipitation. Therefore, it can be argued that effective seeding should produce at least 10 L^{-1} ice crystals in similar conditions.

While seeding-enhanced IPCs were evident over both the Bridger Range and Grand Mesa, associated reductions in cloud liquid water were not discernible. The lack of a clear reduction in liquid water was probably partially caused by natural spatial and temporal variability, but might be evidence that seeding-caused IPCs were lower than optimum for precipitation enhancement.

If at least 10 IN L^{-1} are required for winter orographic cloud seeding, Figs. 4 and 5 show that the temperature of the SLW zone reached by AgI is crucial. It appears unlikely that valley seeding would often be effective unless the AgI was transported to SLW cloud at temperatures lower than -10 °C. Moreover, it should be recalled that Figs. 4 and 5 are based on Plateau-top IN observations. Aircraft measurements made near AgI plume tops, usually within 1000 m of the Plateau top, revealed significantly lower IN concentrations. Therefore, Figs. 4 and 5 may markedly overestimate AgI IN concentrations when their indicated temperatures (-10 and -15 °C) are near aircraft sampling altitudes. Aircraft-observed plume top temperatures were usually higher than -15 °C as discussed further in Sec 9.

8.3 Representativeness of Periods with AgI Ice Nuclei Measurements

The 144 h of AgI IN measurements discussed in this section may be atypical of hours with SLW present. Over 100 h were from a series of storms, observed to have frequent embedded convection, which passed the Plateau between February 28 and March 11. The 144 h subsample was relatively wet, with 59 pct of its hours in the wetter (0.07 mm and above) SLW category as compared to 50 pct of the total 333 h sample in the wetter category. Only 12 pct of the wetter hours had downcanyon flow as compared to 24 pct for the 333 h sample discussed in Sec. 5. Twenty-two pct of the drier hours had downcanyon flow in the 144 h subsample as compared to 46 pct of the 333 h sample. These values suggest that Figs. 4 and 5 may be somewhat optimistic of

winter storms in general. That is, the frequency with which valley-released AgI reaches SLW cloud levels cold enough to nucleate ice crystals may be even less than suggested in Secs. 8.1 and 8.2.

9. IMPLICATIONS FOR CLOUD SEEDING

As previously discussed, precipitation-producing potential was limited for the drier half of all hours with observed SLW. Nevertheless, it was shown that the seeding potential of such hours should not be ignored because even minor precipitation increases become important when accumulated over many hours.

Table 5 shows the most frequent and wettest SLW hours were concentrated between 210-270°. These hours also had the highest average wind speeds. All else being equal, these hours should have the most seeding potential. However, their average temperature at 2700 m on top of the Plateau was a relatively warm -1.9 °C, which makes successful AgI seeding a challenge.

Ongoing analysis of 1991 AgI and SF_6 plume measurements over the Plateau is revealing that the seeding material was usually found only at the lowest aircraft sampling altitudes, in the 3170 to 3750 m (10,400 to 12,300 ft) range. Moreover, the highest concentrations of both AgI and SF_6 were found at the lower, warmer end of this altitude range. Often, no AgI or SF_6 was found as high as 3750 m, and sometimes not at 3170 m. The finding that ground-released seeding plumes were concentrated in a layer less than 1 km above the terrain is in agreement with earlier investigations over other barriers in the intermountain West (e.g., Holroyd et al. 1988; Super et al. 1989).

With typical in-cloud temperature lapse rates, the average 2700-m temperature of -1.9 °C for the wetter SLW hours corresponds to temperatures of about -5 °C at 3170 m and -9 °C at 3750 m. Figure 2 shows few hours colder than -7 °C at 2700 m had much SLW. Corresponding 3170 m and 3750 m temperatures would be about -10 °C and -14 °C, respectively. These values are in agreement with the 12 in-cloud aircraft sampling missions flown during the 1991 field program. Their average 3750-m temperature was -11.3 °C and only 2 missions were colder than -15 °C at the altitude. Similar warm temperatures for the SLW zone were reported by Sassen and Zhao (1993) for the Tushar Mountains of southern Utah.

Figure 4 suggests that AgI concentrations measured on top the Plateau were insufficient for effective seeding (assumed to require 10 IN L^{-1}) unless the AgI reached SLW colder than about -12 °C. But AgI IN concentrations measured at aircraft levels, where such temperatures were found, were markedly below those measured on the Plateau top. The evidence suggests that the operational seeding program may be effective in only a fraction of the cases with seeding potential.

The evidence presented suggests that the Utah operational seeding program cannot be expected to significantly increase precipitation during warmer storm periods. However, in addition to concerns already raised about the NAWC AgI generator calibration and NCAR IN counter measurements, two caveats should be attached to this tentative conclusion. It is possible that AgI is more effective in creating ice crystals at relatively warm temperatures in mountain orographic clouds than in cloud simulation laboratory clouds. It is possible that AgI-nucleated ice crystals sometimes are involved in one or more significant ice multiplication processes that increase precipitation production.

The effective IN concentration estimates presented in this paper may be improved by obtaining a new CSL calibration of the Utah operational seeding generator, and by further comparing an NCAR IN counter with the CSL. In view of the modest costs involved, this laboratory work should be accomplished, and the calculations herein repeated with the newer data. However, the best (although difficult and costly) approach is to obtain more observations of seeding-caused IPCs from winter orographic clouds over typical ranges of temperatures and liquid water contents. It is important that seeding-caused changes in the cloud microphysics be documented to insure that such changes are significant, at least under favorable conditions.

Aircraft and Plateau-top observations planned for the early 1994 Utah field campaign will attempt to document seeding-caused IPCs in orographic clouds. Moreover, attempts will be made to follow seeding-caused crystals to the surface to document precipitation rates caused by seeding. Experience has shown that only a limited number of successful physical "direct detection" experiments should be expected from a 2-mo field effort. But the importance of such physical demonstrations cannot be overstated. The physical basis for winter orographic cloud seeding needs to be significantly enhanced for the field to gain credibility and for the technology to be improved.

10. CONCLUSIONS AND RECOMMENDATIONS

The 1991 data set is encouraging in that many hours had abundant SLW over the west edge of the Plateau top. A large fraction of the wetter hours had no detectable precipitation, suggesting significant seeding potential may exist if ice crystals can be produced in the SLW cloud. The average SLW amount during the wetter hours with precipitation was even higher than during the wetter hours with no precipitation, again suggesting seeding potential.

Huggins et al. (1992) presented estimates of SLW flux per storm episode for the 1991 field season. For the 20 days discussed herein, the estimate of total SLW flux exceeded 2100 Mg per meter of crestline. If that amount of water was converted to precipitation of uniform intensity over the width of the Plateau (about 10 km), the average precipitation would be 8.3 in., almost twice the observed amount. This calculation suggests that a substantial amount of excess SLW was transported over the Plateau as has been found over other mountain barriers in the

intermountain West (e.g., Super and Huggins 1993). The portion of excess SLW that cloud seeding can convert to precipitation has yet to be demonstrated. However, the "raw material" needed for seeding to be effective certainly exists in relative abundance. The availability of abundant SLW has been assumed for decades but has been verified only in the past several years.

The 1991 data set also raises questions about the effectiveness of the Utah operational seeding program. Physical reasoning was presented that suggested seeding rates may be too low, at least for warmer storms. Admittedly, the estimates of effective IN may be flawed by instrumentation limitations and possible unrepresentativeness of CSL generator calibrations for winter orographic clouds. However, in the absence of better information, the observations and calculations presented in this paper indicate there is reason to be concerned. Production of adequate concentrations of seeded ice particles is basic to successful seeding. This topic deserves further investigation in the Utah operational program in particular, and in seeding programs in general.

The main problem for the Utah operational seeding program appears to be the relatively warm SLW temperatures combined with the strong temperature dependence of AgI as an effective IN. This problem could be partially remedied by increasing the source strength of potential IN using improved seeding generators and solutions and higher AgI output rates. However, the SLW is probably too warm for effective seeding with any practical AgI solution and seeding rate some of the time. Even transporting the AgI to higher, colder altitudes by aircraft seeding would frequently be ineffective because the AgI would then be above the SLW needed to nucleate ice crystals.

This is not to suggest that more effective AgI solutions and higher output generators should not be employed. Anything done to increase the output of effective IN should help seeding effectiveness. However, practical limits exist regarding what can be done with AgI. A large fraction of the winter storms, tending to be those with highest SLW amounts, likely cannot be effectively seeded with present AgI solutions because the SLW is simply too warm.

The problem of seeding warm SLW with AgI is not unique to Utah. The statistical analysis of Super and Heimbach (1983) strongly suggested that the warmer, wetter half of Montana winter orographic storms did not respond to AgI seeding, but the colder, drier storms (< -9 ° at 2600 m) clouds did respond. The State of California has been developing a propane seeding technology because the warm SLW problem is severe there (Reynolds, 1991). Propane seeding can create high concentrations of ice crystals at temperatures colder than 0 °C. Remote-controlled propane dispensers are much more economical than remote-controlled AgI generators, and are more reliable because they are much simpler devices. However, they must be located in or very near cloud to be effective.

It is recommended that the State of Utah pursue a number of approaches aimed at increasing the effectiveness of the operational seeding program. High output generators and more effective AgI solutions should be considered. Higher altitude release sites would increase the frequency of targeting SLW clouds. The possibility of high altitude releases from mountains upwind from the target areas deserves further exploration. Ongoing analysis suggests that AgI releases above canyon mouths may be more effective than AgI releases from valley floor locations. Finally, propane seeding should receive serious attention because even warm storms can be seeded as long as the propane dispensers are located at high altitudes within the orographic cloud.

The 1991 field program measurements have confirmed for the Wasatch Plateau of central Utah some of the earlier findings from the Tushar Mountains of southern Utah. Namely, abundant SLW is available during phases of many winter orographic storms which should provide frequent seedable opportunities. Most of the SLW is within 1 km of the mountain crestlines at relatively high temperatures. The challenge is to develop the means to routinely target the SLW zone with adequate concentrations of artificially nucleated ice crystals which can start the precipitation formation processes in naturally inefficient clouds.

Acknowledgements. Many people contributed to the success of the 1991 field program on the Plateau. These include Clark Ogden and Barry Saunders of the Utah Division of Water Resources; Arlen Huggins of the Desert Research Institute; James Heimbach of the University of North Carolina at Asheville; Glenn Cascino, Roger Hansen, Ed Holroyd, John Lease and Jack McPartland of the Bureau of Reclamation; and Don Griffith, Bill Hauze and George Wilkerson of North American Weather Consultants. Gerhard Langer reconditioned the acoustical ice nucleus counters and checked their field operation.

This research was primarily sponsored by the Atmospheric Modification Program of the National Oceanic and Atmospheric Administration, with assistance from the Bureau of Reclamation.

11. REFERENCES

Fukuta, N., E. Lees, M. Murakami and D.C. Tomten, 1988: Ground Microphysical Observations, 1987. Final Report to Utah Division of Water Resources from the Univ. of Utah, Salt Lake City UT. 89 pp.

Griffith, D.A., J.R. Thompson and D.A. Risch, 1991: A winter cloud seeding program in Utah. *J. Weather Mod.*, **23**, 27-34.

Griffith, D.A., G.W. Wilkerson, W.J. Hauze and D.A. Risch, 1992: Observations of ground released sulfur hexafluoride tracer gas plumes in two Utah winter storms. *J. Weather Mod.*, **24**, 49-65.

Heimbach, J.A., and A.B. Super, 1992: Targeting of AgI in a Utah winter orographic storm. Proc. Irrigation and Drainage Session, ASCE Water Forum '92, Baltimore MD, Aug. 2-6, 553-558.

Hogg, D.C., F.O. Guiraud, J.B. Snider, M.T. Decker and E.R. Westwater, 1983: A steerable dual-channel microwave radiometer for measurements of water vapor and liquid in the troposphere. *J. Climate Appl. Meteor.*, **22**, 789-806.

Holroyd, E.W., J.T. McPartland and A.B. Super, 1988: Observations of silver iodide plumes over the Grand Mesa of Colorado. *J. Appl. Meteor.*, **27**, 1125-1144.

Huggins, A.W., M.A. Wetzel and P.A. Walsh, 1992: Investigations of Winter Storms Over the Wasatch Plateau during the 1991 Utah/NOAA Field Program. Final Report to the Utah Division of Water Resources from the Desert Research Institute, Reno, NV. 198 pp. + appendices.

Langer, G., 1973: Evaluation of NCAR ice nucleus counter. Part I: Basic Operation. *J. Appl. Meteor.*, **12**, 1000-1011.

Locatelli, J.D., and P.V. Hobbs, 1974: Fall speeds and masses of solid precipitation particles. *J. Geophys. Res.*, **79**, 2185-2197.

Redder, C.R., and N. Fukuta, 1989: Empirical equations of ice crystal growth microphysics for modeling and analysis. I. Mass and dimensions. *Atmos. Research*, **24**, 247-272.

Reynolds, D.W., 1991: Design and field testing of a remote ground-based liquid propane dispenser. *J. Weather Mod.*, **23**, 49-53.

Sassen, K., and H. Zhao, 1993: Supercooled liquid water clouds in Utah winter mountain storms: Cloud-seeding implications of a remote-sensing dataset. *J. Appl. Meteor.*, **32**, 1548-1558.

Super, A.B., and B.A. Boe, 1988: Microphysical effects of wintertime cloud seeding with silver iodide over the Rocky Mountains. Part III: Observations over the Grand Mesa, Colorado. *J. Appl. Meteor.*, **27**, 1166-1182.

Super, A.B., and J.A. Heimbach, 1983: Evaluation of the Bridger Range winter cloud seeding experiment using control gages. *J. Climate Appl. Meteor.*, **22**, 1989-2011.

Super, A.B., and J.A. Heimbach, 1988: Microphysical effects of wintertime cloud seeding with silver iodide over the Rocky Mountains. Part II: Observations over the Bridger Range, Montana. *J. Appl. Meteor.*, **27**, 1152-1165.

Super, A.B., and E.W. Holroyd, 1994: Estimation of effective AgI ice nuclei by two methods compared with measured ice particle concentrations in seeded orographic cloud. *J. Weather Mod.*, **26**, --.

Super, A.B., and A.W. Huggins, 1992: Investigations of the targeting of ground-released silver iodide in Utah. Part I: Ground observations of silver-in-snow and ice nuclei. *J. Weather Mod.*, **24**, 19-34.

Super, A.B., and A.W. Huggins, 1993: Relationships between storm total supercooled liquid water flux and precipitation on four mountain barriers. *J. Weather Mod.*, **25**, 82-92.

Super, A.B., E.W. Holroyd and J.T. McPartland, 1989: Winter cloud seeding potential on the Mogollon Rim, Final Report to the Arizona Dept. of Water Resources under IGA-88-6189-000-0051, Bureau of Reclamation R-89-02. 173 pp.

ESTIMATION OF EFFECTIVE AGI ICE NUCLEI BY TWO METHODS COMPARED WITH MEASURED ICE PARTICLE CONCENTRATIONS IN SEEDED OROGRAPHIC CLOUD

Arlin B. Super and Edmond W. Holroyd III
Bureau of Reclamation
Denver CO 80225

Abstract. The Utah/NOAA Atmospheric Modification Program conducted a field program during early 1991, with additional support from the Bureau of Reclamation. Several aircraft missions were flown over central Utah's Wasatch Plateau to monitor plumes of AgI (silver iodide) and tracer gas, and microphysical changes caused by the AgI seeding. This paper discusses one mission during which high-altitude, ground-based AgI release resulted in obvious enhancements in ice particle concentration. Fast-response observations of co-released tracer gas, presumably collocated with the AgI plumes, were used to define seeded zones and crosswind control zones.

Two methods were used to estimate concentrations of AgI ice nuclei effective at cloud temperatures sampled by the aircraft. One method used tracer gas concentration measurements while the other was based on acoustical ice nucleus counter observations. Both methods were partially based on a cloud simulation laboratory calibration of the AgI generator done over two decades ago. The methods were compared with the ice particle concentrations apparently caused by the AgI seeding. Both approaches were found to provide a reasonable first approximation for the particular AgI aerosol produced and the sampled cloud conditions. However, caution should be exercised in applying the estimation approaches to other cloud conditions and AgI aerosols.

1. INTRODUCTION

A fundamental problem in winter orographic AgI (silver iodide) cloud seeding is determination of appropriate AgI aerosol release rates for given conditions. Several variables enter into the release rate determination. These include transport and dispersion of the aerosol, ice-forming mechanisms and resulting rates of AgI nucleation at SLW (supercooled liquid water) temperatures reached by the AgI, growth and fallout rates of AgI-nucleated ice particles, and others. As a practical matter, almost all ground-based AgI seeding operations and experiments have used a single release rate with a fixed network of generators. It has been assumed (but seldom demonstrated) that vertical transport and dispersion would often carry the AgI to sufficiently cold SLW cloud levels so that significant ice crystal nucleation, growth and fallout (snowfall) would result.

Few direct measurements of AgI-nucleated IPC (ice particle concentration) in winter orographic cloud have been published in the literature. Most estimates of AgI release rates have been based on AgI effectiveness (number of ice crystals produced per mass of AgI) values from cloud simulation laboratory tests. The best known facility for calibration of AgI generator effectiveness has been the Colorado State University CSL (Cloud Simulation Laboratory).

Publications from scientists associated with the CSL facility have cautioned against applying CSL results to cloud conditions beyond those produced in their cloud chambers. However, in the absence of direct measurements within seeded clouds, cloud seeding experimenters and operators have used results from the CSL and similar facilities to estimate seeding rates. This paper is an attempt to compare estimates of effective AgI IN (ice nuclei) concentrations with direct measurements of seeding-caused IPCs within orographic clouds.

Field experiments were conducted at the Plateau (Wasatch Plateau) of central Utah during mid-January to mid-March 1991, as part of the Utah/NOAA (National Oceanic and Atmospheric Administration) Atmospheric Modification Program. The main goal of these experiments was to document the transport and dispersion of ground-released AgI used in the Utah operational cloud seeding program.

The Utah operational program uses mostly valley floor AgI generators with a few generators located near canyon mouths. However, the experiment reported here used high-altitude co-releases of AgI and SF_6 (sulfur hexafluoride) tracer gas from a site well up the windward slope of the Plateau. The primary purpose of this experiment was to document changes in IPC caused by the AgI seeding at aircraft sampling levels. However, the measurements also allowed for estimation of effective AgI IN concentrations by two methods. This paper compares these estimation methods with the direct IPC measurements apparently caused by AgI seeding.

The AgI and SF_6 plumes were sampled by a specially instrumented NOAA C-90 KingAir aircraft. It was equipped with a 2D-C particle imaging probe to monitor IPCs calculated by the method of Holroyd (1987). Fast-response gas detector (Benner and Lamb 1985) measurements of SF_6 and NCAR (National Center for Atmospheric Research) acoustical IN counter (Langer 1973) observations of AgI IN were used to estimate IPCs which could result from AgI seeding.

It was hoped that one or both of the estimation methods would be useful in the

absence of IPC observations. For example, 2D-C measurements are not always available to evaluate the effectiveness of AgI seeding in creating ice crystals. Even when 2D-C measurements are available, cloud temperatures may be too warm for AgI to nucleate significant ice. In such cases, it may be useful to estimate the expected IPC had the atmosphere been colder. Past studies which have used SF_6 or NCAR IN counter measurements to estimate the IPC expected to result from AgI seeding of winter orographic clouds include, among others, Holroyd et al. (1988), Griffith et al. (1992), and Heimbach and Super (1992).

2. OPERATIONS

The aircraft sampling mission of 17 February 1991 was suitable for estimating concentrations of effective AgI IN from AgI and SF_6 gas plumes, co-released from the HAS (High Altitude Site) at 2500 m (all altitudes are above mean sea level) on the Plateau's windward slope. Figure 1 shows the HAS and 8 valley seeding sites, 5 precipitation gauges and various other instrumentation used in the 1991 field program.

Co-releases of SF_6 and AgI were made from the HAS during some other cloud-sampling missions. During those missions either the plumes rarely ascended to aircraft altitudes or the SLW cloud was too warm for the AgI to noticeably enhance the IPC.

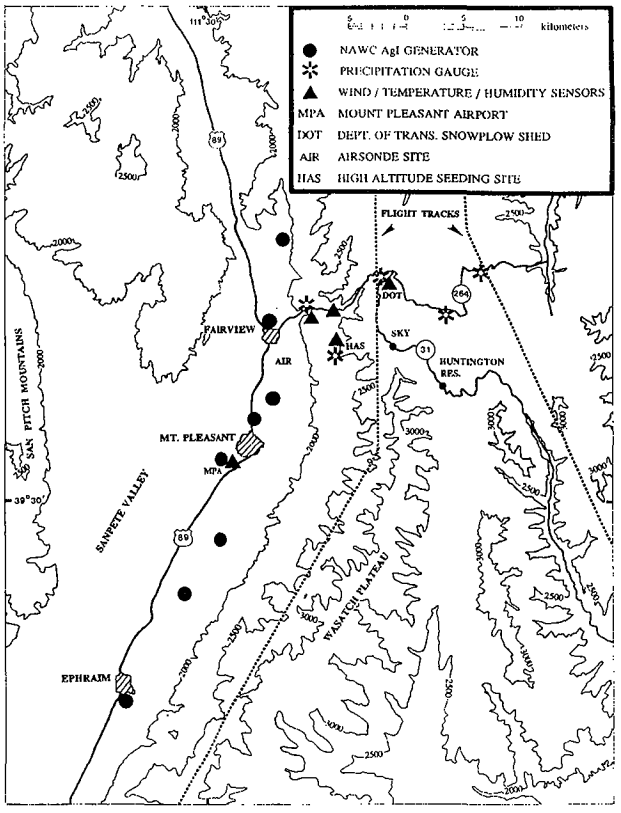

Fig. 1. Map of Wasatch Plateau Experimental Area showing equipment siting for the 1991 field program. Contours are in meters above mean sea level.

The aircraft was flown over two generally north-south (approximately crosswind) tracks above the west (windward) and east (lee) edges of the Plateau's top. These flight tracks are shown on Fig. 1. The Plateau-top elevation increases from north to south. Lowest altitude passes were made by paralleling the terrain elevation, attempting to maintain at least 300 m vertical separation above the highest terrain. These low-level passes were flown under a special waiver from the Federal Aviation Administration since normal minimum vertical separation is 600 m for in-cloud flight. In practice, these low passes were generally about 600 m above the average terrain as measured by a radar altimeter on the aircraft. Higher altitude passes were made at a constant altitude.

All plume penetrations by the aircraft were defined by the maximum extent of the SF_6 plume, ignoring gaps within. Average SF_6 and IN within the plume were used for calculating expected IPC values. On both sides of each plume buffer zones were defined as 12 seconds of flight time (approximately 1 km in length) immediately adjacent to the plume edges. The purpose of the buffer zones was to minimize any contamination by seeded cloud in the event that the AgI and SF_6 plumes were not precisely collocated. Control zones of 24 seconds of flight time were defined immediately beyond the buffer zones. Ice particle concentrations within the SF_6 (and presumably AgI) plume were compared with the natural conditions in the control zones, assuming cloud homogeneity along the flight passes.

Ice particle concentration averages over several plume passages were weighted in a special way. The total count of particles over all plumes was divided by the sum of the sample volumes actually observed. The 2D-C was operated in a limited mode, whereby a maximum of a few buffers of data were recorded each second. Under high concentration conditions this results in a reduction in the volume of air from which particle images were recorded in each second. A simple average of IPC values from each pass can therefore be biased with a high concentration value from a potentially unrepresentative sample. The weighted average errs in the opposite direction, letting a low concentration from a large sample volume dominate the average. Using the weighted IPC average is the more conservative way of assessing possible changes resulting from cloud seeding.

3. AGI GENERATOR OUTPUT

An MSU (Montana State University) generator of the type developed for the Bridger Range Experiment (Super and Heimbach, 1983) was used at the HAS during this experiment. It released 30 g h^{-1} AgI using a 3 percent solution of AgI complexed with NH_4I in acetone. The MSU generator was calibrated at the CSL in 1972 at a liquid water content of 1.5 g m^{-3}. This is admittedly an old calibration and the CSL has been improved over time. A more recent calibration, which might improve the estimation methods to be discussed, is not available at this time.

The MSU AgI generator calibration was done at "natural tunnel draft," equivalent to a wind speed of 2 to 3 m s^{-1} past the burner head (Paul DeMott, personal communication), and under "maximum fan" conditions. Only the former was used in the calculations to be presented because winds at the generator site did not exceed 3 m s^{-1} during the aircraft mission in question. Table 1 lists natural tunnel draft effectiveness value vs cloud temperature from the CSL calibration.

Table 1. - CSL calibration of MSU ground-based AgI generator under natural draft (light wind) conditions.

Temperature (°C)	Ice crystals per gram of AgI
-6	7×10^{10}
-8	2×10^{12}
-10	6×10^{13}
-12	3×10^{14}
-16	6×10^{14}
-20	7×10^{14}

One potentially serious uncertainty in the calculation procedures to be discussed is the representativeness of CSL AgI generator calibrations for winter orographic clouds. Laboratory clouds generally have markedly higher droplet concentrations and liquid water contents, much less turbulence and are much more homogeneous than orographic clouds. Silver iodide nucleation is monitored for an extended period after AgI injection in the CSL. Silver iodide in orographic clouds often has less time to nucleate ice crystals before being transported beyond the SLW zone. Contact nucleation might be expected with the AgI solution used in these experiments, a slow process in laboratory tests (DeMott et al. 1983).

Silver iodide may result in a forced condensation-freezing mechanism immediately after generation within a SLW cloud or ice-saturated atmosphere (Finnegan and Pitter 1988, Chai et al. 1993). During the experiment to be discussed, conditions at the AgI generator sites ranged from in-cloud to about 300 m below cloud base, always at or greater than ice saturation humidities. Therefore forced condensation-freezing was possible, perhaps most of the time. This might have resulted in higher than expected (from the CSL tests) IPCs at the temperature prevailing at the generator altitude. However, that temperature was near -5 °C on 17 February, too warm for significant nucleation by AgI. Moreover, the aircraft sampling temperature was several degrees Celsius colder where AgI nucleation is much more effective. For these reasons, this possible mechanism was unlikely to affect the results to be discussed.

4. NCAR IN COUNTER CHARACTERISTICS

Three similar NCAR IN counters were used in the 1991 Utah field program for detecting the presence of AgI nuclei. One was fixed at the DOT mountain laboratory (see Fig. 1), a second was in a mobile truck, and the third was on the aircraft. All were operated at a cloud chamber temperature near -20 °C. Actual IN counts are multiplied by ten to account for known ice crystal losses (Langer 1973) to the NCAR IN counter's glycol-covered walls and bottom cone of the cloud chamber.

The NCAR IN counter is a semiquantitative instrument based on dated technology. It would be highly desirable to use more quantitative IN counters based on modern technology (e.g., Rogers 1993), but such equipment was not available for the 1991 field program.

Several field comparisons were made between a fixed ground-based NCAR IN counter and a truck-mounted IN counter frequently parked nearby. These comparisons consistently resulted in agreement within a factor of two and usually significantly better. A single field comparison was made between the aircraft unit and the truck-mounted counter parked nearby while both counters were in the plume of an AgI generator operated a few kilometers upwind. The aircraft unit's IN concentrations were consistently a factor of three less than those measured by the truck's IN counter.

Reasons for the discrepancies among the NCAR IN counters are not known but are likely partially caused by differences in outputs of humidifier moisture and atomizer cloud condensation nuclei. NCAR IN counter clouds deliberately have much higher droplet concentrations than orographic clouds to help compensate for the limited time IN are exposed to cloud (1 to 3 min) before being drawn out of the chamber. However, there is no precise control on cloud characteristics which may cause differences between counters. The three units used in the Utah program were overhauled by the system's inventor (G. Langer) just before the field season and were operated by experienced personnel. Nevertheless, the aircraft unit apparently had a lesser response to AgI than the other two IN counters.

In view of the differences between NCAR IN counter clouds and orographic clouds, it is reasonable to question the representativeness of the counter's measurements of IN. Measurements of natural IN at -20 °C were consistently below 1 IN L^{-1} in Utah, which suggests the NCAR IN counter may respond poorly to such nuclei. Good agreement was reported between measurements by an NCAR IN counter and a single observation at the CSL (at -18 °C) for the AgI-NH_4I-acetone seeding agent used in these experiments (Langer and Garvey 1980).

Airborne NCAR IN counter observations of the same type of AgI produced by an MSU generator were used to estimate IN fluxes on several occasions as reported by Super et al. (1975). These estimates were in reasonable agreement with expected generator output from the 1972 CSL calibration for the observed range of surface wind speeds. This observational evidence suggests that a properly maintained and operated NCAR IN counter may provide at least a first approximation estimate of IN from the type of AgI used in Utah operational seeding. However, it

must be admitted that the degree of agreement is not well known between CSL observations and NCAR IN counter measurements of the AgI aerosol used in the 1991 Utah seeding experiments. A thorough test program comparing the two systems would be beneficial to this and similar investigations.

An example of the IPC estimation procedure using NCAR IN counter data for the fifth aircraft pass of 17 February is as follows. The IN counter detected 21 ice crystals after passing through the SF_6 plume. Assuming the AgI plume width was the same as that of the co-released SF_6 plume (32 s transit time) and knowing the IN counter samples 10 L min^{-1} outside air, the NCAR IN counter sample volume is just over 5 L. Using the usual factor of ten correction for known ice crystal losses, 40 IN L^{-1} results as the IN concentration effective at -20 °C, the temperature of the instrument's cloud chamber. The CSL AgI generator calibration curve indicates the effective IN concentration at -14 °C is 61 percent of that at -20 °C. Use of that factor results in an estimate of 24 IN L^{-1} (listed in Table 2 for pass 5) effective at the cloud temperature outside the aircraft.

5. CALCULATIONS FROM SF_6

The SF_6 gas detector was calibrated during each mission by injecting a series of calibration gases of known SF_6 concentration into the detector to establish the system's output voltage vs PPTV (parts per trillion by volume). The mean SF_6 concentration was calculated for each aircraft passage (pass) through the tracer gas plume. The calculation was based on second-by-second observations in PPTV from first to last detection of the SF_6 even if "gaps" existed within the plume where the concentration was less than detectable levels (about 10 PPTV).

The mean SF_6 concentration for each pass and the ideal gas law were used to calculate the gas density at ambient temperature and pressure outside the aircraft. The SF_6 density was multiplied by the ratio of the SF_6 and AgI source strengths to estimate the mean AgI density at the location where the aircraft intercepted the gas plume. Finally, calibrations of AgI generator effectiveness and observed cloud temperature at the aircraft altitude were used to convert AgI density into effective AgI IN L^{-1}.

The following is an example of the IPC estimation procedure using SF_6 gas, again for the fifth aircraft pass of 17 February. The aircraft gas detector observed SF_6 gas for 32 s with a mean value of 57 PPTV. For the ambient temperature of -14.0 °C, pressure of 651 mb, and SF_6 molecular weight of 146.05 g mol^{-1}, the ideal gas law yields an SF_6 density of 2.5×10^{-10} g L^{-1}. The gas release rate was 23.4 kg h^{-1}, while that of AgI was 30 g h^{-1}. The ratio of the release rates multiplied by the gas density yields an estimated AgI density of 32×10^{-14} g L^{-1}. This value was multiplied by the generator effectiveness value for -14.0 °C (4.3×10^{14} ice crystals g^{-1} of AgI), estimated by fitting a curve to all natural tunnel draft data points. An estimate of 138 IN L^{-1} resulted from these calculations, listed in Table 2 along with similar calculations for all other aircraft passes.

6. 17 FEBRUARY 1991 EXPERIMENT

The synoptic setting for this storm is discussed by Huggins et al. (1992). Briefly, cold, moist air was advecting into Utah from the northwest on the back side of a trough. A series of minor short waves passed over the experimental area, one of which may have passed near the end of the mission to be described. Weak convective activity occurred in the post-trough environment. Rawinsondes released from the Mount Pleasant Airport (Fig. 1) between 0900 to 1800 (all times LST) showed convectively unstable layers from about 2000 to 4000 m.

A total of 12 passes was made with the instrumented aircraft over the Plateau between 1135-1405. Within plume temperatures ranged between -13.0 and -15.5 °C. The AgI and SF_6 plumes were released from the HAS beginning at 1100 and continuing until the aircraft departed. The seeding site was in cloud at about -5 °C for part of the experiment but cloud base was about 250 m above the HAS most of the time. Precipitation rates during the experiment were very light, ranging from 0.25 mm h^{-1} (limit of gauge resolution) to undetectable at the 3 Plateau-top gauges shown on Fig. 1.

The 8 valley generators shown on Fig. 1 were also operated during this experiment. They had been run continuously since morning of the previous day. A region of AgI IN was detected with the NCAR IN counter on 5 aircraft passes over the west track, approximately east of the town of Ephraim, believed caused by the valley seeding. No other evidence of valley seeding was found at aircraft levels during this mission. The "Ephraim plume" was far enough south of the HAS plumes so that its IN counter response could be identified and removed from the measurements to be presented.

The HAS plumes did not reach the west flight track until the third aircraft pass, about 70 min after start of release. The plume was first intersected 5.7 km horizontally from the HAS, indicating the average transport speed was only 1.4 m s^{-1}. Average HAS winds were less than 1 m s^{-1} during the first portion of the experiment, while aircraft level winds were about 15 m s^{-1} from 290 degrees.

Passes 5-8 were made over the east flight track, followed by 4 more over the west track, after which the aircraft returned to base. All but the first 2 passes detected both AgI and SF_6 downwind of the HAS as shown in Table 2. All passes were at the lowest possible altitude, maintaining 300 m vertical separation from the highest terrain.

The altitude of encounters with the SF_6 plume ranged from 3.31 to 3.66 km, depending upon where the plume was intercepted along the flight tracks. There was no correlation between altitude and SF_6 concentration or NCAR IN counter

counts per pass so the exact altitude of the plume top is unknown. Ka-band radar tops above the Plateau ranged from about 3.7 to 4.7 km during the aircraft mission, and occasional visual checks of cloud top with the aircraft were near 3.6 km.

Supercooled liquid water was detected on all aircraft passes. Regions with SLW were interspersed among regions without liquid cloud. Mean amounts per pass were typically near 0.05 g m^{-3} along both the west and east flight tracks as measured by a King liquid water probe. Maximum amounts were about 0.5 g m^{-3} on west track passes and 0.3 g m^{-3} on east track passes.

Mean IPCs were calculated for the time periods that the aircraft was within the SF_6 plume, from first to last detection of the gas, and also for the periods within the buffer and control zones. The mean of the north and south control zones is presented in Table 2 for each pass with SF_6 detected. These mean values, ranging from 7-18 ice particles L^{-1}, represent the natural IPC at aircraft sampling altitudes. The difference between the mean control IPC and the IPC within the SF_6 plumes is assumed to represent the concentration of ice particles caused by AgI seeding.

Plume widths, relative to the release site, ranged from 6 to 24° (0.6 to 2.4 km; median 2.0 km) for the west track passes, and from 10 to 17° (2.6 to 4.6 km; median 3.0 km) for the east track passes. The plume's direction of transport from the HAS to the 6 west track passes ranged between 250 to 281° with a median of 273°. The transport direction for the 4 east track passes ranged from 273 to 279°

The low average SF_6 concentrations and low total IN counts on two of the higher plume intersections both suggest that the plume tops were near 3.6 km over the east track. This region, near the Plateau's lee side, was likely in descending air. Plume tops may have been somewhat higher over the west track. Aircraft sampling near the AgI plume top would minimize the effect of seeding-caused ice particles settling from above. Some ice particles sampled by the aircraft probably were nucleated by AgI at higher altitudes, where the seeding agent could be more effective because of lower temperatures. This would result in higher IPCs than estimated from the NCAR IN counter measurements adjusted to sampling altitude temperatures.

Data points for pass 9 have been excluded from the figures to follow as obvious outliers. The SF_6 detector and NCAR IN counter measurements were examined in their most basic available form. The second-by-second SF_6 data (PPTV) were summed for each pass as were the NCAR IN counter counts. The former was divided by the latter and, with the exception of pass 9 which had a ratio of 5, all other ratios ranged between 29 and 137 with a median of 60. The SF_6 plume was only 10 s wide, the second narrowest of Table 2, while the total IN counts were well above those of any other pass. In reference to this pass the aircraft scientist's notes state that, "Looks like the SF_6 had two parts, each one about ten seconds long." Only a single 10 s plume existed in the processed SF_6 data supplied by the contractor responsible for the gas detector, and over 4 min of SF_6 data were missing from this pass. While the reasons are not totally understood, the pass 9 observations are clearly outliers.

7. AGI IN ESTIMATES AND COMPARISONS WITH OBSERVED IPCs

The AgI concentrations for 17 February estimated from the SF_6 and NCAR IN counter observations are plotted on Fig. 2 with pass numbers plotted over the data points. A linear least squares regression line is fitted to the 9 points. The Pearson product-moment correlation coefficient for these data is 0.70, significant at the 5 percent level.

It is perhaps fortuitous that the two types of AgI IN estimates agree as well as they do. Both are based on the same plume widths, determined with the SF_6 detector, and the same CSL AgI generator calibration. Beyond that, the two detection methods are quite different with one based on a quantitative gas detector and the other on the semiquantitative NCAR IN counter which responds to ice crystals formed in a refrigerated cloud chamber maintained near -20°C.

Ratios (SF_6/IN) of the Fig. 2 data points vary from 0.11 to 0.60 with a median ratio of 0.24. This median suggests that overall the AgI IN estimates from the particular NCAR IN counter are low by about a factor of four. Previous discussion indicated the other two NCAR counters used on the project likely would have produced higher counts.

Table 2. - Estimates of effective AgI IN based on SF_6 and NCAR IN counter observations and IPCs measured during the aircraft mission of 17 February 1991.

Pass No.	Flt Trak	In SF_6 (s)	Avg. SF_6 (s)	Altitude (km MSL)	IN counts	Est. IN (L^{-1}) SF_6	Est. IN (L^{-1}) NCAR C.	IPC (L^{-1}) Target	IPC (L^{-1}) Control	IPC (L^{-1}) Diff
3	W	9	112	3.38	13	38	46	56	10	46
4	W	21	91	3.42	14	208	22	102	18	84
5	E	32	57	3.52	21	138	24	28	14	14
6	E	49	4	3.53	7	10	6	26	7	19
7	E	56	20	3.54	19	50	13	20	11	9
8	E	52	8	3.53	7	21	5	32	8	24
9	W	10	26	3.38	48	57	155	124	14	119
10	W	31	35	3.31	32	73	32	61	8	53
11	W	25	51	3.66	27	154	50	112	8	104
12	W	30	42	3.40	33	96	38	47	9	39

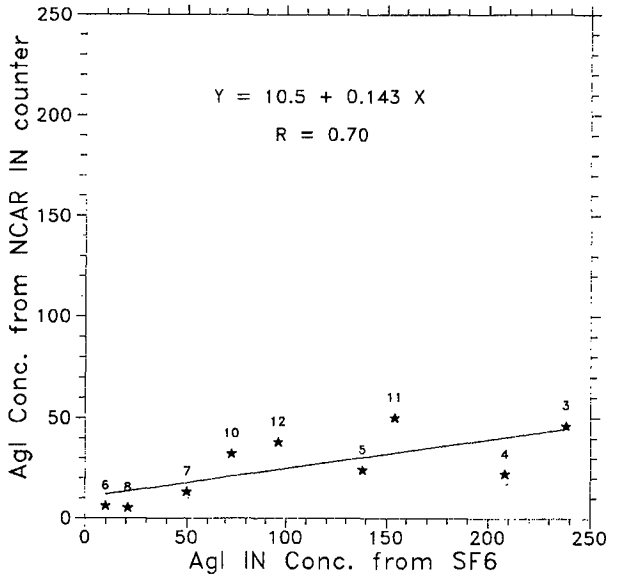

Fig. 2. Concentrations of AgI ice nuclei estimated from SF_6 measurements vs estimates based on NCAR IN measurements for indicated pass numbers on 17 February 1991.

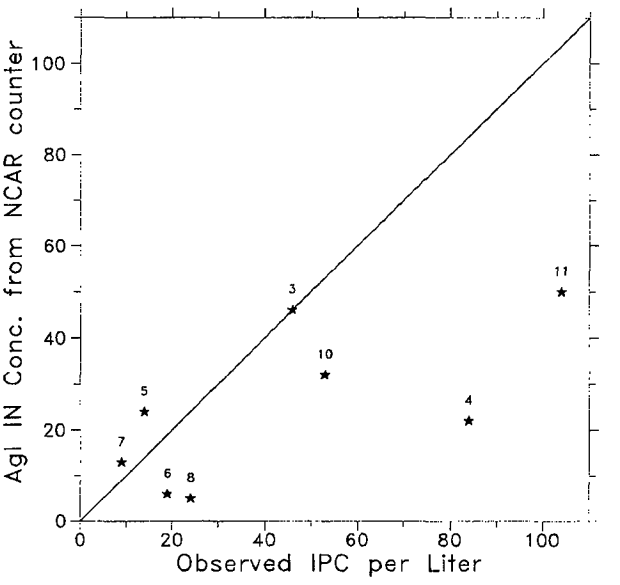

Fig. 4. Concentrations of AgI ice nuclei estimated from NCAR IN counter measurements vs observed ice particle concentrations for indicated pass numbers on 17 February 1991.

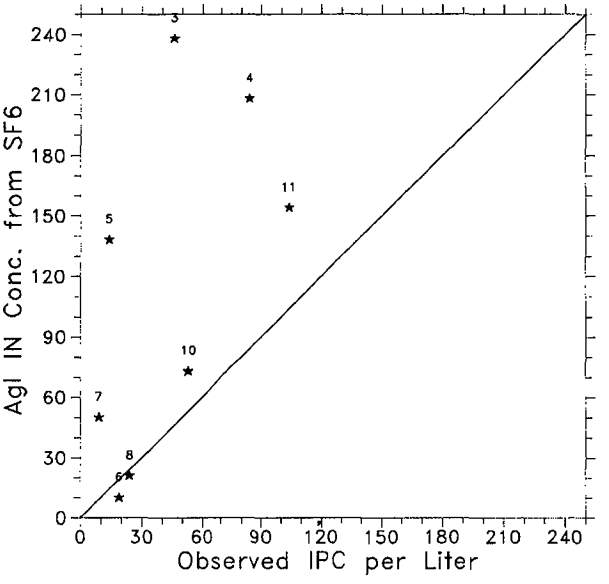

Fig. 3. Concentrations of AgI ice nuclei estimated from SF_6 tracer gas vs observed ice particle concentrations for indicated pass numbers on 17 February 1991.

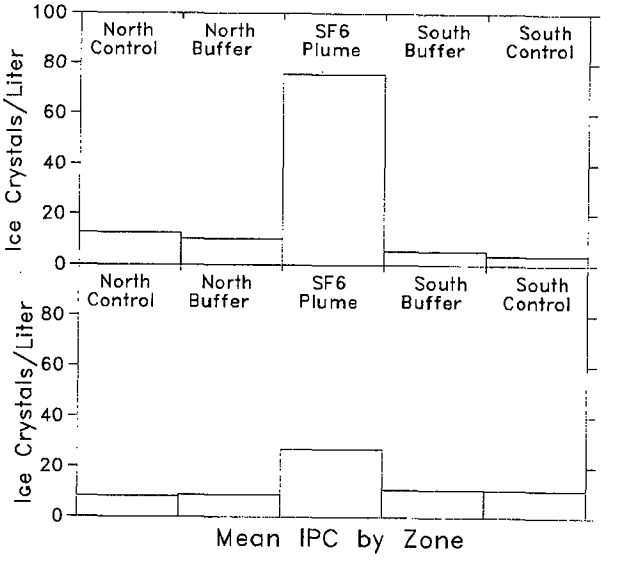

Fig. 5. Ice particle concentration by zone (24 s controls, 12 s buffers, SF_6 plume) for 6 passes over the west flight track (upper panel) and 4 passes over the east track (lower panel) on 17 February 1991.

The estimated AgI IN concentrations from the SF_6 gas detector and NCAR IN counter observations in Table 2 are plotted against the measured IPC (target minus control) in Figs. 3 and 4, respectively.

Figure 3 shows reasonable agreement between the SF_6-based estimates of AgI IN, effective at the sampling temperature, and the observed IPC. The latter tend to be smaller as might be anticipated. While cloud should not constitute a significant sink for SF_6 gas, both scavenging by ice crystals and nucleation can reduce AgI IN concentrations during prolonged passage through cloud. Moreover, not all AgI IN with the potential to nucleate ice at any given temperature necessarily do so (contact nucleation proceeds slowly). These factors should result in fewer ice particles than estimated from the gas measurements as observed in Fig. 3. However, as previously noted, AgI nucleation at colder temperatures above the aircraft can enhance the observed IPC settling past the aircraft's altitude. The data of Fig. 3 suggest this factor was not of major importance during the 17 February experiment.

Figure 4 shows that the estimated IN concentrations from the NCAR IN counter measurements were also in general agreement with observed IPCs. Most observations of IPC were higher than these IN estimates as might be anticipated from Figs. 2 and 3. However, the agreement is better than might be expected when considering the factors mentioned above and various sources of potential error in the estimation method.

The fact that both Figs. 3 and 4 show reasonable agreement suggests that the CSL calibration values may be a good first approximation for AgI nucleation in orographic cloud, at least for the MSU generator at cloud temperatures in the -13 to -20 °C range.

8. MICROPHYSICAL EFFECTS OF AGI SEEDING

Figure 5 shows obvious microphysical effects of the HAS AgI seeding at aircraft levels for 17 February. The bar graph shows weighted average values of IPC within the SF_6 plumes and in the crosswind buffer and control zones. The upper panel shows the averages for the 6 west track passes and the lower panel shows the 4 east track passes.

The IPC enhancement due to AgI seeding is several-fold over the west track's natural IPC, amounting to about 67 L^{-1}. The east track increase is about three-fold, near 17 L^{-1}. It is postulated that the reduction in seeded IPC values over the east track is partially due to the growth and fallout of seeded ice particles below aircraft sampling altitudes.

9. SUMMARY AND CONCLUSIONS

A specially-instrumented aircraft was used to monitor AgI and SF_6 plumes co-released from a high-altitude site on the Wasatch Plateau of central Utah during early 1991. An NCAR IN counter measured AgI while a fast-response detector measured the SF_6 tracer gas. A 2D-C particle imaging probe monitored the IPC within and crosswind of the AgI/SF_6 plumes. Other sensors observed cloud temperature, liquid water content, aircraft position and other variables.

Obvious increases in IPC were associated with the SF_6 plume on the 17 February aircraft mission. Observations from this mission were used to estimate concentrations of AgI IN effective at the sampling temperatures. These estimates were compared with measurements of the IPC enhancement within the SF_6 (and presumably collocated AgI) plume. The IPC enhancement was considered to be the difference between in-plume IPCs and the natural IPCs in crosswind control zones.

Two methods were used to estimate effective AgI IN concentrations. One method was based on SF_6 gas concentration measurements and the other on NCAR IN observations. Both methods relied on cloud simulation laboratory calibrations to establish the source strength and temperature dependence of generated AgI IN. The representativeness of these calibrations for winter orographic clouds is open to question. Nevertheless, in the absence of IPC measurements, cloud simulation AgI generator calibrations have been used in designing several seeding experiments and operational programs.

The ratios of AgI IN estimates by the two methods indicated that the more quantitative SF_6 observations provided on average, about 4-5 times higher values than the NCAR IN counter measurements. The differences in AgI IN estimates may be partially due to AgI losses by nucleation and scavenging and partially to instrumentation limitations. Cloud characteristics and residence times are quite different between winter orographic clouds and NCAR IN counter (and CSL) cloud chambers. The NCAR IN counter uses a dense cloud in an attempt to compensate for the short residence time of IN.

The SF_6 gas measurement method provided first-approximation estimates of measured IPCs with all but one of the estimates within a factor of six. Most estimates were higher than observed IPCs. First-approximation estimates were also provided by the NCAR IN counter method, although values were lower than provided by the SF_6-based method.

The single experiment reported suggests that seeding-caused IPCs can be estimated by tracer gas or NCAR IN counter observations to within about one order of magnitude for the particular AgI generator and aerosol used, and the sampled cloud conditions. While this result is encouraging, further observations would be needed to test whether similar results can be obtained with other AgI generators, AgI solutions and cloud conditions. In view of differences between orographic and simulated clouds, and of known instrumentation limitations, the apparent good agreement from the single experiment may be somewhat fortuitous.

Because of the uncertainties involved in AgI IN estimation, and in ice nucleation processes, it is clearly preferred to directly measure seeding-caused IPCs within winter orographic clouds. More direct IPC measurements must be made if the field of winter orographic cloud seeding is to advance in scientific understanding and credibility. However, such observations are difficult and expensive to obtain, and may be impractical for many programs. Further testing of indirect methods may provide an alternative approach to direct observation of IPCs. It is recommended that any further tests of indirect methods use a current AgI generator calibration from the CSL or similar facility. Use of an improved IN counter, based on current technology, would also be very desirable.

Acknowledgements. Many individuals significantly contributed to the success of the 1991 Utah field program. These included Clark Ogden and Barry Saunders of the Utah Division of Water Resources; James Heimbach of the University of North Carolina at Asheville (aircraft scientist); Dennis Wellman, Stan Wilkison and Joe Boatman of NOAA's Air Quality Group who provided aircraft data; NOAA pilots Tom Gates, Gregg LaMontagne and Mark Finke; Arlen Huggins of the University of Nevada's Desert Research Institute; and Glenn Cascino, Roger Hansen, John Lease and Jack McPartland of the Bureau of Reclamation. Gerhard Langer reconditioned the NCAR IN counters prior to the field program and checked their operation in the field.

The reviewers are thanked for their many helpful comments which improved this paper.

This research was primarily supported by NOAA's Atmospheric Modification Program with secondary support from the Bureau of Reclamation.

10. REFERENCES

Benner, R.L., and R. Lamb, 1985: A fast response continuous analyzer for halogenated atmospheric tracers. *J. Atmos. Oceanic Tech.*, **2**, 582-589.

Chai, S.K., W.G. Finnegan and R.L. Pitter, 1993: An interpretation of the mechanisms of ice-crystal formation operative in the Lake Almanor cloud-seeding program. *J. Appl. Meteor.*, **32**, 1726-1732.

DeMott, P.J., W.C. Finnegan and L.O. Grant, 1983: An application of chemical kinetic theory and methodology to characterize the ice nucleating properties of aerosols used for weather modification. *J. Climate Appl. Meteor.*, **22**, 1190-1203.

Finnegan, W.G., and R.L. Pitter, 1988: Rapid ice nucleation by acetone-silver iodide generator aerosols. *J. Weather Mod.*, **20**, 51-53.

Griffith, D.A., G.W. Wilkerson, W.J. Hauze and D.A. Risch, 1992: Observations of ground released sulfur hexafluoride tracer gas plumes in two Utah winter storms. *J. Weather Mod.*, **24**, 49-65.

Heimbach, J.A., and A.B. Super, 1992: Targeting of AgI in a Utah winter orographic storm. Proc. Irrigation and Drainage Session, ASCE Water Forum '92, Baltimore, MD, Aug. 2-6, 553-558.

Holroyd, E.W., 1987: Some techniques and uses of 2D-C habit classification software for snow particles. *J. Atmos. Ocean. Tech.*, **4**, 498-511.

Holroyd, E.W., J.T. McPartland and A.B. Super, 1988: Observations of silver iodide plumes over the Grand Mesa of Colorado. *J. Appl. Meteor.*, **27**, 1125-1144.

Huggins, A.W., M.A. Wetzel and P.A. Walsh, 1992: Investigations of winter storms over the Wasatch Plateau during the 1991 Utah/NOAA field program. Final Report to the Utah Division of Water Resources, Desert Research Institute, Reno, NV. 198 pp. + appendices.

Langer, G., 1973: Evaluation of NCAR ice nucleus counter. Part I: Basic operation. *J. Appl. Meteor.*, 12, 1000-1011.

Langer, G., and D. Garvey, 1980: Intercomparison of MEE and NCAR ice nucleus counters and the CSU isothermal chamber. *J. Weather Mod.*, **12**, 24-33.

Rogers, D.C., 1993: Measurements of natural ice nuclei with a continuous flow diffusion chamber. *Atmos. Research*, 29, 209-228.

Super, A.B., and J.A. Heimbach, 1983: Evaluation of the Bridger Range winter cloud seeding experiment using control gages. *J. Climate Appl. Meteor.*, **22**, 1989-2011.

Super, A.B., J.T. McPartland and J.A. Heimbach, 1975: Field observations of the persistence of AgI-NH_4I-acetone ice nuclei in daylight. *J. Appl. Meteor.*, **8**, 1572-1577.

A REVIEW OF HYGROSCOPIC SEEDING EXPERIMENTS TO ENHANCE RAINFALL

Robert R. Czys
Atmospheric Sciences Division
Illinois State Water Survey
Champaign, Illinois 61820

and

Roelof Bruintjes
National Center for Atmospheric Research
P.O. Box 3000
Boulder, Colorado 80307

Abstract. Field experiments and computer modeling studies of the possibility to promote the coalescence process by hygroscopic seeding for rainfall enhancement are reviewed. Most previous experiments have focused on the use of water sprays or common salt particles, but the practical delivery of the massive bulk sources of these products has been a limiting factor. Although most past efforts have not provided convincing scientific evidence of seeding effects, they leave the impression that effects were generally consistent with the hygroscopic seeding hypothesis under investigation (i.e., broadening of the cloud droplet distribution, and triggering of coalescence which possibly alters echo morphology). Rainfall enhancement from hygroscopic seeding remains to be demonstrated. Seeding effects beyond those expected on the coalescence process may also be apparently possible. Effects on the initiation and evolution of ice may have been noted perhaps because of the enhanced presence of supercooled drizzle and rain drops, or because rime-splintering may have been enhanced by the presence of broader distributions of supercooled cloud droplet distributions in ice multiplication zones, or for perhaps both reasons. Indications of "dynamic" effects may have been found which possibly occurred either in conjunction with the latent heat of condensation, or from a more active conversion of supercooled water to ice, or for both reasons. Computer modeling has indicated that seeding at cloud base with appropriately sized cloud condensation nuclei to foster Langmuir-type precipitation growth trajectories may be a desirable seeding strategy, and that seeding does not necessary have to be limited to cold based clouds characterized by a marginal coalescence process. The use of "new" hygroscopic seeding flares at cloud base in deep warmer-based South African clouds has produced very encouraging results from a limited amount of experimentation, and the new seeding flares have apparently overcome earlier problems associated with transporting the seeding materials. Thus, the technique of hygroscopic seeding deserves reexamination.

1. INTRODUCTION

Recent investigations into the possible effects of artificial hygroscopic nuclei to enhance the coalescence process in the multicelled storms that grace the eastern Transvaal of South Africa (Mather 1991) have provided some indication of success. The clouds and the multicelled rain cloud systems of that region are similar in many ways to the convective summertime rain clouds that have been the subject of "dynamic seeding" experimentation in Illinois. For example, the convective rain clouds of the eastern Transvaal and those in Illinois tend to be warm based with similar distributions of cloud base temperatures (Johnson 1982). Clouds from both regions tend to initiate precipitation by the condensation-coalescence process, and both tend to originate ice by the coalescence-freezing mechanism (Braham 1986). The only major difference between the clouds being perhaps mean updraft velocities which is typically about 5 m s^{-1} for Illinois (Czys 1991) compared to 8 to 9 m s^{-1} for those in the eastern Transvaal. The similarity between clouds in both regions would provide broad common base from which to make inferences about seeding effects.

The possible successful result of hygroscopic seeding in the Eastern Transvaal, and its potential application in Illinois was cause for us to look back at previous investigation in order to place the recent work in South Africa into proper perspective. In the course of conducting this review, we uncovered an excellent review paper by Cotton (1982) which was prepared for the World Meteorological Organization (WMO) meeting on Warm Cloud Modification held at Kuala Lumpur, Malaysia in March of 1981. Other reviews on this subject have been made by Dennis (1980), Mason (1971), and Hess (1974). As best as we could determine little as been done with respect to hygroscopic seeding since Cotton's fine review was written. However, we believe that the status of warm cloud modification is cast in a sufficiently different light when the South African results are included to warrant revisiting the subject.

2. DEFINITIONS AND SEEDING TECHNIQUES

Since its inception, the term "hygroscopic seeding" has taken on slightly different meaning depending on the experimental design, type of seeding material used, and the

type of cloud that was the subject of experimentation. However, almost in all instances the ultimate goal has been to enhance rain fall by somehow promoting the coalescence process. As will be discussed, alteration of the coalescence processes may have implications on the origin and evolution of precipitation processes involving ice, and on overall cloud dynamics from the redistribution of energy in the form of latent heat releases associated with condensation as well as freezing. By the term "modification of warm cloud processes", we mean any influence that seeding would have on the coalescence process to enhance the production of rain drops. Seeding may help to initiate coalescence when it would otherwise not, or may help to allow coalescence to initiate earlier than it would naturally. The effects of seeding are not necessarily limited to cloud regions that never grow colder than 0°C, nor should the initial effects on the coalescence process not have implications for how other subsequent microphysical and/or dynamical processes might proceed.

The addition of "appropriately" sized cloud condensation nuclei (CCN) and the direct introduction of artificial rain drop embryos with either sprays of water or dilute saline solutions, are the most common previously used hygroscopic seeding techniques, although poisoning of CCN and stimulation of coalescence by electric fields have, at various times, been considered. In this review, we focus on use of water sprays and hygroscopic aerosol particles. The primary objective of adding "larger" CCN is to prevent the activation of the smaller natural CCN to lower the total concentration of initial cloud droplets, and thus, broaden the initial cloud droplet spectra. This is supposed to transform a cloud with a "continental" cloud droplet spectrum to one having a more "maritime" spectra. Thus, the process by which a cloud would initiate precipitation would either 1) enhance the coalescence process, or 2) shift from a mechanism more dependent on ice processes towards the condensation-coalescence mechanism. The primary objective of introducing artificial rain drop embryos is to short circuit the action of the CCN population in determining the initial character of the cloud droplet population, and thus, jump-start the coalescence process.

3. USE OF WATER DROPLET SPRAYS

The first experiments with clouds using hygroscopic seeding materials were made when condensation-coalescence theory was in its very infancy. In the late 1940's and 1950's there was considerable controversy over the importance of the warm rain process in midlatitude convective clouds, which is exemplified in such works as that of Langmuir (1948), Bowen (1950), and Battan (1953), because certainly every rain drop must originate from an ice crystal (Bergeron 1935, Findeisen 1942). In perhaps what was the first scientific attempt at hygroscopic seeding comes from a South African report (Anon: 1948) that rain was produced three hours after five gallons of calcium chloride solution were released into the tops of cumulus reaching about 18,000 ft. There were two other occasions when releases were made; a radar echo developed on one occasion, and on another there was no measurable effect. Thus, in the absence of establishing a direct cause and effect relationship, these early experiments produced no conclusive evidence for seeding effects.

Theoretical investigations into the coalescence process made by Bowen (1950), and by Ludlam (1951), suggested that it may be more efficient to introduce larger-than-average cloud droplets at cloud base rather than to introduce raindrops into cloud top. In the calculations, the growth of larger cloud droplets were traced during their upward trajectory from cloud base followed by their downward fall toward earth. These calculations indicated that a droplet with radius of 30 μm, transported upward at about 3 m s^{-1} from a cloud base at 20°C, would, after traversing an upward and downward trajectory, return to cloud base with a final size of 1.9 mm (achieving an increase of mass of nearly a factor of 2.5 x 10^5). Similarly, a 20 μm drop would return with a radius of 2.5 mm (nearly a 2 x 10^6 increase in mass). Thus, artificial raindrop embryos introduced at cloud base may have an advantage over those introduced at cloud top because the former experience growth over an upward and downward trajectory rather than just a downward trajectory and smaller cloud droplets (~20 μm) have a larger mass growth factor than larger cloud droplets (~30 μm) because the smaller ones experience a longer growth pathway, assuming of course, that sufficient cloud depth exists.

These concepts were tested in Australia using water drops sprays with median droplet radius of 25 μm and dispersal rates of about 30 gallons per minute (Bowen 1952a, 1952b). In-cloud treatments were made about 1,000 ft above cloud base. Results from these experiments supported findings from the original theoretical work. When the cloud thickness was less than 1.5 km (5,000 ft), treated clouds produced virga in six of seven cases, while nearby untreated clouds did not precipitate. When cloud thickness was greater than 1.5 km, rainfall or hail was observed in three of four cases shortly after seeding, while nearby unseeded clouds produced no rainfall. However, it is not possible to be sure that the results did not happen by chance in this small number of samples.

As part of the Cloud Physics Project sponsored by the United States Weather Bureau after World War II, Coons et al. (1948, 1949) reported on twenty-one cumulus clouds that received water spray treatment near cloud top during summertime operations in Ohio. In these experiments, fifteen clouds received drops at a rate of one gallon per mile and the remainder at a rate fifty times higher. Only one cloud in this study produced rain which reached the ground while seventeen showed a tendency to dissipate. This early experiment demonstrated several drawbacks to cloud top seeding with water sprays: the artificial embryos tended to wash out the cloud droplet population, and precipitate loading acted against vertical cloud growth.

Similar experiments involving much larger quantities of water were pursued as part of the Cloud Physics Project in the early 1950's (Braham et al. 1957). Operations occurred in the central United States and the Caribbean. The experiment was divided roughly into two treatment categories, the first was referred to as the "small valve experiment" and the second was called the "large

valve experiment." Only the large valve experiment produced effects that were detected in radar data. In contrast to the suggestions of Bowen (1950), water releases were made into cloud top because of the weak nature of the updrafts in Caribbean clouds. In the large valve experiment, roughly 450 gallons of water per mile were released (see Fig. 1). From data obtained from a series of drop tests over a spatial array of dye impregnated papers arranged on the runway at Chanute Air Force Base, drop sizes were determined to be between 100 and 1500 μm with an exponential decrease in the number counted with size. The water spray itself did not produce a radar echo. Pairs of clouds were selected for experimentation. Only one in each pair received the water spray treatment. A pre-determined randomization scheme was used to guide the decision to seed or not to seed.

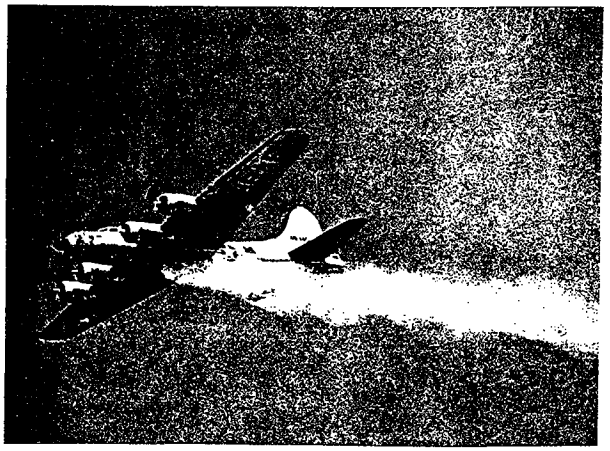

Figure 1. Photograph of the B-17 research airplane that was used to transport 450 gallons (3600 lb.) of water aloft and dumping a water drop spray in the cloud-top seeding that was conducted as part of Project Cloud Catcher (from Braham et al. 1957).

The results from the large valve experiment were much more encouraging than those originally reported in the earlier trials (Coons et al. 1948). Some results from the treatment of cumulus clouds in the Caribbean with the large valve are presented in Table 1. As can be seen in Table 1, there were 17 cases when the treated cloud produced an echo while the untreated cloud of the pair did not. In comparison, there were only 6 cases when the treated cloud of the pair did not produce an echo, while the untreated cloud echoed. The probability that these results occurred by chance was computed to be 0.017 under the null hypothesis that treatment had no effect. However, the results indicate nothing about intensity or total amounts. The data were also used to compute the probability of an echo for the seeded and unseeded cloud pairs in the large and small valve experiments. These probabilities and corresponding 99% confidence intervals are shown in Fig. 2. The computations in Fig. 2 were interpreted to indicate that the large value treatment increased the average probability of an echo from 23 to 48%. The time for the formation of an echo was also computed for these experiments. The computations were made after imposing several limitations on the use of the data including that the clouds were continuously observed, and time and space thresholds related to the characteristics of the radar set. The average time for precipitation initiation (time from treatment to first echo) in the untreated clouds was found to be 11.9 min. This time was computed to be 6.4 and 8.5 min. for the treated clouds in the large and small valve data. Thus, the time required for echo initiation was reduced by about 5 min. in the seeded pairs of the large cloud experiment. This difference was found to be statistically significant at less than the 1% level using a Wilcoxan test. Unfortunately, the sample of water-spray treated clouds in Ohio was too small to base any conclusion on.

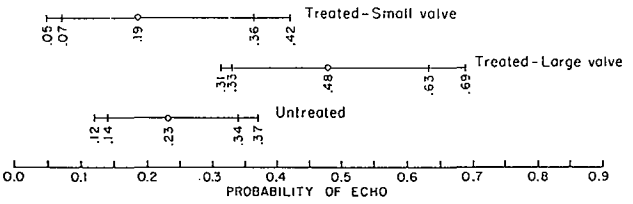

Figure 2. Probability of echo formation determined for untreated clouds, and clouds treated in the large valve and small valve experiments of Project Cloud Catcher (from Braham et al. 1957).

4. USE OF COMMON SALTS

One of the earliest investigations into the use of giant salt nuclei was made in East Africa (Davies et al. 1952) using "bombs" tethered from balloons. Each bomb contained a mixture of gun powder and sodium chloride. The bombs were released from the earth's surface and fused to explode in the length of time it would take for the balloon to carry the bomb to cloud base. When the bomb exploded about 15 g of salt particles, ranging in diameter from 5 to 100 μm, were dispersed. Treatments were delivered on the 38 days. On these days, the rainfall

Table 1. Contingency table for radar echoes from tropical cumuli treated in the large valve experiment (after Braham et al., 1957).

		Treated Cloud of Pair		
		Echo	No Echo	Total
Untreated Cloud of pair	Echo	5	6	11
	No Echo	17	18	35
	Total	22	24	46

downwind of the release was 6 inches greater than on the unseeded days. It was difficult to tell whether the seeding material had any effect because upwind rainfall on seed days was also greater than on treatment days by about 2 to 3 inches. Similar experiments were later repeated except that the seeding was carried out on alternative days over a 90-day period (Sansom et al. 1955). In these experiments 24 of the 33 seeded clouds produced rain such that the downwind rainfall was 2 to 3 inches higher than that on the unseeded days.

Experiments in which salt particles were released from ground based-generators have also been conducted over the Indian subcontinent around Delhi, Jaipor, and Agra (Biswas et al. 1967). In these experiments, hygroscopic particles were released into the boundary layer by either spraying a dilute salt solution into the air, or with a finely ground salt mixture. In the case of liquid sprays, particles in the size range from 7 to 25 μm were released at a rate of 10^9 per second, while estimated particle size for the powder release was 5 μm at a rate of 2×10^{12} per second. The experiment was designed around a four-way blocking scheme of control and target area on both seed and no seed days, and a method of double and single ratios was used to evaluate for seeding effects. Rain gage networks around Delhi, Jaipor, and Agra provided the basic data for analysis.

The experiment was conducted for 8 consecutive seasons beginning in 1960 for Delhi and Agra, and for four seasons beginning in 1960 at Jaipor. Positive seeding results were indicated at Delhi in 7 of the 8 seasons, 5 out of 6 seasons in Agra and 4 of four seasons at Jaipor. Accounting for the fact that the days with frequent or continuous rain were excluded from the experiment, the indicated increase in rainfall was 21%, uncorrected for the fact that seeding occurred for only a small fraction of the time that a 24-hour rainfall total had accumulated. However, because the generators were operated from the ground, there was no certainty that the particles indeed reached cloud base, and if they did, their concentrations were unknown. Thus, it was not possible to be certain that the apparent enhanced rainfall was due to seeding.

Kapoor et al. (1975) reported on effects of seeding on the cloud droplet size distribution for three different regions in India; Poona, Bombay, and Rihand. Operations were conducted during the summer monsoon of 1973. Treatments were delivered at nearly constant altitude of a few hundred feet above cloud base dispersing a mixture of common salt and soapstone in the ratio of 10 to 1 at a rate of up to 10 kg per km of flight path. Cloud droplet distributions were measured by impaction on to magnesium-oxide coated slides.

Cloud droplet data from all three regions showed marked changes in the cloud droplet distribution, consistent with that expected from seeding. Increases in maximum diameter, decreases in total droplet concentrations, increases in liquid water content and increase in median volume diameter were noted for each of the three regions. However, because of the operational procedures it was not possible to be absolutely certain that the observed changes did not happen by chance.

Fournier d'Albe and Aleman (1976) reported on ground-based salt seeding experiments in Mexico. In these experiments, salt was dispersed at a rate of 50 kg/h. The experiment was conducted during the summer and seeding performed during daylight hours when convective activity was at a maximum. The experiment was randomized with 54 days receiving seeding and 22 days being used for control. This experimentation suggested that there was less rainfall on seeded days than on control days. However, the results may have occurred because of exceptionally heavy rainfall on control days, rather than from a true decrease due to seeding.

Differences between the height and temperature of first echoes in salt seeded and unseeded clouds were studied as part of Project Cloud Catcher in the Dakotas (Dennis and Koscielski 1972, and Koscielski and Dennis 1972). A three-way randomization was used in this experiment with treatment being either 1) no seed, 2) AgI seed, 3) salt seed. AgI and salt treatments were not combined on a single day. Salt seeding was accomplished by releasing up to 50 kg of finely ground salt (NaCl) in updraft near cloud base during the first 30 minutes of the treatment. The salt was a 50/50 mixture (by initial bulk mass) that produced particles with mean mass diameter of 25 μm and 150 μm. Particle concentrations within the plume at 0°C were estimated to be one to more than ten per liter. In one exploratory case, Biswas and Dennis (1971, 1972) reported visual evidence that indicated the initiation of a rain shower by salt seeding. However, seeding effects were generally evaluated on the basis of radar data. The experiment produced a total of 22 unseeded cases and 16 salt seeded cases. Results for the salt seeded cases indicated that the average first echo height above cloud base was half that of the no seed cases (5,300 ft compared to 11,000 ft) and that this difference could not be accounted for by natural differences in cloud base heights, cloud base temperature, or maximum updraft velocity. Therefore, it appears that salt seeding in the High Plains may have been responsible for lowering the height of first echoes by initiating coalescence earlier than it would have otherwise.

Heating associated with condensation of water vapor on sodium chloride particles has also been noted. The theoretical amount of heat in humid air for particular values of temperature, pressure and relative humidity has been found to be proportional to the weight of salt added (Woodcock et al. 1963). Woodcock and Spencer (1967) conducted experiments along these lines around Hawaii and found that the salt-laden air was warmer than the ambient air by 0.35°C on average. In their experiments, dry sodium chloride particles, in the size range from 0.5 to 20 μm diameter, were released from an airplane flying about 400 to 500 m above the ocean. Release rates from the 400 kg load were intended to produce airborne salt concentrations of 40 mg per kg of air.

Dynamic responses to salt seeding have also been noted in warm monsoon clouds. Ramanchandra Murty et al. (1975) made visual and in-cloud measurements of six cloud complexes in which a total of 32 cloud seeding traverses were made a few hundred meters above cloud base. The seeding material used was a pulverized mixture

of salt and soap stone mixed in a 10 to 1 ratio with a mode diameter of 10 microns. The seeding rate varied between 10 and 30 kg for every 3 km of flight path, traveling at a mean air speed of 180 kmph.

From this small sample, Ramanchandra Murty et al. (1975) reported that it appeared that deeper clouds tended to show a dynamic response by a gain of cloud top height, and in some cases, a gain in lateral dimensions. On two occasions, when the cloud samples were between 1,000 and 1,500 ft deep, dissipation was observed along with a decrease in horizontal dimension as seeding progressed. One cloud complex approximately 5,000 ft deep was observed to gain 2,000 ft vertically along with a lateral increase in size. Peak liquid water content reportedly increased from 0.5 g m^{-3} to 2.8 g m^{-3} as seeding proceeded. The initial maximum temperature in cloud (16°C) was 2°C colder than the environment, but was observed to increase by about 1°C as seeding proceeded. This cloud group was observed to rain at which time the internal cloud temperature was noted to decrease. A cloud group with initial depth of 4,000 ft was observed to gain 2,000 ft with seeding and also shared similar increases in liquid water content and temperature as did the other 5,000 ft deep complex. Finally, cloud complexes with initial depths of 7,000 and 10,000 ft showed vertical increases in cloud top height of approximately 4,000 ft following seeding both with increases in width and changes of liquid water content from 0.6 to 1.0 g m^{-3} prior to seeding to about 3 g m^{-3} before rain began to fall from these clouds.

Chatterjee et al. (1978) used an X-band 3 cm radar set to evaluate for salt seeding effects on warm maritime cumulus clouds. Their analysis was based on data collected over a six day period in September during which time four isolated cumulus were selected for seeding. For each of the seeded clouds, a neighboring cloud was left unseeded and used as control. They concluded that the seeded clouds lasted longer than the control clouds. The details of the time variation for one of the cloud pairs indicated that the aerial coverage of echo may have initially decreased. However, 12 minutes after, seeding area coverage remains constant and then increases to a maximum about 40 minutes after seeding began. Echo tops which also initially showed a decrease, showed increases shortly after seeding began with two maximum, one 8 minutes, and the other 40 minutes after seeding began. The control cloud in this pair was observed to dissipate 10 minutes after it was selected as a no seed cloud. However, in this small sample, it is not possible to tell whether or not the results occurred by chance.

Parasnis et al. (1982) computed one-dimensional temperature spectra (Corrsin 1951) for one clear air case and for five cloud cases using data primarily collected as part of the salt seeding experiments conducted by Ramanchandra Murty et al. (1975) around Bombay and Puna, India. In this type of analysis, it should be noted that a -5/3 slope is indicative that turbulence is isotropic and that energy input and dissipation are balanced. An increase in the -5/3 slope indicates higher energy dissipation rates. The release of latent heat of condensation generates large wavelengths of spectra while shorter wavelengths represent smaller scale turbulence (Warner 1970). Paresnis et al. (1982) found that the slope of the spectra in salt seeded cases increased with a net energy gain at larger wavelengths (greater than 540 m) and the net loss at shorter wavelengths.

5. COMPUTER SIMULATIONS

Klazura and Todd (1978) developed and used a one-dimensional steady-state condensation-coalescence model to better understand the physical chain of events that occur with hygroscopic seeding. Drop break-up and freezing were simulated in their model. The model was used to trace the growth trajectories of hygroscopically initiated particles. The sizes of the seeds varied from 5 to 400 μm diameter and updraft speeds ranged from 1 to 25 m s^{-1}. Effects on warm- and cold-based clouds were explored. Model results indicated that the relationship between updraft velocity and initial seed diameter must be conducive to the development of raindrops big enough to undergo break-up and set off a Langmuir-type (1948) chain reaction for seeding to be effective. Assuming that sufficient cloud depth exists to allow condensation, coalescence, drop break-up, and freezing to proceed uninterrupted, model results for cloud base temperatures and updraft velocities close to those characteristic of Illinois clouds (5 m s^{-1} and 19.4°C) indicated that smaller "seed" diameters had a growth advantage over larger "seed" diameters because they followed longer (in time and space) growth trajectories; much the same as that originally suggested by the theoretical work of Bowen (1950) and Ludlam (1951). It should be noted that this advantage diminishes for finite cloud depth, and as updraft velocity increases because at high updraft velocities the "seeds" are carried to cloud top, experiencing little growth, and thus remain suspended as part of the cloud's anvil.

The work of Klazura and Todd also produced the following findings:

1. for a given updraft speed, small hygroscopic seeds require a greater cloud depth to grow large enough to fall against the updraft and perhaps experience break-up;
2. a greater cloud depth is required for higher and colder cloud bases for the "seeds" to grow large enough to fall;
3. large hygroscopic seeds will result in drop break-up lower in cloud at any particular updraft speed;
4. stronger updrafts require larger hygroscopic seeds to produce drop break-up and vice versa;
5. vertical depth of the drop break-up regime increases as cloud base temperature increases because longer coalescence growth and later particle freezing combine to expand the drop break-up zone; and
6. hygroscopic seeding was found to produce the greatest water yield from the *warmest* based clouds.

Farley and Chen (1975) used a detailed microphysical model to simulate hygroscopic seeding. In their model, condensate was represented by 52

logarithmically spaced size categories covering a size range from 2 μm to 5 mm radius. Their model simulated the evolution of water drop size distribution as a result of vertical advection, condensation/evaporation, stochastic coalescence, and drop break-up. Seeding was simulated by the introduction of a distribution of raindrop embryos at cloud base.

After making allowances for errors they made in the condensation growth equation and an error in the Raoult effect for the growth of salt particles, model results indicated that raindrop break-up was necessary for cloud seeding to be effective. Because larger drops were introduced at cloud base, they found that rather large (greater than 10 m s^{-1}) updraft velocities and large cloud depths were required for break-up to initiate. When the model was run without break-up, cloud seeding was found to have little effect other than to produce a few raindrops at cloud base. Thus, some sort of raindrop multiplication process must spread throughout the cloud.

Rokicki and Young (1978) used a Lagrangian parcel model to simulate water drop seeding at cloud base. The size of the droplets in the spray was chosen so that the fall speed was not larger than one tenth of the updraft velocity. They simulated deep clouds which eventually carried the condensate aloft where it supercooled. From their model results, they concluded that water spray seeding may have potential use in mid-latitudes as well as in the tropics, and that effects may be potentially larger than can be obtained with AgI seeding without the possibility of overseeding.

Johnson (1980) performed a series of salt seeding simulations that took into consideration that the natural cloud had a broad size distribution of CCN. The particle spectrum included nuclei greater than a few tens of micrometers. Johnson (1980) pointed out that overlooking these potentially important, naturally present, giant nuclei, can make model calculations overly sensitive to salt particle or droplet seeding. Figure 3 shows an example of the type of time-height cross sections that were obtained from Johnson's trajectory model. The shade region indicates the region of the simulated cloud where reflectivities were computed to be in excess of 10 dBZ. The shaded region ends abruptly with a vertical line in each case when the reflectivity, at any level, reached or exceeded 30 dBZ. When this occurred the calculation was terminated. In Fig. 3a, the seeding was delivered at 0.5 km above cloud base, and in Fig. 3b the simulated cloud was seeded at cloud base. The calculation applies to a simulated cloud with base at 5°C, updraft velocity of 4 m s^{-1}, and model runs for salt concentrations of 10^{-2} g m^{-3} and 10^{-4} g m^{-3}. For these rather heavily seeded clouds Fig. 3 clearly suggests that the treatment results in the formation of first echoes slightly lower than the unseeded model run and approximately 5 to 7 minutes sooner than the no seed case. Differences between seeding at cloud base or slightly above are less dramatic, but it does appear that seeding at cloud base results in slightly lower and later echo formation than when seeding at 0.5 km above cloud base. One of the main conclusions from this work was that very large salt concentrations (on the order of that shown in Fig. 3) would be needed to initiate rainfall faster than would occur naturally, implying that hygroscopic seeding may not have

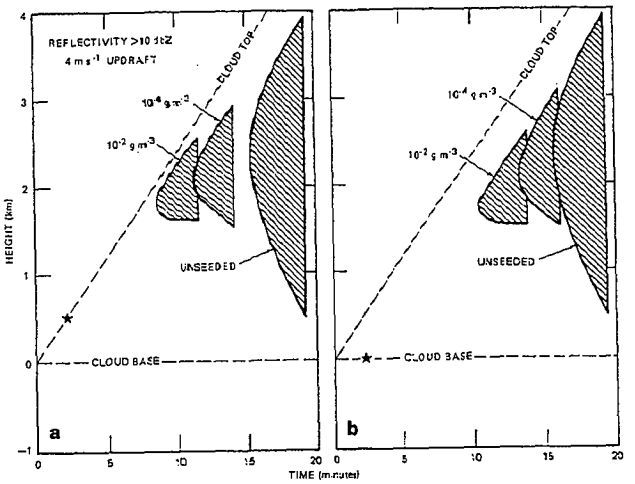

Figure 3. Example of the time-height cross sections obtained from a trajectory cloud model comparing the unseeded case and two seed cases for different seeding concentrations made 0.5 km above cloud base (panel a), and at cloud base (panel b) (from Johnson 1980).

a large effect on clouds with a naturally efficient warm rain process. This result stands in contrast to the model results of Rokicki and Young (1978) which suggested that concentrations on the order of 10^{-7} g m^{-3} would be sufficient to instill an effect.

Recent numerical simulations of the seeding of a warm-based Illinois convective cloud with and without ice multiplication active, have led to speculation about effects that warm cloud seeding may have on ice processes (Orville et al. 1993). In their simulation, a 2-dimensional, time-dependent model (Orville and Kopp 1977; Lin et al. 1983) with bulk water microphysics was applied to the 23 June 1989 exploratory cloud seeding trial conducted as part of the Precipitation Augmentation for Crops Experiment during 1989 (Changnon et al. 1991). Seeding was simulated as the release of AgI at approximately -10°C, as was the technique followed in PACE. Model runs with and without seeding were compared. In addition, two runs were made with ice multiplication active (Mossop and Hallett 1974, Hallett and Mossop 1974), one with and one without seeding.

The seeding simulation on the cloud without an ice multiplication process active, led to a clear signal in rapid transformation of rain to ice precipitation and a rapid increase in radar reflectivity. However, final precipitation at the ground was unchanged. Slight changes in vertical velocities were evident and a change in cloud temperature was positive in the seeded clouds. The results with ice multiplication showed that the seeding signal was almost completely masked by ice multiplication. This interesting result with regard to ice multiplication led to speculation about hygroscopic seeding effects on ice processes, because of the close link that exists between the presence of supercooled drizzle and raindrops, ice initiation, and ice multiplication by graupel interactions with supercooled cloud droplets.

If hygroscopic seeding does indeed lead to an enhancement of raindrop concentrations prior to the parcel reaching 0°C, then ice may originate in higher concentrations than it would have naturally, if the cloud follows a coalescence-freezing mechanism (Braham 1986). This might result in higher initial concentrations of frozen raindrops, and thus a more active graupel process, thereby stimulating ice multiplication by rime-splintering. Thus, the enhanced rate of conversion of water-to-ice might have implications for future microphysical evolution, as well as dynamic effects from the release of latent heat.

6. A "NEW" APPROACH

Recently the potential for rainfall enhancement by promoting the coalescence process has been renewed by radar and aircraft measurements taken of clouds developing in the plume of a large paper mill (Mather 1991). The apparent effects of the paper mill were very similar to those noted by Egan et al. (1974) and Hindman (1976) on the microstructure and precipitation from small cumuli and stratus affected by paper mill effluent. The basic evidence reported by Mather (1991) suggests that large anthropogenic hygroscopic nuclei (perhaps 0.5 to 1 μm diameter) are transported by updraft air into cloud base where they act to promote the early formation of small drizzle drops while inhibiting smaller natural CCN from nucleating. The net effect resulted in a broadening of the initial cloud droplet spectra and earlier initiation of the coalescence process. Mather and Terblanche (1992) suggest that these early effects (determined at cloud base) then mix throughout the cloud and may possibly be transmitted to other clouds (echo cores) in the multicelled system.

7. PRELIMINARY USE OF THE "NEW" FLARE

Because of the large apparent "positive" seeding effect of the paper mill, experiments were pursued to replicate, as closely as possible, the effect of the paper mill effluent on cloud microphysics. This was attempted with the production of a 1,000 g pyrotechnic flare based on a formulation originally developed by Hindman (1978). The South African flare was composed of 5 percent magnesium, 10 percent sodium chloride, 65 percent potassium perchlorate, and 2 percent lithium carbonate, and produced a combustion product which was 21 percent sodium chloride, 67 percent potassium chloride, and 12 percent magnesium oxide (Mather and Terblanche 1992).

Randomized seeding experiments were conducted during the 1991-1992 summer season in two regions in South Africa, the Bethlehem region on the Highveld (where cloud base temperatures are approximately +7°C) and the Carolina region in the eastern Transvaal (where cloud bases are approximately +10°C). A total of 50 seeding trials were conducted, 25 of which were seed and 25 that were unseeded. Twenty-one of the experiments were conducted in the Bethlehem area and the other 29 were conducted in the Carolina area.

The experimental units in either the Bethlehem or Carolina areas were defined by multicellular convective systems that already had a radar echo of at least 30 dBZ. This type of cloud selection is similar to that used in the 1989 Illinois experiment. Flares were ignited at cloud base in strong updraft. A maximum of 10 flares were used in each seed case. Radar estimated rain mass was calculated for the lowest radar scan (1.5° elevation) and at the 6 km level above mean sea level (approximately -10°C). Rain masses were sorted into 10 minute time windows starting 10 minutes before and ending 1 hour after the seed/no-seed decision. Figure 4a and 4b show the mean rain mass for the Bethlehem and Carolina regions at the lowest and the 6-km scan levels, respectively.

Figures 4a and 4b show that the Carolina storms had a much larger rain mass than the Bethlehem storms and that there was an initial bias in favor of the seeded storms in the Carolina area. In general, the rain masses follow the same trend during the first three time intervals, after which the rain masses diverge (approximately 30 to 40 minutes after seeding) with the seeded storms showing greater rain masses than the unseeded storms by about a factor of two. Figure 4 also shows that the apparent response to seeding at 6-km starts one time window earlier than the lowest scan. The high degree of consistency of behavior among the data is also noteworthy. Statistical analysis performed by the Centre for Applied Statistics at the University of South Africa indicated that the differences between the seed and no seed cases are significant at the 10% level.

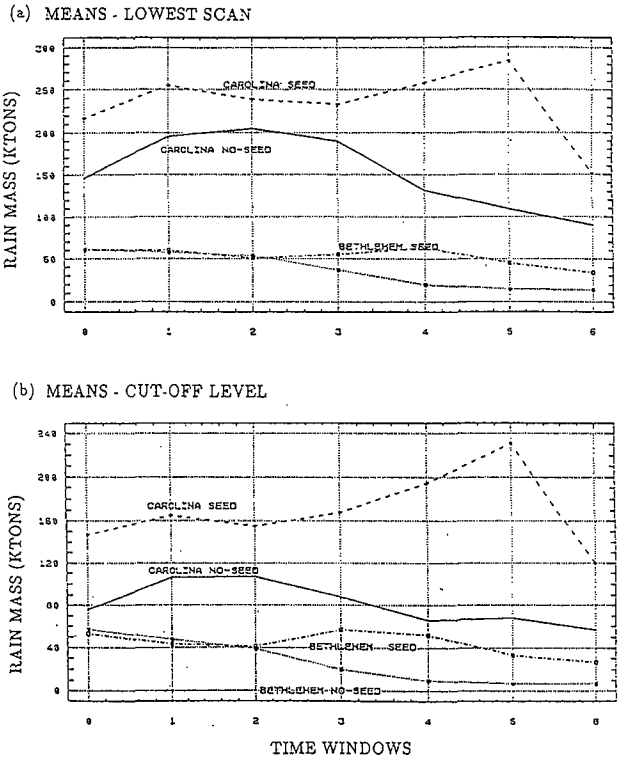

Figure 4. Radar estimated rain mass near cloud base (a) and near the -10°C level (b) sorted according to 10 minute time windows for South African storms at Carolina and Bethlehem using hygroscopic seeding flares just below cloud base (from Bruintjes et al 1993).

In the experiment, an attempt was also made to determine how the seeding material may have affected the initial cloud droplet spectrum. In this attempt, the cloud droplet spectrum were measured near cloud base with an instrumented aircraft flying behind the seeder aircraft. One of the cloud droplet spectrum obtained in the seeded and unseeded areas of cloud base are shown in Figure 5 (Bruintjes et al. 1993). The unseeded spectrum is shown as a dashed line, while the seeded spectrum is shown as a solid line. Figure 5 shows a distinct difference between the cloud droplet distribution in the unseeded area of cloud base, narrow distribution with a peak between 10 and 12 μ m diameter; while the seed spectrum is broader, with a tail extending out to 26 μm diameter. Both distributions represent about the same liquid water content, 0.33 and 0.35 g m^{-3} for the seed and no-seed spectrum. However, the total concentration of the unsceded region was 508 cm^{-3} compared to 280 cm^{-3} in the seeded region.

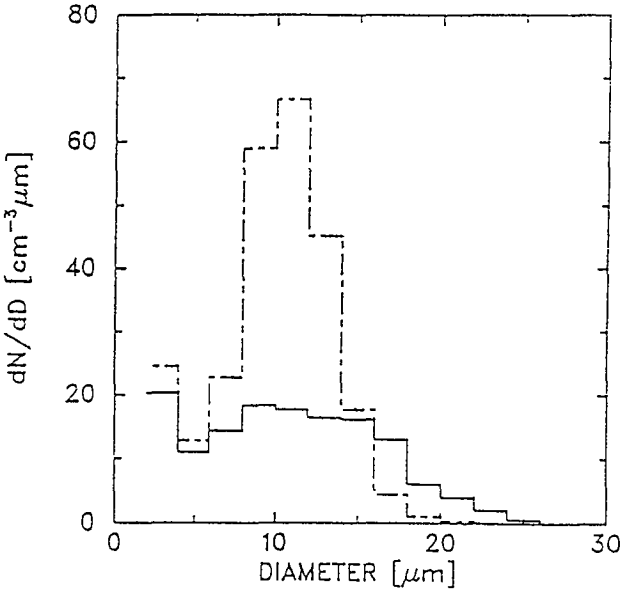

Figure 5. Difference of cloud droplet distribution from FSSP measurements probably taken in the affected (solid line) and unaffected (dashed line) region of cloud near cloud base (from Mather and Terblanche 1992).

Therefore, although it is possible that these differences in a small sample from a single summer may have happened by chance, and it is worrisome that such large apparent effects seem to result from such a modest amount of seeding, the overall results are consistent with the general seeding hypothesis and many aspects of earlier work in that coalescence appears to have been enhanced in the seeded clouds and the effect apparently spreads throughout the cloud system to result in higher radar estimated rain mass (i.e., precipitation enhancement).

8. POSSIBLE EFFECTS ON THE ICE PROCESS

Hygroscopic seeding at cloud base may also have influences on precipitation evolution involving ice because of the strong link that exists between the presence of supercooled precipitation-size drops and the initiation of ice (Koenig 1963, Braham 1964, Czys and Petersen, 1992), and because of the dependence of the rime-splintering mechanism on concentrations of supercooled cloud droplets and on graupel size and concentration (Mossop and Hallett 1974, Hallett and Mossop 1974, Mossop 1976, Mossop 1978a, Mossop 1978b).

Exploratory measurements made in South Africa around the -10°C level in clouds affected by the paper mill (Mather 1991) and in clouds hygroscopically seeded (Mather and Terblanche 1992) have provided some clues about possible effects on the ice process. In one set of measurements, the seeding aircraft released seeding material from two flares, followed by the ignition of two more flares at cloud base with the pairs of ignitions being four minutes apart. Prior to and after these releases, the cloud physics airplane was sampling at -10°C in clouds roughly above the release area. Prior to the time that the affected cloudy air could have reached the -10° level, concentrations of supercooled cloud droplets as measured by the FSSP have distribution concentrations typical of natural clouds (see Fig. 6). However, shortly after, when it would have been possible for the seeding material to reach the sampling level, the concentration of FSSP particles with diameters greater than 32 μm was observed to increase by a factor of near 7, from 0.55 to 3.6 cm^{-3}, with a corresponding broadening of the size spectrum (see Fig. 6). Of course, uncertainty exists over whether or not this change in supercooled cloud droplet distribution is truly due to seeding because there is no direct evidence that the airplane sampled in affected cloud or that the airplane may have caused the perturbation itself (Rangno and Hobbs 1983, Rangno and Hobbs 1984, Kelly and Vali 1991).

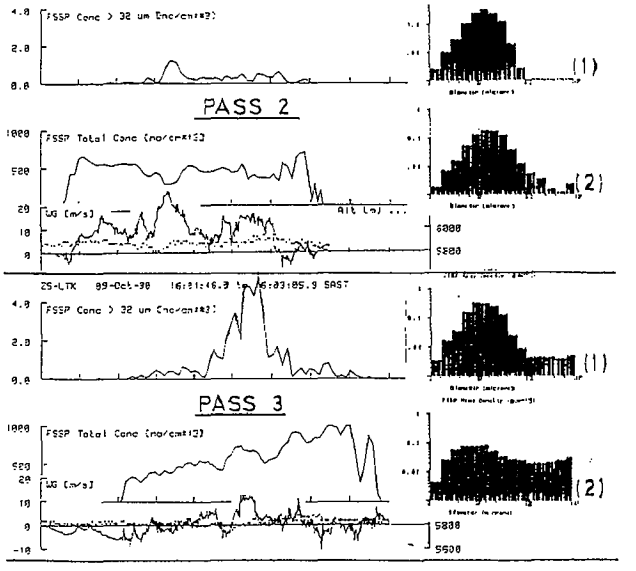

Figure 6. Selected microphysical measurements taken around the -10°C level of clouds in the recent South African experiments which suggest broadening of the spectrum of supercooled cloud droplets that occurred between pass 2 and pass 3 (from Bruintjes et al. 1993).

Assuming that the cloud droplet spectrum is broader at subzero temperatures, and that the presence of increased concentrations of supercooled drizzle and raindrops do indeed result from seeding, some further speculation can be made about effects on the ice process. First, increased concentrations of supercooled drizzle and raindrops may mean higher initial concentrations of "first ice" because first ice concentrations (in the form of frozen raindrops and then graupel) in clouds with an active coalescence process are highly correlated with concentrations of supercooled drizzle and raindrops (Koenig 1963, Braham 1964, Czys 1989, and Czys 1991). Thus, there may be a more active ice process involving graupel. This may in turn enhance precipitation development because of the advantages that graupel growth has over coalescence (Johnson 1987). Furthermore, a more active graupel process may enhance secondary ice production if other conditions exist to permit the rime-splintering process (Mossop 1976, Heymsfield and Mossop 1984).

In fact, limited evidence has been uncovered that rime-splintering may have been triggered in South African clouds affected by effluent of the paper mill (Mather 1991). This evidence was uncovered by the appearance of columnar crystals when they are not usually part of the kind of ice naturally encountered (see Fig. 7). The exact effect that an enhanced secondary rime splintering process would have on cloud and precipitation production is unclear and needs to be explored. Nonetheless, a more rapid glaciation seems physically possible, and this may have effects similar to those expected from dynamic seeding. Thus, hygroscopic seeding may potentially enhance rain production by not only promoting coalescence, but by enhancing ice processes and by dynamic effects that may promote cloud growth from latent heat releases related to freezing as well as condensation.

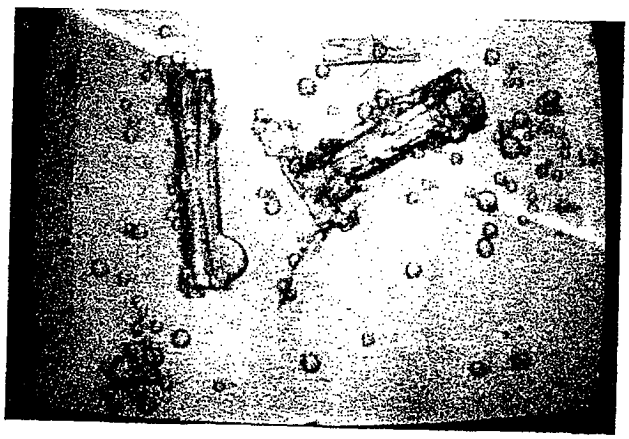

Figure 7. Photograph showing possible evidence of hygroscopie seeding on ice processes which may come about by the effect that broadening of the supercooled cloud droplet spectrum may have on the rime-splintering process (from Mather 1991).

9. POSSIBLE DYNAMIC EFFECTS

It is interesting to note that the clouds in the 1991-1992 South African hygroscopic seeding trials, as well as those supposedly affected by the paper mill (Mather 1991) also seem to have experienced dynamic effects from hygroscopic seeding. Figure 8 shows radar-measured cloud top heights (defined by the 30 dBZ contour) for the seed/no-seed storms, each for 10 minute time windows relative to the time of seeding. Figure 8 shows that the no-seed storm increased in height from time-window 1 to time-window 2, and then decreased thereafter. On the other hand, the seed clouds show a slight decrease from window 1 to window 2, and then show a steady increase. Positive effects on echo top growth rates have also been found in the South Africa data, as well as on heights and growth rates defined in the 45 dBZ contour. Thus, it appears that "dynamic" effects might also accompany microphysical effects in hygroscopic seeding, as was suggested in the earlier experiments. However, the extent to which these effects can be attributed to an enhancement of the latent heat of condensation, latent heat of fusion, both, or some other reason is uncertain and needs to be addressed.

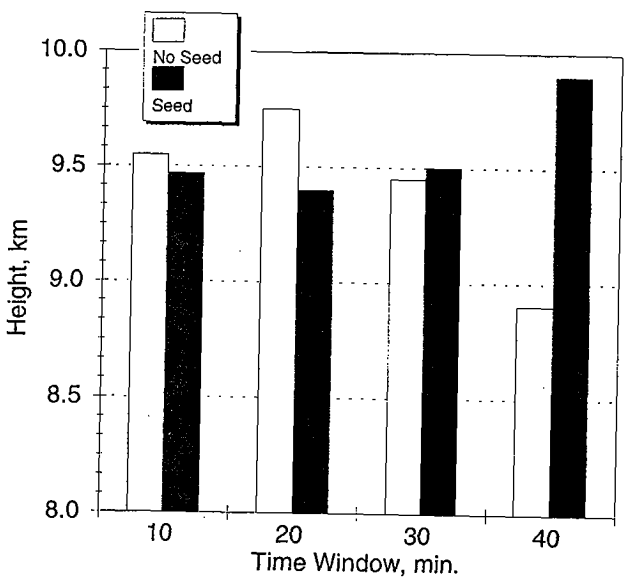

Figure 8. Bar chart showing possible evidence of dynamic effects due to hygroscopie seeding in the South African seeding trials.

10. SUMMARY AND CONCLUSIONS

From the very time that condensation-coalescence theory was accepted as a physical mechanism for the initiation and evolution of precipitation in mid-latitude clouds, attempts were made to use hygroscopic substances to promote coalescence, and thereby enhance rainfall. Although this seeding technique received a great amount of initial attention, interest has diminished over the years in favor of static mode and dynamic mode glaciogenic seeding. It is difficult to assess why interest was lost in hygroscopic seeding. However, one reason may have been the inherent difficulty of delivering adequate amounts of

appropriately sized water droplets or finely ground salts, compared to the relative ease of glaciogenic seeding. Handling is also a problem. Many hygroscopic seeding substances are very corrosive, and chemically incompatible with the materials from which aircraft are constructed.

Almost all of the scientific work related to hygroscopic seeding, was conducted prior to recent major advances in ground-based and airborne measurement systems, and computer modeling. Perhaps this helps to explain why almost all of the previous experiments have failed to provide convincing scientific evidence of hygroscopic seeding effects. More importantly though, many of the previous experiments failed to adequately document the physical chain of events that would have linked cause and effect. This too may have been the result of inadequate or unavailable technologies, if not from other constraints. Although the evidence is far from convincing, it seems that most experiments have shown possible effects that are consistent with that expected from hygroscopic seeding: cloud droplet distribution in some cases have been found to be broader than they would have been naturally, echoes may have formed sooner, lower, or when they otherwise may not. And there are limited indications of "dynamic" effects in the form of higher cloud tops, larger growth rates, or both. However, the earliest experiments never thoroughly tested what the original theoretical analysis indicated should be the most effective treatment technique; releases at or near cloud base in updraft with moderately sized artificial CCN. The most recent South African trials in which near cloud base treatments were tried have produced some encouraging results that deserve noting, and have renewed interest in the technique of hygroscopic seeding.

Acknowledgments. This review was conducted as part of the Precipitation, Cloud Changes and Impacts Project (PreCCIP) under NOAA cooperative agreement COM NA27RAO173. The authors wishs to thank Robert W. Scott and Nancy E. Westcott for their helpful comments during the preparation of this manuscript.

11. REFERENCES

Anon., 1948: Artificial Stimulation of Precipitation. South African CSIR Report (see Mason 1980).

Battan, L.J., 1953: Observation on the formation and spread of precipitation ,in convective clouds. *J. Meteor.*, **10**, 311-324.

Bergeron, T., 1935: On the physics of clouds and precipitation. *Proceedings, 5th Assembly U.G.G.I.*, Lisbon, **2**, 156.

Biswas, K.R., and A.S. Dennis, 1971: Formation of a rain shower by salt seeding. *J. Appl. Meteor.*, **10**, 780-783.

Biswas, K.R., and A.S. Dennis, 1972: Calculations related to formation of rain shower by salt seeding. *J. Appl. Meteor.*, **11**, 755-760.

Biswas, K.R., R.K. Kapoor, K.K. Kanuga, and Bh.V. Ramanamurty, 1967: Cloud seeding experiment using common salt. *J. Appl. Meteor.*, **6**, 1914-1923.

Bowen, E.G., 1950: The formation of rain by coalescence. *Aust. J. Scientific Res.*, **A3**, 193.

Bowen, E.G., 1952a: A new method of stimulating convective clouds to produce rain and hail. *Quart. J. Roy. Meteor. Soc.*, **78**, 37-45.

Bowen, E.G., 1952b: Australian experiments on artificial stimulation of rainfall. *Weather*, London, 7, 204.

Braham, R.R., Jr., 1964: What is the role of ice in summer rain showers? *J. Atmos. Sci.*, **21**, 640-645.

Braham, R.R., Jr., 1986: The cloud physics of weather modification. Part I: Scientific basis. *WMO Bull.*, **35**, 215-221.

Braham, R.R., Jr., L.J. Battan, and H.R. Byers, 1957: Artificial nucleation of cumulus clouds. *Meteor. Monogr.*, **2**, 47-85.

Bruintjes, R.T., G.K. Mather, D.E. Terblanche, and F.E. Steffens 1993: A new look at the potential of hygroscopic seeding in summertime convective clouds. *Proc. 1993 National Conf. Irrigation and Drainage Engineering*, Park City, Utah, July 21-23, ASCE, 496-503.

Changnon, S.A., R.R. Czys, R.W. Scott, and N.E. Westcott, 1991: The Illinois precipitation modification program. *Bull. Amer. Met. Soc.*, **72**, 587-604.

Chatterjee, R.N., A.S. Ramachandra Murty, K. Krishna, and Bh.V. Ramana Murty, 1978: Radar evaluation of the effect of salt seeding on warm maritime cumulus clouds. *J. Wea. Modif.*, **10**, 54-61.

Coons, R.D., E.L. Jones, and R. Gunn, 1948: Second partial report on the artificial production of precipitation - cumuli formed clouds, Ohio, 1948. *Bull. Amer. Meteor. Soc.*, **29**, 544-546.

Coons, R.D., E.L. Jones, and R. Gunn, 1949: Fourth partial report on artificial production of precipitation: cumulus clouds, Gulf States, 1949. *Bull. Amer. Meteor. Soc.*, **30**, 289-292.

Corrsin, S., 1951: On the spectrum of isotrophic temperature fluctuations in an isotrophic turbulence. *J. Appl. Phys.*, **22**, 469-473.

Cotton, W.R., 1982: Modification of precipitation from warm clouds - A review. *Bull. Amer. Meteor. Soc.*, **63**, 146-160.

Czys, R.R., 1989: Ice initiation by collision forcing in warm based cumuli. *J. Appl. Meteor.*, **28**, 1098-1104.

Czys, R.R., 1991: A preliminary appraisal of the microphysical nature and seedability of warm based midwestern clouds at -10°C. *J. Wea. Modif.*, **23**, 1-17.

Czys, R.R., and M.S. Petersen, 1992: Observations of first ice in Illinois cumulus. *Proc. 11th Intnl. Conf. Clouds and Precip.*, Montreal, Canada, 264-267.

Davies, D.A., D. Hepburn, and H.W. Sansom, 1952: Report on experiments at Kongwa on artificial control of rainfall, Jan-Apr 1952. *E. Afr. Met. Dep. Mem.*, **2**, No. 10.

Dennis, A.S., 1980: *Weather Modification by Cloud Seeding.* Academic Press, New York. 267 pp.

Dennis, A.S., and A. Koscielski, 1972: Height and temperature of first echoes in unseeded and seeded convective clouds in South Dakota. *J. Appl. Meteor.*, **11**, 994-1000.

Egan, R.C., P.V. Hobbs, and L.F. Radke, 1974: Particle emissions from a large Kraft paper mill and their effects on the microstructure of warm clouds. *J. Appl. Meteor.*, **13**, 535-552.

Farley, R.D., and C.S. Chen, 1975: A detailed microphysical simulation of hygroscopic seeding on the warm rain process. *J. Appl. Meteor.*, **14**, 718-733.

Findeisen, W., 1942: Ergebnisse von Wolken - und Niederschlags-beobachtungen bei Wetterkundungesflugen uber See. *Reichsamt f. Wetterdienst Forsch. u. Erfahrungsberichte, B.* **No. 8**, 3-12.

Fournier d'Albe, E.M., and P. Mosino Aleman, 1976: A large-scale cloud seeding experiment in Rio Nazas Catchment Area, Mexico. *Proc. Second WMO Sci. Conf. Wea. Modif.*, Boulder, CO, 143-149.

Hallett, J., and S.C. Mossop, 1974: Production of secondary ice crystals during the riming process. *Nature*, **249**, 26-28.

Hess, W.H., 1974: *Weather and Climate Modification.* John Wiley and Sons, New York. 842 pp.

Heymsfield, A.J., and S.C. Mossop, 1984: Temperature dependence of secondary ice crystal production during soft hail growth by riming. *Quart. J. Roy. Meteor. Soc.*, **110**, 765-770.

Hindman, E.E., 1976: Observations of effects on clouds and rainfall caused by affluence from paper mills. *J. Wea. Modif.*, **8**, 84-92.

Hindman, E.E., 1978: Water droplet fogs formed from pyrotechnically generated condensation nuclei. *J. Wea. Modif.*, **10**, 77-96.

Johnson, D.B., 1980: Hygroscopic seeding of convective clouds. SWS Contract Report 244, Illinois State Water Survey, Champaign, IL. 221 pp.

Johnson, D.B., 1982: Geographical variations in cloud based temperature. Preprints, *Conf. Cloud Physics*, Chicago, IL, Amer. Meteor. Soc., 187-189.

Johnson, D.B., 1987: On the relative efficiency of coalescence in riming. *J. Atmos. Sci.*, **44**, 1672-1680.

Kapoor, R.K., S.K. Paul, A.S. Ramachandra Murty, K. Krishna, and Bh.V. Ramana Murty, 1975: Study of drop size distribution in warm clouds subject to repeated seeding. *J. Wea. Modif.*, 7, 116-126.

Kelly, R.D., and G. Vali, 1991: An experimental study of the production of ice crystals by a twin turbo-prop aircraft. *J. Appl. Meteor.*, **30**, 217-226.

Klazura, G.E., and C.J. Todd, 1978: A model of hygroscopic seeding in cumulus clouds. *J. Appl. Meteor.*, **17**, 1758-1768.

Koenig, L.R., 1963: The glaciation behavior of small cumulus clouds. *J. Atmos. Sci.*, **20**, 29-47.

Koscielski, A., and A.S. Dennis, 1972: Seeding effects in convective clouds in western South Dakota. *J. Wea. Modif.*, **4**, 149-171.

Langmuir, I., 1948: The production of rain by a chain reaction in cumulus clouds at temperatures above freezing. *J. Meteor.*, **6**, 175-181.

Lin, Y.L., R.D. Farley, and H.D. Orville, 1983: Bulk parameterization of the snowfield in a cloud model. *J. Climate Appl. Meteor.*, **22**, 1065-1092.

Ludlam, F.H., 1951: The production of showers by coalescence of cloud droplets. *Quart. J. Roy. Meteor. Soc.*, 77, 402.

Mason, B.J., 1971: *The Physics of Raincloud.* Claredon Press, Oxford. 671 pp.

Mather, G.K., 1991: Coalescence enhancement in large multicell storms caused by the emissions from a Kraft paper mill. *J. Appl. Meteor.*, **30**, 1134-1146.

Mather, G.K., and D.E. Terblanche, 1992: Cloud physics experiments with artificially produced hygroscopic nuclei. *Proc. 11th Intnl. Conf. Clouds and Precip.*, Montreal, Canada, 147-150.

Mossop, S.C., 1976: Production of secondary ice particles during the growth of graupel during riming. *Quart. J. Roy. Meteor. Soc.*, **102**, 45-57.

Mossop, S.C., 1978a: The influence of drop size distribution in the production of secondary ice particles during graupel growth. *Quart. J. Roy. Meteor. Soc.*, **104**, 323-330.

Mossop, S.C., 1978b: Some factors governing ice particle multiplication in clouds. *J. Atmos. Sci.*, **35**, 2033-2037.

Mossop, S.C., and J. Hallett, 1974: Ice crystal concentrations in cumulus clouds: Influence of drop spectrum. *Science*, **186**, 632-634.

Orville, H.D., and F.J. Kopp, 1977: Numerical simulation of the life history of a hailstorm. *J. Atmos. Sci.*, **34**, 1596-1618.

Orville, H.D., F.J. Kopp, R.D. Farley, and R.R. Czys, 1993: Numerical simulation of the cloud seeding of the warm base Illinois convective cloud with and without ice multiplication active. *J. Wea. Modif.*, **25**, 50-56.

Parasnis, S.S., A.M. Selvam, A.S. Ramachandra Murty, and Bh.V. Ramana Murty, 1982: Dynamic responses of warm monsoon clouds to salt seeding. *J. Wea. Modif.*, **14**, 35-37.

Ramachandra Murty, A.S., A.M. Selvam, and Bh.V. Ramana Murty, 1975: Dynamic effect of salt seeding in warm cumulus clouds. *J. Wea. Modif.*, **7**, 31-43.

Rangno, A.L., and P.V. Hobbs, 1983: Production of ice particles in clouds due to aircraft penetrations. *J. Climate Appl. Meteor.*, **22**, 214-232.

Rangno, A.L., and P.V. Hobbs, 1984: Further observations of the production of ice particles in clouds by aircraft. *J. Climate Appl. Meteor.*, **23**, 985-987.

Rokicki, M.L., and K.C. Young, 1978: The initiation of precipitation updrafts. *J. Appl. Meteor.*, **17**, 745-754.

Sansom, H.W., D.J. Bargman, and G. England, 1955: Report on experiments on artificial stimulation of rainfall at Mitiana, Uganda, Sept-Dec 1954. *E. Afr. Met. Dep. Mem.*, **3**, No. 4.

Warner, J., 1970: The microphysical structure of cumulus clouds. Part III: The nature of updraft. *J. Atmos. Sci.*, **27**, 682-688.

Woodcock, A.H., and A.T. Spencer, 1967: Latent heat released experimentally by adding sodium chloride particles to the atmosphere. *J. Appl. Meteor.*, **6**, 95-101.

Woodcock, A.H., D.C. Blanchard, and C.G.H. Rooth, 1963: Salt-induced convection in clouds. *J. Atmos. Sci.*, **20**, 159-169.

Statistical Evaluation of the 1984–88 Seeding Experiment in Northern Greece

R.C. Rudolph,[1] C.M. Sackiw[2] and G.T. Riley[3]
INTERA Technologies Ltd.
Calgary, AB, Canada

Abstract. A randomized crossover hail suppression seeding experiment conducted in northern Greece during 1984–88 was evaluated using hailpads distributed over approximately 2000 km^2 with a mean separation of 4.5 km. A total of 196 hailpads were collected on 37 hail days and a Wilcoxon Signed Rank test was applied to 10 target and control hailpad parameters. All parameters showed a reduction due to treatment ranging from 19 to 85%. The associated P–values range from 0.003 to 0.392. Three hail crop insurance parameters showed reductions from 18 to 59% with associated P–values between 0.11 and 0.54. Reductions due to treatment were evident in the five year aggregate size distributions in which target hailstones were 38 to 100% fewer than control hailstones in 12 size categories. The average size reduction was 55% with a P–value of 0.002. Similar reductions were observed in each year of the experiment.

1. INTRODUCTION

Those familiar only with the glorious summer sun and sandy beaches of the Greek islands may be surprised by the need for a hail suppression program in that country. Yet vacationers to northern Greece will recall the rugged terrain – broad river valleys ringed by 2 km high mountain ridges – that forms the breeding ground of almost daily convective activity in the April to July period and beyond. These same fertile river valleys are the backbone of Greek agriculture where farmers grow a wide assortment of fruits, vegetables, cotton, tobacco, rice and cereal crops.

The Greek National Hail Suppression Program (GNHSP) was established in 1984 under the auspices of the National Agricultural Insurance Institute, now known as EL.G.A. The primary objectives of the program were to reduce hail damage to crops in the agricultural valleys of northern Greece using airborne seeding technology and to evaluate the program by means of a fully randomized crossover seeding experiment. This paper summarizes the statistical evaluation of the seeding experiment conducted during 1984–88.

2. GNHSP PROGRAM OVERVIEW

2.1 Experimental Design

The GNHSP was designed to protect three agricultural areas of northern Greece (Karacostas, 1984, 1989). Area 1 was designated as the experimental area (Fig. 1) where randomized crossover seeding was conducted while Areas 2 and 3 were fully seeded. Area 1 was divided into approximately equal northern and southern sub–areas, with the orientation of the dividing line determined by mean storm motion, terrain and the spatial variability of crops. No buffer zone seperated the two sub–areas. Hence, contamination of pads could occur if seeded cells crossed the dividing line, consequently reducing the distinction between target and control estimates. Partly because the sub–areas are physically adjacent, the correlation of hail occurrence is expected to be high and thus reduce the variance of target–control differences.

The experimental unit was a declared "hail day." On each day meeting seeding criteria, operations were conducted in either the northern or southern sub–area, depending on the random number of the day. The seeding criteria was a reflectivity of 35 dBZ or more measured in convective cells located either inside, or within 20 minutes of entering, the designated target area at altitudes corresponding to temperatures between -5° and -30°C (Flueck *et al.*, 1986). A hailpad network provided an objective measure of target–control differences.

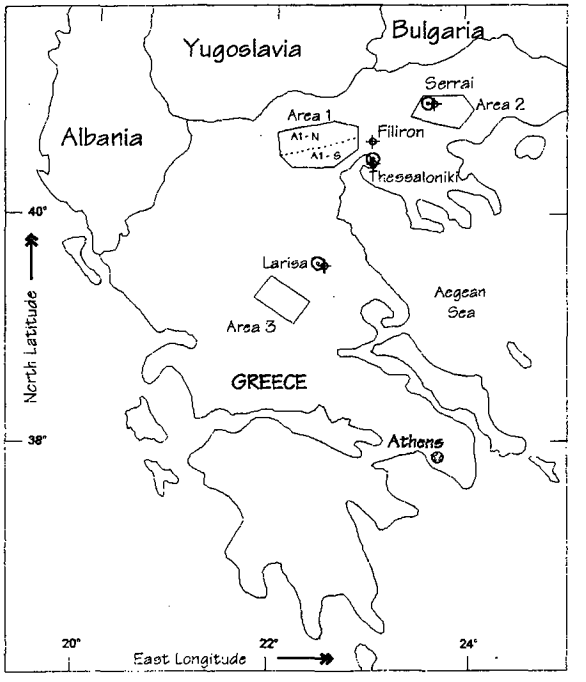

Fig. 1. The three areas of the GNHSP, circa 1984. Crossed circles indicate locations of project radars over the course of the experiment. Area One was divided into northern and southern sub–areas for the randomized experiment. (After Henderson, 1986.)

[1] Current affiliation Colorado International Corporation, Boulder, CO, USA.

[2] Current affiliation Atmospheric Environment Service, Trenton, Ontario, Canada.

[3] Current affiliation Atmospherics Incorporated, Fresno, CA, USA.

2.2 Seeding Hypothesis

The GNHSP was not designed with an "official" seeding hypothesis but pragmatic versions have evolved during the program. In 1984–85, Atmospherics Incorporated applied the concept of Limiting Supercooled Liquid Water as the rationale for operations. As the name implies, this approach aims to reduce the amount of supercooled water available to the storm by converting it to ice so that it is then unavailable for hailstone growth (Solak *et al.*, 1985). Since that time, the working hypothesis has been broadly based on Beneficial Competition Theory which assumes a lack of natural ice nuclei in the environment. Adding silver iodide (AgI) is thought to result in the production of a substantial number of "artificial" ice nuclei. The natural and artificial nuclei then compete for the available supercooled water in the hailstone growth regions within the storm. If enough nuclei are added it is possible that the hailstones will be small enough to melt completely before reaching the ground. No additional microphysical details of a hypothesis have been introduced because of the limited in–cloud measurements made on the program.

Operationally, the cloud seeding experiment concentrated on the time–evolving updrafts of ordinary (single) cells and on the updrafts of developing feeder clouds that flank mature multicell storms. Stated most simply (Henderson, 1986), this technique limits the available supercooled liquid water within those cloud volumes where hailstone birth and growth are assumed to occur.

Limited microphysical observations in Greek convective clouds (Krauss and Papamanolis, 1989) support the ice phase or graupel embryo precipitation process and are consistent with the beneficial competition theory. These observations include the presence of conical graupel embryos, average cloud base temperatures near 10°C and a continental drop size distribution. Furthermore, convective clouds with tops warmer than -10°C have not been observed to produce rain. The presence of an active coalescence process, which does not appear likely from observations, would invalidate the beneficial competition premise that seeded cloud volumes and volumes where hailstone embryo formation and growth occur are coincident.

2.3 Experimental Conduct

The experiment was operated during 1 May to 30 September in each of the years 1984–88. Seeding was conducted with five light, twin–engined (Cessna 340A or Piper Aztec) aircraft equipped with seeding racks containing both ejectable and end–burning AgI flares. TB–1 pyrotechnic mixtures were used in all years. At most, three aircraft seeded a single storm (in 1984) but typically no more than two aircraft could conduct seeding operations in the experimental area at any one time due to operating logistics and Air Traffic Control policy.

Weather surveillance in the experimental area was provided by two radars, an Enterprise WSR74 10 cm S–band set located at Macedonia International Airport in Thessaloniki with backup from an Enterprise WR100 5 cm C–band radar located near the town of Serres in 1984–85 and near the village of Filiron in 1986–88. A radar watch was maintained as required by forecast and observed convection 7 days per week during 1984–86. During 1987–88 the watch was standardized at 20 hours per day (0600 to 0200 local) and was extended to 24 hours if cells were observed or forecast. Storms were not observed to generate hail large enough to damage hailpads after 2300 local.

Several seeding methodologies were used depending on factors such as storm type, visibility, terrain proximity and time of day to enable delivery of seeding material to actively growing storm regions in as many conditions as possible. Seeding material was released in one or more of the following locations:

- growing cloud towers (feeder cells) on the upshear flanks of mature multicell storms;
- regions of identifiable liquid water and/or updraft in single convective cells;
- weak updraft regions below the base of feeder cells;
- the main updraft region below the base of single convective cells; and
- regions of expected storm inflow based on ground radar information in the absence of good visibility.

In practise, seeding was begun on storms that moved or propagated toward the experimental area when the leading edge of the storm above seeding criteria first entered the buffer zone (1984–85) or when the leading edge of the 35 dBZ contour first entered the buffer zone (1986–88). Storms frequently reached seeding criteria within the area and were seeded as soon as possible thereafter.

The nominal seeding rate during 1986–88 for penetrations near -10°C was one 20 g flare every 5 s, resulting in a seeding rate of 240 g/min. In practise, these rates were adjusted both upwards and downwards by up to 50% depending on conditions. Seeding at cloud base was conducted by burning one or two 150 g flares over a 4 minute period for a seeding rate of 40 or 80 g/min.

3. EVALUATION DATASETS

3.1 Hailpad Network Installation and Service

Each hailpad site in the Area 1 network consisted of a levelled aluminum frame designed to firmly hold a piece of styrofoam with an exposed surface of 27 x 27 cm at a height of 1.5 m above ground. The network varied considerably during the 5 years of the experiment. In 1984, the network was established with a 4.5 km mean spacing with 123 sites distributed within approximately 2300 km^2. Of these sites, 56 lay in the north (1150 km^2), 60 in the south and 7 were located outside of Area 1 and excluded from the analysis.

At the beginning of 1985, the northeast portion of the area was expanded by about 40 km^2; 6 new sites were added and several were removed. The result was 63 sites in the north and 62 in the south. On 1 June, the boundary between north and south was moved southward to re–equalize the size of the sub–areas, leaving 69 sites in the north and 57 in the south.

Before the start of the 1986 season, approximately 100 additional sites were added to the "regular" network to create two, small "dense" networks with a mean spacing of 1.5 km for improved hailswath resolution. A standard rain gauge was also installed at each regular site and several sites were relocated. During the season, most of the sites were upgraded to improve hailstand stability with little interruption in service. The final

1986 configuration consisted of 69 regular sites in the north, 59 in the south and 1 outside the boundaries of the area.

The 1987 and 1988 networks were similar to that of 1986 although one site was relocated due to flooding. For these years, the network consisted of 68 sites in the north, 60 in the south and 1 outside of the area. Fig. 2 is a map of the 1988 network.

Pads were routinely changed within 24 hours of possible storm damage as indicated by radar, or within 10 days (14 days in 1984–85) of deployment if no storms occurred. In practice, a new experimental day was not declared until hailpad crews reported that all damaged pads from previous storms had been changed.

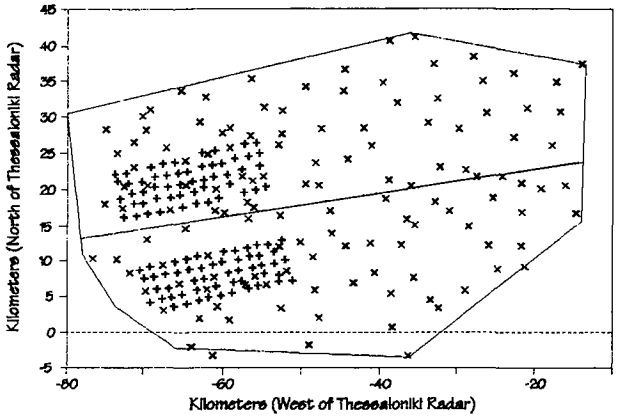

Fig. 2. The 1988 hailpad network in Area One showing the distribution of regular (x) and dense (+) sites.

3.2 Hailpad Data Set

Hailpad styrofoam varied somewhat in composition from year to year and batch to batch according to availability. To account for changing characteristics, all types of hailpad material used on the program were calibrated using steel balls dropped from varying heights to match hailstone energy (Dalezios *et al.*, 1991; Lozowski *et al.*, 1978). Hailstone size was calculated based on the calibration data and stones less than 5 mm in diameter (the minimum detectable stone size of the least sensitive pad material) were excluded from analysis.

Methods of digitizing hailstone dents varied somewhat during the experiment. In 1984–85, pads were inked and dents measured using a video scanning technique (Henderson, 1986). In 1986–88, pads were inked and dents were measured using a digitizing tablet (bitpad). In both techniques, artifacts (e.g., bird damage and pebble impact dents) were either not digitized or were removed graphically based on the experience of the operator.

In 1984–86, random numbers (i.e., the identification of the target/control sub-areas) were known ahead of time by the aircraft controllers who worked from an authorized list of such numbers. To our knowledge, this information did not result in any effort to conduct seeding operations in other than an objective manner. Furthermore, due to penalty clauses in the operations contract for not seeding on hail damage days, crew alert status was very high. This knowledge of the target was eliminated in 1987–88 by using sealed envelopes which were opened only when seeding criteria were met. Random numbers were drawn twice on three days in 1986 due to incorrect instructions but in all cases, the first number drawn was used to identify the target area for analysis and no seeding was conducted after the second number was drawn.

Four datasets were originally identified for analysis of the 1984–88 period. The SC (Seeding Criteria) dataset included all days when seeding criteria were met (119 days including all days in 1984 when seeding or reconnaissance flights occurred). The DR (Days at Risk) dataset included all days at risk, consisting of 76 days when hail damage to pads was observed and/or seeding operations were conducted. The DE (Damage in Either) dataset contained 37 days with damage to hailpads in either the target or control. A fourth dataset (DB) consisted of 12 days with hailpad damage in both target and control. This fourth dataset was considered only in preliminary analyses (Rudolph *et al.*, 1989a) and because of its small size is not discussed further in the present paper. It is recognized that events following the randomization decision should generally not determine the composition of the evaluation database. This suggests that SC should be the dataset of choice for evaluation. However, as will be seen, the results were independent of whether the SC, DR, or DE dataset was used.

Hailpad estimators were summed for each day in the dataset, weighted by the slight differences in pad placement density in the northern and southern sub-areas, and normalized by the total number of *regular* network pads exposed. Weighting factors for pad density ranged from 0.963 to 1.124. Table 1 contains a summary of the hailday and hailpad dataset (for details of the dataset, see Rudolph *et al.*, 1989b). Dense network pads have not been included in this analysis.

Table 1. Number of days in each dataset and number of regular network hailpads collected.

	Days			Hailpads	
Season	**SC**	**DR**	**DE**	**Target**	**Control**
1984	26	16	6	15	18
1985	21	13	5	14	24
1986	26	11	6	6	7
1987	22	16	4	19	24
1988	24	20	15	36	33
Total	119	76	37	90	106

At the end of the exploratory phase of the experiment and based on physical appropriateness, ten estimators of treatment effect were identified during the 1986 season. Most estimators chosen (summed over a hail day, weighted and normalized) were functions of hailstone diameter and included:

- number of damaged pads (Pad);
- total number of hailstones (Stone);
- median hailstone diameter (Med);
- maximum hailstone diameter (Max);
- total pad area covered by hailstones (Cov);
- total hailstone volume (Vol);
- impact energy (KE); and
- reflectivity (Refl, defined as hailstone diameter to the sixth power).

Two additional estimators, SSI (Spatial Severity Index) and AVA (AVerage Area), were multiplicative functions of several simpler estimators (Solak *et al.*, 1985). While somewhat

redundant, they are intended to identify small variations in the other parameters.

The list of estimators above represents all of the hailpad parameters examined in the evaluation, not a subset. Many of the estimators are therefore expected to be correlated since all those of higher order were calculated from stone diameter. Specifically, this includes the area of the pad covered by hailstone damage, stone volume, kinetic energy, and reflectivity. It is also expected that SSI and AVA will be correlated with other, simpler, estimators. While kinetic energy was formally identified as the primary parameter in the seeding experiment, it has not been used as the sole determinant of experimental success.

3.3 Hail Crop Insurance Data

All agricultural land within the project areas is covered by mandatory government hail crop insurance, with EL.G.A. collecting and archiving all claims. The mandatory nature of the insurance eliminates many of the policy coverage problems normally associated with accurately determining treatment effects (Changnon, 1985). Insurance payouts are governed by crop type, stage of growth, commodity prices, agricultural subsidies and currency fluctuations and therefore do not strictly reflect physical characteristics of hail damage. However, the program is funded with the explicit goal of reducing payouts and therefore crop insurance data are relevant to the evaluation.

Insurance data made available to the GNHSP include the storm (damage) date, the number of reports for each village but not the exact location of the damage, the number of fruit trees or field crop area damaged and the total payout. Claims must be filed within 48 hours of the storm. No payments are made when damage is less than 20% of the value of the crop, which accounts for records of damage with no payout. The procedures of the field adjustors did not change significantly during the experimental period.

Three insurance parameters were considered: payout (Pay); damaged area (Area); and number of reporting villages (Vill). On some occasions the number of damaged trees was reported instead of the size of the damaged area. In these cases, the area was determined on the basis of 30 trees per 1000 m^2. Payout was based on the value of 1988 drachmas with inflationary adjustments for earlier years (Rudolph and Ganniaris–Papageorgiou, 1991).

4. RESULTS

4.1 Treatment Effect

Means (M) of target and control daily values were used to define a relative target–control difference (D) such that:

$$D = M_t / M_c - 1$$

where t and c refer to target and control values respectively. Results for 1984–88 (Fig. 3) show that target estimates of hailpad damage and insurance parameters are consistently less than those in the control, in the direction of a beneficial (negative) treatment effect.

Negative differences ranged from 19 to 85% for the five–year hailpad dataset and from 18 to 59% for the insurance dataset. These results are similar to those of Flueck *et al.* (1986) and Rudolph *et al.* (1989a) who performed analyses for subsets of the data. Furthermore, the results were identical for the SC, DR, and DE datasets because of the paired differences.

It is clear that not all of the reductions in hailpad parameters shown in Fig. 3 are independent. As stated earlier, higher order parameters were calculated functions of hailstone diameter and are expected therefore to be highly correlated. One would expect differences for these variables to be of the same sign.

4.2 Significance of Results

The Wilcoxon Signed Rank test (WSR) examined the strength of the target–control relative differences (Fig. 4). The WSR test was chosen because of its nonparametric character and robustness, and because the randomized experiment produced pairs of target–control values. Values for the SC, DR and DE datasets were identical because paired zeroes are ignored. Two–tailed P–values (probabilities) ranged from 0.003 to 0.392 for the hailpad dataset, indicating the treatment effects were not due to chance for most variables. P–values for the insurance dataset ranged from 0.11 to 0.54.

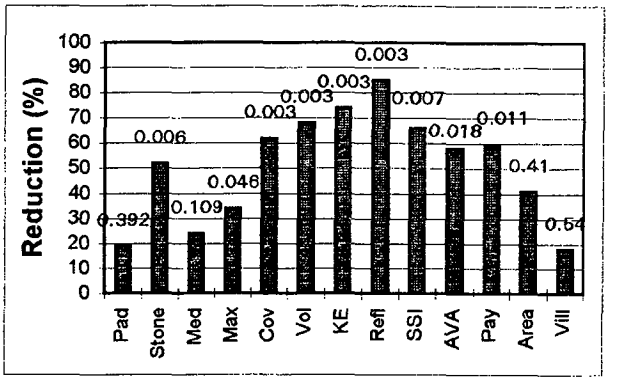

Fig. 3. Hailpad and crop insurance estimated treatment effects. Associated P–values are shown above the column.

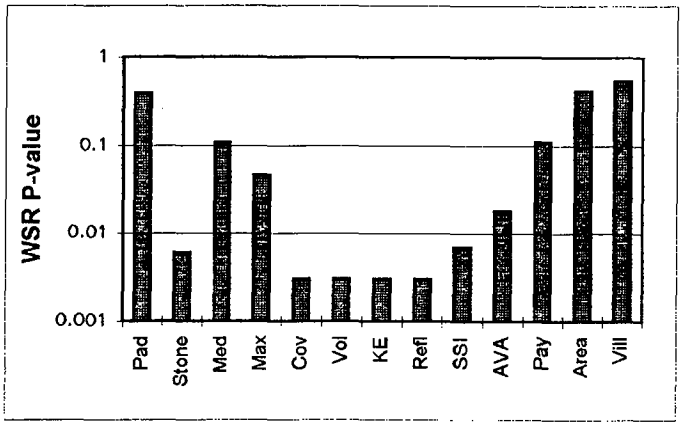

Fig. 4. Hailpad and crop insurance WSR P–values.

4.3 Hail Day Contingency Analysis

Following the methodology of Flueck *et al.* (1986), contingency tables were constructed for the presence of hail in the target and control sub–areas during 1984–88. The results, shown in Table 2, with two–tailed Fisher Exact probabilities of 0.31 for the DE

dataset and X^2 significance level of 0.385 for the DR dataset, suggest that the control is indeed associated with more days with hail damage than the target, although not significantly so.

Table 2. Contingency analyses of target and control for DR and DE datasets

	DR		DE	
	No Hail	Hail	No Hail	Hail
Control	49	27	9	27
Target	54	22	14	22

The contingency coefficients for the five–year dataset were 0.12 and 0.06 for DE and DR, respectively, indicating a weak association between hail occurrence and sub–area. Two possible explanations for the magnitude of this coefficient are:

- seeding is not completely eliminating damage to hailpads or;
- an underlying relationship exists between hail in target and control.

The first explanation is clearly valid and in keeping with a hail suppression (as opposed to prevention) project. The second is also expected due to the immediate proximity of the sub–areas, although the contingency coefficient includes a treatment effect which will reduce the association.

Further examination of Table 2 for the DR dataset shows that 27 of 76 days (36%) were associated with hail in the control while 22 of 38 days (29%) were associated with hail in the target. For the DE dataset, 27 of 36 days (75%) were associated with hail in the control and 22 of 36 days (61%) with hail in the target.

4.4 Hailstone Size Distributions

Hailstone target–control count differences, divided by control counts, and partitioned into 12 stone diameter size categories (e.g., 5 to 7 mm, centered at 6 mm), are shown in Fig. 5. It is apparent that target counts are less than control counts in all 12 categories, from 38% less in the smallest size categories to 100% less in the largest size categories. The mean estimated treatment effect is 55% over the 12 size categories.

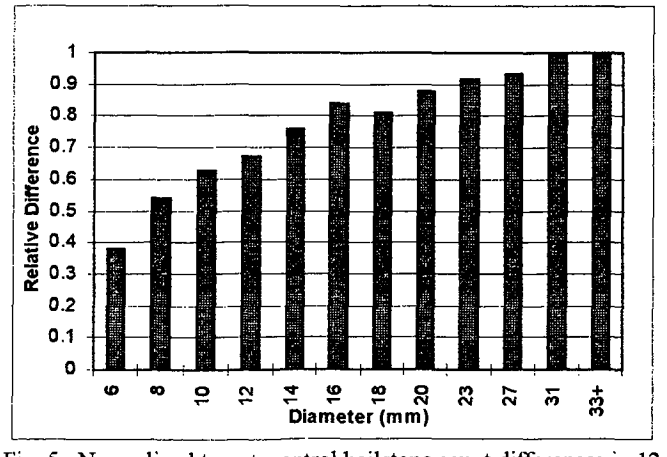

Fig. 5. Normalized target–control hailstone count differences in 12 size categories, 1984–88.

Table 3 presents size distribution estimated treatment effects for each of the 5 years of the experiment. With two exceptions (20 and 27 mm size categories in 1987), all of the size categories in each year indicated a positive treatment effect. Also, with the exception of 1987, each of the years indicated a stronger treatment effect in larger size categories. The evidence shows a decrease in the number of hailstones in the target, as compared to the control, in all size categories except the 27 mm group in 1987. With that sole exception, the larger sizes were not observed in the target area in all other years. In fact, for some years (e.g., 1984), the maximum stone size in the target was at least 33% smaller than in the control. Based on the size distribution data in Table 3, it appears that 1986 was the least severe hail year and 1987 was the most severe although 1988 produced the most damaged hailpads. However, it is worth noting that the large stones in 1987 occurred in association with one storm cell which developed in what is for Greece, an unusually convective environment. This storm was – perhaps – the only claimant to supercell status observed over the course of the experiment.

The WSR test was applied separately to the differences of each year. The resulting two–tailed P–values show very little probability (e.g., 0.01 in 1986) that the beneficial treatment effects are due to chance.

Further evidence on the possible physical effects of treatment on hailstone size is available by examining the number of stones in each category normalized by the total number of stones. Fig. 6 is a relative frequency diagram for the target and control sub–areas. In the 6 mm size category, the target had relatively more stones than the control. In the 8 mm category, relative frequencies were approximately equal. In all larger size categories, target relative frequencies were less than control. These observations are consistent with a beneficial competition process which inhibits the growth of large stones and increases the relative number of small stones (Sackiw, 1991).

Size distributions were further investigated by determining the inverse cumulative number concentration N(D) (Smith, 1982; Smith and Waldvogel, 1989) given by:

$$N(D) = \int_D^\infty n(D)dD$$

where n(D) is the hailstone number concentration. If the underlying size distribution for the population is of the Marshall–Palmer exponential form $n(D) = n_0 e^{-\Lambda D}$, then N(D) will have the same slope parameter Λ but intercept n_0/Λ compared to n(D).

Target and control values of five–year n(D) and N(D) distributions are shown in Table 4. N(D) distributions are closely exponential with R^2 values greater than 0.99 for each. Λ values were 0.42 and 0.31 mm^{-1}, with standard errors of 0.005 and 0.009 mm^{-1}, for target and control distributions, respectively. This suggests there is little likelihood that the differences are due to chance (P–value less than 0.005).

Values of the N(D) intercept, $\ln(n_0/\Lambda)$, were 11.31 and 11.28 mm^{-1}, with standard errors of 0.15 and 0.19 mm^{-1}, for target and control distributions, respectively. The intercepts are not significantly different and support the observation that the effect of

treatment seems to be reducing the total number of hailstones, especially in the larger sizes.

Table 3. Annual size distribution estimated treatment effects.

Dia. (mm)	1984	1985	1986	1987	1988	1984–88
6	-0.41	-0.81	-0.74	-0.37	-0.08	-0.38
8	-0.35	-0.58	-0.94	-0.58	-0.36	-0.54
10	-0.49	-0.63	-0.98	-0.67	-0.49	-0.63
12	-0.42	-0.77	-0.97	-0.72	-0.57	-0.67
14	-0.64	-0.87	-1.00	-0.77	-0.71	-0.76
16	-0.85	-0.94	-1.00	-0.73	-0.90	-0.84
18	-0.79	-0.94	-1.00	-0.64	-0.85	-0.81
20	-0.97	-1.00		-0.50	-1.00	-0.88
23	-1.00	-1.00		-0.44	-1.00	-0.92
27	-1.00	-1.00		0.00		-0.93
31	-1.00	-1.00				-1.00
≥33	-1.00					-1.00
Wilcoxon Sign–Rank Two–tailed P–values						
	0.002	0.003	0.01	0.02	0.006	0.002

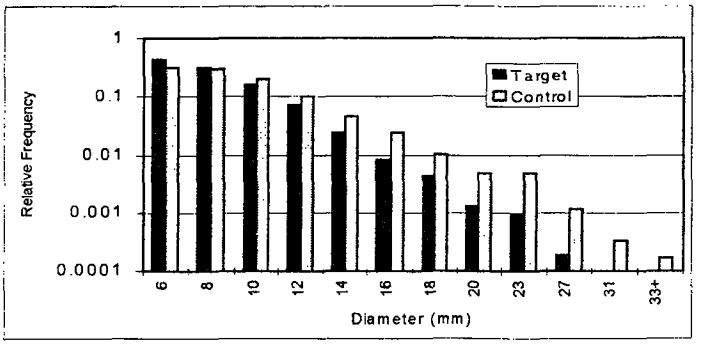

Fig. 6. Target and control relative differences in 12 hailstone size categories, 1984–88.

Table 4. Five–year hailstone size distributions.

Size Range (mm)	n(D) Target	n(D) Control	N(D) Target	N(D) Control
5–7	2251	3639	5335	11793
7–9	1641	3593	3084	8154
9–11	854	2332	1443	4561
11–13	380	1148	589	2229
13–15	127	537	209	1081
15–17	45	283	82	544
17–19	24	124	37	261
19–21	7	58	13	137
21–25	5	59	6	79
25–29	1	14	1	20
29–33		4		6
>33		2		2

5. SUMMARY AND DISCUSSION

The results presented in this paper summarize a five–year randomized–crossover seeding experiment conducted during 1984–88 in northern Greece within the context of the GNHSP. The experiment was evaluated using hailpads from a network with a mean spacing of 1 pad in 20 km^2.

Target estimates of hail damage were consistently less than control estimates, with reductions in all hailpad parameters of 19 to 85%. Associated P–values ranged from 0.003 to 0.392. The reductions in hail crop insurance payout ranged from 18–59% with P–values of 0.11–0.54. The results suggest that the seeding treatment likely did not reduce the number of haildays in the target area (hailday contingency analysis P–value >0.3). Nor did it reduce the number or areal extent of the storms in the target area (number of damaged pads P–value 0.39), the number of villages claiming insurance damage (P–value 0.54), or the areal extent of insurance claims (P–value 0.41). However, there is strong support for concluding there was a real reduction in the intesity of the storms in the target area (P–values ≈ 0.1 or less) as indicated by all of the remaining hailpad and insurance parameters. These results are consistent with a seeding methodology that targets specific storms in or near the target area and reduces, but does not eliminate, hail in these storms rather than one which broadly seeds upwind in an effort to reduce the number of storms. It is also interesting to note that these lower P–values are associated with the parameters exhibiting the greatest reductions.

Hailstone size distributions showed clear evidence of beneficial treatment effects. Target counts ranged from 38 to 100% less than control counts in all 12 size categories, with an average reduction of 55%. On an annual basis, P–values of the treatment effect ranged from 0.002 to 0.02. The P–value for the five–year experiment was 0.002.

To put the results of the program in Greece into perspective, let us summarize the results from a few of the other major hail suppression programs. Mather (1977) reported on the Nelspruit, South Africa project which used airborne AgI seeding from 1970–1977. He found reductions in hail damage of 48 to 59% with P–values of 0.01 using a non–randomized single target method. In Switzerland, the 1977–81 Grossversuch IV results, as originally reported by Mezeix and Caillot (1983), showed no increase or decrease in hail damage in a randomized single target method using rockets. The National Hail Research Experiment (Crow *et al.*, 1979) reported a 75% non–significant increase in damage using randomized airborne seeding. North Dakota reported reductions in insurance parameters as a result of seeding that ranged from 17 to 41% (Miller and Fuhs, 1987). In Alberta, the hail suppression project reported a qualified 20% reduction in the insurance loss–risk ratio that could be attributed to cloud seeding (Humphries *et al.*, 1987).

While the hailpad and crop insurance data for treated GNHSP hailstorms support a conclusion of reduced damage, there is a lack of direct physical evidence to substantiate the statistical reductions. Nonetheless, the evidence at hand suggests the following possible chain of events. Krauss and Papamanolis (1989) documented a narrow, continental cloud drop distribution. Cloud base temperatures near 10°C suggest that coalescence is not the dominant precipitation growth process and therefore substantial broadening of the spectrum is not expected to occur. Federer and Waldvogel (1978), for storms with similar mean cloud base temperatures and cloud top heights, and an active coalescence process normally leading to larger hail, found 5% of hailstones to be larger than 25 mm in diameter. Table 4 shows <0.2% of Greek control hailstones and <0.02% of target hailstones to be "large." This too, suggests coalescence is not the dominant process in most storms although conical, ellipsoidal, and spherical graupel embryos

have all been observed in Greek hailstones. In addition, GNHSP Λ values are somewhat smaller than those reported elsewhere. For example, Federer and Waldvogel (1978) indicated that an average value for Swiss hailstones is about 0.5 mm^{-1} and Cheng *et al.* (1985), showed a similar average number for Alberta hailstone size distributions. The combination of very low numbers of large stones and small Λ suggests relatively small n_0 values and low total hailstone numbers in natural Greek clouds. These factors suggest that Greek clouds are relatively inefficient, lending themselves well to a beneficial competition type of approach to seeding, and furthermore that the small stones are more likely to melt completely below cloud base.

Certainly, a great deal more remains to be learned about the hailstone formation process in Greece. The recent re-introduction of digitally recorded radar data on the GNHSP is a good step in that direction. A modest field program with an instrumented aircraft and time-resolved precipitation measurements would address several remaining questions about the statistical experiment.

Acknowledgments. The authors gratefully acknowledge the work and guidance of Dr. John Flueck who performed parts of the GNHSP hailpad analysis under contracts with both Atmospherics Inc. and Intera Technologies Ltd. and whose influence goes well beyond his cited references. We also thank the GNHSP controllers, pilots and hailpad network crews who performed their duties conscientiously. Dr. Larry Davis suggested examining the size distribution slope and intercept and we appreciate the comments of the two anonymous reviewers.

6. REFERENCES

Changnon, S., 1985: Use of crop-hail insurance data in hail suppression evaluation. *4th WMO Conf. Wea. Modif.*, Geneva, Switzerland, 563–567.

Cheng, L., M. English and R. Wong, 1985: Hailstone size distributions and their relatioship to storm thermodynamics. *J. Climate Appl. Meteor.*, **24**, 1059–1067.

Crow, E.L., A.B. Long, J.E. Dye, A.J. Heymsfield and P.W. Mielke, 1979: Results of a randomized hail suppression experiment in northeast Colorado, Part II, Surface data base and preliminary statistical analysis. *J. Appl. Meteor.*, **18**, 1538–1558.

Dalezios, N.R., M.V. Sioutas and T.S. Karacostas, 1991: A systematic hailpad calibration procedure for operational hail suppression in Greece. *Meteor. Atmos. Phys.*, **45**, 101–111.

Federer, B., and A. Waldvogel, 1978: Time-resolved hailstone analyses and radar structure of Swiss storms. *Quart. J. Roy. Meteor. Soc.*, **104**, 69–90.

Flueck, J.A., M.E. Solak and T.S. Karacostas, 1986: Results of an exploratory experiment within the Greek National Hail Suppression Program. *J. Wea. Mod.*, **18**, 57–63.

Henderson, T.J., 1986: The hail suppression program in Greece. *J. Wea. Mod.*, **18**, 51–56.

Karacostas, T.S., 1984: The design of the Greek National Hail Suppression Program. Preprints, *9th Conf. Wea. Modif.*, Park City, UT, Amer. Meteor. Soc., 26–28.

_____, 1989: The Greek National Hail Suppression Program: Design and conduct of the experiment. Preprints, *5th WMO Sci. Conf. Wea. Modif. and Appl. Cloud Phys.*, Beijing, China, 605–608.

Humphries, R.G., M. English and J. Renick, 1987: Weather modification in Alberta. *J. Wea. Mod.*, **19**, 13–24.

Krauss, T.W., and N. Papamanolis, 1989: Precipitation formation processes within hailstorms of northern Greece. Preprints, *5th WMO Sci. Conf. Wea. Modif. and Appl. Cloud Phys.*, Beijing, China, 321–324.

Lozowski, E.P., R. Erb, L. Wojitiw, G.S. Strong, R. Matson, A. Long, D. Vento and P. Admirat, 1978: The hail sensor intercomparison experiment. *Atmos.-Ocean*, **16**, 94–106.

Mather, Graeme K., 1977: An analysis of a possible crop response to hail suppression seeding: The Nelspruit hail suppression project. *J. Appl. Meteor.*, **16**, 959–970.

Mezeix, J-F., and P. Caillot, 1983: A confirmatory evaluation of the Grossversuch IV experiment using hailpad data (French network 1977–1981). *J. Wea. Mod.*, **15**, 1–6.

Miller, J.R., and M.J. Fuhs, 1987: Results of hail suppression efforts in North Dakota as shown by crop hail insurance data. *J. Wea. Mod.*, **19**, 45–49.

Rudolph, R.C., C. Ganniaris-Papageorgiou, C. Boufidis and J. Flueck, 1989a: Hellenic National Hail Suppression Program – summary of exploratory statistical results. Preprints, *5th WMO Sci. Conf. Wea. Modif. and Appl. Cloud Phys.*, Beijing, China, 621–624.

_____, C.M. Sackiw, T.W. Krauss and A.G. Davis (eds), 1989b: Greek National Hail Suppression Program 1988 Annual Report. Agricultural Insurance Institute (EL.G.A.) Athens, Greece, 280 pp.[available from EL.G.A., Patission 30, Athens].

_____, and C. Gannaris-Papageorgiou, 1991: Effects of cloud seeding on hail insurance statistics in northern Greece. Preprints, *2nd Yugoslav Conf. Wea. Modif.*, Mavrovo, Yugoslavia, 202–209.

Sackiw, C., 1991: Statistical evaluation of hailpad data from a five-year randomized crossover cloud seeding experiment. Preprints, *2nd Yugoslav Conf. Wea. Modif.*, Mavrovo, Yugoslavia, 263–273.

Smith, P.L., 1982: On the graphical presentation of raindrop size spectra. *Atmos.-Ocean*, **20**, 4–16.

_____ and A. Waldvogel, 1989: On determinations of maximum hailstone sizes from hailpad observations. *J. Appl. Meteor.*, **28**, 71–76.

Solak, M.E., D.C. Melita, R.B. Allan, T.J. Henderson, D.W. Duckering and S.D. Pinion, 1985: A summary of cloud seeding activity including operations, maintenance, data collection and analysis, a randomized exploratory experiment, evaluations, and the conduct of a training program for the Hellenic Republic during the periods May-September 1984 and 1985 and an independent statistical analysis by John A. Flueck. Prepared for and available from the National Agricultural Insurance Institute (OGA, now EL.G.A.), Division of Economic Services. Patission 30, Athens. 201 pp.

TESTING OF DYNAMIC COLD-CLOUD SEEDING CONCEPTS IN THAILAND
PART I: EXPERIMENTAL DESIGN AND ITS IMPLEMENTATION

William L. Woodley[1], Daniel Rosenfeld[2], Warawut Khantiyanan[3]
Wathana Sukarnjanaset[3], Prinya Sudhikoses[3] and Ronit Nirel[4]

[1] Woodley Weather Consultants, Littleton, Colorado
[2] Dept. of Atmospheric Sciences, Hebrew University of Jerusalem, Israel
[3] Royal Rainmaking Research & Development Institute, Bangkok, Thailand
[4] Dept. of Statistics, Hebrew University of Jerusalem, Israel

Abstract. Dynamic, cold-cloud, seeding concepts are being tested in Thailand in the context of the Applied Atmospheric Resources Research Program (AARRP). This work was conducted under a contract with the Bureau of Reclamation as part of a U.S. Agency for International Development-sponsored program to upgrade Thailand's weather modification capability. The AARRP is a component of Thailand's national program of weather modification under the direction of the Royal Rainmaking Research Development Institute (RRRDI). Part I focuses on the design and execution of the Thai, exploratory, randomized, cold-cloud experiments and on the conceptual model that is guiding these investigations. The treatment units for these experiments are the convective cells, which contain cloud towers that meet the liquid water and updraft requirements. In the Thai design, it is the cell that receives the on-top silver iodide treatment, and any effect of seeding should manifest itself first on this scale before it is seen in the experimental unit that contains the cells. The experimental unit consists of the small multiple-cell convective system located within a radius of 25 km and centered at the location of the convective cell that qualifies the unit for the first treatment. Evaluation of the experiments is to be accomplished using an S-band (10-cm) radar that is located near Omkoi in northwestern Thailand.

Fifteen experimental units (8 Seed and 7 No Seed) have been obtained to date, and they appear to be well-matched. Bias does not appear to have been a factor in the selection of these random cases and in the subsequent cloud treatments. Evaluation of these units and the convective cells contained within them is presented in Part II.

1.0 HISTORICAL BACKGROUND

Since the late 1960's, scientific and technical organizations in the Kingdom of Thailand have been involved with a series of experiments and operational programs to increase rainfall through cloud seeding. This effort has been under the direction of His Majesty King Bhumibol Adulyadej. A national program of weather modification under the direction of the Royal Rainmaking Research Development Institute (RRRDI) was formalized in 1975.

Since program inception, RRRDI leadership has attempted to improve the effectiveness of their program by taking advantage of the latest scientific findings. In recent years, His Majesty the King recognized the need for the development and implementation of a more comprehensive scientific approach to the design, operation, and evaluation of Thailand's weather modification program. Therefore, the Royal Thai Government (RTG) requested assistance of the U.S. Agency for International Development (USAID), which agreed to sponsor a visit by a team of experts to assess the RRRDI program and make suggestions for improvements. This assessment, which was conducted under the auspices of the U.S. Bureau of Reclamation at the request of USAID, was made by four scientists who visited Thailand from 7-26 September 1986. Their assessment and recommendations are contained in a report entitled "Weather Modification Assessment: Kingdom of Thailand" (Silverman et al., 1986).

The report recommended a comprehensive 5-year developmental program to improve the technical capabilities of the RRRDI through training, additional equipment and a demonstration cloud seeding project. These recommendations were accepted by USAID and a new, broadly-based program known as the Applied Atmospheric Resources Research Program (AARRP) was established.

Subsequent to the report by Silverman et al. (1986), a core training course was conducted in February and March 1988 to acquaint AARRP participants with the scientific principles, terminology and technology of weather modification as a water augmentation tool. Simultaneous with and following this training, a number of studies were conducted in preparation

for the demonstration cloud seeding project. These are described in a report by Medina et al. (1989).

The basic concepts to be tested in Thailand, involving either warm-cloud seeding to increase the coalescence of liquid drops or cold-cloud seeding to produce dynamic effects and increased rainfall, were investigated using a number of cloud models. The model runs indicated that both seeding approaches have potential for increasing rainfall in Thailand and that perhaps 35 percent of the potential operational days might be suitable for seeding for dynamic effects.

Preliminary work on the design of the demonstration extended beyond the numerical studies of possible responses to seeding. After visiting potential experimental sites, officials of the RRRDI and Reclamation selected the Nám Mai Tun River area of western Thailand for the conduct of the demonstration project (Figure 1). The Field Operations Center was located first (1991) at the Bhumibol Dam site and later (1992) moved to Chiang Mai Airport, and a weather radar was installed in 1991 at a site about 9 kilometers southeast of Omkoi on a ridge (height 1,160 m) which provides a good view of the Nam Mai Tun River drainage.

Part I focuses on the design and execution of the Thai experiments and on the conceptual model that is guiding these investigations. Part II presents the initial results of this experimentation. This work was done under a contract with the Bureau of Reclamation as part of a program sponsored by the U.S. Agency for International Development to upgrade Thailand's weather modification capability.

2.0 SUMMARY OF RESULTS OF RELEVANCE TO THAILAND

The most systematic investigation of the potential of "dynamic seeding" for rainfall enhancement began in clouds over the Caribbean Sea in the mid-1960's (see Simpson et al., 1967) and continued in Florida in the series of experiments that came to be called the Florida Area Cumulus Experiment (FACE). Although the FACE program did not provide conclusive proof that seeding had increased the areal precipitation, the estimated rainfall increases ranged between 10 and 25% for the target area covering 1.3×10^4 km^2 and between 20% and 50% for groups of treated convective clouds within the target area (called the "floating target") (see Woodley et al., 1982; 1983).

The FACE program also provided strong evidence for substantial increases in rainfall from individual convective clouds and cells. The first experiment (in 1968 and 1970) indicated that the rainfall from individual clouds could be increased by over 100% (Simpson & Woodley, 1971). A

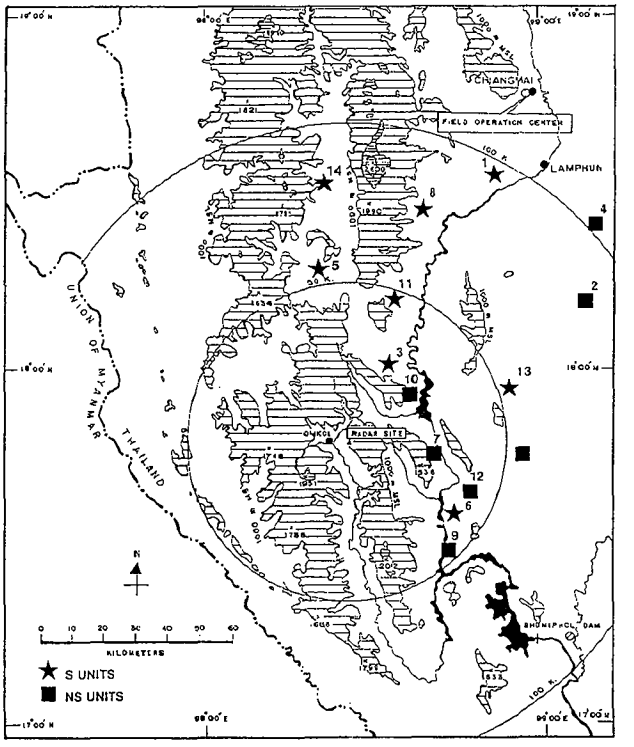

Fig. 1. Map of the project area. The range rings (in km) are relative to the AARRP radar. The locations of each experimental unit are plotted on the map as either solid squares (NS cases) or stars (S cases). The numbers identify the units in the order that they were qualified, beginning in 1991. See Table 3 for listing.

major breakthrough in the second of the two experiments (in 1978-1980) was made with the development of a sophisticated method to identify, track and assess the properties of the treated clouds throughout their lifetimes. Use of this technique permitted a more comprehensive analysis of the effect of seeding on the individual convective cells. Again, the results indicate rain increases of over 100% (Gagin et al., 1986).

These results for tropical clouds in Florida provided the impetus for continuation of dynamic seeding research in Texas. The Texas research to date indicates that dynamic seeding has enhanced the rainfall from individual cells by over 100%, thereby replicating many of the Florida results. In addition, rain increases of 25-30% are indicated for the experimental unit (i.e., the small mesoscale convective cluster) that covers

nearly 2,000 km^2 (Rosenfeld and Woodley, 1989, 1993). This effort is continuing.

In summary, the scientific evidence from cloud seeding research programs in Florida and Texas that have employed dynamic seeding techniques indicates that rainfall can be increased from convective clouds by over 100% on the scale of individual cells, by 25 to 50% percent on the scale of groups of convective clouds and by 10% to 25% over targets up to 13,000 km^2 in size. The strength of the evidence for enhanced rainfall decreases, therefore, as the scale of the rainfall increases. The evidence is strongest for individual cells where the seeding signal is largest and weakest for large target areas where the seeding signal is small.

3.0 THE DYNAMIC SEEDING CONCEPTUAL MODEL

The revised dynamic seeding conceptual model has been discussed recently by Rosenfeld and Woodley (1993). The main departure of the new dynamic seeding model from the "classical" model of the past (Woodley, et al., 1982) is the realization that dynamic seeding can also produce a substantial increase in convective rainfall without a large increase in the maximum height of the seeded entity.

The steps in the new conceptual chain are supported by new and old scientific findings from a number of research projects. These findings have been combined with the new results to synthesize a revised conceptual model for dynamic seeding, that in no way contradicts the precepts of the old, but merely builds and expands on them in places where physical insight was lacking.

In building on the conceptual models that guided the Florida and Texas experimentation, it is suggested that seeding for dynamic effects operates to produce more rain from individual cells and groups of cells through the following steps that are listed in Table 1:

Table 1

CONCEPTUAL MODEL FOR DYNAMIC CLOUD SEEDING
(Revised as of July 1992)

Lifecycle Stages of Suitable Unseeded Clouds

1. Cumulus Growth Stage
Warm-based growing cumulus cloud with vigorous updraft and active warm-rain processes.

2. Supercooled Rain Stage
Active updraft thrusts large amounts of supercooled rain and cloud water from the 0°C level toward the -10°C level. This is the seeding time window.

3. Cloud Rainout Stage
Increased drop sizes and precipitation loading causes most of the supercooled rain to fall back into the warm portions of the cloud without freezing; that which remains glaciates. The falling rain suppresses the lower portions of the updraft, thus terminating the growth of the cloud.

4. The Downdraft Stage
The rain and associated downdraft reach the surface, resulting in a short-lived rain shower and gust front.

5. The Dissipation Stage
The cloud dies.

The above sequence of stages is an idealization. Dissipation may follow the glaciation stage of seeded clouds or any subsequent stage, if the required conditions are not present.

Lifecycle Stages of Clouds Following Seeding

Cloud-top seeding to produce a vertical curtain of ice nuclei is done at the **Supercooled Rain Stage**, such that the nucleant is dispersed in the supercooled volume as it ascends through the -10°C level.

3. Glaciation Stage
The raindrops freeze and continue their growth as graupel particles with increased growth rates and reduced fall velocities. All or a portion of the released latent heat supports the increased precipitation loading. Leftover buoyancy induces added vertical cloud growth. This prolongs the updraft at lower levels, which carries additional water into the supercooled region to increase precipitation mass.

4. Unloading Stage
The increased precipitation mass eventually descends. The unloaded cloud top, which still contains some of the released latent heat, renews its vertical growth, producing additional ice precipitation. In many cases, this cloud tower reaches cumulonimbus stature. The unloaded precipitation initiates a downdraft at the lower levels.

5. Downdraft and Merger Stage
The enhanced precipitation and downdraft reaches the surface, resulting in increased outflow, increased convergence at the gust front, new cloud growth and merger.

6. Mature Cumulonimbus Stage
Growth continues in the convergent regions, leading to an expansion of the cloud system and the formation of a mature cumulonimbus system.

7. Convective Complex Stage
Application of seeding to several suitable towers results in additional cloud growth and merger, leading potentially to a small mesoscale convective system and greater overall rainfall.

This is an idealized sequence of events. Dissipation may follow the glaciation stage or at any subsequent stage, if the required conditions are not present.

It is important to note that the above model applies to convective clouds in which the coalescence process is active to produce rain drops in the supercooled region. It is the freezing of these raindrops that produces the bulk of the fusion heat release (see Lamb et al., 1981). A useful guideline for distinguishing between clouds that are likely to produce supercooled rain and those that will not, involving parcel buoyancy at 500 mb and cloud-base temperature, is provided by Mather et al. (1986).

This conceptual model applies optimally to clouds having mean updrafts strong enough to carry the rainwater to temperatures where it can be nucleated artificially but not having updrafts strong enough to carry the rainwater to heights where the temperature is cold enough for complete natural freezing. The updraft velocities should be at least comparable to the terminal fall velocity of the raindrops at that level (i.e., about 10 m/sec). Assuming that the rate of ascent of cloud top is half the peak updraft velocity, a minimum of 5 m/sec vertical growth rate is required for the cloud top, while growing through the 0 to -10C levels. This means that a suitable cloud must cover the 1600 m vertical distance that normally exists between the 0°C and -10°C levels in at most 5 minutes.

To be effective, several seeding flares should be ejected into the updraft region to ensure that the freezing will be completed before the updraft begins to wane. Although one flare contains a sufficient number of ice nuclei to seed a typical updraft, there may not be enough time to disperse this material within the updraft during the short time (< 5 min) that the supercooled rainwater exists at the seeding level.

The consequences of seeding too late in the life cycle of a cloud is usually accelerated dissipation. This occurs when a mass of supercooled rainwater is glaciated artificially without an attendant updraft. The released heat, which is not sufficient to re-generate a significant updraft, remains aloft while the frozen precipitation continues downward. When this frozen precipitation eventually melts and cools the cloud, it destroys the updraft and/or enhances the downdraft, resulting in the destruction of the cloud.

It must be emphasized that artificial seeding merely imitates a natural process, which is often the mechanism that transforms cumulus convection to cumulonimbus convection. Seeding is most effective, however, when this transformation is unable to proceed naturally. It is crucial, therefore, that seeding tests be conducted during these marginal conditions and not when deep, vigorous, natural cumulonimbi are prevalent.

This rather complex conceptual model is backed by observations that taller convective cells precipitate more. Observations of natural convective rain clouds in Florida (Gagin et al., 1985) and in Texas (Rosenfeld and Woodley, 1989) indicate that an increase of cell top height by 20% nearly doubles its rain production. If a seeding-induced enlarged cloud behaves as a natural cloud reaching the same top height, the rainfall from the treated cloud will be increased accordingly. This was nearly the case in two Florida studies (Simpson and Woodley, 1971; Gagin et al., 1986), where 20% increases in mean cell height explained about 70% of the factor of 2.60 seeding effect on the rainfall.

This has not been the case in Texas, however, where it now appears that more than a doubling of the rainfall has been associated with only about a 7% increase in mean maximum cell height. This finding in conjunction with the evidence that seeded clouds in Texas produce more rainfall than unseeded clouds of the same height suggest that additional physical processes are at work in enhancing the rainfall by seeding. These have been addressed in the new model.

The revised conceptual model is different from the original model in several important respects. It was assumed implicitly in the early model that the AgI treatment would produce high concentrations of very small ice crystals and, in effect, "overseed" (i.e., too many nuclei for the available water supply) portions of the treated volume, resulting in less efficient precipitation processes. This possible outcome was viewed "as a small price to pay" in exchange for the release of fusion heat that would lead eventually to a larger, longer-lasting cloud in which natural precipitation processes would dominate.

More recent thinking, however, suggests that this "over-seeding" concept may not be valid in vigorous warm-based clouds (Rokicki and Young, 1978). A large amount of supercooled water normally exists at the seeding level in such clouds. Although seeding produces an obvious glaciation signature (Sax et al., 1979), it is rare to encounter an extensive overseeded region. The normal circumstance in cloud immediately following seeding is a mix of cloud water, seeding-induced ice crystals and raindrops, a situation that should be conducive to the formation of graupel through the aerodynamic capture of the ice crystals by the raindrops which then

freeze (Lamb et al., 1981). Under such circumstances, much of the cloud's water mass may be intercepted before it can be evacuated in the anvil.

Once the enhanced graupel mass exists, Johnson (1987) indicates that the graupel will fall slower and grow faster than water drops of comparable mass. This means that the seeding-induced graupel will reside in the cloud tower longer and achieve greater size than a population of water drops within a similar unseeded cloud.

This effect is consistent with the increased reflectivity aloft after seeding, accompanied by some decrease of reflectivities at lower levels. This area of larger reflectivity reaches cloud base as additional rainfall about 40 minutes after initial seeding. Bruintjes et al. (1992) have also noted increases in the reflectivities aloft after seeding clouds in South Africa, which he attributes to the same effect of conversion from rain to graupel, as suggested by Johnson (1987).

The increased precipitation loading in the seeded tower will require greater cloud buoyancy and a stronger updraft to keep it aloft. It is possible, therefore, that some of the increased buoyancy in Texas clouds is expended in carrying the larger precipitation load, leaving little buoyancy left over for the production of higher cloud tops. In Florida, however, the fusion heat releases should be higher because of higher rainwater contents. This may allow seeded Florida clouds to carry the increased precipitation load and still have enough buoyancy left for additional vertical cloud growth. Only with numerical cloud modeling with explicit microphysics will it be known for sure.

The retention of the increased ice mass high in the cloud is an important new aspect of the dynamic seeding conceptual model. It may help explain how an effect of seeding is communicated immediately to the rest of the cloud. If the precipitation mass can be held aloft as a result of the seeding, the downdraft is delayed. This provides additional time for the growth of the cloud tower. Only until this precipitation mass begins to move downward is the updraft in jeopardy. Under conditions of vertical wind shear, the precipitation may fall adjacent to the parent updraft and not disrupt it. In addition, the decreased precipitation loading in the cloud tower that formerly contained the water mass may allow it to renew its growth to greater heights, possibly reaching cumulonimbus stature. This second surge of growth is a common phenomenon in natural clouds, especially in the tropics where warm-rain processes are most active. Seeding may also produce this second surge of growth in clouds that could not have done so naturally.

There is no doubt that downdrafts are vitally important to the development of a cloud system. This is why the dynamic seeding conceptual model incorporates the ideas of Simpson (1980), regarding the role of the downdraft following seeding. It is doubtful, however, that the downdraft can explain the explosive initial growth of the seeded tower that sometimes occurs following seeding, since this growth often occurs prior to or simultaneous with the rain reaching the ground.

Evidence in support of the portion of the conceptual model dealing with increased cloud growth, greater cloud duration, more mergers and additional rainfall has been presented earlier by Rosenfeld and Woodley, 1989; 1993). The observational evidence to date clearly supports these links in the conceptual chain.

4.0 DESIGN OF THE THAI COLD-CLOUD EXPERIMENTS

4.1 Aircraft and Radar Systems

An Aero Commander 690B turbo-prop aircraft was provided to the RRRDI and its AARRP effort under lease from Thai Flying Service. This turbo-prop aircraft was equipped with an airborne data acquisition and seeding system and served as the cloud physics platform and seeder for the program. In addition to standard avionics and flight instrumentation, the Aero Commander was equipped with the following instrumentation: a Johnson-Williams-type liquid water content meter manufactured by Cloud Technology, Inc., a thermo-electric dew point hygrometer, a reverse flow thermometer, a Ball variometer and a satellite-based (GPS) navigation system that permits location of the aircraft to within 100 m. A forward-looking nose video camera was mounted in the cockpit and provided a continuous view of cloud conditions during flight through the extreme right side of the windshield.

The liquid water hot wire and the Ball variometer were configured to measure water contents and draft speeds up to 6.0 gm/m^3 and 2,000 ft/min, respectively. No Thai cloud had water contents approaching 6.0 gm/m^3, so this threshold was never exceeded. Many Thai clouds did, however, have drafts exceeding 2,000 ft/min, particularly during pre-monsoon conditions, so the measured maxima and the calculated mean maxima are underestimates of the true values.

The main operational and research radar for the AARRP effort is an Enterprise Electronics Corporation (EEC) Model DWSR-88S S-band (10-cm) Doppler Weather Surveillance Radar with a 1.2° conical beam. The AARRP radar is situated on a hill 9 km southeast of Omkoi (17° 47'54"N; 98° 25'57"E) at an elevation of 1,160 m. The surrounding terrain is below

1° elevation except between 225° and 275° azimuth, where one hill top extends up to 2.3° elevation. During the program the radar was operated 24 h per day in either the surveillance or volume-scan modes. The characteristics of this radar are provided in Table 2.

Table 2

Characteristics of Thailand's DWS-88S Doppler Weather Radar*

Frequency	2.7-2.9 GHz
Wavelength	10.8 cm (S-band)
Peak Trans. Power	500 kW
Pulse Dur. (width)	2.0 μs for intensity mode (reflectivity) 0.8 μs for velocity mode
Pulse Rep. Freq.	250 pulses/sec for intensity mode Dual 600 to 1000 pulses/sec for velocity mode
MDS	-106 dBm
Antenna diameter	6.1 m (beamwidth approximately 1.2°

* Manufactured by Enterprise Electronics Corporation

4.2 Experimental Layout

The Thai experiments were carried out in accordance with the Design Document and AARRP Operations Plans by Woodley et al. (1991). This was an exploratory experiment and the design changed slightly from 1991 to 1993 as is characteristic of exploratory efforts. The treatment decisions were randomized on a unit-by-unit basis and all suitable convective cells within the unit received the same treatment -- silver iodide (AgI) in the case of a seed (S) decision or simulated AgI in the case of a no seed (NS) decision.

The selection of the experimental unit was based upon the following requirements:

1. The qualification cloud must have a maximum (1-sec values) liquid water content $\geq$ 1.0 g m^{-3} and a maximum (1-sec value) updraft $\geq$ 1,000 ft min^{-1} (i.e., $\geq$ 5 ms^{-1}), as determined from real-time readouts aboard the aircraft.

2. The experimental unit consists of the small multiple-cell convective system located within a radius of 25 km and centered at the location of the convective cell that qualified the unit for the first treatment.

3. All cells within the experimental unit at the time of initial treatment had to have echo tops $\leq$ 10 km AGL.

4. At least some of the subject cells had to have top temperatures of -10°C or colder.

5. At the time of selection, the center of the experimental unit had to be at least 40 km from cumulonimbus clouds, displaying radar reflectivities of 50 dBz or greater in the vicinity.

During the experimentation on a particular experimental unit, the following requirements applied:

1. The center of the experimental unit is to be positioned at the location of the qualification pass of the aircraft. This position is to be advected with time with the mean direction and speed neighboring convective cells.

2. All untreated cells contained entirely within the 25-km circle become potential seeding targets and, by definition, become a part of the experimental unit.

In the Thai design, therefore, the treatment units are the convective cells, which contained cloud towers that met the liquid water and updraft requirements. It is the cell that receives the treatment, and any effect of seeding should manifest itself first on this scale before it is seen in the experimental unit that contains the cells.

Prior to commencement of the 1993 experiments, it was decided to allow for relaxation of the stringent requirements for qualification of an experiment. Specifically, the 1.0 gm/m^3 requirement was relaxed to 0.5 gm/m^3 and the requirement that no cell within the unit shall have an echo top exceeding 10 km was eliminated, as was the 40 km separation distance between the center of the prospective unit and nearby 50 dBz cores. This was done in the hope of qualifying more units with the intention of stratifying them later during the analysis phase.

During the actual experimentation, however, the flight scientists "attempted to play by the old rules." As best can be determined, all units were qualified by the old protocol with no loss in unit qualifications as a consequence of adhering to the old qualification rules.

The randomized seeding instructions for the single-cell experiment were prepared by the Bureau of Reclamation in Denver, Colorado, USA. In 1991, the blocking of the randomization was based on the time that the first cumulonimbus echo in Thailand, having a top exceeding 10 km, formed within 159 km of the radar. There were three blocks:

Block 1 - Used on days when the first

Cb echo forms in the study area prior to 1300 LST.

Block 2 - Used on days when the first Cb echo forms in the study area after 1300 but before request for a treatment decision.

Block 3 - Used on days when no Cb echo has formed in the study area prior to request for a treatment decision.

This blocking scheme was developed to account for the fact that the weather is different on days with early deep convection from days on which deep convection is delayed until late in the day.

By 1993, however, the view prevailed that the blocked randomization was too complex for the initial Thai experiments. A new set of randomized instructions without blocking was prepared and used in the 1993 experiments. Thus, only one experimental unit was qualified with the blocked scheme and 14 were qualified with the simple randomization.

The AgI nucleant that was used in this experiment was the EJ-20-E-20 type FA6 formulation manufactured by Atmospherics Inc., in Fresno, California, USA. This flare is complexed with chlorinated hydrophilic material that allows it to nucleate at a faster rate (i.e., 90% activation in the first 3 min) than the modified TB-1 formulation (i.e., 10% activation in the first 3 min) that has been used in Texas. According to tests at the Cloud Simulation and Aerosol Laboratory at Colorado State University, the EJ-20/FA6 and the modified TB-1 flares produce about 3 x 10^{14} and 8 x 10^{14} ice crystals per gram of silver iodide, respectively, at -10°C. Both flares yield about 10^{13} ice crystals per gram of silver iodide at -7°C (Figure 2).

The flares were ejected at the seeding flight altitude (normally 21,500 ft) from the project Aero Commander 6903 turbo-prop aircraft. When ejected at seeding altitude, each flare normally burns for at least 50 sec and falls more than 1.5 km in still air. The actual fall distances were likely less because the flares normally were dropped into vigorous updrafts. The seeder aircraft carried 200 20-gm flares on each flight.

5.0 EXPERIMENTAL PROCEDURES

During the randomized experimentation, suitable supercooled convective cloud towers within the convective cells received either simulated AgI treatment or actual AgI treatment near their tops (typical tops heights of 6.0 to 7.0 km and top temperatures -7°C to -9°C). Between 1 and 10 flares normally were ejected during a seeding pass. The flare ejection button was pressed approximately every second while the cloud liquid water

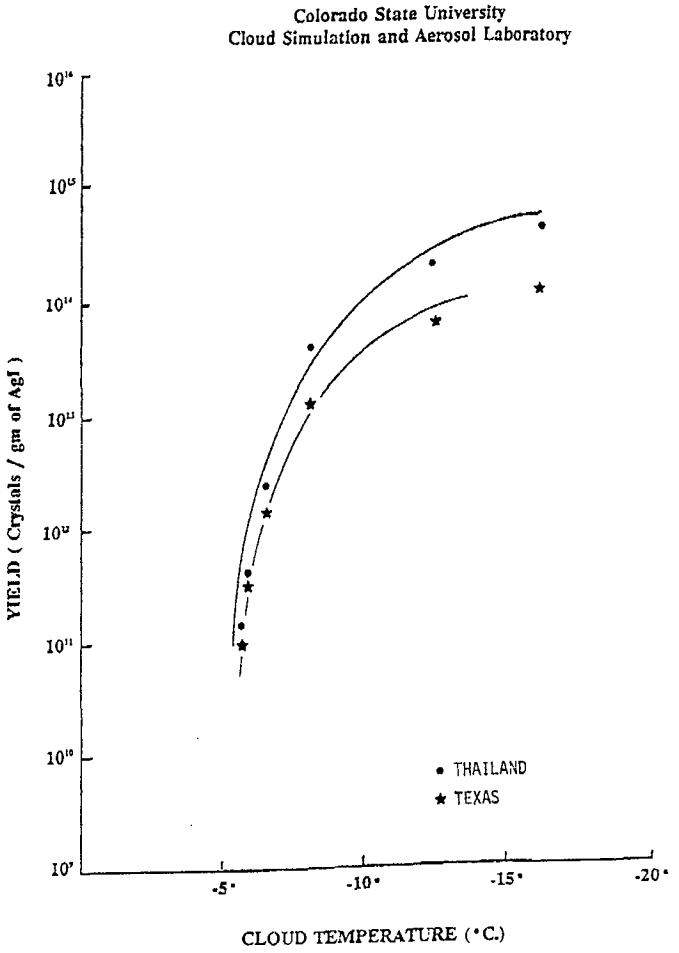

Fig. 2. The yield in ice crystals per gram of silver iodide as a function of temperature for two pyrotechnic formulations produced by AI, Inc. of Fresno, CA. The top curve corresponds to the EJ-20/FA6 flare that is used in Thailand and the bottom curve corresponds to the modified TB-1 flare that is used in Texas. The tests were performed in the Cloud Simulation and Aerosol Laboratory at Colorado State University in Ft. Collins, CO.

reading was greater than 0.5 g/m^3 and the aircraft was in updraft (the 1.0 gm/m^3 and 5 m/sec requirement applied only to the initial qualification pass). In some cases, seeding or simulated seeding was done 1,000 ft or less over the top of an especially vigorous hard tower, when previous cloud passes on a particular day had established the suitability of the subject clouds. In the simulated seeding passes no flares were actually ejected when the button was pressed, but the event was still recorded in the aircraft data system by activating an event switch.

The treatment decision for each experimental unit was revealed after the qualification pass. This was done to maximize the learning experience of the Thai scientists and to avoid the extra costs that would have been incurred through the use of placebo flares. This decision is not without its risks, however, since knowledge of the treatment decision could result in inadvertent bias either in the conduct of a given experiment and/or in the selection of the next experimental unit. This potential problem is discussed in more detail in the next section.

Once the decision on a particular unit had been made, it was irrevocable, and could not be changed, nor could the unit be eliminated from the sample. Only failure of the radar can result in elimination of a unit from the sample. Without the radar, no rainfall data will be available to evaluate the unit.

During the operations the pilots and flight scientists attempted to make certain that all seeding or simulated seeding passes took place within the confines of the experimental unit (i.e., within 25 km of the qualification point). The "cloud pointer" on the aircraft was used to mark the position of the qualification pass, and this pointer was used to keep the aircraft within the unit. As the unit moved, however, the flight scientist sought a new center position from the radar operator, who was plotting the unit on the radar display and moving it along with the motion evident in the radar echoes nearby. This position was then used to update the pointer aboard the aircraft.

Regardless of the treatment decision, the flight patterns were essentially the same. The object was to recognize what nature was trying to do with a particular cloud or cloud group and then seeding to enhance the natural tendencies. This usually required multiple passes through suitable young towers growing on the upshear flanks of the parent cloud, and the ejection or simulated ejection of about 1 AgI flare per sec while in suitable conditions.

Doing the seeding within young vigorous clouds, as they moved through the treatment level, required teamwork between the flight scientist and the pilots. Care was taken not to fly into mature large clouds that could have beat up the aircraft and were not suitable for seeding in any case. This generally meant that young upshear towers were worked at angles to the shear vector, so that the large cloud, which was normally downshear, was not penetrated. The echo cores could be located on the aircraft radar. Most cloud towers more than 5,000 ft above the aircraft already had echo cores and were unsuitable. Flight patterns requiring a 90° left turn and then a 270° degree right turn (or vice versa) frequently were helpful, as were race-track patterns that permitted visual monitoring of the cloud on one of the legs of the racetrack and repenetration of suitable towers and seeding on the other. Sometimes no set patterns were possible because of intervening cloud clutter, and the aircraft was flown in whatever way necessary to get the job done.

A good unit was one that had a treatment duration of at least 1 hour following qualification and had 20 to 30 treatment passes, which resulted in the ejection or simulated ejection of 100 or more AgI flares. This could not always be controlled, however, and one was left to make the best of a particular situation.

Seeding continued in the unit as long as there were suitable towers, regardless of the treatment decision. There was no set limit to the duration of seeding and to the amount of nucleant that was expended in each experimental unit. As long as cloud conditions were suitable, treatment continued. In a few cases treatment was terminated, when the aircraft ran out of fuel and/or the experimental unit moved beyond 159 km quantitative range from the radar.

6.0 OPERATIONAL SUMMARY

One experimental unit was qualified in 1991 and 14 experimental units were qualified in 1993 for a total of 8 Seed and 7 No Seed units. Information for these cases is provided in Table 3, and a plot of their locations is provided in Figure 1. Further details are provided by Woodley and Rosenfeld (1993).

Although the Operations Plan allowed for relaxation of the qualification criteria that had been observed in 1991, it did not prove necessary. Only on April 21 was a unit qualified with a SLWC < 1.0 gm/m^3. The qualification value was 0.74 gm/m^3, but there is some uncertainty concerning the accuracy of this measurement, because the heater on the hot wire probe failed entirely three passes after the qualification pass. It is possible also that one cloud in the experimental unit of 9 May 1993 may have exceeded 10 km on its southern boundary for about 5 minutes around the time of the qualification pass.

Potential bias in the conduct and evaluation of a cloud seeding experiment should be evaluated wherever possible. It is important, therefore, to determine whether bias may have played some role in the Thai cold-cloud seeding experiments. At this point there is no evidence that deliberate or unintended bias has been a factor in the selection of the random cases, at least for the qualification pass, as can be seen in Table 4 for which maximum SLWC and updraft have been listed.

Table 3

SUMMARY OF RANDOMIZED CASES

DATE	CLOUD BASE TEMP (°C)	TIME OF QUALIF PASS (LST)	POSITION OF QUALIF PASS (LAT; LONG)	TREATMENT DECISION (S OR NS)	# OF FLARES FIRED	# OF TREATED TOWERS	TIME OF 1ST TREATMENT (LST)	TIME OF LAST TREATMENT (LST)	TREATMENT DURATION (MINUTES)
8/7/91	22	15:34	18 34.8;98 51.6	S	29(29)	13	15:40	17:11	92
4/15/93	18	14:53	17 59.8;99 16.7	NS	45(0)	9	15:04	15:46	42
4/18	11	15:41	17 55.7;98 36.7	S	57(57)	12	15:45	16:33	48
4/20	15	15:19	18 13.6;99 17.3	NS	79(0)	13	15:30	16:36	66
4/21	15	13:59	18 16.8;98 21.0	S	112(112)	18	14:04	16:10	126
4/22	18	15:40	17 34.2;98 44.3	S	70(70)	13	15:47	17:11	84
4/23	18	14:20	17 45.0;98 41.0	NS	91(0)	17	14:27	16:19	112
4/25	16	14:45	18 27.4;98 36.2	S	118(118)	25	14:56	17:32	160
4/29	19	15:18	17 28.6;98 41.5	NS	96(0)	17	14:26	15:50	84
5/4	22	15:17	17 52.0;98 40.2	NS	57(0)	17	14:30	17:11	101
5/7	21	13:52	18 09.9;98 34.0	S	77(77)	18	14:02	15:46	104
5/8	15	14:50	17 38.3;98 44.7	NS	89(0)	18	14:59	17:20	141
5/9	18	14:26	17 50.6;98 56.8	S	156(156)	29	14:34	17:26	172
5/27	22	14:36	18 30.8;98 18.8	S	124(124)	25	14:47	17:15	148
6/4	21	15:08	17 41.7;98 57.4	NS	124(0)	22	15:13	17:42	129

Note: In the "# of Flares Fired" column, the first number for the Seed cases is the number of flares attempted and the second number in parentheses is the number of flares actually fired. For the Seed cases all of the flares did fire --- a remarkable performance for the seeding system. For the No Seed cases, the first number refers to the number of times that a toggle switch was activated to simulate seeding. Each activation was recorded by the data system. The second number in parentheses is zero (0), because no actual seeding was done and no flares left the rack.

Table 4

LISTING OF SLWC AND UPDRAFT VALUES
FOR THE QUALIFICATION PASSES

Seed Cases			No Seed Cases		
Date	Max SLWC (gm/m^3)	Max Updraft (ft/min)	Date	Max SLWC (gm/m^3)	Max Updraft (ft/min)
8/7/91	3.57	1300			
4/18	3.05	1100	4/15	1.89	2000+
4/21	0.74	1900	4/20	1.36	2000+
4/22	1.43	2000+	4/23	1.43	1400
4/25	1.47	2000+	4/29	1.61	2000+
5/7	1.17	2000+	5/4	1.07	2000+
5/9	1.20	1900	5/8	3.53	2000+
5/27	1.22	1600	6/4	1.45	1300
Avg.	1.73	1725	Avg.	1.77	1866

Table 5

LISTING OF THE ECHO DURATIONS WITHIN
THE EXPERIMENTAL UNITS
AFTER THE QUALIFICATION PASS

Seed Cases			No Seed Cases		
Time of No Echo	Qual. Time	Dur. (min)	Time of No Echo	Qual Time	Dur. (min)
2130	1534	356			
1715	1453	97	1650	1453	117
1900	1359	301	1710	1519	111
1955	1540	255	1750	1420	220
1715	1445	150	1901	1518	223
1820	1352	268	1740	1517	143
2031	1426	249	1715	1450	145
1728	1447	199	2155	1508	407
Means:		234			195

A second concern is whether the conduct of the experiment might have been biased after the treatment decision had been revealed. This possibility is more difficult to investigate, because the effect of seeding itself may be a confounding factor. For example, the mean number of AgI flares expended and simulated in S and NS units were 93 and 83, respectively. The corresponding mean treatment durations (i.e., time of last treatment minus time of first treatment) were 117 min and 96 min, respectively. Are these flare expenditure and treatment duration differences indicative of a bias in the conduct of the experiment, or do they indicate that the AgI-treated clouds last longer and provide more seeding opportunities?

Listed in Table 5 are the durations of echoes within each experimental unit after the qualification pass, obtained from the set of radar analyses to be discussed in Part II. Note that the 8 S units lasted 39 minutes longer on radar than the NS units. When the longest duration unit is eliminated from both the S and NS samples as a sensitivity test, the S vs NS disparity increases to 56 minutes. This indicates that the S systems lived longer and, thereby, provided more seeding opportunities. Although this result could have occurred by chance, it is consistent with an effect of seeding.

Looking further at the question of bias, the mean number of treatment passes per day are 19 and 16 for the S and NS cases, respectively. This is consistent, of course, with the longer treatment durations for the S cases. Some might still view it as an indication of bias. It is interesting, however, that the treatment rate (i.e., # of AgI or simulated AgI flares per pass) is virtually identical for the two treatment categories --- 4.9 flares per pass for the S cases and 5.2 flares per pass for the NS cases.

7.0 SUMMARY AND CONCLUSIONS

The Thai cold-cloud experiments have gone very well to date. The clouds are highly suitable microphysically for glaciogenic seeding intervention and they appear to be responsive to seeding as is described in Part II. The experimental design has been implemented without problem. Its great similarity to that for the Texas experiments (Rosenfeld and Woodley, 1993) will make it possible to compare the results for both regions. This is illustrated in Part II. Such an interactive process should enhance the learning experience for the scientists involved in both projects.

8.0 REFERENCES

Bruintjes, R.T., D.E. Terblanche, G.K. Mather, F.E. Steffans, L. van Heerden and L. Fletcher, 1992: Additional Evidence of Increases in Precipitation Due to Cloud Seeding of Summertime Convective Clouds over South Africa. Proceedings of Symposium on Planned and Inadvertent Weather Modification, 9 January 1992, Atlanta, Georgia, Sponsored by the American Meteorological Society., Boston, MA., 115-120.

Gabriel, K.R., and P. Feder, 1969: On the distribution of statistics suitable for evaluating rainfall stimulations. Technometrics, 11, 149-160.

Gagin, A., D. Rosenfeld and R.E. Lopez, 1985: The relationship between height and precipitation characteristics of summertime convective cells in South Florida. J. Atmos. Sci., 42, 84-94.

Gagin A., D. Rosenfeld, W.L. Woodley and R.E. Lopez, 1986: Results of seeding for dynamic effects on rain cell properties in FACE-II. J. of Climate and Appl. Meteor., 25, 3-13.

Johnson, D.B., 1987: On the relative efficiency of coalescence and riming. J. Atmos. Sci., 44, 1671-1680.

Lamb, D., R.I. Sax and J. Hallett, 1981: Mechanistic limitations to the release of latent heat during the natural and artificial glaciation of deep convective clouds. Quart. J. Roy. Meteor. Soc., 107, 935-954.

Mather, G.K., B.J. Morrison, and G.M. Morgan, Jr., 1986: A preliminary assessment of the importance of coalescence in convective clouds. J. Atmos. Sci., 20, 29-47.

Medina, J.G., R.M Rasmussen, A.S. Dennis and B.A. Silverman, 1989: Applied Atmospheric Resources Research Program in Thailand. Interim Scientific Report Submitted to the U.S. Agency for International Development Under Participating Agency Service Agreement No. ANE-0337-P-IZ-0821-00, 134 pp.

Rokicki, M.L., and K.C. Young, 1978: The initiation of precipitation in updrafts. J. Appl. Meteor., 17, 745-754.

Rosenfeld, D., 1987: Objective method for tracking and analysis of convective cells as seen by radar. J. Atmos. Sci., 4, 422-434.

Rosenfeld, D., and W.L. Woodley, 1989: Effects of cloud seeding in west Texas. J. Appl. Meteor., 28, 1050-1080.

Rosenfeld, D., and W.L. Woodley, 1993: Effects of cloud seeding in west Texas: Additional results and new insights. J. Appl. Meteor., 32, 1848-1866.

Sax, R.I., J. Thomas, and M. Bonebrake, 1979: Ice evolution within seeded and non-seeded Florida cumuli. J. Appl. Meteor., 18, 203-214.

Silverman, B.A., S.A. Changnon, J.A. Flueck, and S.F. Lintner, 1986: Weather Modification Assessment: Kingdom of Thailand, Bureau of Reclamation, Denver, Colorado, 117 pp.

Simpson, J., 1980: Downdrafts as linkages in dynamic cumulus seeding effects. J. Appl. Meteor., 19, 477-487.

Simpson, J., and W.L. Woodley, 1971: Seeding cumulus in Florida: New 1970 results. Science,172, 117-126.

Simpson, J., G.W. Brier, and R.H. Simpson, 1967: Stormfury cumulus seeding experiment 1965: Statistical analysis and main results, J. Atmos. Sci., 24, 508-521.

Woodley, W.L. and D. Rosenfeld, 1991: Testing Dynamic Seeding in Thailand. A Report to the U.S. Bureau of Reclamation on Contract No. 1-CS-81-17780. 78 pp.

Woodley, W.L. and D. Rosenfeld, 1993: Analysis of Randomized Experiments in Thailand. A Report to the U.S. Bureau of Reclamation on Contract No. 1425-3-CS-81-19050. 62 pp.

Woodley, W.L., J. Jordan, J. Simpson, R. Biondini, J.A. Flueck and A. Barnston, 1982: Rainfall results of the Florida Area Cumulus Experiment, 1970-1976, J. Appl. Meteor., 21, 139-164.

Woodley, W.L., A. Barnston, J.A. Flueck and R. Biondini, 1983: The Florida Area Cumulus Experiment's Second Phase (FACE-2), Part II: Replicated and confirmatory analyses. J. Clim. & Appl. Meteor., 27, 365-375.

Woodley, W.L., D. Rosenfeld, B. Silverman, and C. Hartzell, 1991: Design and Operations Plan for a Randomized Cold-Cloud Seeding Experiment Focused on Individual Convective Cells. July 1991. 126 pp.

TESTING OF DYNAMIC COLD-CLOUD SEEDING CONCEPTS IN THAILAND
PART II: RESULTS OF ANALYSES

Daniel Rosenfeld[1], William L. Woodley[2], Warawut Khantiyanan[3], Wathana Sukarnjanaset[3], Prinya Sudhikoses[3], and Ronit Nirel[4]

[1] Dept. of Atmospheric Sciences, Hebrew University of Jerusalem, Israel
[2] Woodley Weather Consultants, Littleton, Colorado
[3] Royal Rainmaking Research & Development Institute, Bangkok, Thailand
[4] Dept. of Statistics, Hebrew University of Jerusalem, Israel

Abstract. Part II provides the results of analyses of Thailand's randomized, exploratory, cold-cloud, seeding effort. The sample is small and caution should be exercised in interpreting the results of these analyses.

A total of 151 convective cells (87 seeded and 64 nonseeded) have been identified within the experimental units and their properties computed through analysis of three-dimensional, volume-scan, S-band radar data using cell tracking software. The results indicate that AgI seeding may have increased the maximum cell areas by 25%, durations by 14% and rain volumes by 69%. Little effect is indicated on maximum cell heights, which may be due in part to underestimation of the glaciated tops of AgI-treated clouds by the S-band radar. Additionally, within the height range of 7 to 11 km, seeded cells of a given maximum echo top produced more rain volume than unseeded cells of the same height. None of the results has strong statistical support.

Partitioning by cloud base temperature increased the apparent effect of seeding to 71%, 33% and 125% for cell areas, durations and rain volumes, respectively, within the warm base ($T > 16^{o}C$) partition. The apparent effect on maximum cell height is on the order of +6%.

The results for the small sample (i.e., 7 Seed and & 7 NS) of experimental units also show more S than NS rainfall. All results are comparable to what has been reported by the first two authors for a similar program in Texas, and are discussed in the context of the conceptual model guiding both experiments.

This work was conducted under a contract with the Bureau of Reclamation as part of a program sponsored by the U.S. Agency for International Development to upgrade Thailand's weather modification capability.

1.0 INTRODUCTION

Part I presented the historical and conceptual framework for the exploratory randomized cold-cloud seeding experiments in Thailand, a discussion of their design and procedures, and a description of the aircraft and radar systems that were available to the effort. The operational summary then provided the context for the analyses of the radar data that are discussed in this paper. The sample is quite small, which complicates the search for evidence of effects of silver iodide (AgI) treatment. Nevertheless, past experience elsewhere suggests that inference of seeding effects might be possible despite the limited sample.

The philosophy or approach to the analyses for seeding effects and their interpretation has the following components:

a) The results cannot depend on the approach to the analyses.

b) Statistically significant results should be evident ultimately, if the sample is large enough and if some means are found to account for the natural variability.

c) Seeding effects should be indicated in most of the analyses, even when no individual indication is statistically significant.

d) The results should be consistent with the conceptual model, or, if not, suggest a plausible alternative explanation.

e) The outcomes should be compatible with the findings in similar experimentation conducted elsewhere, especially that in Florida and Texas where the conceptual model and the design and its implementation are comparable to what has been done in Thailand.

In essence, therefore, the analysis process must not boil down to an exercise in statistics. All results must be plausible, reasonable and physically consistent, if they are to be believed.

This work was conducted under a contract with the Bureau of Reclamation as part of a U.S. Agency for International Development-sponsored program to upgrade Thailand's weather modification capability.

2.0 ANALYSIS OF THE RADAR DATA

The three-dimensional structures of the convective rain cells were monitored and recorded by the Enterprise S-band radar which was located at Omkoi (see Part I for specifications). The radar scanned the whole volume of the troposphere in the target area every 5 minutes. The recorded radar data are the primary source of information for the scientific evaluation of the effect of seeding.

The three-dimensional matrices of radar reflectivity factor, which were used in the next steps to specify the history of the three-dimensional structures of the cells, were saved in 5-minute time intervals. The data were already recorded by the SIGMET radar processor in dBz units.

The initial focus of this study is on individual convective cells within clouds and cloud systems rather than on multi-cell echoes, because the cell is the fundamental building block of all convective weather systems. As in earlier work (Gagin et. al., 1985 and 1986; Rosenfeld, 1987, Rosenfeld and Woodley, 1989, 1993), convective cells are defined as entities with at least three closed radar reflectivity isolines, spaced at 1 dBZ intervals, at the cloud-base level. All the radar echoes greater than 12 dBZ are partitioned between these entities, with the division lines coinciding with the trough lines on the reflectivity map.

A special method, developed by Rosenfeld (1987), for the study of cells that compose convective rain systems. This method consists of a package of computer programs that use pattern recognition techniques on three-dimensional digital radar data to identify the rain cells, track them with time and calculate their properties. The product of the computations is a comprehensive data base of physically meaningful properties of rain cells, which can be used to infer the internal structure and the dynamics of convective rain systems. This includes the production of time-height reflectivity cross-sections of the tracked cells, which are very useful to obtain a physical understanding of the precipitation evolution in the clouds.

The cell tracking programs produce a data base of the tracked cells. Their data base consists of tables of cell properties during their lifetimes. There are 90 INSTANTANEOUS values for each scan at which the cell was scanned by the radar (usually 5 minutes apart). Each cell also has LIFECYCLE values, which contain cumulative cell properties or the life-cycle maximum of the instantaneous properties.

It is possible to analyze the cell data with both the "short track" and "long track" approaches. The "short track" approach follows the cells until they either dissipate or merge with neighboring cells at a particular reflectivity contour. The "long track" is an objective approach that allows for cell tracking after merger. It appears to be superior to "short track", because it permits a more complete history of each cell (Rosenfeld and Woodley, 1989). This is the analysis emphasized in this paper.

A total of 151 cells were treated (AgI or simulated AgI) in 1991 and 1993 and subsequently tracked in the long-track analyses. These are the input data for the ensemble cell analyses that follow. All rainfalls were calculated from the reflectivity (Z) Rainfall Rate (R) relationship: $Z = 300R^{1.4}$, which was used by Woodley (1970) for radar estimation of rain from convective clouds over south Florida.

No analysis was possible for 18 April 1993 on which AgI seeding was done. The radar was not operated properly on this day, resulting in the loss of the data necessary to track the cells and calculate their properties. Thus, there are 14 experimental units (7 S and 7 NS) available for the inference of treatment effects. These are discussed in the next section.

3.0 SEARCH FOR EFFECTS OF COLD-CLOUD SEEDING

3.1 Statistical Significance Tests

The probability that the AARRP cell results are due to chance was calculated by a refinement of the Monte Carlo rerandomization test (Gabriel and Feder, 1969). This was done in the following steps:

a) A randomization reallocation of the experimental random cases to seeded (S) and non-seeded (NS) was made. All the treated cells in an experimental random case were assigned the same treatment which was drawn for the case.

b) The single ratio (SR) between all the S and NS cells, pulled together from all the S and NS randomized cases was calculated.

c) Steps a) and b) were repeated for 3000 permutations and a sorted vector of the SR's, obtained in the permutations, was produced.

d) The fraction (P, in %) of the randomly obtained SR's, which are larger than the observed one in the real experimental allocation, is the chance that the experimental result is due to the natural variability. This chance is referred to as the "significance level."

3.2 Results of the Cell Analyses

The mean cell properties for the Thailand data set are provided in Table 1. NS refers to cells that were not seeded and S to cells that received AgI treatment. NCLMAX is the mean maximum number of cells within each cell cluster. S/NS is the single ratio of S to NS cell properties and the significance of each observed SR was calculated using rerandomization procedures.

Examination of the presentation in Table 1 suggests that the S cells produced more rainfall than the NS cells by virtue of covering more area and having greater durations and larger rain volume rates. This result, while physically plausible and in agreement with the results in Texas (Rosenfeld and Woodley, 1989; 1993), could well be due to chance because of the small sample. No single result can be seen to have a significance value anywhere near 5%.

The next step was to examine only those cases having warm cloud bases, when coalescence would be more active and rainwater would be present in vigorous updrafts above the freezing level. It can be seen from Table 3 in Part I that the sample had rather variable cloud-base temperatures, ranging from 11°C to 22°C.

The cool cloud bases might strike the uninitiated scientist as rather odd, considering the tropical location of the experimentation. As discussed by Woodley and Rosenfeld (1993), however, high, cool, cloud bases are fairly typical of Thailand during the pre-monsoon period, when conditions are relatively dry. It is during the monsoon itself that cloud bases are lower and warmer. Woodley and Rosenfeld (1993) estimate that the onset of the monsoon at Chiang Mai in 1993 took place on 19 May. Both random units obtained after this date have base temperatures > 20°C.

The Thai cell results for those 10 cases in which the cloud base temperature was > 16°C are provided in Table 2. (The 16°C cutoff is purely arbitrary, but, in examining the data in Table 1 of Part I, it seemed as logical as any other.) Note that the ratio of S to NS has increased for every listed parameter, except for the number of cell mergers, which stayed the same. The apparent effect on cell rainfall has increased to 2.25, which is comparable to what has been observed in Texas (Rosenfeld and Woodley, 1993). All significance values have improved as well, but they are still far short of what is needed for high confidence in ascribing the results to AgI seeding.

It is interesting to note from the presentations in Tables 1 and 2 that the apparent 100% increases in mean cell rainfall have taken place without an appreciable increase in mean cell heights.

This too was the case in Texas, where the increase in mean cell height was < 10%. In Florida, on the other hand, the mean increase in cell height was on the order of 20%. A potential explanation for these results, involving the expenditure of the seeding-induced buoyancy to sustain the increased water mass and leaving little left over for increased vertical growth of the cloud, has been addressed by the conceptual model that was discussed in Part I.

At this point, however, one cannot discount the possibility that AgI seeding may have made the clouds less reflective near cloud top than comparable unseeded clouds. This would result in underestimation of the growth of the seeded clouds by the S-band radar.

These Thai results were the impetus for re-examining the Texas cell results (Rosenfeld and Woodley, 1993) as a function of cloud base temperature. It was found that even in the cold base partition (i.e., $T \leq 16^{o}$) the SR of S to NS rainfalls is a factor of 2.08, but the SR of S to NS echo top heights is only 0.95. Thus, in the cooler cloud base situation there is still a 100% increase in cell rainfall, but increased vertical cloud growth is apparently not associated with the rain increases.

In the warm base partition (i.e., T > 16°C), the apparent effect of treatment in west Texas is even larger at a factor of 2.85, and the SR of echo top heights is 1.23, which is comparable to what has been observed in Florida. This suggests that in the warm base situation, when the concentration of rainwater at the level of treatment should be greater, the seeding-induced buoyancy is large enough both to sustain the increased water mass and to increase echo top height.

Further quantification of the apparent seeding effect as a function of cloud-base temperature is provided in Figure 1, which shows plots of the ratio of mean S to NS values (the Seeding Effect Ratio) versus cloud-base temperature for echo height and rain volume in Texas and in Thailand. The plots were constructed by including cases cumulatively, beginning with the case with the coldest cloud-base temperature. The right edge of each plot, therefore, represents the S/NS ratio of cell height and rain volume for all cases. Note that the plots for both regions show increasing S/NS values for cell heights and rain volumes as cloud base temperature increases.

One of the more interesting Thai analyses is the presentation in Figure 2, which is a semi-log plot that shows the mean S and NS rainfalls by height interval. Note that in the interval

Table 1: Means, single ratios and the rerandomization significance levels of the ratios for the various cell properties for the 14 experimental units obtained in Thailand through 1993. The data are for the long-tracked cells.

Variable	No. of Cells		S	NS	S/NS	Rerand. Sig. (%)
	S	NS				
R_{vol} (10^3 m^3)	87	64	190.6	113.1	1.69	38.4
H_{max} (km)	87	64	9.6	9.8	0.98	59.6
Z_{max} (dBZ)	87	64	43.1	42.7	1.01	47.0
A_{max} (km^2	87	64	69.6	55.8	1.25	21.0
DUR (min)	87	64	43.1	37.8	1.14	30.8
RVR_{max} (10^3 m^3/h)	87	64	413.8	290.5	1.42	33.1
NCLMAX	87	64	19.5	11.9	1.64	27.5
MERGERS	87	64	1.9	1.7	1.07	40.5

Table 2 Means, single ratios and the rerandomization significance levels of the ratios for the various cell properties for the 10 experimental units obtained in Thailand whose cloud base temperatures were > 16°C. The data are for the long-tracked cells.

Variable	No. of Cells		S	NS	S/NS	Rerand. Sig. (%)
	S	NS				
R_{vol} (10^3 m^3)	61	47	261.1	115.9	2.25	30.0
H_{max} (km)	61	47	10.0	9.4	1.06	34.1
Z_{max} (dBZ)	61	47	46.4	42.2	1.10	16.2
A_{max} (km^2	61	47	82.4	48.1	1.71	3.2
DUR (min)	61	47	52.4	39.4	1.33	11.9
RVR_{max} (10^3 m^3/h)	61	47	535.4	256.4	2.09	19.8
NCLMAX	61	47	24.5	13.7	1.78	23.6
MERGERS	61	47	1.9	1.7	1.07	38.0

between 7 and 11 km the S cells produce more rainfall than NS cells of the same height. This suggests a more efficient microphysical process in the S cells whereby more water mass is accumulated within its interior than exists within NS cells of the same height. This is very similar to the results that were obtained in Texas (see Figure 4 in Rosenfeld and Woodley, 1993).

Plots of the mean properties of the S and NS cells as a function of time for all cells and for those cells in units with base temperatures > 16°C are provided in Figures 3 and 4, respectively. The means are for those cells that existed at each time interval.

Examination of the plots for all cells (Figure 3) shows somewhat greater echo areas and rainfalls for the S cells both before and after the initial treatment. The S and NS reflectivity plots are little different, while the S and NS height plots suggest slightly taller NS cells. By one hour after initial treatment, all differences favor the NS cells, although less than one-third of the cells remain in the sample at this time.

Examination of the plots for all cells with warm bases (Figure 4) shows essentially the same picture, although the S and NS differences before and after treatment are somewhat larger. Again, the few NS cells remaining in the sample by one hour after initial treatment are stronger than the S cells. This is different from the Texas results that showed the S vs NS differences increasing with time (Rosenfeld and Woodley, 1993).

A more representative picture of the effect of seeding on mean cell areas and rainfall flux is the calculation by time interval that includes the zero (0) values of those cells that had already dissipated. The plots for all cells are provided in Figure 5 and for only those cells with warm bases in Figure 6.

The all cells plots (Figure 5) show smaller pre-treatment and post-treatment differences, with the S cell areas and rain fluxes generally exceeding the NS values until 60 min after initial treatment. The plots for only the warm-based cells (Figure 6) show essentially the same picture as in Figure 5, although the S-NS differences are substantially greater.

Many readers might feel intuitively that the somewhat higher mean rainfall for the S cells prior to treatment represents a bias favoring the S sample. This does not appear to be the case for this sample, however, as can be seen in the scatter plot for the NS and S cells of total pre-treatment cell rainfall vs the total rainfall produced by the cell in its lifetime (Figure 7). The scatter is large in both plots. Note that all but one of the cells in both samples, producing $> 10^6$ m^3 in rain volume, had zero pre-treatment rainfalls. The one exception in the S sample had a modest pre-treatment rainfall and its position in the plot could well be a function of the seeding intervention. Note further that all cells having pre-treatment rainfalls $\geq 40 \times 10^3$ m^3 had very small lifetime rainfalls. If these cells are eliminated from both samples, the new ratio of mean S to NS post-treatment cell rainfalls is 1.77 vs the original value of 1.69 shown in Table 1. It appears, therefore, that it is a liability to a cell's post-treatment rainfall for it to have a large pre-treatment rainfall.

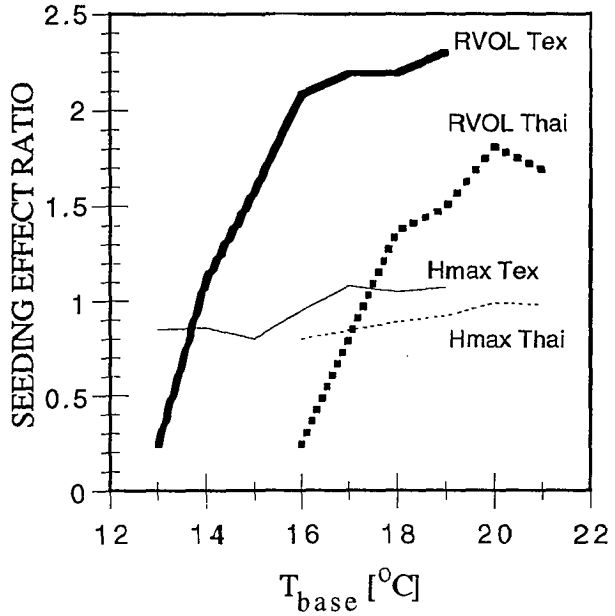

Figure 1. The indicated seeding effects on cell rain volume and maximum echo top height in Texas and Thailand as a function of cloud-base temperature. The cases are considered cumulatively beginning at the coldest observed cloud-base temperature. The right terminus of each line provides the overall effect from all cases.

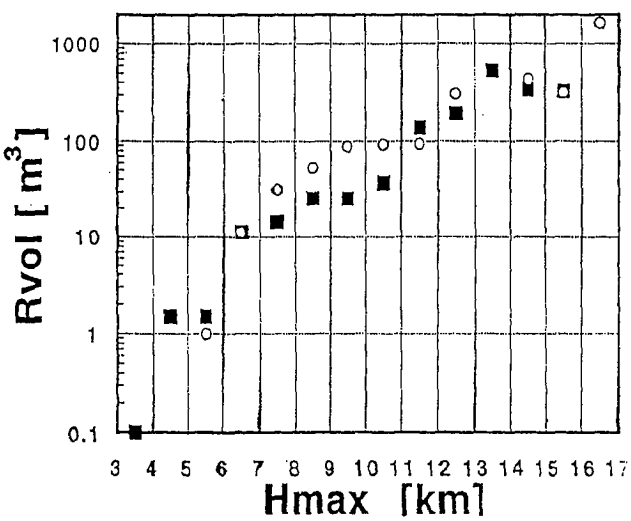

Figure 2. Semi-log plots of mean S and mean NS cell rain volumes within 1 km height intervals. The open circles represent S data and the solid squares represent NS data.

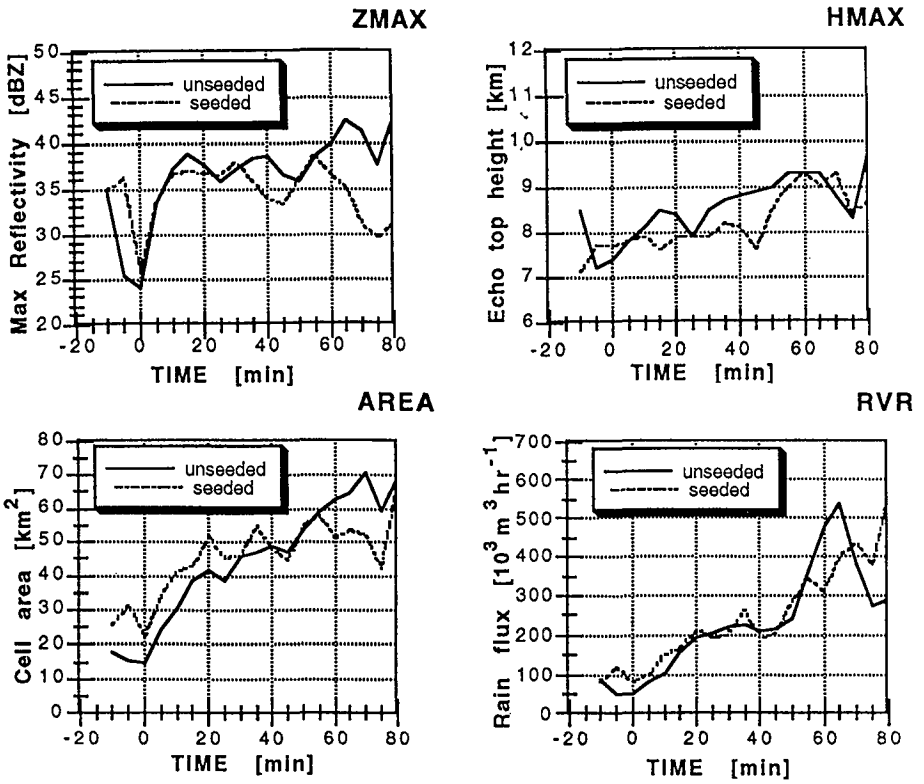

Figure 3. Line plots of mean S and mean NS reflectivities (upper left), cell heights (upper right), areas (lower left) and rain volume rates (lower right) for all of the cell data. The means have been calculated at each interval based on the number of cells in the sample at that time.

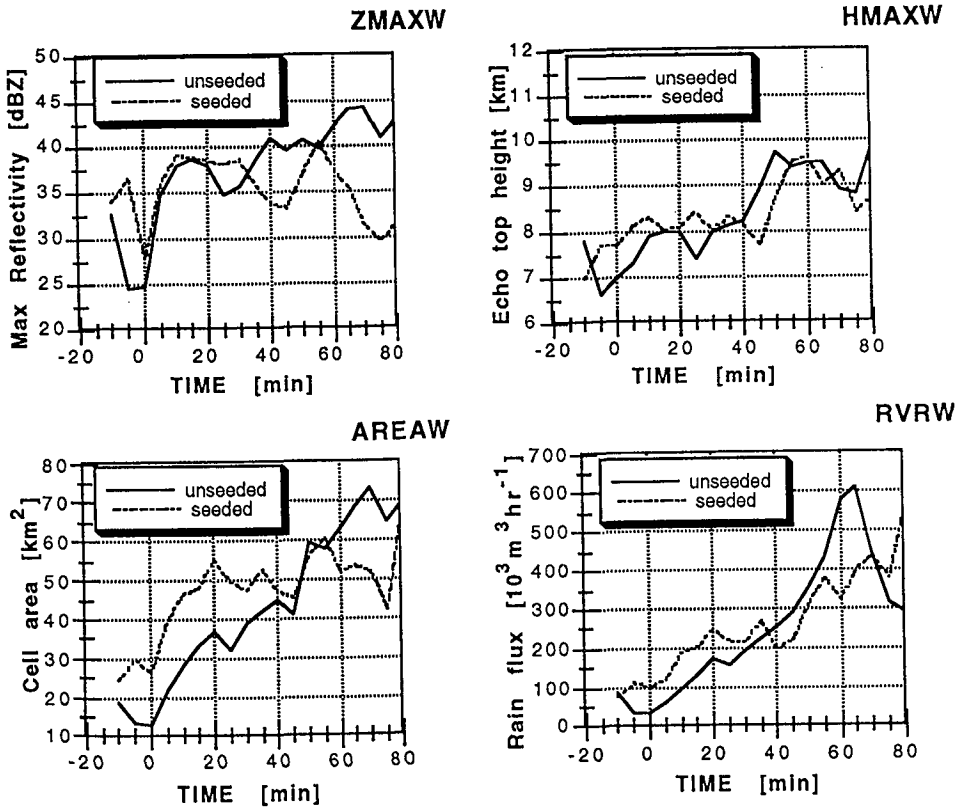

Figure 4. As in Figure 3, but for the cell data when cloud-base temperatures exceeded 16°C.

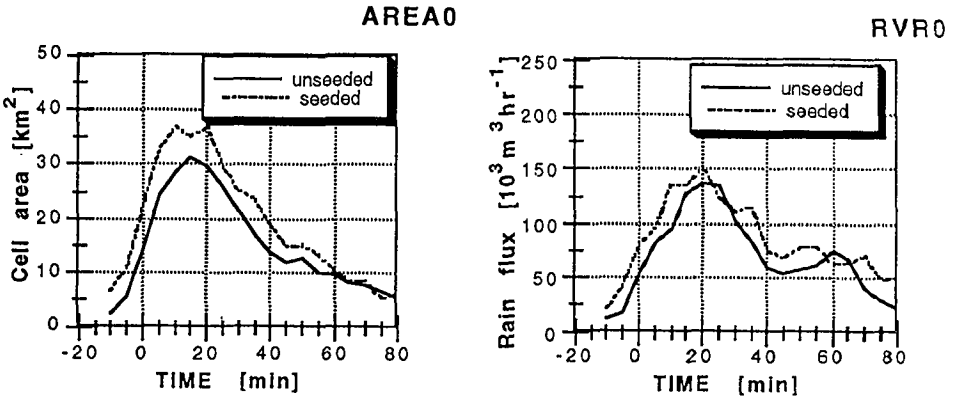

Figure 5. Line plots of mean S and mean NS cell areas (A) (at top) and rain and rain volume rates (R) (at bottom) for all of the cell data. The mean A and R values for each time interval were calculated by inputing zero values for those cells that had dissipated previously.

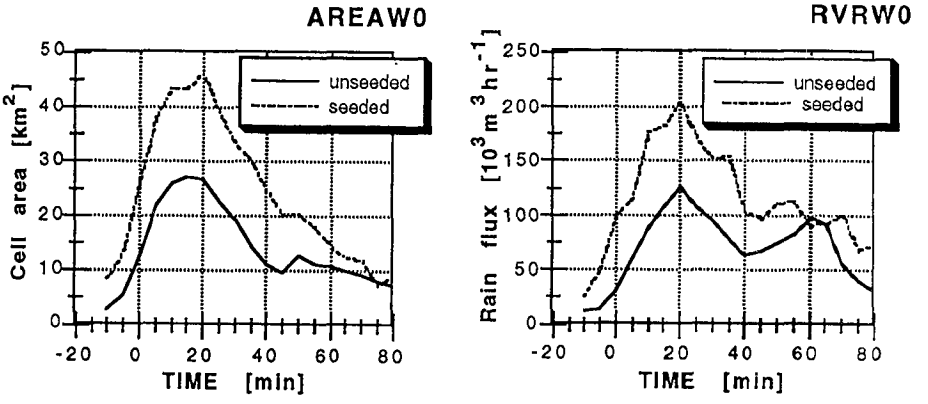

Figure 6. As in Figure 5, but for the cell data when cloud-base temperatures exceeded 16°C.

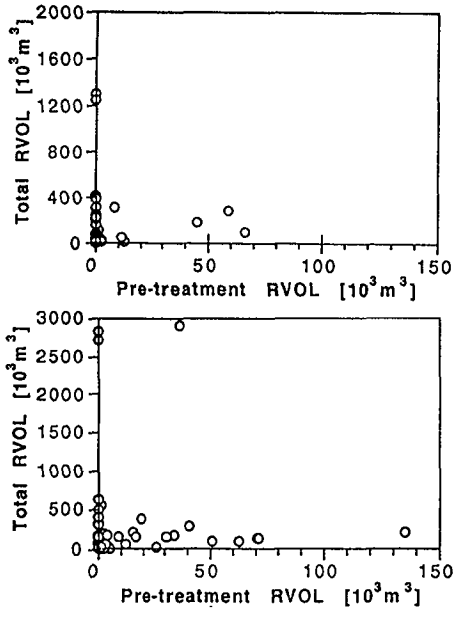

Figure 7. Scatter plot of the total rainfall produced by the NS (top) and S (bottom) cells (units: $m^3 \times 10^3$) prior to real or simulated treatment vs the total rainfall produced by the cells in their lifetimes.

Further physical insight into the cell results was provided by the construction of time-height reflectivity cross sections for the entire cell data set (not shown), and for the cells having base temperatures > 16°C in Figure 8. The numbers above the abscissa indicate the number of cells that contributed to the composite versus time. The S cross-section for the cells with warm cloud bases (top) appears to be more stratified than the comparable NS cross-section (bottom), beginning 30 minutes after initial seeding. The NS cells left in the sample at that time are also taller than the S cells that remain, in contrast with the results obtained in Texas.

Only after subtracting the patterns of Figure 8 (i.e., S time height profile minus NS time height profile) does something of interest appear (Figure 9). Note that there is a positive reflectivity difference of up to 11 dBz centered between 6 and 8 km at the time of initial treatment which persists until about 30 minutes thereafter.

Such a difference pattern was observed also in Texas, although the differences were initially smaller in

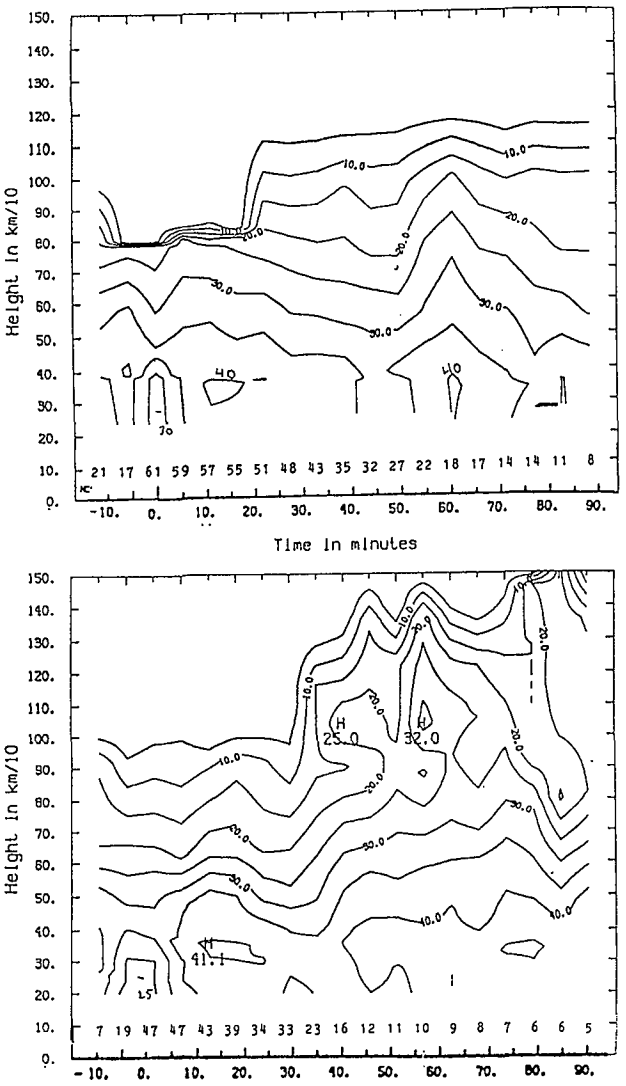

Figure 8. Composite time-height reflectivity plots of the cells with cloud-base temperatures > 16°C that were treated with AgI (top) or received simulated AgI treatment (bottom). The numbers above the abscissa refer to the number of cells (NC) in the sample at that time interval. The "0" time refers to the time of real or simulated treatment.

Texas than in Thailand (See Figure 3c in Rosenfeld and Woodley, 1993). Such positive reflectivity differences are consistent with the formation of graupel particles following AgI seeding as postulated in the conceptual model. Beyond that, however, the difference patterns in Thailand and Texas are quite disparate. The S-NS reflectivity differences in Thailand become slightly negative (below 10 km) with time, indicating that the few NS cells that remain in the sample are stronger than the few S cells that persist. In Texas, on the other hand, the differences become strongly more positive with time, indicating stronger S than NS cells long after the initial treatment.

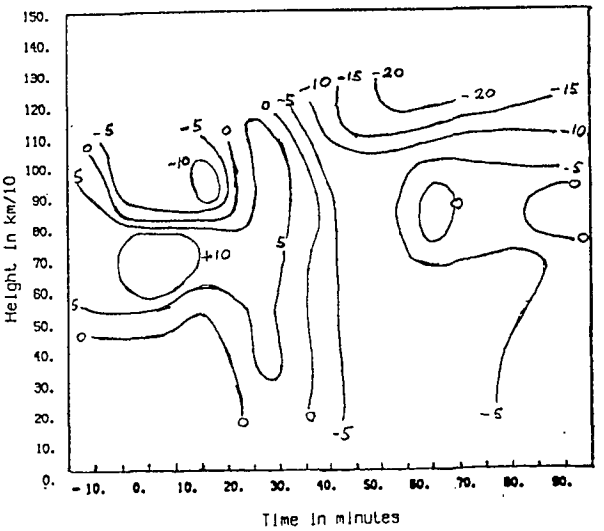

Figure 9. Difference (i.e., S-NS) composite time-height reflectivity plots for the cells having cloud-base temperataures > 16°C. The "0" time marks the time of initial treatment (AgI or simulated AgI).

3.3 Results for the Experimental Units

The last step in the analysis progression was an investigation of the effect of treatment on the experimental units themselves. Fourteen (7 S and 7 NS) experimental units were available for analysis. A listing of the input data by case, presented cumulatively in 30 min intervals relative to the time of initial treatment is provided in Table 3.

Examination of Table 3 reveals enormous case-to-case variability in the recorded values. It is imperative, therefore that the sample be increased and that predictors be found that can account for some of the natural rainfall variability that is inherent in the Thai experiments.

The mean cumulative rainfalls by time period for the S and NS samples and the ratios of the former to the latter are provided in Table 4. There are two listings in the table. The first provides the mean S and NS rainfalls and the ratios of the former to the latter. The second provides the same information but with the wettest day in each sample deleted. This is done to see how sensitive the results are to outliers. No significance testing of the ratios has been done, because such an exercise would have little meaning at this point in the Thai experiments. The sample is still much too small.

In examining the data presented in Tables 3 and 4, a reader's first impression is that a bias favored the S units, because the mean S rainfalls exceed the mean NS rainfalls by about a factor of

Table 3

Cumulative Rainfall from the Experimental Units in Time Intervals Relative to the Time of Initial Treatment (Units: $m^3 \times 10^3$)

SEED CASES

Date	0 to -60	0 to -30	0 to 30	0 to 60	0 to 90	0 to 120	0 to 150	0 to 180	0 to 210	0 to 240	0 to 270	0 to 300
8/7/91	829.3	518.8	879.3	1723.9	2077.1	2302.0	2595.0	3712.1	5452.0	7548.0	9673.3	11312.0
4/21/93	18.6	5.0	3.9	25.8	48.4	69.0	69.4	74.7	782.5	2200.7	3208.2	3761.5
4/22/93	44.9	42.2	238.1	916.2	1625.3	2338.0	4248.7	6321.5	6730.9	6763.1	6769.1	
4/25/93	18.6	16.3	48.3	189.3	533.4	991.7	1092.2					
5/7/93	0.1	0.1	33.8	250.3	700.5	2301.3	6001.8	7872.1	8225.9	8330.0	8375.8	
5/9/93	170.3	139.1	233.3	890.8	1556.9	1630.6	1644.4	1792.0	2197.3	2197.5		
5/27/93	351.1	196.5	265.0	519.3	656.1	763.1	888.5	979.7	987.2			
NO SEED CASES												
4/15/93	161.1	132.9	145.9	380.2	488.7	494.3						
4/20/93	1.4	1.2	19.6	559.1	985.1	1102.5						
4/23/93	27.3	27.3	518.9	1894.9	3469.3	4635.5	5139.6	5904.4	6957.5	7081.4		
4/29/93	343.1	248.7	292.9	636.2	1048.5	1380.7	1535.4	1541.9				
5/4/93	88.8	45.7	19.1	23.7	23.8	23.9						
5/8/93	0.1	0.1	151.8	429.7	755.6	883.8	887.9					
6/4/93	20.9	16.9	34.7	136.1	315.9	543.5	757.5	854.8	890.1	1020.2	1310.2	1487.5

Table 4

Mean Cumulative Rainfalls for the Experimental Units Relative to the Time of Initial Treatment (Units: $m^3 \times 10^3$)

All Data

	0 to -60	0 to -30	0 to 30	0 to 60	0 to 90	0 to 120	0 to 150	0 to 180	0 to 210	0 to 240	0 to 270	0 to 300
S	204.7	131.1	243.1	645.1	1028.2	1485.1	2362.8	3120.6	3638.3	4159.8	4586.2	4927.9
NS	91.8	67.5	169.0	580.0	1012.4	1294.8	1420.2	1544.2	1730.5	1736.0	1777.4	1802.8
S/NS	2.23	1.94	1.44	1.11	1.02	1.15	1.66	2.02	2.10	2.40	2.58	2.73

Data with Wettest Unit from the S and NS Samples Deleted

S	100.6	66.5	137.1	465.3	853.4	1349.0	2324.1	3022.0	3336.0	3595.1	3771.7	3863.9
NS	102.6	74.2	110.7	360.9	602.9	738.0	800.3	817.5	859.3	845.1	893.4	923.0
S/NS	0.98	0.90	1.24	1.29	1.42	1.83	2.90	3.70	3.88	4.25	4.22	4.19

two in the hour prior to initial treatment. This impression may not be correct, because there appears to be no correlation between the pre-treatment rainfalls and the rainfalls that are produced by the experimental units subsequently. This can be seen in the log-log plot for the NS cases of the rainfall in the hour before initial treatment vs the rainfall in the two hours after initial treatment (Figure 10). (The S units were not used in this exercise, because AgI treatment is postulated to have altered the natural rainfalls.) The scatter is great and there is no evidence from this limited sample that the pre-treatment unit rainfalls are a predictor of the rainfall that will be produced subsequently within the unit. If anything, the limited sample suggests a negative correlation (i.e., more rainfall prior to treatment means less rainfall afterwards). This is virtually the same result that was obtained for individual cells.

The presentation in Table 4 and the plot of the S to NS ratios in Figure 11 show that the sample is quite sensitive to the deletion of the wettest unit from the S and NS samples. First, note that the

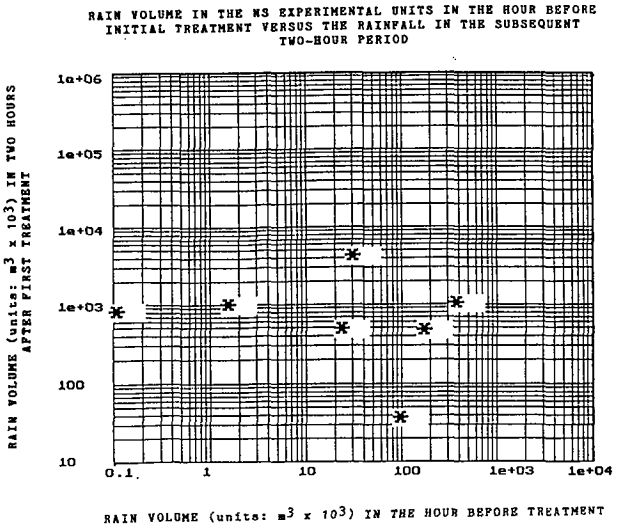

Figure 10. Log-log plot of the rain volume for the NS experimental units in the hour prior to initial simulated treatment versus the unit rain volume in the subsequent two hours.

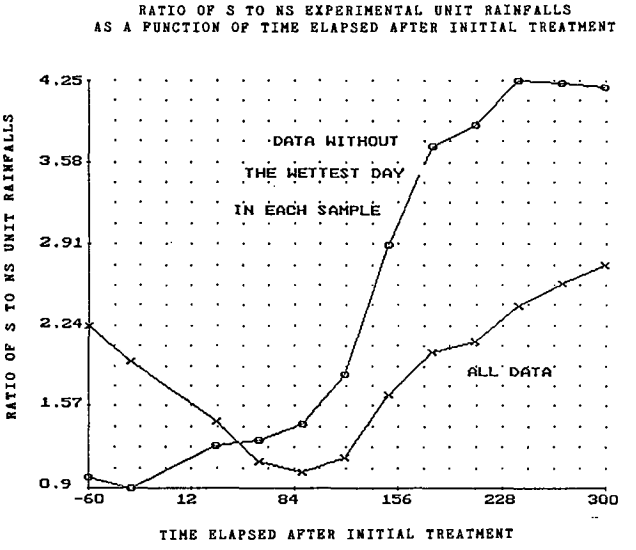

Figure 11. Plot of ratios of S to NS unit rain volumes by 30-min time intervals relative to the time of initial treatment. The solid line is for all data. The dashed line plot is for the ratios that were calculated after the wettest day in the S and NS samples had been deleted.

apparent pre-treatment bias in the S sample totally disappears after deleting the wet case on 7 August 1991. Second, notice that the ratio of S to NS mean rainfalls increases continuously after the initial treatment when the wettest S and the wettest NS units are deleted.

The reader is urged to be cautious with the interpretation and dissemination of these results. Although they do provide the impetus to continue with the Thai experiments, no unequivocal argument that AgI treatment produces large increases in rainfall within the experimental units is justified at this time. With patience and a lot of hard work to increase the sample, such an argument might have some basis in the future.

4.0 SUMMARY AND CONCLUSIONS

Scientific progress with the Thai cold-cloud seeding effort has been substantial. It is now known that Thailand presents a rich harvest of supercooled clouds that are suitable for seeding intervention for the enhancement of their rainfalls. Thai pre-monsoon clouds are different from those that exist typically during the monsoon over the region of study. Cloud-base temperature is the major determinant of cloud conditions. When bases are high and cool, as is often the case in the pre-monsoon period, much of the water within the cloud apparently is concentrated in small cloud drops. Seeding of these clouds appears to result in rather slow glaciation and a rather weak vertical growth response of the cells. This is in agreement with the predictions of Lamb et al. (1981) that glaciation in clouds with small supercooled drops will proceed rather slowly. When the bases are low and warm, as is the usual case during the monsoon, a substantial amount of the water that is encountered within the cloud at temperatures of about -8°C is apparently in raindrops. Seeding of these clouds appears to result in rapid glaciation and in explosive vertical growth in some circumstances. Although rainfall increases may be produced in both cloud types, the largest increases are likely produced in the clouds with warm cloud bases. This is consistent with the conceptual model as presented and discussed in Part I. Having such a model to guide the effort has been a major plus for the program.

The results of cold-cloud seeding to date are consistent in most respects with the results that have been published previously for Florida and Texas (Gagin et al., 1986; Rosenfeld and Woodley, 1989; 1993). Initial results suggest that AgI seeding may have increased the cell rainfalls by as much as 100% or more for cells having cloud bases > 16°C. As is the case in Texas, these increases have been produced by broader cells with longer durations. Vertical cell growth of the S cells has been small relative to the growth of the NS cells and does not, therefore, appear to be a requirement for the rain increases. An important finding is that AgI-treated cells in both Texas and Thailand produce more rainfall than non-seeded cells having the same echo top

height. How this might take place is addressed extensively in the conceptual model (see Part I).

It is also possible, however, that the vertical growth of the S cells may have been underestimated by the S-band radar operative in Thailand. Visual inspection of the clouds in real time and on video tape suggests a more stratified glaciated structure of the tops of the S cells relative to those that have not been seeded. This might mean lesser reflectivity near the tops of the AgI seeded clouds. Further study is needed to resolve this uncertainty.

The results for the 14 experimental units (7 S and 7 NS) for which analysis is possible are consistent with a positive effect of seeding. The natural variability is great and the results are highly sensitive to removal of the wettest unit from each of the S and NS samples.

The Thai cold-cloud experiments appear to be on the right track, and the obvious recommendation is that they continue. The present design appears to be well suited for the continuation, considering the progress that has been made so far.

5.0 REFERENCES

Gabriel, K.R., and P. Feder, 1969: On the distribution of statistics suitable for evaluating rainfall stimulations. Technometrics, 11, 149-160.

Gagin, A., D. Rosenfeld and R.E. Lopez, 1985: The relationship between height and precipitation characteristics of summertime convective cells in South Florida. J. Atmos. Sci., 42, 84-94.

Gagin A., D. Rosenfeld, W.L. Woodley and R.E. Lopez, 1986: Results of seeding for dynamic effects on rain cell properties in FACE-II. J.of Climate and Appl. Meteor., 25, 3-13.

Lamb, D., R.I. Sax and J. Hallett, 1981: Mechanistic limitations to the release of latent heat during the natural and artificial glaciation of deep convective clouds. Quart. J. Roy. Meteor. Soc., 107, 935-954.

Rosenfeld, D., 1987: Objective method for tracking and analysis of convective cells as seen by radar. J. Atmos. Sci., 4, 422-434.

Rosenfeld, D., and W.L. Woodley, 1989: Effects of cloud seeding in west Texas. J. Appl. Meteor., 28, 1050-1080.

Rosenfeld, D., and W.L. Woodley, 1993: Effects of cloud seeding in west Texas: Additional results and new insights. J. Appl. Meteor., 32, 1848-1866.

Woodley, W.L., 1970: Precipitation results from a pyrotechnic cumulus seeding experiment. J. Appl. Meteor., 9, 242-257.

Woodley, W.L. and D. Rosenfeld, 1991: Testing Dynamic Seeding in Thailand. A Report to the U.S. Bureau of Reclamation on Contract No. 1-CS-81-17780. 78 pp.

Woodley, W.L. and D. Rosenfeld, 1993: Analysis of Randomized Experiments in Thailand. A Report to the U.S. Bureau of Reclamation on Contract No. 1425-3-CS-81-19050, 62 pp.

Woodley, W.L., D. Rosenfeld, B. Silverman, and C. Hartzell, 1991: Design and Operations Plan for a Randomized Cold-Cloud Seeding Experiment Focused on Individual Convective Cells. July 1991, 126 pp.

CRITERIA FOR A REMOTE GROUND GENERATOR NETWORK IN LEON (SPAIN)

J. L. Sánchez, A. Castro, J. L. Marcos, M. T. de la Fuente, R. Fraile
Lab. Física de la Atmósfera
Universidad de León, Spain

1. INTRODUCTION

In 1985, the Agriculture Department of the Province of León (Diputación de León), worried about the frequent occurrence of hailfalls, asked the Laboratorio de Física de la Atmósfera de la Universidad de León to perform research on hail climatology and the economic repercussions of hail on agriculture. In order to do that, a target area was defined (Fig. 1) in which the agrarian production is high, and a network of meteorological observers was established in a density of one for each 17 km². This network has provided a useful data base for the summer hail period since 1986 when the project started. The target area comprises a good part of the provinces of León and Zamora and has an extent of 12,500 km².

After three years, the results allowed us to develop an action project of hail suppression, named PALA, for the problem caused by the hailfalls and the possible losses to agriculture they cause, to be carried out from 1989 to 1992. The main aim has been to obtain climatological information on the hailfalls and establish risk maps of high or low hail incidence. There are many references about the results found (Sánchez *et al.*, 1987, 1991, 1992; Fraile and Sánchez, 1989; Fraile *et al.*, 1991, 1992; Castro *et al.*, 1992; de la Madrid and Sánchez, 1989).

In 1993, following the initial project, the first stage of a planned four-year operating project was initiated, and the first experimental actions of cloud seeding with glaciogenic nuclei started. The PALA sponsors, that is to say, the provincial and regional Departments of Agriculture, have taken special care in trying to follow the suggestions emanated from the WMO. They are looking for a balance between the practice of an operational programme to reduce hail damage without forgetting the need for seeding control and research associated with this kind of activity.

In this paper, we describe the characteristics of the seeding systems and the criteria used for their implementation.

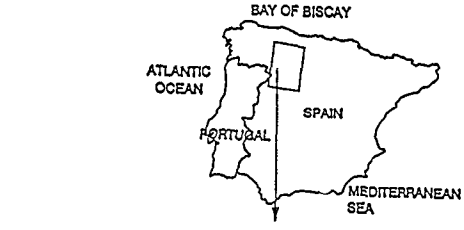

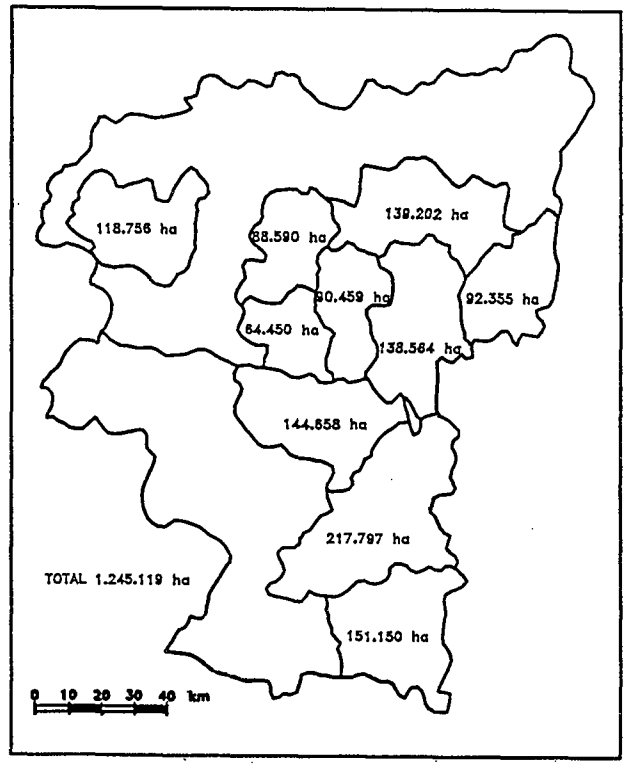

Fig. 1: The target area is divided into areas which size is shown.

2. SOME CLIMATOLOGIC CHARACTERISTICS OF THE FORMATION OF STORMS

2.1 Introduction

In the southeast of the Iberian Peninsula, the first studies carried out in 1976 showed that the occurrence of hailstorms is usually highly connected to the geographical area on which they take form (Dávila *et al.*, 1978). Since then, in other places on the Peninsula, analogous results have been found (Sánchez and Castro, 1990; Sánchez *et al.*, 1986, 1988; Castro and Sánchez, 1990; Castro *et al.*, 1989, 1990, 1991). For these reasons, one of the first aims of the current programme was the determination of geographical areas more inclined to the formation of storms.

The determination of these areas can be carried out with the help of a radar. In our case from 1989 to 1992, we used a digitized C band radar, which has allowed us to achieve this aim as well as to determine some characteristics of the summer storms.

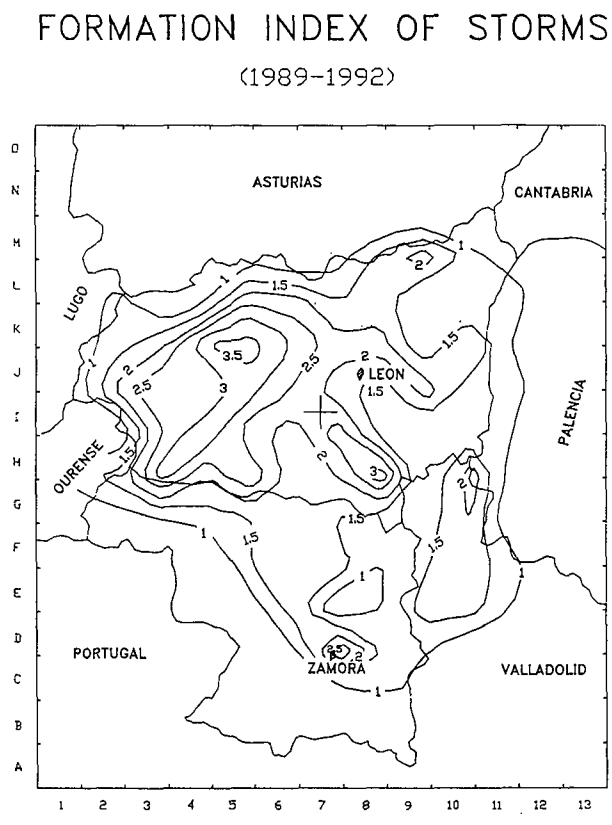

Fig. 2: Spatial distribution of the storms' formation indexes.

2.2 Storm Formation Climatology

2.2.1 Formation index. In a previous paper (Sánchez *et al.*, 1985), a dimensionless index was defined. The index shows the areas with a higher probability of storm formation. The value of the index is expressed in such a way that the higher the index, the higher the risk of the formation of storms in that area. In order to do that, we have established over the provinces of Léon and Zamora, as well as the bordering areas, a grid of 169 squares of 20 km on a side. Figure 2 shows isolines of the spatial distribution of this index in the period between 1989 and 1992, with a sample of 769 storms. The results show that there are basically:

1) An area of about 20 squares which goes from map index H3 to K6 in which, in comparative terms, the formation of storms is very frequent. This area corresponds with a mountainous area formed by various ranges with heights that, in some cases, go beyond 2000 m.

2) Two small areas associated with squares H8 and D7 which also have high index values without, in this case, any relevant reason from the geographical point of view.

2.2.2 Storm trajectories. With the help of the information supplied by the radar, we have calculated the trajectories of the storms which caused severe precipitation over the target area shown in Fig. 1. The trajectories were classified into 16 different directions and the results are shown in Fig. 3. The most frequent trajectories are the ones that

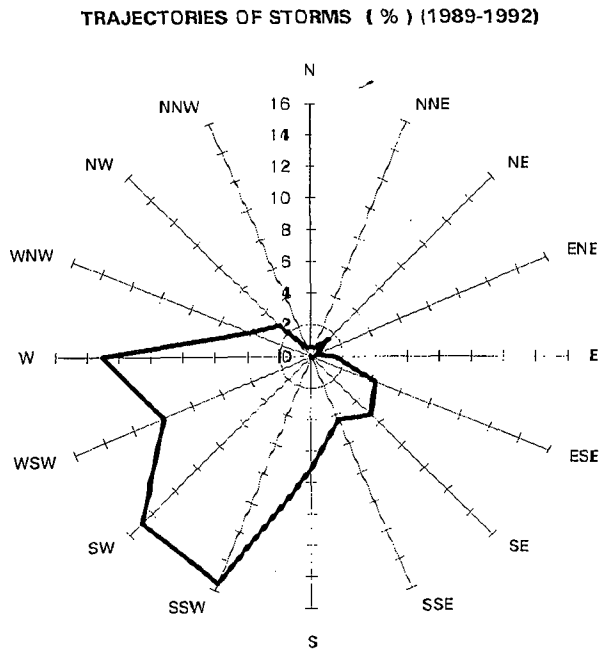

Fig. 3: Trajectories followed by the storms and calculated with the help of the meteorological radar.

have components of the third quadrant (W, WSW, SW, SSW, S). It is proper to bring out that 13% of the storms were stationary.

Taking into account the number of hail days recorded in the summers of 1986-1992 (Fig. 4), we can interpret that

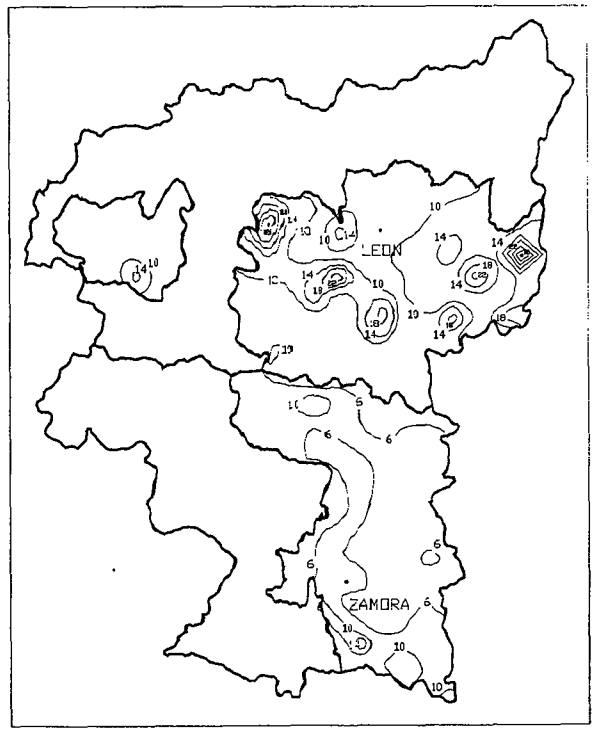

Fig. 4: Spatial distribution of the total number of days in which have been recorded hail on the ground in summer (1986-1992).

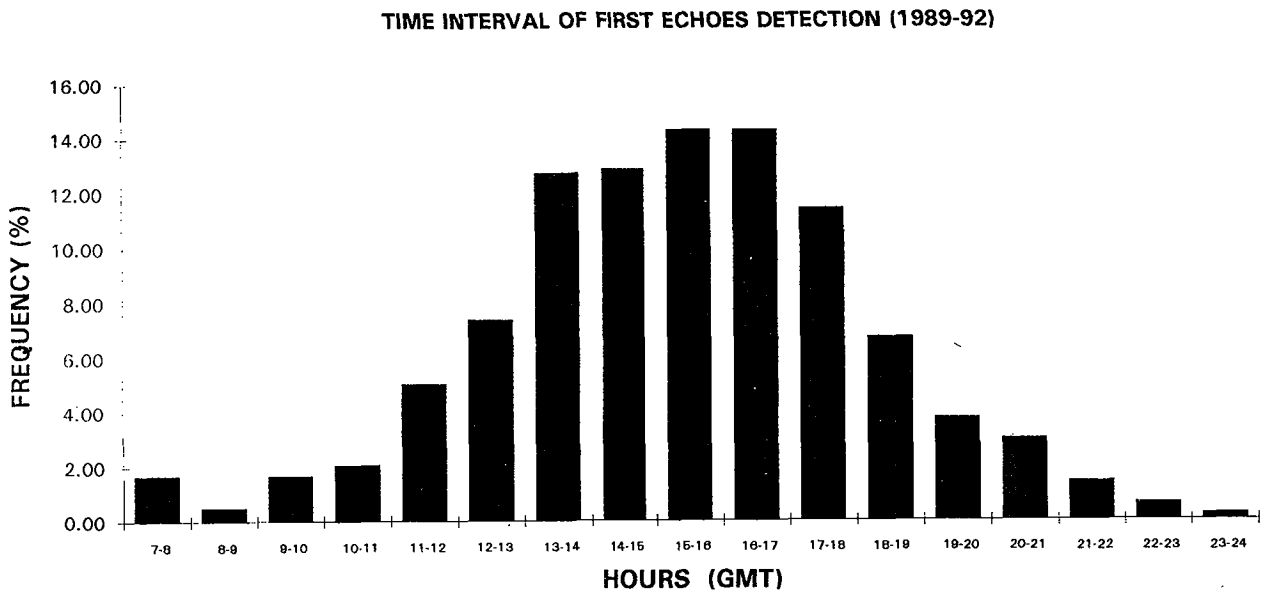

Fig. 5: Time interval of storms' formation.

many storms generated in the high index areas referred to in section 2.2.1 follow trajectories that give rise to the occurrence of hail in the regions with higher agrarian production and cause important economic losses.

2.2.3 *Time interval of storms' formation.* In Fig. 5, we have represented the fraction of storms formed in each time interval. Almost 80 percent of the storms form between 10 and 18 hours, with a sharp decrease after 18 hours; few storms form at night.

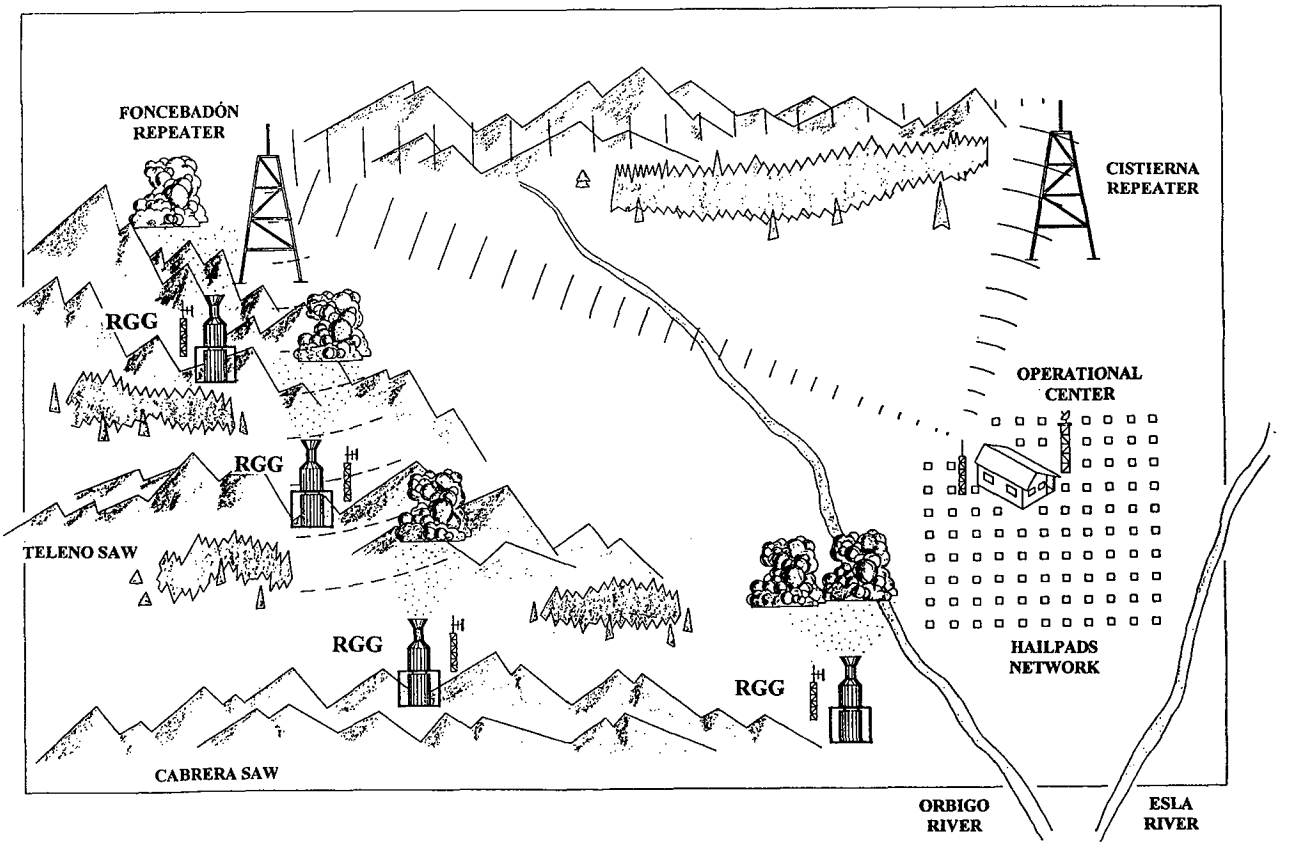

Fig. 6: Schematic operation of the generator network: the central station, two signal repeaters, and the RGG which are the nuclei generators.

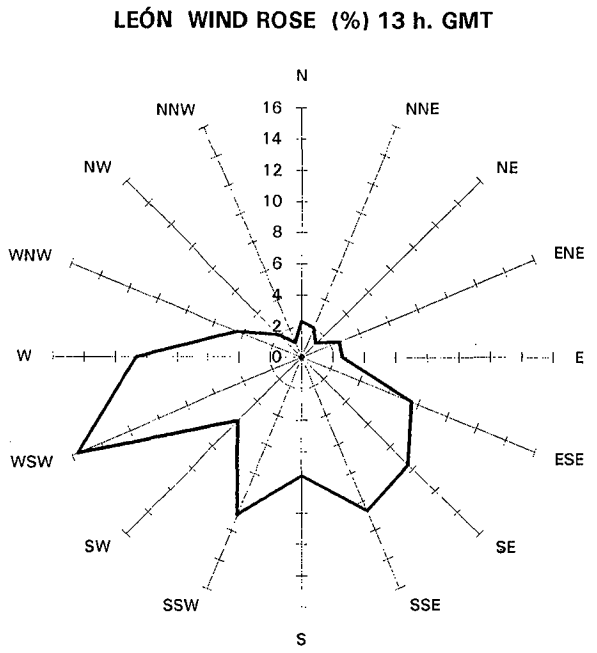

Fig. 7: Wind rose of the low levels corresponding to a historic series of 25 years and calculated starting from the data obtained in the days in which storms were recorded.

3. DESCRIPTION OF THE SEEDING SYSTEM

3.1 General Criteria for the Selection of the Seeding System

The target area to which we have referred in Fig. 1 is a geographically flat area but very close to the mountainous ranges, where navigation aids are not enough to be able to guide seeding from airplanes with security guarantees. Taking into account that cloud seeding projects elsewhere in Spain (Dessens, 1986; ANELFA, 1993), and in a good part of eastern Europe, use ground generators, and that especially in France they have much experience in the effectiveness of ground generators, the PALA sponsors selected this system. According to the climatologic study, from the radar data, the storms form mainly in the mountainous areas close to the target area. Since these sites are remote and not close to populated areas, it was necessary to set up a network of automatic ground generators controlled by radio signals.

3.2 Characteristics of Remote Ground Generator Network

After various tests, we decided to select the model RG288-A/P made by Atmospherics, Inc., using a system of communications based on Motorola Intrac 2000 System equipment. In this way and by means of a system of signal boosters, the operation is controlled from the central station. In Fig. 6, we show schematically the operation of the network.

The maker showed us some nucleation yields that *a priori* seemed satisfactory for our aims. Nevertheless, with the help of a cloud chamber, we checked that they were accurate and obtained the values that are shown in Table 1.

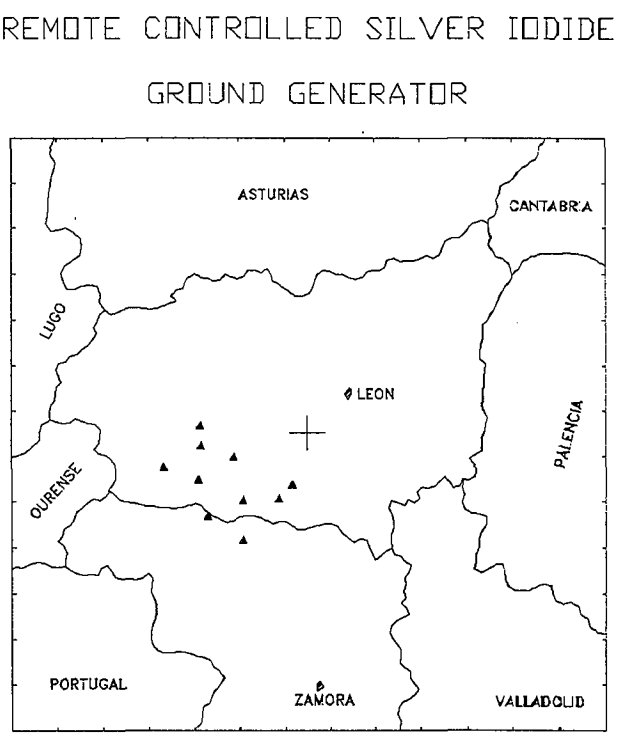

Fig. 8: Location of the 10 automatic generators.

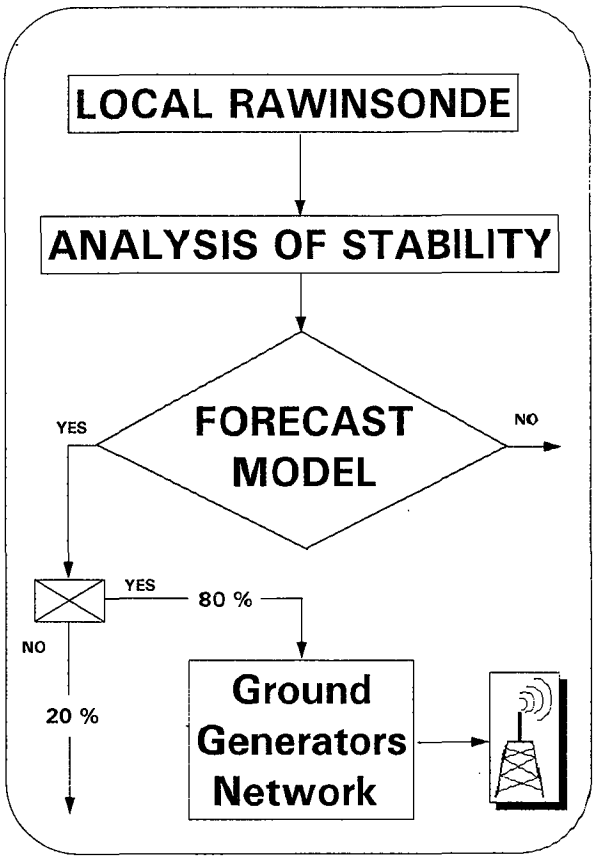

Fig. 9: Scheme of the methodology followed in order to declare seeding or non-seeding days.

TABLE 1

Formation of Ice Crystals Per Gram of Nucleant for AgI Aerosols Produced by Combustion of 1.2 AgI, Acetone

Cloud Temperature (°C)	-8	-13	-17
Yield (Crystal/g AgI)	10^{12}	$2*10^{14}$	$9*10^{14}$

3.3 Selection of the Priority Area

The chosen seeding system has two basic determinants:

a) The seeding system must work provided that there is enough warming of the lower level cumulus clouds to transport nucleant material towards higher atmospheric levels. It implies, in practice, an operation time of 6 or 7 hours more or less, that is to say from 10 (Z) to 17 (Z).

b) The trajectory of the plume of the nucleant material formed at the end of the stack of the generator is determined by the horizontal component of the wind. Taking into account that the directions of the winds in the low levels in the target area (Fig. 7) fall in the third quadrant in a majority of cases, the PALA managers decided to give priority protection to the area on which the agrarian production is higher, with irrigated crops more sensitive to the falling of hail. The said area, shown in Fig. 8, has an extent of more or less 5000 km^2. This priority area is smaller than the target area, and an objective for the future is the progressive increasing of the area until both coincide.

3.4 Location of the Generators

From the beginning, one of the PALA aims has been to be able to establish an evaluation of the seeding. In section 2 and especially in the analysis of Fig. 3, we showed that the hailstorms are generated mainly in a mountainous area. That is why we decided to seed exclusively from that area, trying to increase significantly the number of ice nuclei in these areas where a high number of storms are formed. That is to say, the aim is to introduce into the environment of the surface layer of air a high concentration of ice nuclei in order to ensure that the storms that will be formed ingest significant amounts of nuclei. Thus it will be possible to say that they have been seeded with the aim of increasing the beneficial competition.

We established a network of 10 automatic generators taking into account:

a) The characteristics of the plumes of the nucleant material in various conditions of atmospheric stability, which affect the dispersion of the nucleant material and the characteristics of the emission.

b) The number of active AgI nuclei that the generator is able to produce with the solution in use.

c) The geographic situation of the priority area to be protected and the area of formation of storms (Figs. 2 and 8).

d) The need for the significant increase of the concentration of ice nuclei mainly in the area of formation of storms.

In Fig. 8, we have the location of the generators that are placed at elevations which range from a high of 2050 m to a low of 900 m.

4. METHODOLOGY FOR THE SEEDING ACTIONS

The seeding system chosen needs a short-term prediction system that will be reliable. Early in the morning, we launch a radio sounding. Based on the data received, we evaluate with a prediction model (de la Fuente, 1993) the probability of hailfall in the priority area. The model uses discriminant analysis as a statistical procedure, which allows us to obtain a criterion for classification of risk situations of having or not hailfalls.

Following the scheme in Fig. 9, we can see that once a hail producing condition is predicted, in 80% of the cases we proceed to activate the system of generation of freezing nuclei. The remaining 20% is used to obtain a natural storm evolution pattern, that is to say, a control series, and in this way to be able to establish the effectiveness of the system.

The knowledge of the activity at the ground is acquired by means of:

1) A network of more than 500 meteorological observers that send a card daily with observations.

2) A network of 250 hailpads, each representing 4 km^2 of area.

3) A network of 50 pluviometers.

The trajectories and the characteristics of the storms are determined through the information given by the radar and by means of the analysis of the Meteosat PDUS images.

5. DISCUSSION ABOUT THE SEEDING ACTIONS FOR THE PRIORITY AREA OF PROTECTION

With the seeding system chosen, that is to say ground generators, we are inserting "on many occasions" the ice nuclei in the low levels somewhat like seeding of clouds in the base. In contrast with the placing of the ANELFA generators in France, where the goal is to keep a concentration of ice nuclei constant in the entire area of protection, we have carried out a previous study to locate the AgI generators in the places that have been considered more advantageous from the point of view of the formation of storms. Depending on the results that we are measuring, we will carry on with this location or it will be complemented by the installation of additional generators.

The determination of the "defended area" is not easy since after setting up the existing generator network, we can find some storms that follow trajectories in such a way that they do not pass over the priority area. When this happens, the defended area is not the priority area of protection. On the other hand, we can have storms which form in areas located south of the operational area, where there are no generators for the seeding nuclei, and then more over the area to be protected. We can also find that during the time of operation of the generators there have been been storms that have given rise to hailfalls, but still storms with hail will be registered in the agrarian areas.

In order to establish if the storms that cause precipitation in the priority area of proection were seeded by means of our system of hail suppression, we need a day-by-day, hour-by-hour analysis, both of the activity registered on the gound and of the characteristics of the formed storms. The creation of this data base will allow us to establish an adequate evaluation of the effectiveness of the designed hail suppression system.

REFERENCES

ANELFA, 1993: Campagne Antigrele 1991. **No. 40**. 64 pp. [In French]

Castro, A., and J.L Sánchez, 1990: Indices de formación de tormentas y su relación con factores geográficos y topográficos en el Valle Medio del Ebro. *Revista de Geofisica,* **46**, 181-191. [In Spanish]

Castro, A., J. L. Sánchez, R. Fraile and J.L. de la Madrid, 1989: Análisis de la estructura de las tormentas del valle medio del Ebro. *Boletin de Sanidad Vegetal - Plagas,* **15**, 149-160. [In Spanish]

Castro, A., J. L Sánchez, M.L. Sánchez, J.L. de la Madrid and R. Fraile, 1990: Comparación entre los indices de crecimiento de las tormentas de Albacete y Aragón. *Boletin de Sanidad Vegetal - Plagas,* **16**, 625-633. [In Spanish]

Castro, A., J.L. Sánchez, R. Fraile and M.T. de la Fuente, 1991: Influence zone of formation in the characteristics of storms in the middle valley of the Ebro (Spain). II International Meeting on Agriculture and Weather Modification, Zamora (Spain), 107-118.

Castro, A., J.L. Sánchez and R. Fraile, 1992: Statistical comparison of the properties of thunderstorms. *Atmos. Res.*, **28**, 237-257.

Dávila, M., A. Aparicio and L. Garcia de Pedraza, 1978: Campana Experimental de Antigranizo del Levante. Ministerio de Agricultura. 46 pp. [In Spanish]

de la Fuente, M.T., 1993: Un modelo estadistico para la predicción de tormentas en León. Universidad de Leon. 95 pp. [In Spanish]

de la Madrid, J.L., and J.L. Sánchez, 1989: Evaluación de las pérdidas ocasionadas por el pedrisco en León y Zamora (1985 - 1988). Excmas. Diputaciones Provinciales de León y Zamora y Junta de Castilla y León. 100 pp. [In Spanish]

Dessens, J., 1986: Hail in southwestern France I: Hailfall characteristics and hailstorm environment. *J. Clim. Meteor.*, **25**, 35-47.

Fraile, R., and J.L. Sánchez, 1989: Análisis de los tipos de tiempo para situaciones tormentosas en León y Zamora (1984-1988). *Excmas. Diputaciones Provinciales de León y Zamora y Junta de Castilla y León.* 72 pp. [In Spanish]

Fraile, R., J.L. Sánchez, J.L. de la Madrid and A. Castro, 1991: A network of hailpads in Spain. *J. Wea. Mod.*, **23**, 56-62.

Fraile, R., A. Castro and J. L. Sánchez, 1992: Analysis of hailstone size distributions from a hailpad network. *Atmos. Res.*, **28**, 311-326.

Sánchez, J.L., and A. Castro, 1990: Analysis of the characteristics of storms in the Middle Ebro Valley (Spain); preparation for a new stage of hail suppression. *J. Wea. Mod.*, **22**, 98-105.

Sánchez, J.L., J.L Casanova and M. Dávila, 1985: On set system to suppress the hail in Spain. *Proc. Fourth WMO Scientific Conf. on Wea. Modif.*, **Vol. II**, 575-578.

Sánchez, J.L., A. Castro, M.L. Sánchez and M. Dávila, 1986: Comparison between seeded and unseeded storms in Albacete (Spain). *J. Wea. Mod.*, **18**, 43-46.

Sánchez, J.L., M.L. Sánchez, A. Castro and M.E. López, 1987: Bases to prepare a hail suppression project. *Proc. I International Meeting on Agriculture and Weather Modification,* Leon, Spain, 1-12.

Sánchez, J.L., M.L. Sánchez, A. Castro and M.C. Ramos, 1988: Some results related to the suppression hail project in Albacete. *J. Wea. Mod.*, **20**, 31-36.

Sánchez, J.L., A. Castro, R. Fraile and J.L. de la Madrid, 1991: Some characteristics of severe storms on León and Zamora (Spain). II International Meeting on Agriculture and Weather Modification, 1991, Zamora (Spain), 1-10.

Sánchez, J.L., A. Vega, A. Castro, M.T. de la Fuente and R. Fraile, 1992: Classification of convective clouds. *Proc. 9th Meteosat Scientific Users Meeting,* EUMETSAT & SMA, 147-154.

INVESTIGATION OF THE EFFECT OF ICE NUCLEI FROM A CEMENT PLANT ON DOWNWIND PRECIPITATION IN SOUTHERN ALBERTA

Daryl V. O'Dowd
Department of Geography
University of Alberta
Edmonton, Alberta

Abstract. In an earlier study, ice nuclei were measured in airborne effluent over a cement producing facility in southern Alberta. To investigate the possibility of inadvertent weather modification due to the effluent, two predictor schemes were developed using five weather stations to determine whether precipitation amounts or precipitation events were anomalous at a sixth station downwind of the facility. Despite departures from predicted values, no linear correlation could be confidently made between mill production and precipitation anomalies at Calgary, the downwind and sixth station, during the ten year analysis period from 1981 to 1990. Inadvertent precipitation modification does not seem to have taken place.

1. INTRODUCTION

In southern Alberta, on the eastern edge of the Rocky Mountains, there is situated a large, isolated industrial complex that has been in operation since the late 1800's. Located on the Bow River at Exshaw, three cement and calcination plants produce large quantities of waste heat, water vapour and airborne particulate matter. Located 80 km downwind of the facility (Fig. 1) and situated in rolling prairie farmland, is the city of Calgary, a large urban centre with a population of 775,000. The hub of farming, ranching and oil and gas activity in western Canada and the site of the 1988 Winter Olympics, Calgary has a large regional recreational and agricultural economy that is particularly sensitive to precipitation amounts and events.

In June of 1985, *ad hoc* Alberta Research Council airborne particle sampling flights using an NCAR (National Centre for Atmospheric Research) IN (ice nuclei) counter were made over and downwind of the Exshaw site, the author in attendance. Nuclei concentrations from the single cement producing plant measured several km downwind were 5/litre at an altitude of 7,500 feet, with an NCAR chamber temperature of -20°C. In direct plume penetration, however, concentrations became comparable to those produced by commercial airborne cloud-seeding equipment (Heimbach, 1986). Over 3300 IN were measured in a single penetration pass of less than 1 minute, producing a measured IN concentration minimum of 320/litre. However, unlike a commercial seeding operation, this IN source is virtually a continuous one running 24 hours a day, 365 days a year, barring equipment overhaul or breakdown (J. Brown, personal communication, 1986), and only two complete shutdowns occurred in the ten year period from 1981 to 1990. The aim of this paper is to determine whether Calgary shows climatological evidence of anomalous precipitation and, if present, whether such precipitation can be unequivocally related to industrial output at the suspect Exshaw facility.

2. WEATHER MODIFICATION PRINCIPLES

Modification of supercooled clouds using ice nucleating agents is possible due to a lower saturation vapour pressure over ice than over liquid water. This difference, an important component of the Bergeron nucleation process (Dennis, 1980), causes an ice crystal to grow by vapour deposition at the expense of nearby supercooled liquid water droplets. The two results of this process are that ice crystals grow faster than they would through normal coalescence and collision, and that increased buoyancy results from latent heat release, augmenting cloud updrafts (Braham, 1986). The role of most seeding agents (natural and artificial) is to mimic the inter-molecular dimensions and hexagonal shape of a natural ice

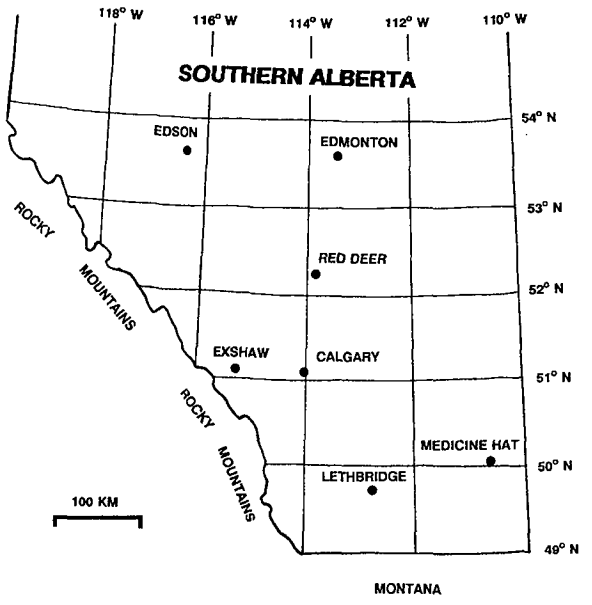

Figure 1. Map of southern Alberta. The five predictor control stations are shown (Edson, Edmonton, Red Deer, Lethbridge and Medicine Hat) as well as the ice nuclei source (Exshaw) and the target station (Calgary).

crystal and thus provide a substrate for ice deposition. This improves the efficiency of precipitation processes and consequently increases rain and snow fall, and through embryo competition, reduces hail size. Naturally occurring IN include true ice crystals from the glaciation of strong vertical cumuliform growth as well as solid particles of dust swept aloft by wind, volcanic aerosols, meteoritic debris, gas precipitates, spores and bacteria (e.g., Pseudomonas Syringae).

While the introduction of IN improves precipitation processes to a point, overseeding by the same mentioned cloud processes has the potential of reducing and even preventing precipitation where natural IN concentrations are optimal. An excess of IN can result in smaller sized precipitation droplets or crystals, thus increasing the likelihood of complete evaporation prior to reaching the ground. Virga, consequently, is more likely to occur in overseeded situations. Incomplete or insufficient seeding of hail situations also has the potential of creating unexpected hail damage by increasing the number of stones but not sufficiently to limit their growth. Indeed the attendant risks associated with deliberate weather modification programs has seen a number of States in the USA and Provinces in Canada enact legislation to regulate or at least monitor such operations (Miller, 1992).

3. ICE NUCLEI AND ACCIDENTAL INDUSTRIAL WEATHER MODIFICATION

High concentrations of IN from industrial sources have rarely been directly observed in experiments to date. However, the release of such nuclei has often been hypothesised where climate data reveals anomalous precipitation or storm events. One of the first observations made of weather modification through industrial process was in England by Ashworth (1929). He noted that Sunday rainfall amounts, the day factories were regularly shut down, were lower than during the rest of the week and hypothesized that "the fine flue dust ejected by the draught up the chimney may supply an abundance of nuclei which promote the formation of rain". Almost forty years later, an association between increased iron and steel production in Chicago, Illinois and increased precipitation and storm events downwind at La Porte, Indiana was evaluated and statistically defended as being plausible (Changnon, 1968). The conclusions drawn in METROMEX (Metropolitan Meteorological Experiment) similarly suggested that increased rainfall and storm activity observed over and downwind of St. Louis, Missouri were due to urban/industrial effects, with anthropogenic IN considered to be a contributing factor (Changnon, 1981).

In contrast, some instances have been noted where a suspect industrial complex does not show evidence of downwind weather modification, despite favourable indicators for the contrary. Although investigation by Telford (1960) revealed IN concentrations of 300/litre at -22°C in the effluent of steel plants in the Newcastle/Sydney (Australia) area, downwind impact was determined to be negligible (Ogden, 1969). The validity of some of Ogden's results, however, was challenged in later discussion (Changnon, 1971). In an investigation of the downwind climatological impact of a single steel complex in Hungary, Lowry and Probald (1978) similarly found no evidence to support the release of IN and consequent weather modification.

A hybrid situation arose in the results presented by Hobbs *et al.* (1970). In their investigation of airborne effluent from a variety of isolated industrial complexes in the State of Washington, using airborne IN detection equipment, they noted anomalously high CCN (cloud condensation nuclei) concentrations but low or absent IN concentrations. They sampled plumes from a copper smelter, a steel furnace, a ferroalloy plant, an aluminum smelter, a Kraft mill and a saw mill, with only the ferroalloy plant producing measurable IN at close to background levels. However, annual precipitation and stream flow amounts were found to increase in the vicinity of many of these operations, despite the low IN values. The excess CCN appeared to provide fertile ground for periodic injections of naturally occurring IN, triggering, through this two-step process, anomalously high precipitation amounts. It is considered to be a hybrid situation as weather modification evidence is present, but IN are absent.

None of the above mentioned industrial processes contains any reference to cement

production. Furthermore, the literature is exceedingly sparse in discussions of the nucleating and hygroscopic effects of cement kiln effluent. Budilova *et al.* (1969) noted that a possible 5 % increase in precipitation fall could be realized during seeding of convective clouds with a halite and cement mixture, and Murty and Murty (1972) confirmed the nucleating properties of Portland cement through laboratory testing. They showed that the threshold nucleation temperature of Portland cement to be -4.6°C to -5.0°C, between that of silver iodide (-4.0°C) and lead iodide (-6.5°C).

4. EXSHAW INDUSTRY

Three separate mineral beneficiation processes take place at the industrial complex at Exshaw, each under the auspices of a separate company. These companies are Lafarge Canada Inc., Continental Lime Ltd., and Baymag, all three providing data and information on their operations for this study, as presented below.

Lafarge Canada Inc. (Lafarge), one of Canada's largest producers of cement, is believed to be the source of ice nuclei detected in aerial sampling tests reported by Heimbach (1986). In the manufacture of cement, raw materials are initially crushed, blended, ground together and then introduced into long, gently sloping rotating kilns. At 900°C, calcination takes place, and at final temperatures of 1450 - 1650°C, aluminum and calcium complexes form. The kiln product, referred to as clinker, is ground and with a small amount (5%) of gypsum becomes Portland cement. Lafarge currently uses two such kilns, each kiln having a primary kiln stack and secondary cooler stack.

The principal sources of heat, vapour and particulates are the kiln stacks, located at the upper end of the kiln complex. The exhaust gas temperatures average 146°C for kiln five and 336°C for kiln four. Kilns one and two were shutdown in 1976 and kiln three was transferred in October 1982 to Baymag (see below).

Particles released include complex dicalcium and tricalcium silicates, tricalcium aluminate and tetracalcium alumino ferrite. Chemical assays provided by Lafarge show highest concentrations by weight of calcium and silicon, with decreasing amounts of magnesium, potassium, sulphur, aluminum and iron. The greatest percentage of particles released are less than 0.3 μ in diameter, accounting for approximately 83% (by weight) of the solids released, with 6% between 0.3 and 10 μ, and 11% larger than 10 μ. It was noted by Telford (1960) that effluent from Australian steel mills was inert, with high amounts of manganese and silicon, and that particles released were initially in the size range of 0.1 to 1.0 μ, with later coagulation to larger than 10 μ. Table 1 presents a comparison of particle size distributions for the three facilities.

The cooler stacks, located at the lower end of the kiln complex, release gas at comparable velocities but at lower temperatures than the main stacks - kiln four at an average of 146°C and kiln five at an average 169°C. These stacks exhaust air used in cooling the resulting clinker to temperatures that can be handled elsewhere in the facility. Both kilns are fuelled by natural gas, using some 400,000 cubic metres per day. The raw materials used in the process include limestone from the Palliser Formation of Exshaw Mountain, immediately behind the plant, sandstone from the Belly River Formation, shale from the Wapiabi Formation, industrial iron and fly ash. Ash and shale are recognized as common, naturally occurring ice nucleating agents (Dennis, 1980) although during the manufacturing process they become part of the complex cement phyllosilicate and tectosilicate structure, and their individual mineralogical structure is lost. On hydration, the cement complex becomes extensively cross-linked and hardens to form the construction material known as concrete.

Exhaust that exits each of the two kiln stacks is cleaned of 99.7 % of particulates by an electrostatic precipitator (ESP). The secondary cooler stack exhaust is cleaned by gravel bed filters of similar efficiency. The ESP, responsible for limiting average particulate outputs to less than 55 kg/hour, is periodically subject to shutdown for a number of production reasons, including but not limited to the presence of explosive concentrations of volatiles. During these brief transient events, which are carefully logged and reported to Alberta Environment, the Provincial Government department responsible for air quality, particulate loading can increase, theoretically, by two orders of magnitude. This would be anticipated to result in a similar increase in the downwind IN concentration of the effluent from the observed 5/litre to 500/litre, comparable in magnitude with those concentrations measured by Telford (1960) over steel mills in Australia.

Table 1. Average size distributions of effluent particles based on particulate weight. Reported size refers to particle diameter.

	< 0.3 μ	0.3 - 10 μ	> 10 μ
Lafarge	83 %	6 %	11 %
Continental Lime Ltd.	2 %	64 %	34 %
Baymag	1 %	34 %	65 %

The other two facilities located at Exshaw include Continental Lime Ltd. and Baymag. Both firms, like Lafarge, are mineral processors. Continental Lime Ltd., located 5 km east of Lafarge, uses two rotating horizontal kilns for the calcination of limestone ($CaCO_3$) into quicklime (CaO), and a short kiln for drying crushed limestone. Limestone is from the Mount Head

Formation, located 13 km away. Particulate output is significantly lower than at Lafarge, averaging less than 5 kg/hour. Baymag, adjacent to Lafarge, uses the former Lafarge kiln 3 for the formation of magnesium oxide (MgO) through the calcination of magnesite and dolomite, obtained from the Cathedral Formation of Brussilof Mountain, 70 km away. Despite low production amounts, typically 180 tonnes/day, and the use of an ESP, exhaust stack particulate amounts are comparable to Lafarge kiln stacks, averaging 45 kg/hour.

5. METHODOLOGY

The evaluation of a potential seeding impact at Calgary due to anthropogenic ice nuclei (ANIN) was carried out in two parts. The first sought to determine whether the precipitation at Calgary (both amount and number of events) was anomalous by developing a scheme for predicting what the unseeded precipitation at Calgary should be and thereby produce residuals. The second part was dependent on the first, with an attempt to quantify the relationship between Lafarge production over the ten year period from 1981 to 1990 and both (i) calculated event and amount residuals and (ii) the ratio of observed to predicted events and observed to predicted amounts (eg. Thompson and Griffith, 1981).

5.1 Part 1

In attempting to determine any anomalous nature to the precipitation at Calgary, methodologies frequently used by researchers, and in particular by weather modification operators, were considered. The most difficult problem posed here, and indeed in most weather modification evaluation schemes, was determining what would have happened had there been no seeding treatment. As it is not possible to observe what naturally happens and then retroactively apply a seeding agent, indirect schemes for predicting the background or natural state have been developed over the years. These include the target-only, target-control and crossover designs. All three, however, require that for some period, weather parameters (in this case precipitation amount and incidence) be measured when seeding *isn't* or *hasn't* happened. This presents considerable difficulty in the present case as mill records prior to 1980 are vague and shutdown periods cannot be determined prior to this period. Furthermore, in the 120 month sample data set complete shutdown of both kilns occurred only on 4 months (January 1981, February 1981, November 1984, December 1984), insufficient to create a predictor useful for the entire 10 year period. Monthly Lafarge production is presented in figure 2.

A solution to this problem was to use data from other Alberta meteorological stations in a modified target-control approach, and determine whether there was a relationship between precipitation and an independent variable that could be used for predicting what the "unseeded" precipitation at Calgary should be. Partial support for this approach was the good correlation observed by Longley (1974) between precipitation amounts at prairie stations with less than 400 km separations. Five first order stations were used, all latitudinally displaced from Calgary but in a band of roughly equivalent longitudinal displacement from the mountain barrier (Fig. 1). The stations included Red Deer, Edmonton, Medicine Hat, Lethbridge and Edson.

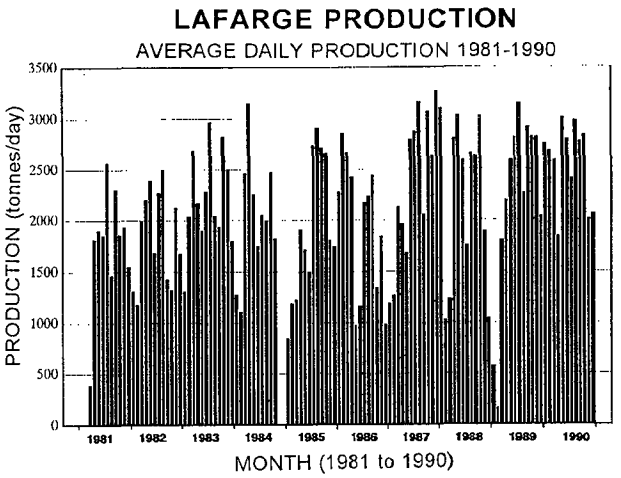

Figure 2. Average daily cement production at Lafarge. Only four months had zero output (January 1981, February 1981, November 1984, December 1984).

Testing of various relationships between monthly precipitation (e.g., measurable precipitation amounts and events in westerly flow, total precipitation, precipitation in non-westerly flow, and ratios of the above) and time (e.g., days per month of westerly flow, days per month of westerly flow in which measurable precipitation fell, days of non-westerly flow, days of non-westerly flow with precipitation, and ratios of the above) were carried out. It was found that the most consistent relationships were between the number of days in a given month that the prevailing surface wind was from the west (250 to 290 degrees) and both the amount of precipitation that fell in westerly flow (type A predictor) and the number of precipitation events during westerly flow (type B predictor). By combining data from all five stations, the strength of a least squares linear correlation could be evaluated for each predictor on a month by month basis, 120 months in total. The coefficients of determination for each predictor and for each month of the ten year period are presented in figures 3 and 4.

Of concern was spacial variability of precipitation due to geographic situation, particularly latitude, and rigorous filtering of the predictor months was initiated to eliminate suspect values. A threshold coefficient of determination of 0.90 was established as the minimum, corresponding to a significance level of approximately 0.01. Any predicted value from a month with an r^2 value below 0.90 was rejected.

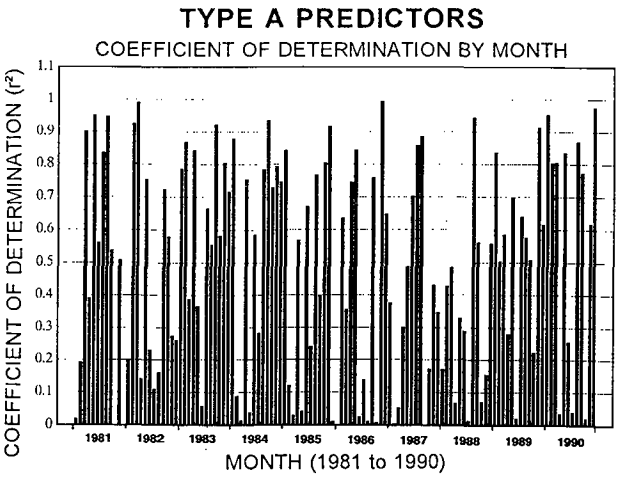

Figure 3. Coefficients of determination (r^2) for the type A predictor. Type A used a correlation between the amount of monthly precipitation that occurred during west flow and the number of days for a given month that had prevailing westerly winds.

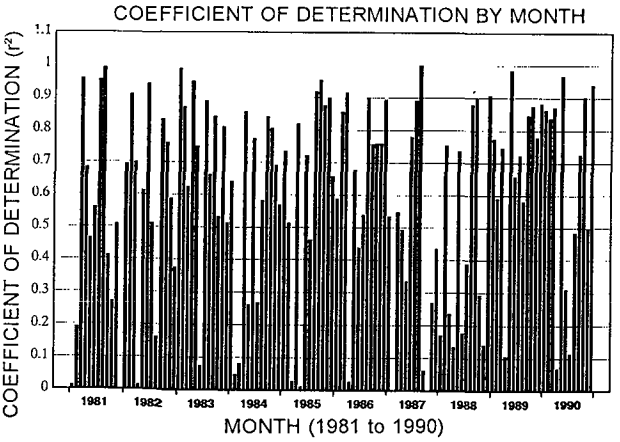

Figure 4. Coefficients of determination (r^2) for the type B predictor. Type B used a correlation between the number of monthly precipitation events that occurred during west flow and the number of days for a given month that had prevailing westerly winds.

As a check of the validity of the relationships as predictors, it was noted that for January 1981, February 1981, November 1984, and December 1984, the inclusion of Calgary data did not change the coefficient of determination by more than 0.04. While this supports the premise that Calgary precipitation should not be anomalous for those months in which there was no seeding taking place, it is by no means conclusive as the coefficient of determination in all four cases was below the 0.90 rejection threshold.

5.2 Part 2

The type A and type B residual data, extracted as above, as well as the ratios of observed to predicted precipitation amounts and precipitation events were then compared through a least squares linear regression with weighted production amounts at the Lafarge facility. Raw Lafarge production data took the form of total monthly kiln production measured in tonnes, and the weighted production values took the form of daily estimated production (monthly tonnage divided by the number of days in the month) multiplied by the number of days for that month in which prevailing wind at Calgary was from the west. Type A results are presented in table 2 and type B results are presented in table 3.

Figure 5 illustrates the relationship between residual precipitation amounts (the difference between what was observed and what was predicted to have fallen had there been no seeding influence) and weighted production, the three positive values indicative of precipitation augmentation and the nine negative values indicative of precipitation suppression. The single zero value indicated no seeding influence. Figure 6 illustrates the same relationship for precipitation events, rather than amounts, with five instances of augmentation, eight instances of suppression, and three instances of no impact.

Figures 7 and 8 illustrate the relationship between ratios of observed to predicted precipitation amounts (figure 7) and precipitation events (figure 8). Values in excess of unity suggest precipitation augmentation and values below unity suggest precipitation suppression. Values of unity indicate no seeding influence, and values of zero indicate a complete absence of a precipitation event where one was predicted. Figure 7 presents three instances of augmentation and nine of suppression, and figure 8 presents four instances of augmentation, eight of suppression, and one of no impact. Data points in both figures were culled (one in figure 7 and three in figure 8) where the predicted precipitation amount or event value was zero, resulting in a zero in the ratio denominator and an undefined ratio value.

In all four figures the least squares linear regression coefficients of determination were low (0.04 for figure 5, 0.23 for figure 6, 0.02 for figure 7 and 0.03 for figure 8) and clearly not significant at a 0.05 confidence level. These results are discussed further in section 7.

6. DATA

Lafarge Canada Inc., the suspected IN producer, has provided monthly production data for the 1981-1990 period. These production figures can be concluded to be proportional to stack effluent amounts, the electrostatic precipitation (ESP) equipment used in particulate capture being fairly uniform in efficiency

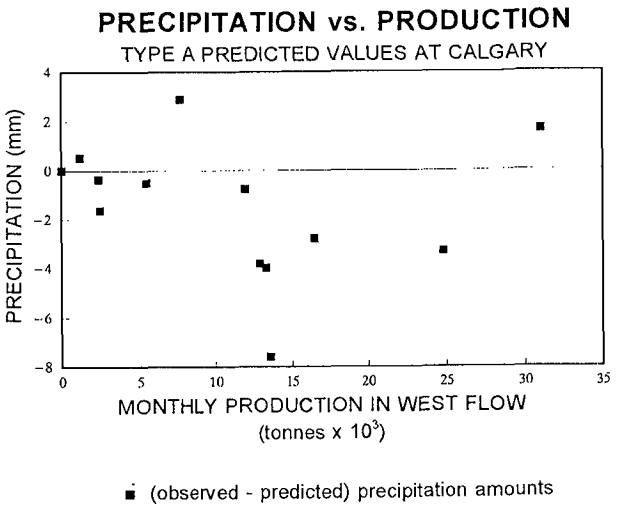

Figure 5. Relationship between type A residual precipitation amounts (determined when the predictor coefficient of determination was in excess of 0.90) and production amounts during westerly flow.

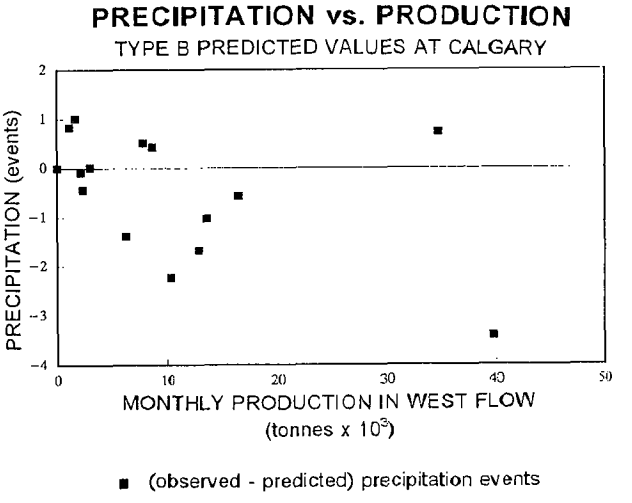

Figure 6. Relationship between type B residual precipitation events (determined when the predictor coefficient of determination was in excess of 0.90) and production amounts during westerly flow.

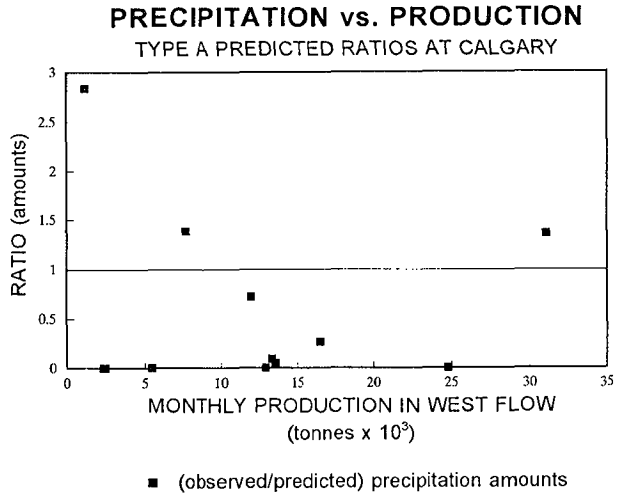

Figure 7. Relationship between the ratio of observed and type A predicted precipitation amounts (determined when the predictor coefficient of determination was in excess of 0.90) and production amounts during westerly flow.

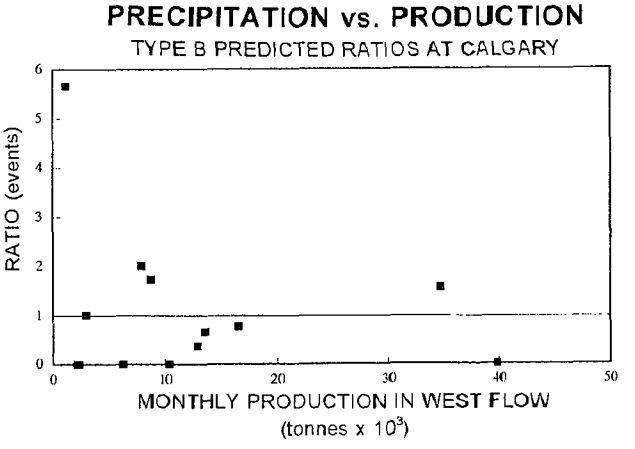

Figure 8. Relationship between the ratio of observed and type B predicted precipitation events (determined when the predictor coefficient of determination was in excess of 0.90) and production amounts during westerly flow.

regardless of the output rate (J. Brown, personal communication, 1988). In order to make the target-control separation, the production amount under downwind conditions had to be separated from the production amount under non-downwind conditions.

Particulate emission data were obtained from independent laboratory results provided by Lafarge and Continental Lime Ltd., and by personal communication for Baymag (B. Walsh, personal communication, 1986).

All precipitation data was provided by the Atmospheric Environment Service, Canada's national weather forecasting and climate data service. As indicated, only first order meteorological stations in southern Alberta with precipitation and daily prevailing wind data were used. Prevailing wind was defined as the most commonly occurring two minute mean wind as measured every hour in a 24 hour period, and in this case covered azimuths of 250 to 290 degrees true. Precipitation was measured in millimetres, or the

Table 2. Type A observed, predicted and residual precipitation amounts as used in figures 5 and 7. Weighted production amounts and coefficients of determination are also shown.

Month	Observed Pcpn (mm)	Calculated Pcpn (mm)	Residual Pcpn (mm)	Ratio (Obs/Cal)	Predictor r^2 value	Weighted Production (tonnes)
3: Mar 81	0.8	0.28	+ 0.5	2.9	0.902	1163
5: May 81	10.4	7.53	+ 2.9	1.4	0.952	7624
8: Aug 81	0.0	0.0	0.0	undefined	0.948	0
14: Feb 82	0.0	0.36	- 0.4	0.0	0.926	2365
15: Mar 82	2.0	2.77	- 0.8	0.7	0.992	11953
33: Sep 83	0.4	8.00	- 7.6	0.1	0.923	13562
45: Sep 84	0.0	1.63	- 1.6	0.0	0.938	2472
59: Nov 85	0.0	0.52	- 0.5	0.0	0.916	5433
71: Nov 86	0.0	3.82	- 3.8	0.0	0.995	12908
92: Aug 88	0.4	4.48	- 4.0	0.1	0.944	13307
107: Nov 89	6.2	4.57	+ 1.6	1.4	0.915	31051
109: Jan 90	0	3.32	- 3.3	0.0	0.954	24791
120: Dec 90	1.0	3.80	- 2.8	0.3	0.976	16491

melted equivalent if the precipitation was snow or hail, and precipitation events were marked by any day in which measurable precipitation was received.

7. RESULTS

An initial total of 13 type A and 16 type B residual and ratio values were produced after filtering. Paired t test comparisons of the calculated precipitation amounts with the observed values (type A predictor) indicated significant differences at the 0.07 confidence level for precipitation amounts alone and 0.11 for ratios of observed to calculated precipitation amounts. Comparison of the calculated precipitation events with the observed events (type B predictor) had significance differences at the 0.15 confidence level for events alone and 0.89 for ratios of observed to calculated events. Nonparametric comparisons using Mann-Whitney U tests revealed threshold confidence levels of 0.05 and 0.02 for the type A residuals and ratios, and 0.24 and 0.25 for the type B residuals and ratios, similar to t test values. As noted by Griffith *et al.* (1991), these statistical tests are indicators of validity rather than proof, the randomness and independence requirements not being completely fulfilled.

Despite the statistical strength of the type A predictor in producing residual and ratio values indicative of anomalous precipitation at Calgary, no linear correlation was evident between precipitation amounts or events and weighted Lafarge production. In all four cases (type A and B), the coefficient of determination was below 0.23 and not significant at the 0.05 confidence level. However, the type A residual results did have a nonlinear trend (Fig. 5). Below 11000 tonnes weighted monthly production, residual precipitation wavers between mild surplus and deficit. Between 11000 and 29000 tonnes, there was a strong deficit in precipitation, and beyond 29000 tonnes a surplus, as if the negative effect of possible overseeding gave way to some other factor at high production amounts, possibly heat or water vapour (e.g., Hindman, 1977). The pattern is almost sinusoidal, with the amplitude of the residual increasing with increasing production amounts. If the initial fluctuations are discounted, the curve is also suggestive of a cubic function.

8. CONCLUSION

Cement production at the Lafarge facility, on the basis of the tests carried out in this study, cannot be confidently linked to precipitation amount or event anomalies determined at Calgary. Despite the majority of points in figures 5 to 8 lying in the precipitation suppression zones of these graphs, the trend described in the results section must be considered consequential rather than causal, with concrete evidence of cement plant effluent affecting Calgary's precipitation still lacking.

There are a number of reasons why the indicators are inconclusive. Anomalous precipitation at Calgary could be due to some situational feature not present at the other five stations used in producing the residual. Also, there may not be a completely linear relationship between kiln production and stack effluent

Table 3. Type B observed, predicted and residual precipitation events as used in figures 6 and 8. Weighted production amounts and coefficients of determination are also shown.

Month	Observed Pcpn Events	Calculated Pcpn Events	Residual Pcpn Events	Ratio (Obs/Cal)	Predictor r^2 value	Weighted Production (tonnes)
3: Mar 81	1	0.18	+ 0.8	5.6	0.957	1163
7: Jul 81	1	2.68	- 1.7	0.4	0.954	12847
8: Aug 81	0	0.00	0.0	undefined	0.991	0
14: Feb 82	0	0.44	- 0.4	0.0	0.908	2365
18: Jun 82	1	0.00	+ 1.0	undefined	0.942	1687
25: Jan 83	1	0.49	+ 0.5	2.0	0.988	7878
28: Apr 83	0	0.10	- 0.1	0.0	0.948	2168
56: Aug 85	1	0.58	+ 0.4	1.7	0.918	8729
57: Sep 85	2	3.00	- 1.0	0.7	0.953	13588
63: Mar 86	2	1.28	+ 0.7	1.6	0.915	34689
80: Aug 87	0	0.00	0.0	undefined	0.998	0
96: Dec 88	0	1.39	- 1.4	0.0	0.907	6283
101: May 89	0	2.23	- 2.2	0.0	0.984	10376
113: May 90	1	0.99	0.0	1.0	0.968	3012
118: Oct 90	0	3.42	- 3.4	0.0	0.902	39766
120: Dec 90	2	2.58	- 0.6	0.8	0.941	16491

amount (varying ESP efficiency). Furthermore, it is possible that there exists a sink that deactivates or scours IN from the air downwind of Exshaw. This may be manifest simply as deactivation through particulate coagulation, as noted in steel mill plumes in Australia (Telford, 1960) and in cement effluent in the former Soviet Union (Vdovin *et al.*, 1974), or as aggravated particulate settling due to mesoscale phenomena (i.e., subsidence over Ghost Lake, located 20 km east of Exshaw).

It is also possible that the source of IN was mis-identified during the original sampling flights, and that Continental Lime Ltd. or Baymag may contribute to the release. Murty and Murty (1974) noted that quicklime (CaO) also acted as a nucleating agent in laboratory tests, although they also noted that the nucleating effect decayed rapidly on wetting due to solution effects.

Planned further study will take the form of analyzing ESP dust samples for nucleating ability and collecting rain samples in Calgary in order to carry out an analysis for cement plant effluent. Such effluent has a distinctive mineralogical signature (Arslan and Boybay, 1990) and downwind samples should be distinguishable from natural dust on the basis of the mineralogical "fingerprint" determined from ESP dust samples provided by Lafarge.

9. ACKNOWLEDGEMENTS

Thanks are extended to M. Pawlicki, J. Brown and J.D. Catillon of Lafarge Canada Inc., J. Elliot of Steel Brothers Ltd. (now Continental Lime Ltd.) and B. Walsh of Baymag, for providing extensive production and effluent data. Thanks are also due to T. Thompson and thesis advisor R. Charlton of the University of Alberta for providing data and discussion, M. Swarbrick for library services, J. Heimbach for providing the initial IN results and thoughts on analysis, P. Sweeney for assigning me to the Istanbul rain project and thereby indirectly funding part of this project, and the two anonymous reviewers for their suggestions and comments. This project is part of a M.Sc. research thesis at the University of Alberta at Edmonton, Alberta.

10. REFERENCES

Arslan, M., and M. Boybay, 1990: A study on the characterization of dustfall. Atmos. Environ., 24A, 2667-2671.

Ashworth, J.R., 1929: The influence of smoke and hot gases from factory chimneys on rainfall. R. Meteor. Soc., 55, 341-350.

Braham, R.T., 1986: Precipitation enhancement - a scientific challenge. In: Precipitation Enhancement - A Scientific Challenge. R. Braham (ed.), Meteorological Monograph, vol. 21, no. 43, Amer. Meteor. Soc., Boston, 1-5.

Budilova, E.P., E.E. Kornienko, V.T. Lenshin and D.D. Stalevich, 1969: Practical experiments with a mixture of sodium chloride and cement as a reagent for seeding large cumulus clouds. Army Foreign Science and Technology Centre, Washington, D.C. 14 pp.

Changnon, S.A., 1968: The La Porte weather anomaly - fact or ficton? Bull. Amer. Meteor. Soc., 49, 4-11.

Changnon, S.A., 1971: Comments on "The effect of rainfall on a large steelworks." J. Appl. Meteor., 10, 165-168.

Changnon, S.A., 1981: Impacts of urban modified precipitation conditions. In: METROMEX: A Review and Summary, S. Changnon (ed.), Meteorological Monograph, vol. 18, no. 40, Amer. Meteor. Soc., Boston, 153-177.

Dennis, A.S., 1980: Weather Modification by Cloud Seeding. International Geophysics Series, vol. 24, Academic Press, Toronto. 267 pp.

Griffith, D.A., J.R. Thompson and D.A. Risch, 1991: A winter cloud seeding program in Utah. J. Weather Mod., 23, 27-34.

Heimbach, J.A., 1986: Ground based plume tracing in Alberta, July 1985. Final Report submitted to the Alberta Research Council, March 1986.

Hindman, E.E., 1977: Cloud condensation nuclei from a paper mill - Part 2: Calculated effects on rainfall. J. Appl. Meteor., 16, 753-755.

Hobbs, P.V., L.F. Radke and S.E. Shumway, 1970: Cloud condensation nuclei from industrial sources and their apparent influence on precipitation in Washington State. J. Atmos. Sci., 27, 81-89.

Longley, R.W., 1974: Spatial variation of precipitation over the Canadian prairies. Mon. Weather Review, 102, 307-312.

Lowry, W.P., and F. Probald, 1978: An attempt to detect the effects of a steelworks on precipitation amounts in central Hungary. J. Appl. Meteor., 17, 964-975.

Miller, J.R. (ed.), 1992: Legal regulation of weather modification in the United States and Canada. J. Weather Mod., 24, 126-129.

Murty, A.S.R., and Bh.V.R. Murty, 1972: Ice nucleation by ordinary Portland cement. Tellus, 14, 581-585.

Murty, A.S.R., and Bh.V.R. Murty, 1974: Identification of quick lime as ice nucleant. J. Weather Mod., 6, 79-86.

Ogden, T.L., 1969: The effect of rainfall on a large steelworks. J. Appl. Meteor., 8, 585-591.

Telford, J.W., 1960: Freezing nuclei from industrial processes. J. Meteor., 17, 676-679.

Thompson, J.R., and D.A. Griffith, 1981: Seven years of weather modification in central and southern Utah. J. Weather Mod., 13, 141-149.

Vdovin, B.I., G.G. Velichko, I.M. Zrazhevskii, S.A. Kon'kov, R.I. Onikul, G.A. Panfilova and N.S. Shmorgunenko, 1974: Propagation patterns of discharges from alumina cement plants into the atmosphere. In: Air Pollution and Atmospheric Diffusion 2, M.E. Berlyand (ed.), John Wiley & Sons, Toronto, 233-241.

ATMOSPHERIC FEATURES OF HAIL PERIODS IN SERBIA

Djuro Radinović
Institute of Meteorology, University of Belgrade

Abstract. From 1969 to 1986, there were 222 periods of several successive hail days registered in the target area covered by the hail suppression system in Serbia. In order to have the features of the atmosphere on hail days clearly outlined, a thorough analysis of the synoptic situation and some other important meteorological elements of the periods had to be made. The analysis proved the assumption that Cb cloud development is stimulated by the synoptic situation accompanying a hail period. On the other hand, no direct connection could be found between the occurrence of hail and some other meteorological elements, suggesting that the synoptic-scale conditions studied here are necessary ones, though not sufficient for the development of hailstorms.

1. INTRODUCTION

Ever since the introduction of the hail suppression system in Serbia, it has been noticed that the periods of successive hail days regularly appear in the target area several times a year. That is when widespread hailstorms leave large hail swaths in parts of the target area.

Some of the typically prevailing synoptic situations of the periods are identified, suggesting that such periods could be characterized by some of the specific features of the atmosphere, probably closely connected with the development of hailstorms. This study deals with the synoptic situations and some of the important meteorological elements during hail periods in Serbia.

2. HAIL PERIOD STATISTICS

In the 18-year time period from 1969 to 1986, there were 222 periods with a total of 876 hail days registered in Serbia (Fig. 1).

The annual frequency and duration of the storms during these periods (Table 1) indicate that the annual frequencies and mean length of the hail periods are rather uniform. This is not the case with frequencies at a meteorological station, because a station experiences hail at random, while it is a regular phenomena in an area throughout the year.

Table 2 shows the distribution of the hail periods according to number of days in the period. The frequencies suggest that there are at least three different mechanisms governing the hail processes. The first mechanism corresponds to the hail periods of two- to five-day duration; the second one seems to govern the seven- to nine-day lasting processes; while the third covers the processes exceeding ten-day periods. These possible mechanisms provide a convenient separation of the data for this study.

The data for the distribution of hail periods according to their monthly frequencies are presented in Table 3. More than 50% of all the cases occurred in May and June, which corresponds to the annual thermal and pluviometric regimes. Namely, these months are known to have the greatest increase in surface temperature in Serbia, as well as maximum amount of precipitation. The mean values of the duration of hail periods are very similar, too.

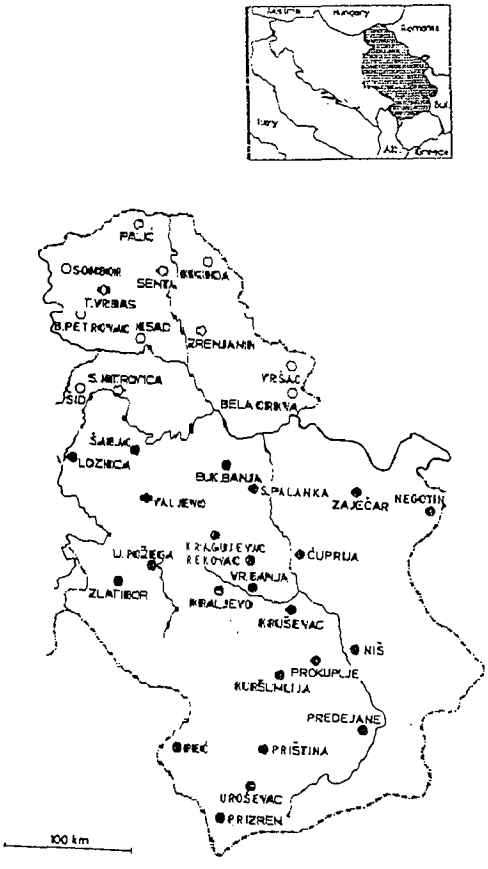

Fig. 1. Territory of Serbia, covered by hail suppression system (full circles, showing main synoptic stations). The insert in the upper right-hand corner shows the region relative to the remaining parts of former Yugoslavia and surrounding countries.

3. SYNOPTIC CONDITIONS

For the purpose of this study, each hail period was extended to include the day before it began and the one after it ended. This enabled us to see the differences in

Table 1. Frequency and duration of hail periods in Serbia.

Year	No. of periods	No. of days	Mean duration (days)	duration (days)
1969	13	47	3.6	8
1970	17	63	3.7	12
1971	8	35	4.4	9
1972	10	42	4.2	11
1973	10	44	4.2	15
1974	10	35	3.5	8
1975	14	67	4.8	17
1976	15	63	4.2	11
1977	16	63	3.9	9
1978	13	46	3.5	9
1979	13	49	3.8	12
1980	12	41	3.4	7
1981	10	43	4.3	9
1982	13	51	3.9	9
1983	14	41	2.9	5
1984	13	40	3.1	6
1985	10	45	4.5	12
1986	11	61	5.5	14

atmospheric features before, during, and after the hail periods. The synoptic conditions for these periods were studied from the series of synoptic charts and the radiosonde observations from Belgrade were used to calculate the mean values for the standard isobaric levels of 1000, 850, 700, and 500 hPa, as well as the mean thickness of the layers between these levels. Mean mixing ratio and the mean values of windshear, vorticity, and static stability were also calculated.

Table 2. Frequency of hail periods according to duration in days.

No. of Days	No. of Periods
2	79
3	61
4	28
5	18
6	4
7	6
8	6
9	10
10	0
11	3
12	3
13	0
14	2
15	1
16	0
17	1

Table 3. Monthly frequencies and duration of hail periods.

Month	No. of periods	No. of days	Mean duration (days)	Maximum duration (days)
April	8	28	3.5	6
May	52	211	4.0	14
June	60	247	4.1	17
July	47	192	4.1	15
August	42	158	3.8	9
September	13	40	3.1	7

Meteorological conditions of the shorter periods, lasting from two to five days, are mostly characterized by a cold front, usually passing from a NW to SE direction.

The hail periods with medium duration of some seven to nine days mostly coincide with large slow-moving upper air trough or depression. It was noticed in some cases that the considered area was in the weak surface gradient field or even on the surface pressure ridge during the first part of the hail period, while the cyclonic circulation prevailed during the second.

The long-lasting hail periods of more than 10 days duration mostly coincide with stationary deep trough, the top of which, after some time, cuts off and forms an upper depression cold pool over the area.

4. STANDARD ISOBARIC FEATURES

Tables 4, 5, and 6 show the mean monthly values of the standard isobaric surface anomalies in decameters (dkm) in Belgrade, the day before, during, and the day after the hail periods.

Table 4. Mean monthly anomaly (dkm) values of the standard isobaric levels in Belgrade, the day before the hail periods in Serbia.

Month	Level (hPa)			
	1000	850	700	500
April	-1	0	0	-3
May	-2	0	0	-1
June	-1	0	0	-1
July	-1	0	0	1
August	0	1	1	1
September	-1	1	2	1

Table 5. Mean monthly anomaly values (dkm) of the standard isobaric levels in Belgrade, during the hail periods in Serbia.

Month	Level (hPa)			
	1000	850	700	500
April	-3	-2	0	-2
May	-3	-2	-2	-2
June	-2	-1	-1	-1
July	-3	-2	-1	-1
August	-2	-1	-2	-2
September	-2	-1	-1	0

Table 6. Mean monthly anomaly values (dkm) of the standard isobaric levels in Belgrade, the day after the hail periods in Serbia.

Month	Level (hPa)			
	1000	850	700	500
April	0	0	0	-2
May	-2	-1	-3	-4
June	-1	-1	-3	-4
July	-2	-2	-4	-4
August	-1	-1	-3	-4
September	-2	-2	-3	-5

Table 4 indicates that in the first three months, the 1000 and 500 hPa height anomalies were negative, while the 850 and 700 hPa height anomalies were zero. That corresponds to low pressure at the surface and cold advection in the middle of the atmosphere. In the last three months, the anomalies of the isobaric heights were positive except the 1000 hPa, showing that the day before hail occurrence, the atmosphere was somewhat warmer than normal.

Table 5 shows that the values of all the standard isobaric levels are below normal in hail periods. The negative deviations are greatest on the 1000 hPa, indicating that hail periods are characterized by the existence of low pressure in Serbia.

The day after the hail periods, as can be seen in Table 6, the values of all the isobaric levels were below normal. However, comparing the data of the hail periods to data of the day after, we can see that the values for 1000 and 850 hPa increased, while those for 700 and 500 hPa decreased. Accordingly, the pressure in the lower level of the atmosphere rose, while the middle of the atmosphere was cooled by the cold air.

5. THICKNESS FEATURES

Tables 7, 8, and 9 show that the day before and during the hail periods, the surface layer (1000/850 hPa) gets warmer than it normally is. The thickness (or the mean temperature) of the other two layers is mostly normal or below normal. The day after the hail periods, the thickness of the upper layers is mostly normal or below normal. The day after the hail periods, the thickness of the surface layer is more normal, while the thicknesses of the upper layers have become less than normal, showing signs of cooling aloft.

6. ATMOSPHERIC FEATURES OF THE LONGEST HAIL PERIODS

Between 1969 and 1986, there were four hail periods registered in Serbia, lasting two weeks or even more. They are:

i) June 29 - July 13, 1973
ii) May 15 - May 28, 1975
iii) June 16 - July 2, 1975
iv) June 10 - June 23, 1986

A detailed analysis of meteorological conditions and synoptic situations of the periods showed that there was an anticyclone prevailing, with the center situated somewhere over central or northern Europe, covering Serbia with the southeast part of the storm. A northerly stream with cold advection on the eastern side of the anticyclone formed an upper trough which extended meridionally from the north of Europe to the Mediterranean Sea. Associated with that trough, a long-lasting cyclonic circulation (an upper depression) that was established in southern Europe and Serbia came to be under the domination of that cyclonic circulation. This type of synoptic situation proved to be very steady.

The sea level pressure was below normal throughout 40 of the 60 days that formed the lengthier hail periods. Only in 20 out of the 60 was it above normal. The thickness of the layer between the standard isobaric levels was mostly above normal, except for the layer of 1000/850 hPa, which was below that value. The lapse rate during the longest hail periods, according to radiosonde observations performed at Belgrade 00 UTC, was close to average (0.6°C/100 m) in the majority of days, being below normal only in a few.

Table 7. Mean monthly thickness (dkm) anomalies in Belgrade, the day before the hail periods in Serbia.

Month	Layer (hPa)			
	1000/ 850	850/ 700	700/ 500	1000/ 500
April	1	2	-2	1
May	2	0	0	1
June	1	0	-1	1
July	1	0	0	1
August	1	-1	0	0
September	1	1	0	-2

Table 8. Mean monthly thickness anomalies (dkm) in Belgrade during the hail periods in Serbia.

Month	Layer (hPa)			
	1000/ 850	850/ 700	700/ 500	1000/ 500
April	1	0	-3	-2
May	2	0	0	1
June	1	0	-1	0
July	1	0	0	2
August	1	-1	0	1
September	2	1	-1	2

Table 9. Mean monthly thickness (dkm) anomalies in Belgrade, the day after the hail periods in Serbia.

Month	Layer (hPa)			
	1000/ 850	850/ 700	700/ 500	1000/ 500
April	0	0	-2	-2
May	1	-1	-2	-2
June	0	-1	-2	-3
July	0	-1	-2	-3
August	0	-2	-1	-3
September	-1	-1	-1	-3

The analysis of vorticity of the isobaric surface, obtained by the Laplacian with 50 km distance and centered in Belgrade, was negative in all the standard levels, in the majority of days. It was more pronounced at the surface and less in the upper levels. During the longest hail periods, the wind was mostly light and variable in all the standard isobaric levels, while the mixing ratio throughout the atmosphere for the corresponding months was about or even below normal in a majority of days.

7. VORTICITY FEATURES OF HAIL PERIODS

The mean vorticity values, calculated for the days before the hail periods throughout the entire warm half of the year, show the greatest negative value at 850 hPa, and a positive one at 500 hPa only, which indicates that apart from the high pressure on the surface, the lowest layer of the air also had a high mean temperature.

An anticyclonic vorticity which decreased with the altitude showed that cold air advection was taking place in the middle of the troposphere. That advection caused a decrease of thickness as well as a decrease of static stability in the upper layer of the air.

The mean hail periods' vorticity values compared to values for the day before hail periods show that anticyclonic vorticity was decreasing, while the cyclonic one

was increasing in all standard levels. The mean vorticity values of the day after the hail periods show that anticyclonic vorticity was increasing in lower levels, just as the cyclonic one was in the higher levels.

The above-derived analyses of the mean vorticity values for the day before, during, and the day after the hail periods in Serbia indicate that in the standard isobaric levels, vorticity is in accordance with the general conditions corresponding to the hail periods. However, if we analyze some individual cases, it can be seen that every combination of cyclonic and anticyclonic vorticity is possible in different levels, during different hail periods. Thus the conclusion is that the vorticity of surface pressure and geopotential fields is not a determinant factor for the appearance of hail periods. In other words, it seems that the cyclonic vorticity is a necessary, although at the same time is not a sufficient, condition for the occurrence of hail.

8. STATIC STABILITY OF THE ATMOSPHERE

The static stability changes are usually caused by cold or warm advection in different layers of the atmosphere. The relations between thicknesses of the layers 1000/700, 700/500 and 1000/500 hPa (Radinović, 1966) during the hail periods, as well as for the day before and the day after each hail period, provide the necessary data for the study.

In about 75% of the hail cases, the static stability values of the atmosphere in hail periods were between the values of the day before and the days after the hail periods.

If so, it can be concluded that the static stability of the atmosphere, considered this way, showed no specific features during the hail periods.

9. RICHARDSON NUMBER

In order to estimate the effect of the application of the Richardson number in the forecast of Cb cloud development in Serbia, Ćurić and Janc (1988, 1989) selected 28 days, from the different hail periods, for which they calculated the Richardson number. These studies showed that the criteria for the forecast of Cb clouds based on the Richardson number (Ludlam, 1980), as well as on the modified Richardson number (Setter and Kuo, 1983), proved inapplicable in Serbia. According to Ćurić and Janc, the reason is a rather pronounced orography which directs the spilling of the cold air masses along the valleys.

10. SUMMARY AND CONCLUSIONS

After thorough analyses of the characteristics of hail periods in Serbia consisting of several successive days of hailfall, it was possible to summarize the following:

1) There are several types of synoptic situations which cause the occurrence of hail periods and determine their duration, such as cold front, thermal trough, and upper air depression.

2) Before the appearance of the hail periods, the surface pressure is, on the average, usually below normal, while the values of the upper-air isobaric levels are above normal. This relation is just the opposite of the one from the end of the hail periods.

3) The studies of the cold and warm air mass outbreaks and the advection show that a warm advection usually appears before the occurrence of hail periods.

4) A study on the vorticity of geopotential fields before, during, and after the hail periods shows that every combination of cyclonic and anticyclonic vorticity in different levels and during different hail periods is possible.

5) The mixing ratio in the standard isobaric levels during the hail periods is close to the normal ones for the corresponding months.

6) The studies of the Richardson number in days of the hailfall in Serbia show that these numbers cannot be successfully used in prediction of the hailstorm developments.

Having taken into consideration all of these features of the atmosphere during the hail periods, it may be concluded that they represent a necessary condition, though not a sufficient one, for the development of hailstorms in Serbia. However, the formation of hail and hailfall is a phenomenon of a local nature, being decisively influenced by the local conditions whose scale is considerably less than the synoptic one.

Acknowledgments. This research was supported by the Serbian Science Association and the Hydrometeorological Institute of the Republic of Serbia, Belgrade.

Appreciation is extended to Mr. Aleksandar Opra for his valuable suggestions and help in preparation of the data. The author also wishes to thank Mrs. Ljubica Radoja and Mrs. Verica Vesić for typing the manuscript.

The reviewers' suggestions for improving the manuscript are appreciated and have been incorporated.

REFERENCES

Chisolm, A.J., 1973: Radar case studies and airflow models in Alberta hailstorms. *Meteor. Monogr.*, **No. 36**, Amer. Meteor. Soc., 1-36.

Ćurić, M., and D. Janc, 1988: Modified Richardson number analysis. The hail suppression research project. Annual Report, 1988. The Hydromet. Institute of Serbia and Faculty of Physics, Belgrade, 81-89.

Ćurić, M., and D. Janc, 1989: Modified Richardson number as predictor of Cb development in mountainous regions. *Fourth Intnl. Conf. on Carpathian Meteor.*, Sofia.

Ludlam, F.H., 1980: *Clouds and Storms.* Penn. State Univ. Press. 404 pp.

Radinović, D., 1966: Orographic influence on air stream deformation in variable static stability of the atmosphere. *Third Conf. Carpathian Meteor.*, Belgrade, SHMZ and PMF, 266-271.

Seitter, K.L., and H.L. Kuo, 1983: The dynamical structure of squall line type thunderstorms. *J. Atmos. Sci.*, **40**, 2831-2854.

The North Dakota Tracer Experiment: Tracer Applications in a Cooperative Thunderstorm Research Program

Bruce A. Boe
North Dakota Atmospheric Resource Board
State Water Commission
Bismarck, North Dakota 58505

Abstract

Radar chaff and sulfur hexafluoride gas were used in the North Dakota Tracer Experiment to tag air parcels which were subsequently tracked through actively growing convective clouds and sampled by cloud physics aircraft and Doppler radars. The scope and objectives for this cooperative thunderstorm research program conducted in south-central North Dakota during June and July 1993 are presented. The project organization and resulting data base are summarized, and the course of analysis efforts charted.

1. INTRODUCTION

Western North Dakota is one of the permanent high hail incidence areas in the upper Great Plains and midwestern United States. Changnon (1984) attributed the high hail incidence to synoptic scale factors including high frequencies of cyclone and cold front passage in the summer. This makes the region of interest contrast to the location of other recent major hailstorm studies (the Black Hills of South Dakota, northeast Colorado, or central Alberta) where orographic factors play a prominent role. North Dakota suffers the highest dollar loss due to crop damage by hail of any state (Changnon 1977), and the southwestern corner of North Dakota has historically had among the highest crop-hail insurance loss costs in the United States.

Interest in hail suppression and rainfall augmentation has driven operational weather modification efforts in North Dakota for over three decades (Rose 1986, Boe 1992). From the early 1950's to the present, convective clouds have been treated with glaciogenic nuclei each June, July, and August. While the first efforts were undertaken with ground-based generators, seeding since 1961 has been exclusively airborne. Nuclei have been released within updrafts at cloud base and within supercooled updrafts by direct penetration. Numerous evaluations have been conducted of the impacts on rainfall (Eddy and Cooter 1979, Schaffner *et al.* 1983, Johnson 1985) and on hail damage (Butchbaker 1970, Smith *et al.* 1987, Johnson *et al.* 1989), and of possible combined effects (Smith *et al.* 1992). All of these evaluations suggest positive results, providing the sponsoring counties ample encouragement for continuing the program.

Still, lack of complete understanding of the physical effects of the seeding fueled speculation as to the cause of the perceived effects. The need to explore and document these processes was recognized, and in 1978 the National Oceanic and Atmospheric Administration's (NOAA's) Federal-State Cooperative Program in Weather Modification Research, now known as the NOAA Atmospheric Modification Program (NOAA/AMP) was born (Reinking 1985). Through this initial funding, the North Dakota Atmospheric Resource Board (ARB) began to coordinate efforts aimed at addressing the uncertainties of their operational seeding program, starting with the transport of seeding agent from the release aircraft into updrafts encountered below rain-free cloud bases. Early on it was decided that a "chain of events" approach would be taken, in which each step in the seeding process would be identified and experimentally examined to test the operational methodology. The data collection efforts began with instrumented aircraft, radars, and other equipment sampling clouds in a brief 1984 field program. Follow-on investigations were conducted in 1985, and on significantly larger scales in 1987, 1989 (the North Dakota Thunderstorm Project, Boe *et al.* 1992), and most recently, the 1993 North Dakota Tracer Experiment, reported herein. This paper examines the objectives of the North Dakota efforts, the approach employed, and provides an overview of the data base assembled through the 1993 field effort.

2. OBJECTIVES

The goals and objectives of the North Dakota program are summarized in Tables 1 and 2. In general, the short-term goals are those which appear fairly straightforward and on which specific efforts are already in progress; the long-term goals those which are predicated on the completion of the short-term goals.

Table 1. Long-Term Goals	
1.	Determine and quantify the physical processes that lead to the development of rainfall in northern Great Plains convective clouds.
2.	Determine the physical processes which result in the production of hail, and develop means to predict hail formation *a priori*.
3.	Improve the understanding and predictability of weather hazards, including damaging winds and cloud-to-ground lightning, on the northern Great Plains.
4.	Determine the feasibility of significantly altering the hail and precipitation formation processes towards improved agricultural productivity.

The more numerous short-term objectives listed in Table 2 are in most cases considerably more specific, but none are trivial. To date significant progress has been made in addressing Short-Term Goals (1), (2), (3), and (8). Additional progress has been made with Short-Term Goals (5) and (6). A single season's cloud-to-ground lightning data have been examined in the course of initial attempts to address (7). While some progress has been made towards goals (4) and (9), much work remains with these objectives. Data which will allow (10) and (11) to begin to be addressed have been collected during the NDTE field effort.

3. FACILITIES

Facilities employed in the NDTE are summarized in Table 3; locations for most are shown in Fig. 1. All aircraft, the C-band Doppler radar, and the project Operations Center were based at the Bismarck Airport. The X-band radar was deployed ~50 km west of the Operations Center (see Fig. 1).

Regional surface weather data were recorded by the *North Dakota Agricultural Weather Network* (NDAWN, Enz *et al.* 1992), operated by North Dakota State University and UND Aerospace. A 900-member statewide volunteer network (not shown) is maintained by the ARB which records daily precipitation and reports hail.

Atmospheric aerosols were sampled from the operations center, and aerosol samples collected aloft by the Citation were processed immediately after each flight, affording some quantitative feel for ice nucleus and cloud condensation nucleus concentrations.

Table 2. Short-Term Goals	
1.	Determine the cloud-scale transport, dispersion, entrainment, and mixing processes in High Plains cumulus and cumulonimbus.
2.	Determine whether glaciogenic seeding agents, as applied in the ongoing county-sponsored operational cloud seeding project, reach and fill the targeted (supercooled) portion of the treated cloud.
3.	Determine the dominant primary ice initiation mechanism(s) in Northern High Plains cumuliform clouds.
4.	Determine what concentrations of artificial ice nuclei are required to significantly influence the precipitation process.
5.	Employ appropriate cloud models to simulate seeded and non-seeded cloud conditions, and compare the results of the simulations to: a) observations of similar real clouds, and b) the expected cloud behavior based on the seeding conceptual model.
6.	Apply *in situ* aircraft, tracer, radar, and other data to verify various aspects of the cloud models.
7.	Examine the effects of seeding on cloud-to-ground lightning production in and out of operational seeding target areas.
8.	Conduct preliminary assessments of benefits accrued from seeding in North Dakota.
9.	Determine the relation of cloud transport, glaciation and precipitation processes to cloud structure, organization, and life cycle using radar, satellite, aircraft, and other observations in conjunction with numerical simulations.
10.	Characterize northern Great Plains atmospheric aerosols (cloud condensation nuclei and ice nuclei) which influence cloud processes near the surface and aloft.
11.	Identify the conditions and circumstances under which warm-cloud precipitation processes are important in northern Great Plains convective clouds.

This and previous field efforts in North Dakota have combined radar measurements with *in situ* aircraft sampling in building a foundation of knowledge on the

TABLE 3. NDTE Facilities		
AIRCRAFT	Agency	Function
Cessna Citation II	UND	Cloud physics, tracer detection
North AmericanT-28	SDSMT	Cloud physics, tracer detection
Beechcraft Duke	WMI	Tracer release
RADARS		
X-Band Doppler Radar	NOAA/ETL	TRACIR, radar reflectivity, Doppler velocity
C-Band Doppler Radar	UND	Radar reflectivity, Doppler velocity
SUPPLEMENTAL		
CLASS Mobile Sounding System	NCAR	Proximity soundings
McIDAS	ARB	Satellite imagery display, archival
National Lightning Detection Network	ARB	Cloud-to-ground lightning detection
Forecasting Workstation	AES	Upper air forecasting, analysis
Aerosol Sampling Equipment	CSU	IN and CCN measurement
Numerical Modeling Workstation - SD	SDSMT	Predictive numerical cloud modeling
Numerical Modeling Workstation GCE	NASA/GSFC	Predictive numerical cloud modeling
North Dakota Ag. Weather Network	UND/NDSU	Regional weather observations
ND Cooperative Raingauge Network	ARB	Daily rain and hail reporting

AES - Atmospheric Environment Service, Winnipeg, Manitoba, Canada
ARB - North Dakota Atmospheric Resource Board, Bismarck, North Dakota
CSU - Colorado State University, Fort Collins, Colorado
NASA/GSFC - National Aeronautics and Space Administration, Goddard Space Flight Center, Greenbelt, Maryland
NCAR - National Center for Atmospheric Research, Boulder, Colorado
NDSU - North Dakota State University, Fargo, North Dakota
NOAA/ETL - National Oceanic and Atmospheric Administration, Environmental Technologies Laboratories, Boulder, CO
UND - University of North Dakota, Grand Forks, North Dakota
WMI - Weather Modification, Inc., Fargo, North Dakota

cloud scale. These modest field programs have remained focussed on the specific objectives of the ND/AMP. The North Dakota PI's remain dedicated to this concept, sometimes termed "medium-sized science", in which the goals always remain in sight, and the scale of the field programs never becomes so large that focus is lost or that conflicting demands for the data collection resources dilute the effort.

Part of this approach includes the belief that documentation of natural processes will ultimately allow the verification of the effects of cloud seeding efforts.

That is, the most direct means of demonstrating the efficacy of the technology will be through physical measurements of the storms themselves, and ***not solely by statistical evaluations***. This approach allows verification of targeting of the seeding agent, while enabling more to be learned about cloud processes. Thus, inconsistencies in the seeding conceptual model can be identified and corrected.

Some improvements over earlier North Dakota field programs included simultaneous release of radar chaff and SF_6 from the *same* aircraft, aircraft tracking by GPS (global positioning system) rather than FAA flight tracks,

real-time downlinking of aircraft positions directly to the operations center, and real-time display of the Duke tracer release aircraft position relative to the Citation tracer detection aircraft *within the cockpit of the detection aircraft*. Another very important addition was the sampling of atmospheric aerosols which are believed to play a critical role in the determination of storm precipitation efficiency (Stith *et al.* 1992). The NDTE also employed a mobile Cross-chain Loran Atmospheric Sounding System (CLASS) to obtain soundings in the vicinity of the subject cloud complexes.

The experiments were designed to gather detailed microphysical information (*in situ* aircraft sampling), afford in-cloud tracing capability (SF_6 detection), reveal detailed cloud structure (radar reflectivity data) and internal cloud motions (Doppler velocity data, sometimes coordinated dual-Doppler scanning), and provide cloud-scale transport information. The dual-circularly-polarized NOAA radar can differentiate between echoes resulting from chaff and meteorological echoes through the use of the circular depolarization ratio (CDR), a technique dubbed TRACIR, for TRacking of Air with CIrcularly-polarized Radar (Moninger and Kropfli 1987, Martner and Kropfli 1989, Martner *et al.* 1992).

4. INFRASTRUCTURE

Research efforts were directed from an Operations Center collocated with the UND Doppler radar at the Bismarck Airport. The UND radar was controlled from the Operations Center through a fiber-optic link to the radar van. In addition to the radar reflectivity and Doppler velocity displays, the Operations Center contained the ARB's McIDAS workstation; the NLDN lightning display station; VHF and FM radio links to project aircraft and the NOAA radar, respectively; direct radio downlinks from the project aircraft; and an AES workstation with software for a variety of forecasting/nowcasting tasks, including sounding analysis.

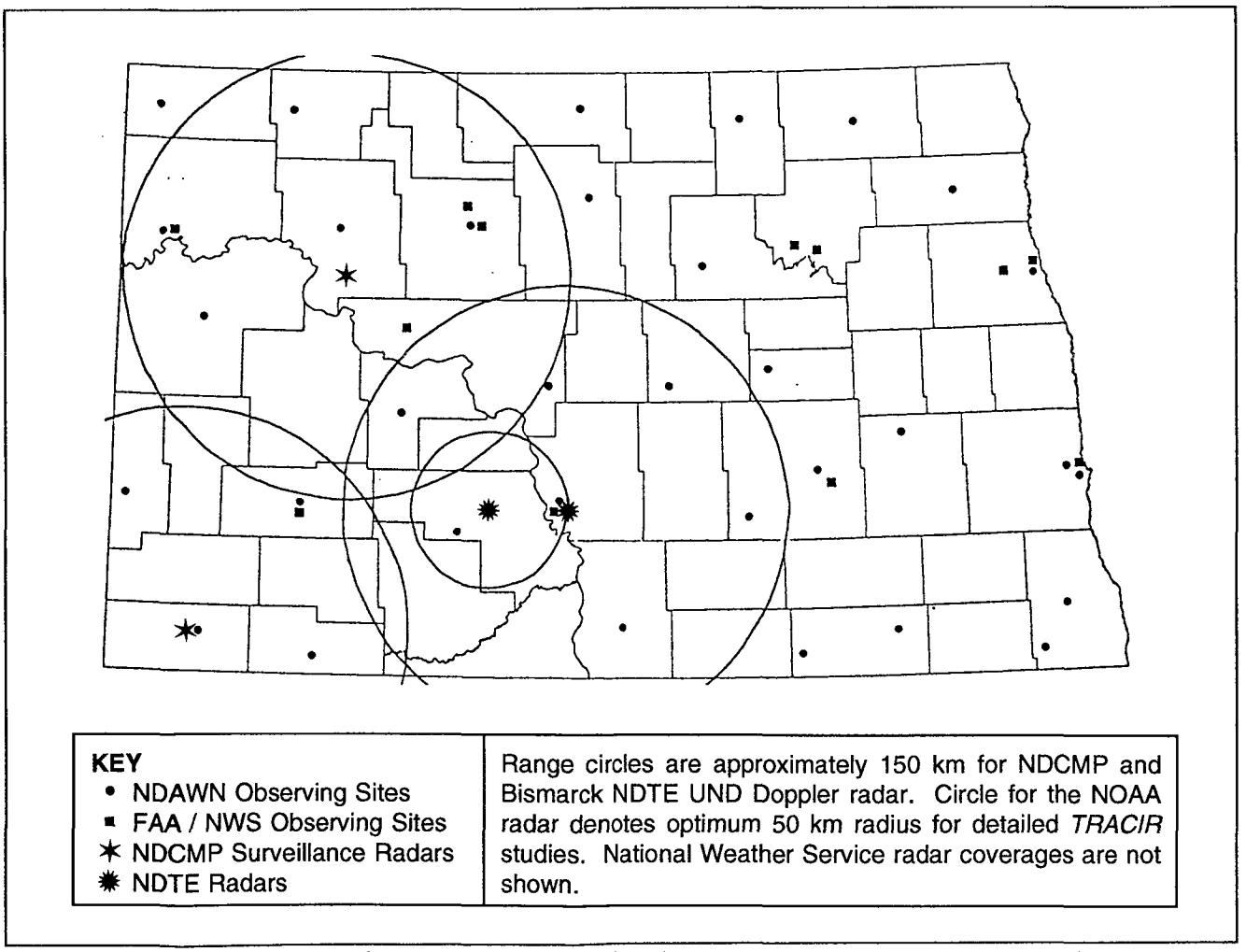

Figure 1. *The NDTE facilities and supporting data collection sites.*

A numerical modeling workstation which accessed an NCAR Cray supercomputer to run the SDSMT two-dimensional, time-dependent cloud model (*e.g.* Kopp and Orville 1994); and another which accessed either the UND Aerospace Cray or the Goddard Space Flight Center Cray (depending on which was affording better speed) to run the NASA Goddard Cumulus Ensemble (GCE) cloud model (Stith and Scala 1993) did so through Internet connections via the North Dakota University System.

Aircraft positions reported by on board GPS receivers were telemetered to the Operations Center, processed into the radar data stream, and displayed in real-time on the PPI's as they were refreshed. For continuity, a series of past positions was displayed for each aircraft, creating a "tail" behind each aircraft plotted.

Within the Operations Center, activities were coordinated by an Operations Director (OD), aided by an Assistant Operations Director (AOD). Three persons served as OD on a continuous nine-day rotation, wherein each individual would be free from duty for three days, then became the AOD for three days, and finally the OD for three days. In that manner, the AOD always became the OD prior to having days off, ensuring continuity in the day-to-day conduct of data collection efforts.

Storm intercept activities and the mobile CLASS team were directed by the Intercept Coordinator, with input from the OD. All project aircraft were directed by the Aircraft Coordinator. During operations, nowcasting was handled by a team from the ARB and the Atmospheric Environment Service (AES) Prairie Weather Centre, Winnipeg, Canada. When dual-Doppler sampling of a subject cloud was appropriate, coordinated scanning by project radars was directed by the Radar Coordinator, always an experienced Doppler radar meteorologist. A Research Experience for Undergraduates (REU) program, sponsored by the National Science Foundation (NSF), allowed students from universities nationwide to participate in the NDTE field effort (*e.g.* Orville and Knight 1992). On a rotating basis, the students served on storm intercept and the mobile CLASS teams. They ran a one-dimensional cloud model daily, served as assistants to the forecasters and radar coordinator, and worked with the research aircraft crews, flying on board the UND Citation when circumstances allowed. Without the REU students, the program could not have been conducted as it was.

5. DATA COLLECTION

Fourteen discrete experimental designs were set forth in the *NDTE Field Operations Plan.* At least one attempt was made at conducting every experimental design except one. Designs were explicitly expressed in the field operations plan document by number, title, and a discussion of the experimental procedure. Required facilities were also listed, and reference illustrations provided where applicable. The design for Experiment One is presented herein as Figs. 2 and 3. Other designs are presented in the *NDTE Field Operations Plan.*

Experiments were designed to address the following hypotheses which reflect various aspects of the conceptual model for hydrometeor development:

Experiment 1

TRANSPORT AND HYDROMETEOR EVOLUTION IN FEEDER CLOUDS

Mid-cloud Treatment

Reference Illustration: Fig. 4.1.

	Summary:	A volume of air in an individual tower in the flanking line of a mature storm will be tagged with tracer(s) and (on about one-third of the cases) seeding agent during a single pass at mid-cloud. Treatment may include any combination of the following: (a) **SF_6**, (b) **X-band chaff**, (c) **AgI-AgCl aerosol**, and (d) **fluorescent particles** (FP). Subsequent sampling of treated cloud turret and neighboring cells will be done by aircraft and radar, with collection of hailstones at the ground in case (d). The T-28 will penetrate at mid-cloud levels (around -8°C), in cells evolving into/merging with the mature (main) cell, while the Citation penetrates the same cell near cloud top. A subsequent treatment pass (or passes) will be flown by the Duke, at intervals of approximately ten minutes or so, depending on the time required for the treatment aircraft to return to the cloud. Aircraft penetrations will continue until the subject cloud (1) grows too intense to safely penetrate, (2) dissipates, or (3) evolves so that the original cloud volume can no longer be identified.
Facilities:	Aircraft:	Duke and Citation or T-28, or all three.
	Radar:	Both preferred, can be done with either radar alone when circumstances preclude using both due to range or storm position.
	Surface:	Mobile CLASS, Storm Intercept Teams (especially for FP/hail experiments.)

Figure 2. *Description for NDTE Experiment 1 as it appeared in the Field Operations Plan. The schematic for Experiment 1 is shown in Figure 3.*

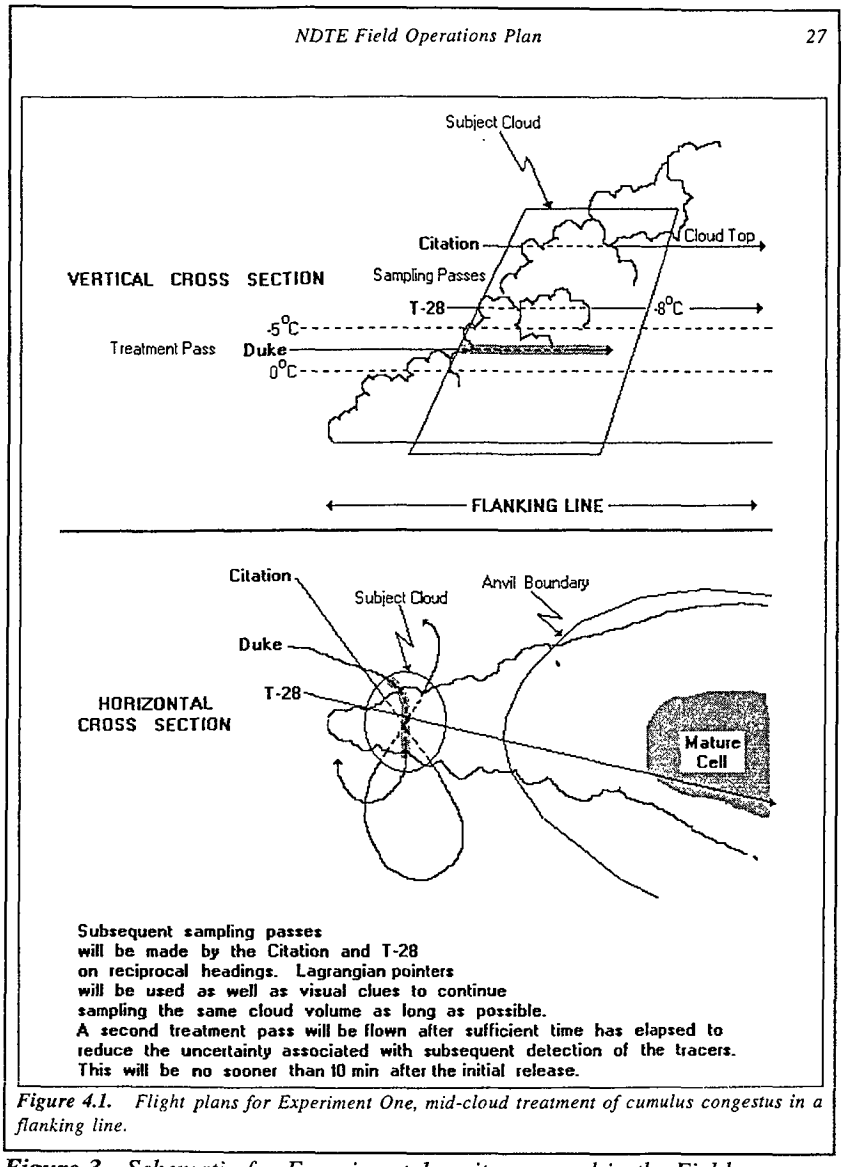

Figure 4.1. Flight plans for Experiment One, mid-cloud treatment of cumulus congestus in a flanking line.

Figure 3. *Schematic for Experiment 1 as it appeared in the Field Operations Plan.*

1. Transport at mid-levels between feeder cells and adjacent mature cells in a multicell thunderstorm can be a significant source of hailstone embryos.

2. Transport of seeding material upward from the base of a feeder cloud occurs initially in narrower plumes, but by the time the -10°C level is reached, dispersion across the updraft region is substantially complete.

3. The transport time from cloud base to the -10°C level in cumulus congestus is a significant fraction of the lifetimes of most such clouds.

4. Material in updrafts at mid-cloud levels in cumulus congestus disperses across updraft regions fairly rapidly.

5. Cloud-top entrainment occurs mainly by transport of air from above the cloud downward into the cloud periphery, followed by ingestion through the cloud sides.

6. The evolution of ice particles that nucleate and grow in clouds with weak vertical motions (and hence at roughly constant temperature) matches that observed in cloud chamber experiments.

Of the fourteen experimental designs, eleven were based on the sampling of convective clouds. Two of the remaining three were predictive numerical cloud modeling experiments; the other, aerosol sampling, was conducted with or without pre-existing convection.

The forty-day period proved to be extraordinarily active both in terms of convective activity and precipitation. The Bismarck National Weather Service precipitation total for the month of July was 34.9 cm (13.75 inches), the wettest for any month since records had been kept beginning in 1885. The disbenefit to such abundant precipitation from the scientific viewpoint was that often skies were excessively cloudy, and coordination of aircraft on subject storms was more difficult than would have normally been the case.

Clouds within range of the dual-Doppler radar coverage and, depending upon experimental intent, within range of the NOAA radar, were given priority over those in other areas. Clouds outside the primary research area identified above, but within aircraft range (about 150 km of the C-band Doppler radar) were considered for experimental purposes only when no suitable candidates could be found in preferred locations. Feeder cloud studies were accorded the highest priority, and were conducted whenever circumstances allowed. Cumulus congestus experiments were given the next highest priority, with subcloud thermodynamic studies assigned the lowest priority.

The NOAA radar was able to employ the circular depolarization ratio (CDR) signal from chaff (released by the Duke) to track the chaff *within the greater cloud volume.* Chaff was released above cloud tops, at cloud bases (in updrafts), in lines through the mid-cloud regions, and in circles in clear air around the perimeters of the clouds at various altitudes. Quantitative estimates of chaff

concentration can be computed in post-processing from the radar reflectivity of the chaff measured by the cross-polarized channel.

The mean Doppler velocity and variance of the Doppler velocity spectrum were also routinely measured and will be useful in studies of turbulence and chaff dispersion rates. In most cases chaff and SF_6 were released simultaneously. The Citation and T-28 subsequently detected the SF_6 while collecting microphysical, thermodynamic, kinematic, and electric field measurements during cloud penetrations. The *in situ* microphysical and tracer measurements complement the large-scale continuous CDR measurements of the chaff. Narrow sector scans centered on the treated cloud maximized the spatial and temporal resolution of the NOAA radar data. Resolution of about 150 m in *x, y,* and *z* dimensions was achieved within a range of 30 km of the radar. Occasional 360° sweeps made by the C-band radar provided surveillance of the storm environment.

Additional objectives that did not compete for resources with the higher priority experiments were also addressed as circumstances allowed. These include radar studies of storm evolution and electrification, which in many respects are natural by-products of the other experiments. Such studies could be conducted with or without aircraft participation, so they were prime candidates for late-day or nocturnal studies. Also included were dual-Doppler radar studies which were conducted when storms of interest passed sufficiently close to the radars, and when aircraft were not engaged in coordinated tracer studies requiring the radars to operate in other modes.

About two-thirds of the NDTE experimental clouds were to have been treated with SF_6, or SF_6 and chaff only (no-seed treatment), and the other third with SF_6 and AgI aerosol as well (seeded treatment). This approach would have allowed comparison of the AgI-treated regions with the non-seeded regions to quantify differences in ice initiation and development. Recent work at the Colorado State University (CSU) Cloud Simulation Laboratory has documented the rates of nucleation and numbers of effective silver iodide nuclei for different water-to-ice conversion mechanisms (DeMott 1990). However, only a few clouds were actually treated with seeding agent, as the record wet July weather made even the appearance of rainfall augmentation activities undesirable after 8 July.

The attempts made to execute each of the fourteen experimental designs appear as Table 4. In addition to the numerical modeling and aerosol sampling experiments (Experiments 9, 10, and 12) conducted almost daily, 62 cases were conducted according to the other experimental designs. Days with multiple experiments of a single type are indicated in Table 4 by parenthetical numbers in the "Dates Conducted" column.

6. ANALYSIS PLANS

Interactions and collaborations are *essential* for the satisfactory completion of analyses. For example, the storm morphology of the 1 July 1993 Bismarck hailstorm (described in Sec. 6.1) is being explored jointly by scientists at UND Aerospace, NSSL, and ETL. Once the morphology is established, studies of ice initiation and subsequent development of rain and hail by researchers at SDSMT, UND, and CSU will be provided a larger scale context. The behaviors of the storm will be examined by numerical modelers at NASA and SDSMT, who will compare their respective predictive models with the field observations.

One of the strengths of the NDTE data base is that specific clouds and cloud systems were sampled simultaneously on the microphysical level, the turret-scale (chaff and SF_6), the storm scale (two Doppler radars, ground-based storm intercept teams), and the synoptic scale, supplemented by proximity upper air soundings and the NDAWN surface weather data. The most complete pictures of the subject storms can only be developed by examining all relevant data, which reaffirms the need for intensive collaboration among individual analysts and agencies/universities.

There are three categories of the NDTE analysis efforts:

*1. **INDIVIDUAL CASE STUDIES**, of experiments like that described below, to elucidate details of the transport, dispersion, ice initiation and hydrometeor evolution processes in the context of the cloud environment and flow fields deduced from the Doppler radar and aircraft observations. The intent will be to obtain a comprehensive description of the cloud under study, and evaluate our understanding of the processes taking place within it, in comparison to the various hypotheses being tested.*

*2. **ANALYSES OF GROUPED EXPERIMENTS**, e.g., all cases of Experiment 1, to assess the implications with respect to the applicable experimental hypotheses. These analyses can include any applicable experiments from the 1989 North Dakota Thunderstorm Project. They can also consider how well the experimental designs worked out in practice, and identify changes that might improve the designs for future projects.*

*3. **NUMERICAL MODELING SIMULATIONS**, in support of the foregoing analysis thrusts. Investigations of cloud processes by modeling have an advantage in that individual components which contribute to specific aspects of cloud development can be isolated more readily.*

Table 4. NDTE Experiments

Aircraft and Radar Experiments

No.	*Title*[1]	*Cloud Class*	*Treatment Agent(s)*[2]	*Treatment Location*	*Dates Conducted*
1	Transport and Hydrometeor Evolution in Feeder Clouds	Cb, feeder clouds	Chaff, SF_6, FP	mid-cloud (linear)	22 June, 1 July, 3 July (5), 8 July (2), 15 July, 18 July (2)
2	Transport, Dispersion, and Hydrometeor Evolution in Feeder Clouds	Cb, feeder clouds	Chaff, SF_6	cloud base (orbit)	1 July, 6 July, 9 July (2), 23 July, 27 July
3	Transport, Dispersion, and Hydrometeor Evolution in Cu Cg	TCu	Chaff, SF_6, AgI	cloud base (orbit)	6 July, 27 July
4	Dispersion and Hydrometeor Evolution in CuCg	TCu	Chaff, SF_6, AgI	mid-cloud (linear)	22 June, 25 June, 29 June, 30 June, 1 July (2), 8 July, 27 July
5	Entrainment and Hydrometeor Evolution in CuCg	TCu	Chaff, SF_6	upper cloud (linear)	24 June (3), 25 June, 14 July, 15 July (2), 23 July
6	Entrainment and Hydrometeor Evolution in CuCg	TCu	Chaff, SF_6, AgI	upper cloud edge (orbit)	30 June (2), 22 July (2), 25 July
7	Subcloud thermodynamic Studies	Flanking line	Chaff, SF_6	cloud base	none
8	Anvil Studies	Mature Cb	Search for SF_6, O_3, electricity studies, microphysics		1 July, 3 July, 27 July
11	Thunderstorm Evolution Studies	Cu to Cb	none	N/A	1 July, 9 July (2), 22 July
13	First Echo Development	Cu	none	N/A	1 July, 16 July, 23 July, 25 July
14	Area-Time Integral Studies	Mature Cb	none	N/A	22, 23, 29 June, 1, 8, 15, 16, 21-22, 22-23, 26-27 July

Real-time Numerical Modeling Forecasting Experiments

No.	*Title*	*Model*	*Computing Facility*	*Initialization*	*Dates Forecasts Made*
9	Real-Time Two Dimensional Cloud Modeling[3]	SDSM&T 2D-TD	NCAR CRAY Y-MP	BIS NWS, CLASS	22-25, 27, 29-30 June, 1-3, 5-7, 9-10,12-16,18-28, 30 July.
10	Real-Time Predictive Utilization of the Goddard Cumulus Ensemble (GCE) Model[4]	Goddard Cumulus Ensemble	UND CRAY X-MP, or Goddard CRAY Y-MP	NGM forecast soundings	22 June, 24-25 June, 27 June - 3 July, 5-9 July, 12-16 July, 18 July, 20-27 July, 30 July.

Atmospheric Aerosol Measurement Experiment

No.	*Title*	*Equipment*	*Measurement Locations*	*Sampling Dates*
12	Aerosol Sampling, Surface and Aloft	Continuous flow diffusion chamber, CCN counter	Operations Center at Bismarck Airport, airborne samples collected at altitude by UND Citation	Daily from the Operations Center on 5-23 July. Airborne samples: 6 July, 8 July, 14 July, 18 July (2), 23 July (2)

[1]For complete descriptions of each experimental design, refer to the NDTE Field Operations Plan.
[2]Treatment may have utilized any or all of the listed agents, depending upon cloud size and position relative to the radars. "FP" denotes fluorescent particles (coated polystyrene beads) of approximately 300 μm diameter.
[3]Support provided by the National Science Foundation.
[4]Support provided by NASA Goddard Space Flight Center.

6.1 A Case Day Sample - 1 July 1993

A series of modestly tall (11-12 km) but intense thunderstorms formed in west-central North Dakota during the afternoon of 1 July 1993. These storms moved through the Bismarck area in succession, producing heavy rains and some very damaging hail. The first deep convection occurred west of Bismarck at ~13:00 CDT, when a number of cells developed southwest of the Bismarck operations center. Aircraft began working the cells by 15:00, with a mid-cloud release of chaff and tracer gas as described in Experiment 1. The first storms were sampled by radar and all three project aircraft until after 16:00, when aircraft returned to Bismarck to refuel.

The second storms of the day began as isolated cells which quickly became very intense, exploding along a north-south line west of Bismarck and subsequently moving southeast into the research area. The three largest of these storms all produced mesocyclonic circulations detectable with the UND Doppler radar. At one point distinct mesocyclones were simultaneously observed north of Bismarck, just north of the NOAA radar, and west-southwest of Bismarck! The strongest of these storms tracked directly over south Bismarck, inflicting an estimated $30 million in damages to vehicles, homes, and other property. Though the mesocyclone of the Bismarck storm was unmistakable, no funnels or tornadoes ever developed. This might be attributable to the storm's prolific rain and hail production and associated outflow which repeatedly cut off the spinning up mesocyclone.

The early stages of this storm's development were recorded by the NOAA radar, which was located ~20 km south of the first mesocyclone, and also by the UND radar. Dual-Doppler analyses will be possible for much of the storm's lifetime. A cloud base tracer release (Experiment 2) was conducted beneath a vigorous tower in the flanking line as well, and the cell was located favorably for hail trajectories to be calculated from Doppler analyses. The chaff was quickly carried aloft and toward the higher reflectivity regions of the mature cell (Figs. 4 and 5). As the chaff and SF_6 were transported upward and mixed into the storm, the Citation and T-28 penetrated the cloud, tracking the progression of the SF_6 while documenting the microphysical evolution within the treated volume.

A *third* round of storms of the day formed as a squall line ~100 km northwest of the operations center. An upper wave moved into the state and added some dynamic support to a surface frontal boundary. This line became well organized while still west of the NOAA radar, producing heavy rains and surface winds in excess of 30 m s^{-1} as it passed that radar. The squall line remained intense as it quickly caught up with the isolated storms of round two, absorbing them about 50 km east of Bismarck.

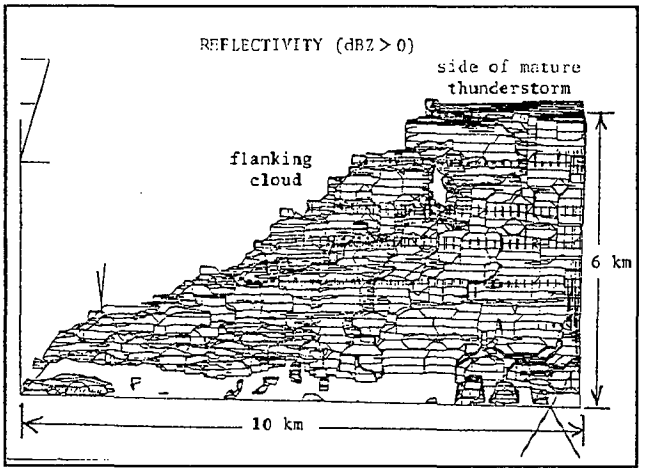

Figure 4. *Three-dimensional reflectivity reconstruction of thunderstorm flanking line recorded by the NOAA radar at 18:12 CDT, 1 July 1993.*

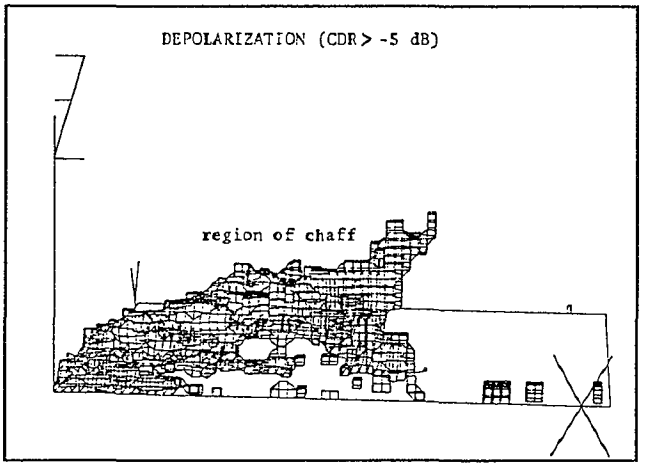

Figure 5. *The depolarization defines the approximate chaff boundary at 18:12 CDT, 6 min after a chaff-SF_6 release on 1 July 1993.*

Confluence at the base of the updraft on the order of 25 m s^{-1} was recorded as the line approached the operations center.

7. CONCLUSIONS

The success of the NDTE data collection efforts demonstrates that productive, medium-sized field programs remain possible. If core programs are defined and funded with sufficient advance notice, additional scientists with compatible interests are provided the lead time required to bring additional resources to the field, greatly strengthening the overall program-- offering more "bang for the buck".

A year or more is often required before review, revision, and funding occurs.

Real-time aircraft tracking using GPS data telemetered directly to the project operations center is a significant improvement on FAA positioning data, particularly when the nearest FAA radar is well-removed from the project area. Radar skin paints of project aircraft were commonplace, confirming the accuracy of the system. The use of GPS is made even more attractive by FAA regulations which now require considerable paperwork just to request access to the FAA data stream. Such requests must now be routed through the Department of Defense and the Drug Enforcement Agency as well as the FAA, a process which requires a lead time on the order of one year.

The simultaneous use of cloud physics aircraft and Doppler radars in combined chaff/gas tracer experiments affords the cloud microphysics to be examined in the context of cloud-scale motions and structure, particularly if one of the radars is circularly-polarized and capable of TRACIR studies. Radars employed in the NDTE were characterized by beam widths less than 1°, and many cases were within less than 50 km range, so considerable detail was recorded which supports the microphysical data collected by the aircraft.

The transport, dispersion, and mixing within the subject clouds carries strong implications for the behavior of plumes of seeding agent within targeted clouds. In this respect alone, the chaff/SF_6 experiments afford the following opportunities:

1. ***Comparisons of the chaff data with the in situ tracer data.*** Such analyses may reveal the concentration of the tracer in the various parts of each storm. The *in situ* tracer offers the relatively high spatial resolution (~100 m), while the radars provide documentation of essentially the entire cloud volume. This data set affords the first opportunity to apply these techniques used simultaneously.

2. ***Documentation of the in situ microphysics*** (particle size spectra, hydrometeor types and habits) and the dynamics (up- and down-drafts, turbulence, buoyancy) in the tagged regions, at least until cloud growth renders the turrets impenetrable.

3. ***Determination of the destinations of tagged regions***, especially as the tagged regions initially become incorporated into the mature storm cloud volume. The progression of the chaff can be used to continue to follow parcels beyond the point where Citation (and most other aircraft) can continue to safely penetrate the subject clouds (into hail growth regions). This is a first-of-a-kind opportunity to determine the trajectories of the air (and small hydrometeors, to the extent they remain with the parcels) in and near convective storms.

4. ***Integration of the results of (2) and (3) above with larger-scale storm structure*** as determined by analysis of radar reflectivity and Doppler velocity data. Dominant or recurrent storm features may be identifiable, particularly as they relate to ice initiation and hydrometeor development.

5. ***Comparisons of the results of (2), (3), and (4) above with the output of the numerical cloud models*** used during the NDTE in real-time. This will aid in validation of these models. For example, both of these models can produce parcel trajectories for comparison with observed clouds. Mechanisms responsible for observed storm behaviors may also be identified.

6. ***Comparisons of the behavior and hydrometeor development within tagged regions*** also containing AgI with similar tagged but unseeded parcels. In essence this makes use of the limited seeding done in the NDTE as a perturbation tool.

7. ***The in situ measurements present an opportunity to compare measured dispersion rates under a variety of cloud conditions.*** On a number of experimental days multiple encounters with the SF_6 plumes were recorded by both the Citation and T-28. Turbulence on these days ranged from light to severe. Observed tracer gas concentrations can be compared to turbulence measured by the Citation, using the approach used by Weil *et al.* (1993).

ACKNOWLEDGEMENTS

The author gratefully acknowledges the efforts of all NDTE field personnel. G. Haug of the Bismarck Airport Authority was very helpful with arrangements for the Operations Center site. Figures 4 and 5 were provided by B. Martner, NOAA/ETL. A special thanks to L. Dollinger, whose efforts kept the project on time and under budget. This research was sponsored by NOAA Cooperative Agreement NA27RA0178-01 and the State of North Dakota. The contributions of the National Science Foundation are also gratefully acknowledged.

REFERENCES

Boe, B.A., 1992: Hail suppression in North Dakota. Preprints, *AMS Symposium on Planned and Inadvertent Weather Modification*, Atlanta, GA. 58-62.

Boe, B.A., J.L. Stith, P.L. Smith, J.H. Hirsch, J.H. Helsdon, H.D. Orville, A.G. Detwiler, B.E. Martner, R.F. Reinking, R.J. Meitín, and R.A. Brown, 1992: The North Dakota Thunderstorm Project: A cooperative study of High Plains thunderstorms. *Bull. Amer. Meteor. Soc.*, **73**, 145-160.

Butchbaker, A.F., 1970: Results of the Bowman-Slope hail suppression program. *Farm Research*, **27**, 11-16. North Dakota Agricultural Experiment Station Reprint #697.

Changnon, S.A. Jr., 1977: The climatology of hail in North America. In Hail: A Review of Hail Science and Hail Suppression. *Amer. Meteor. Soc. Meteor. Monogr.*, **16**, 107-128.

Changnon, S.A. Jr., 1984: Temporal and spatial variations in hail in the upper Great Plains and the Midwest. *J. Clim. Appl. Meteor.*, **23**, 1531-1541.

DeMott, P.J., 1990: *Quantifying ice nucleation by silver iodide aerosols.* Ph.D. dissertation, Dept. Atmospheric Science, Colorado State University, Fort Collins, CO. 253 pp.

Eddy, A., and E. Cooter, 1979: The Evaluation of Operational Cloud Seeding in North Dakota: Some Preliminary Findings. Final report to the North Dakota Weather Modification Board. *Amos Eddy, Inc.*, Norman, Oklahoma. 43 pp.

Enz, J., C. Brenk, R. Egeberg, and D. Rice, 1992: North Dakota Agricultural Weather Network (NDAWN). Weather, Software Users Guide 11. NDSU Extension Service, North Dakota State University, Fargo, ND.

Johnson, H.L, 1985: An Evaluation of the North Dakota Cloud Modification Project. A final report to the North Dakota Weather Modification Board, June, 1985. 35 pp.

Johnson, J.E., R.C. Coon, and J.W. Enz, 1989: Economic Benefits of Crop-Hail Reduction Efforts in North Dakota. Agricultural Economics Report No. 247, Department of Agricultural Economics, North Dakota State University, Fargo. 26 pp.

Kopp, F.J., and H.D. Orville, 1994: The use of a two-dimensional, time-dependent cloud model to predict convective and stratiform clouds and precipitation. *J. Wea. Forecast.* [accepted].

Martner, B.E., and R.A. Kropfli, 1989: TRACIR: A radar technique for observing the exchange of air between clouds and their environment. *Atmos. Envir.*, **23**, 2715-2721.

Martner, B.E., J.D. Marwitz, and R.A. Kropfli, 1992: Radar observations of transport and diffusion in clouds and precipitation using TRACIR. *J. Atmos. Ocean. Tech.*, **9**, 226-241.

Moninger, W. R. and R. A. Kropfli, 1987: A technique to measure entrainment included by dual-polarization radar and chaff. *J. Atmos & Ocean. Tech.*, **4**, 75-83.

NDTE Field Operations Plan, 1993: North Dakota Atmospheric Resource Board, State Water Commission, Bismarck, ND 58505. 76 pp.

Orville, H.D., and N.C. Knight, 1992: An example of a Research Experience for Undergraduates. *Bull. Amer. Meteor. Soc.*, **73**, 161-167.

Reinking, R.F., 1985: An overview of the NOAA Federal-State Cooperative Program in Weather Modification Research. *4th WMO Scientific Conference on Weather Modification*, Honolulu, HI. August 12-14. World Meteorological Organization, Geneva, 643-648.

Rose, R.L., 1986: The North Dakota Experience. Preprints, *Tenth Conf. on Planned and Inadvertent Weather Modification.* May 27-30. 323-325.

Schaffner, L.W., J.E. Johnson, H.G. Vruegdenhil, and J.W. Enz, 1983: Economic Effects of Added Growing Season Rainfall on North Dakota Agriculture. Agricultural Economics Report No. 172, Department of Agricultural Economics, North Dakota State University, Fargo. 19 pp.

Smith, P.L., J.R. Miller, Jr., and P. W. Mielke, Jr., 1987: An Exploratory Study of Crop Hail Insurance Data for Evidence of Seeding Effects in North Dakota. Report SDSM&T/IAS/R-87/01, Consortium for Atmospheric Resource Development, SD School of Mines & Technology, Rapid City, SD. 21 pp.

Smith, P.L., L.R. Johnson, D.L. Preignitz, and P.W. Mielke, Jr., 1992: A Target Control Analysis of Wheat Yield Data for the North Dakota Cloud Modification Project Region. Report SDSM&T /IAS /R-92 /05, Consortium for Atmospheric Resource Development, SD School of Mines & Technology, Rapid City, SD. 38 pp.

Stith, J.L., and J. Scala, 1993: Summer storms provide abundant research opportunities for the North Dakota Tracer Experiment. *The Earth Observer*, July-August 1993, 28-30.

Stith, J.L., D.A. Burrows, and P.J. DeMott, 1992: Initiation of ice in clouds: Comparison of numerical cloud model results with observations. Preprints, *11th International Conference on Clouds and Precipitation*, 17-21 August, Montreal, Canada.

Weil, J.C., R.P. Lawson, and A.R. Rodi, 1993: Relative dispersion of ice crystals in seed cumuli, *J. Appl. Meteor.*, **32**, 1055-1073.

"REVIEWED"

NUMERICAL SIMULATION OF CLOUD SEEDING USING A THREE-DIMENSIONAL CLOUD MODEL

Richard D. Farley, Phuong Nguyen, and Harold D. Orville
Institute of Atmospheric Sciences
South Dakota School of Mines and Technology
501 E. St. Joseph Street
Rapid City, South Dakota 57701-3995

Abstract. This preliminary study is concerned with the numerical modeling of cloud seeding effects in three dimensions for the deep convective cloud case of 19 July 1981 from the CCOPE field experiment. The observed cloud was relatively isolated and grew rapidly to about 11 km height. An extensive anvil was produced. For the first time in our 3D modeling efforts, a silver iodide (AgI) seeding agent is introduced into a three-dimensional cloud model. Ice and precipitation formation occurs 2 min earlier in the seeded case. Maximum mixing ratios show only slight increases (about 5% for graupel/hail) compared to the unseeded case. Domain totals of graupel/hail and rain indicate a more pronounced seeding effect, consistent with surface rainfall estimates of a 20% increase for the seeded case. For the 3D case in this study, 10% of the AgI remains unactivated, caught in a dead zone of virtually no net transport to the southeast of the cloud around 4 km AGL. The use of an inert agent, sulfur hexafluoride, for comparison purposes helps to illustrate the region of activated AgI.

1. INTRODUCTION

Extensive work has been done by our modeling group and others using two-dimensional, time-dependent (2DTD) cloud models to simulate cloud seeding experiments (Hsie *et al.*, 1980; Kopp *et al.*, 1983; Orville and Chen, 1982; Orville *et al.*, 1984; Farley, 1987). Results of these and other studies have shown that the seeded clouds exhibit earlier development of precipitation, relatively slight dynamic enhancement of the updraft, sometimes dramatic differences in cloud life history, and normally precipitation increases of a few to several tens of percent in moderate size convective cells. The results have emphasized the strong interactions of microphysics and dynamics in the model clouds such that precipitation decreases result sometimes. The hypothesis normally tested is the microphysical one of increasing the precipitation efficiency of a cloud.

The code for the cloud seeding methods has been added to the Clark and associates 3D cloud model in addition to the ice microphysics of the Institute of Atmospheric Sciences (IAS) cloud models. This preliminary report shows the results of seeding a moderate size convective cell using a 3D cloud model.

The atmospheric conditions used as initial conditions for the model are taken from a CCOPE case (19 July 1981) that has been studied extensively in WMO workshops and results published in several papers (e.g., Helsdon and Farley, 1987; Dye *et al.*, 1986). The atmospheric conditions (Fig. 1) produce an active cell that first reaches cumulonimbus proportion, produces one lightning flash, some rain and small hail, and an extensive anvil. Updrafts of 10 - 15 m s^{-1} were observed; the simulations show over 20 m s^{-1} maximum updrafts.

The general results for this 3D case are that ice and precipitation formation occur 2 min earlier in the seeded case than in the unseeded case. Maximum mixing ratios show only slight increases (about 5% for graupel/hail) compared to the unseeded case. Domain totals of graupel/hail and rain indicate a more pronounced seeding effect, consistent with surface rainfall estimates of a 20% increase for the seeded case. For this case, 10% of the AgI remains unactivated, caught in a dead zone of virtually no net transport to the southeast of the cloud around 4 km AGL.

A few of the results that lead to these conclusions are given in the following pages.

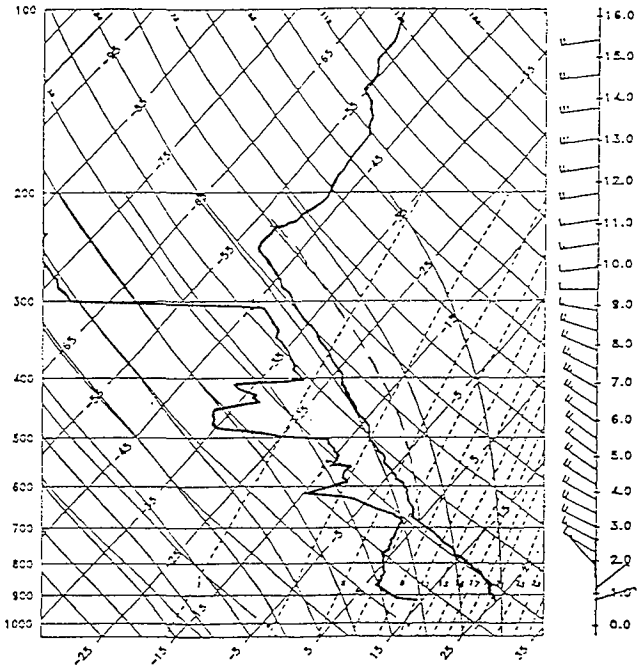

Fig. 1: A representative sounding taken at 1440 MDT (Mountain Daylight time) from Miles City on July 19, 1981.

2. BRIEF THREE-DIMENSIONAL MODEL DESCRIPTION

The three-dimensional cloud model used in this study was developed by Clark and associates (Clark, 1977, 1979, 1982; Clark and Farley, 1984). The model uses the deep anelastic equations of Ogura and Phillips (1962) and originally employed bulk water microphysics similar to Kessler (1969) for cloud water and rain mixing ratios. Recently, this model has been modified to use the bulk water parameterization scheme of Lin *et al.* (1983) with additional microphysical refinements. These are graupel/hail formation via snow (of a certain critical size) accreting supercooled cloud water as explained by Farley *et al.* (1989) and a parameterization of the rime-splintering ice multiplication scheme as described in Aleksić *et al.* (1989). Sub-grid scale turbulence is parameterized according to the first-order theory of Smagorinsky (1963) and Lilly (1962). The eddy mixing coefficients are functions of the flow field and the local Richardson number, so that both wind shear and thermal stability determine the magnitude of the coefficients. Open boundary conditions are used at the side boundaries as described in Clark (1979). The domain of the model is 20 km x 20 km x 15 km with grid intervals of 400 m x 400 m x 250 m in the x, y, z-directions. Time steps of 6 s are used.

For this study, the seeding agent field has been added to the 3D model. This development allows for the seeding agent to be an inert tracer such as sulfur hexaflouride (SF_6) or an artificial ice nucleation agent such as silver iodide (AgI), or dry ice (CO_2). The treatment of AgI follows the scheme outlined in Hsie *et al.* (1980) and that for dry ice is handled as described in Kopp *et al.* (1983). In this paper, only the SF_6 and AgI treatments will be discussed.

Farley *et al.* (1992) discuss simulations of the 19 July 1981 CCOPE case using single and nested model configurations of the 3D model used in this study, concentrating on comparisons to observations. The current set of 3D simulations differ from those in Farley *et al.* (1992) in that the subcloud moisture has been reduced slightly, the direction of the low-level winds has been modified, and a weaker perturbation has been used to initiate the convection. All of these changes were made to produce a less active cloud, especially in the early stages, to create a larger time window for seeding. Consequently, comparison of these results with the particular observations from 19 July 1981 is not pertinent.

3. THREE-DIMENSIONAL MODEL RESULTS

3.1 General Appearance of the Cloud Field

Figure 2 shows three-dimensional depictions of the cloud life cycle viewed from the northeast (NE) at 4-min intervals starting at 8-min simulation time. The perspectives were produced by plotting the surface of the combined cloud water and cloud ice field at $q_{cw} + q_{ci} = 0.1$ g kg^{-1}. Initial cloud formation was at 6 min after initiation. The cloud grows quite rapidly, and the upper portion extends toward the south and east by 16 min. At 20 min, the formation of an anvil becomes apparent. The anvil top develops into an irregular, rough shape and begins to break apart after 30 min. The cloud grows further toward the north and east by 32 min with the low-level support still concentrated along the west side. The turrets appear to be tallest at this time. The lower level of the cloud expands and by 36 min, new growth generated by the outflow shows up. Additional weak new growth can be seen at later times.

3.2 Silver Iodide Evolution

Figure 3 displays 3D depictions of the evolution of the AgI field viewed from the northeast. The numbers on the left corner are the simulation time in minutes. These 3D depictions display the 10^{-3} μg kg^{-1} surface of the silver iodide (AgI) field. The AgI was introduced at the cloud top at 8 min with a maximum value of 3.5 E-10 g g^{-1}. The pattern of seeding gives a total of approximately 47 g of AgI spread over nearly 3.5 km in the horizontal (elongated in the x-direction) and over about

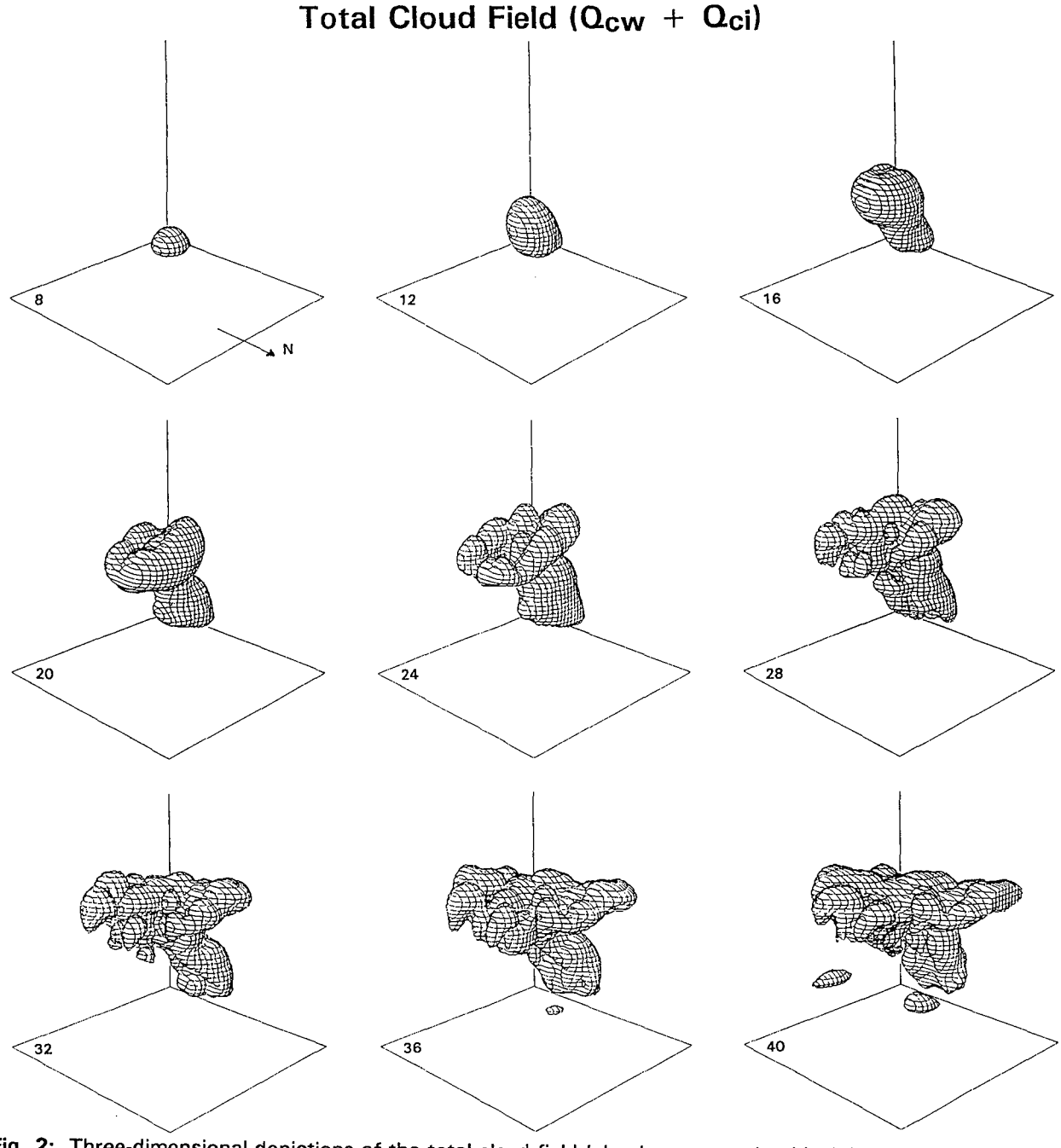

Fig. 2: Three-dimensional depictions of the total cloud field (cloud water + cloud ice) for the unseeded case viewed from the northeast. The 0.1 g kg^{-1} surface is indicated in these panels. The numbers on the left corner are the simulation time in minutes.

1 km in the vertical. The AgI spreads out towards the south and east directions. At 12 min, it forms a wicket shape as the unactivated AgI is draped over the southeast quadrant of the cloud. Also at 12 min, much of the AgI has been used up in the upper portion of the cloud. This can be seen quite clearly at 14 min. The AgI is continually activated as long as it stays above -5°C. By 20 min, only a small amount of AgI at lower levels remains. At 22 min, that portion of the AgI field which has not been activated has been diffused to values less than the plotting threshold of 10^{-3} μg kg^{-1}.

Figure 4a shows the X-Z and X-Y cross sections of the AgI field at 10 and 12 min. The panels at 10 min show some of the AgI has been used up and some has been transported to the east. The portion which is advected to the southeast quadrant is not activated since it is transported outside the cloud and quickly descends to a region where the temperature is warmer than -5°C (the activation temperature for AgI). The unactivated AgI transported to the southeast is also clearly shown in the lower right panel. Most of the AgI to the west has been activated by 14 and 16 min,

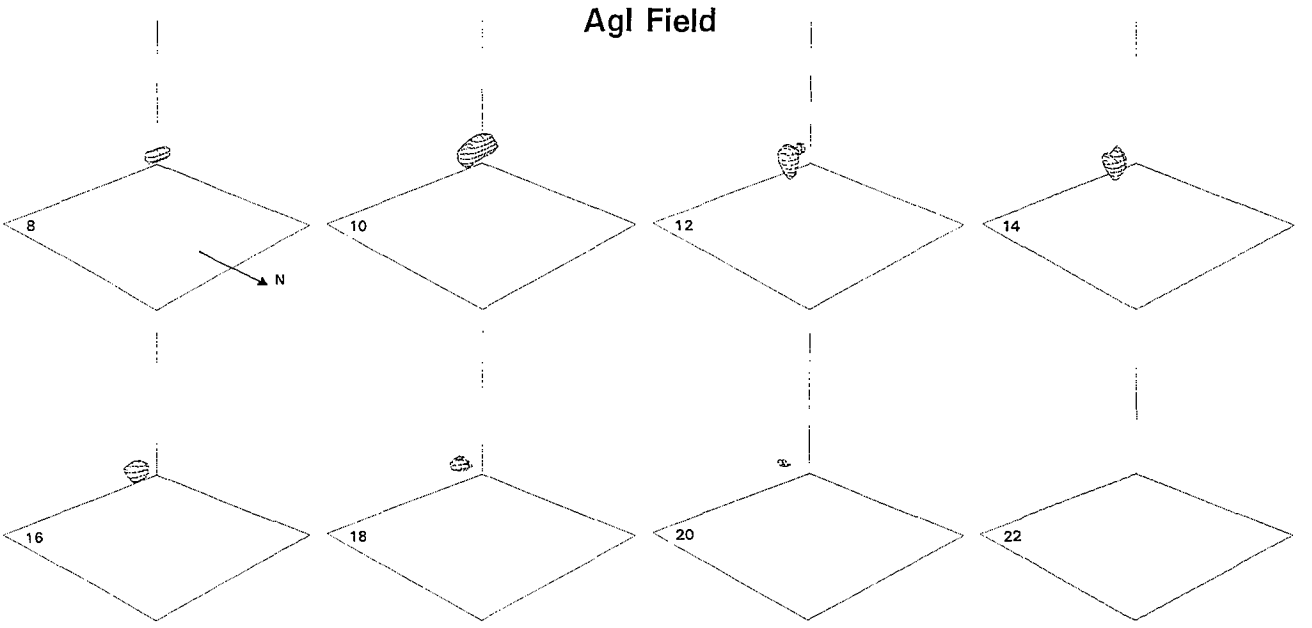

Fig. 3: The silver iodide (AgI) evolution viewed from the northeast. The numbers on the left corner are the simulation time in minutes .

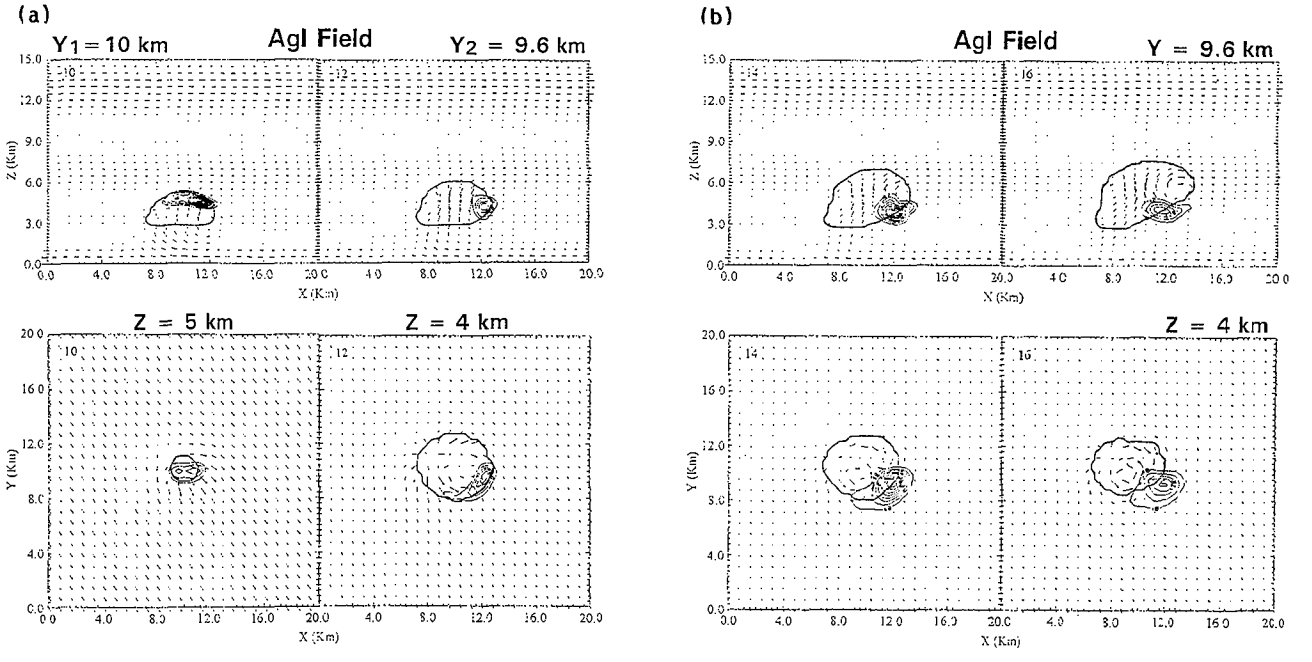

Fig. 4: (a) Top two panels are the vertical X-Z cross sections of the AgI field at y = 10 km at 10 min and y = 9.6 km at 12 min. The bottom two panels are horizontal X-Y cross sections at z = 5 km (left) and z = 4 km (right). The contour interval is 0.0025 μg kg^{-1} for 10 min and 0.001 μg kg^{-1} for 12 min. The arrows show the two dimensional representation of the wind appropriate for the particular plane. The bold solid line indicates the cloud outline. (b) Top two panels are X-Z cross sections of the AgI field at y = 9.6 km at 14 and 16 min. The bottom two panels are X-Y cross sections at z = 4 km at the same times. The contour interval is 0.0004 μg kg^{-1}.

as shown in Fig. 4b. The remaining AgI is concentrated in a "dead zone" to the southeast as can be seen quite clearly in this figure. There is little net transport of the AgI out of this dead zone as the AgI is slowly diffused.

3.3 Inert Tracer Field (SF_6) Evolution

An inert tracer, sulfur hexafluoride (SF_6), is simulated to illustrate where the AgI would have diffused if it had not been activated. Figure 5 illustrates the evolution of the inert tracer field (SF_6) in 3D depictions viewed from the northeast. The number in the left corner of each panel indicates the simulation times in minutes. These 3D depictions display the 10^{-3} μg kg^{-1} surface of the inert tracer (SF_6) field. The SF_6 is introduced at the cloud top at 8 min in the same manner that AgI was applied. By 12 min, the SF_6 extends to the south and east and begins to form a wicket shape. At 16 min, the diffusion of the SF_6 is becoming evident with the SF_6 plume spreading out towards the south and east. Diffusion continues until the field is broken into isolated pockets in excess of the plotting threshold, first evident at 22 min. By 26 min, the figure shows that the top part of the SF_6 field has diffused below the plotting threshold and only an isolated pocket of concentrated SF_6 is evident. By 32 min, the entire SF_6 field has been diffused below the threshold value.

Figure 6a,b shows the evolution of the SF_6 field in X-Z and X-Y cross sections from 10 to 16 min. From this figure, it is easy to see the transport of the SF_6 toward the south and east and downward at 12 min. Figure 6b shows the continuing tendency of SF_6 to be concentrated in the southeast quadrant at around 4 km AGL. Referring back to Fig. 4a, we see that the unactivated AgI tends to be concentrated in the same region. By comparing Fig. 6 with Fig. 4, we also get a good picture of where the AgI is being activated, namely at all elevations above approximately 5 km.

We next look at the development of some of the microphysical fields in the unseeded and seeded cases. The cloud ice and snow fields are not shown here but are analyzed in the thesis by Nguyen (1993).

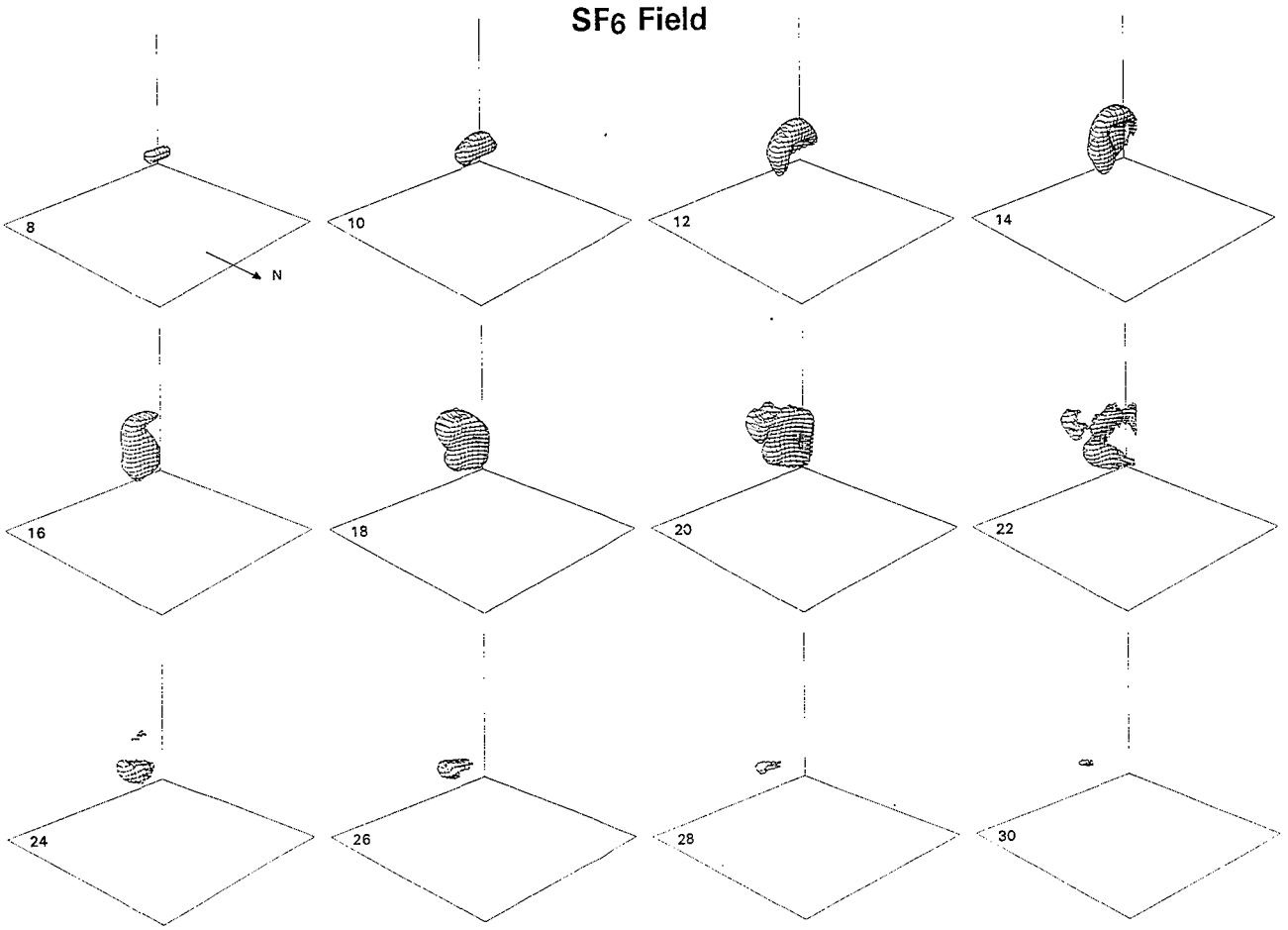

Fig. 5: The inert tracer (SF_6) evolution viewed from the northeast. The numbers in the left corner are the simulation time in minutes.

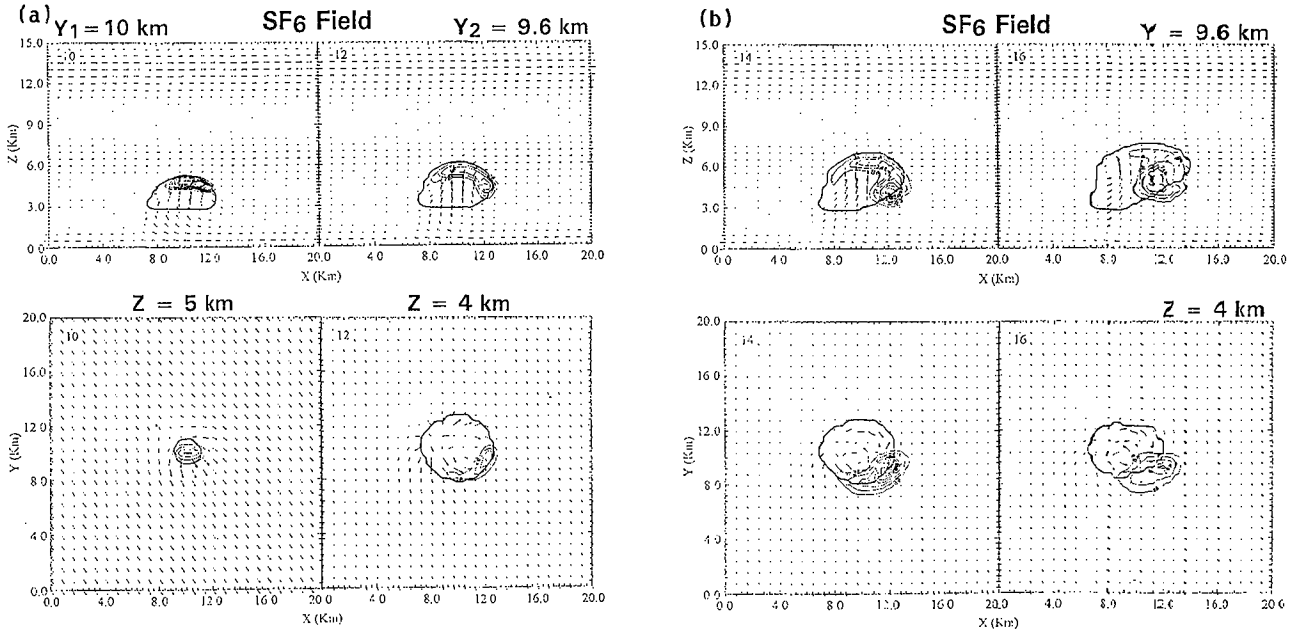

Fig. 6: (a) Top two panels are X-Z cross sections of the SF_6 field at y = 10 km at 10 min and y = 9.6 km at 12 min. The bottom panels are X-Y cross sections at z = 5 km at 10 min and z = 4 km at 12 min. The contour interval is 0.005 μg kg^{-1} at 10 min and 0.002 μg kg^{-1} at 12 min. The arrows show the two-dimensional representation of the wind appropriate for the particular plane. (b) Top panels are X-Z cross sections of the SF_6 field at y =9.6 km at 14 and 16 min. The bottom panels are X-Y cross sections at z = 4 km at the same times. The contour interval is 0.0008 μg kg^{-1} for all panels.

3.4 Development of the Unseeded Graupel/Hail Field

At 16 min, graupel/hail has formed through riming of the snow particles. This initial graupel/hail formation occurs in the updraft core between 6 and 7 km above ground level (AGL). The maximum value of graupel/hail at this time is 1.3 E-4 g kg^{-1}. By 18 min, the maximum amount increases to 0.47 g kg^{-1}. At 20 min, the graupel/hail field is located close to the updraft core, mainly from around 6 to 9 km above the ground level. Two minutes later (22 min), portions of the graupel/hail field have been carried downstream and begin descending toward the ground, and by 24 min, the graupel/hail particles begin to fall out of the cloud on the downshear side of the updraft. This is illustrated in Fig. 7a. The X-Z cross sections (upper panels) of this figure clearly indicate three hail cores. A strong development can be seen in the core to the left (west) which is still within the updraft region. The other two cores are weakening. As the graupel/hail falls below the 0°C isotherm, which is located at 3.25 km AGL, melting begins to occur, leading to the formation of rain.

Figure 7b shows the later development of the three cores at 26 and 28 min. The top panels show that the middle and the right cores of graupel/hail have been melting at lower levels. The decrease which is seen on the east side of the cores in the bottom panels indicates that most of the hail in these cores has fallen out. The maximum value of graupel/hail is recorded at 26 min (2.32 g kg^{-1}). It decreases slowly until 38 min and then increases again. This is due to a new cell to the northwest which has grown tall enough for significant graupel/hail development.

3.5 Development of the Seeded Graupel/Hail Field

Graupel/hail has first formed at 14 min in the seeded case (2 min earlier compared to the unseeded case). The maximum value of graupel/hail at this time is 1.2 E-3 g kg^{-1}. It increases two orders of magnitude by 16 min. By 18 min, the maximum amount increases to 1.2 g kg^{-1}. This is one order of magnitude larger compared to the unseeded case at the same time. By 22 min, the development of the three graupel/hail cores is clearly shown (Fig. 8a). Greater amounts of graupel/hail are indicated at these times compared to the unseeded case shown in Fig. 7a. It is noted that the graupel/hail particles in this case begin to fall out around 22 min. This is also the time when the first significant rain can be seen for the seeded case. The maximum graupel/hail mixing ratio is 2.6 g kg^{-1} occurring at 24 min (2 min earlier than the unseeded case maximum).

Figure 8b shows the later evolution of the same cross sections at 26 and 28 min. At these times, the graupel/hail field for the seeded case is very similar to the unseeded case results shown in

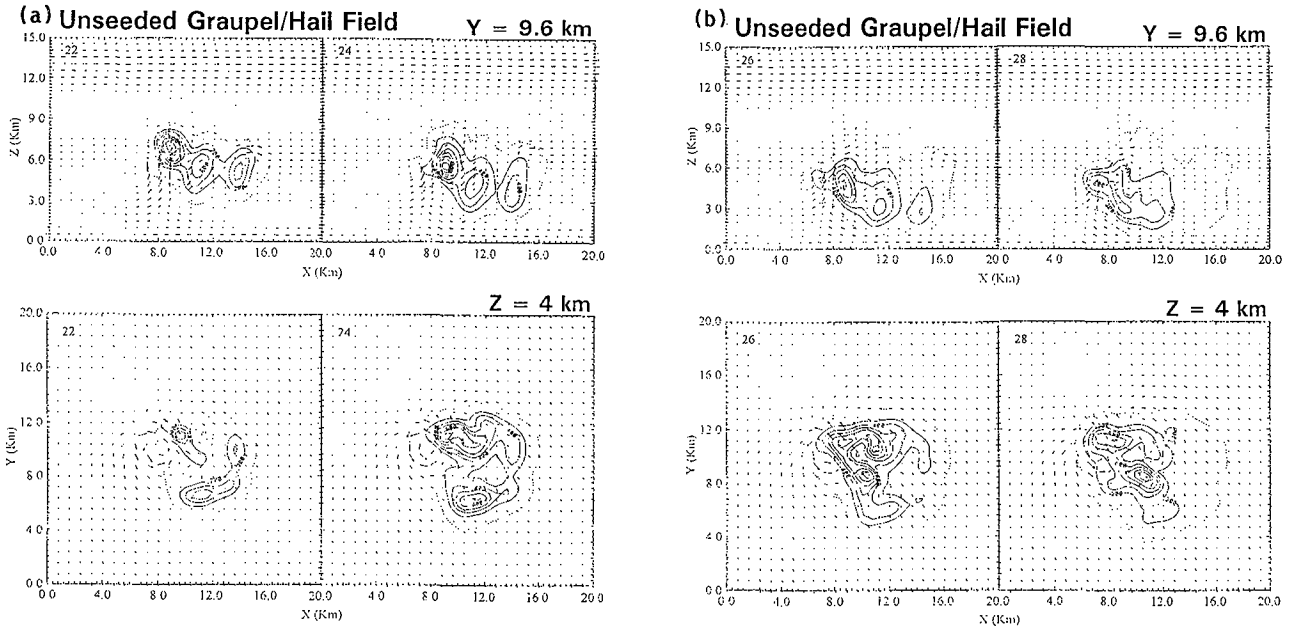

Fig. 7: (a) Top two panels are X-Z cross sections of the graupel/hail field at y = 9.6 km at 22 and 24 min for the unseeded case. The bottom two panels are X-Y cross section at z = 4 km for the same times. The contour interval is 0.2 g kg^{-1}. The arrows shows the two-dimensional representation of the wind appropriate for that particular plane. (b) As in Fig. 7(a), but at 26 and 28 min.

Fig. 7b. The maximum graupel/hail mixing ratio for the seeded case decreases until 38 min, and then increases slowly up to 1.4 g kg^{-1} by 44 min.

3.6 Development of the Unseeded Rain Field

Figure 9 shows the development of the rain field, which forms from the melting of graupel/hail, beginning around 24 min. The maximum mixing ratio at this time is 0.19 g kg^{-1}. It is obvious that the development of these two rain cores is the result of the melting process operating on the lower portions of the center and the right cores of the graupel field shown in Fig. 7a at 24 min. Both cores are growing rapidly and approaching the ground by 28 min. The left core reaches the

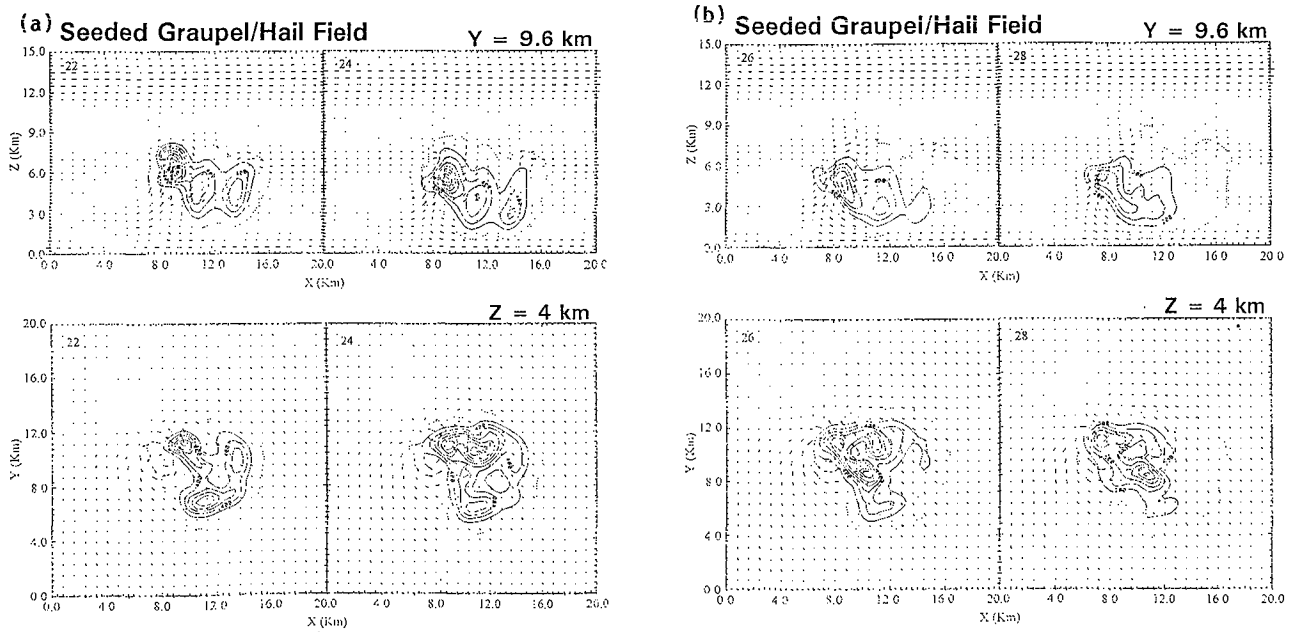

Fig. 8: (a) Top two panels are X-Z cross sections of the graupel/hail field at y = 9.6 km at 22 and 24 min for the seeded case. The bottom panels are X-Y cross sections at z = 4 km for the same times. The contour interval is 0.2 g kg^{-1} in all panels. The arrows show the two-dimensional representation of the wind appropriate for that particular plane. (b) As in Fig. 8(a), but at 26 and 28 min.

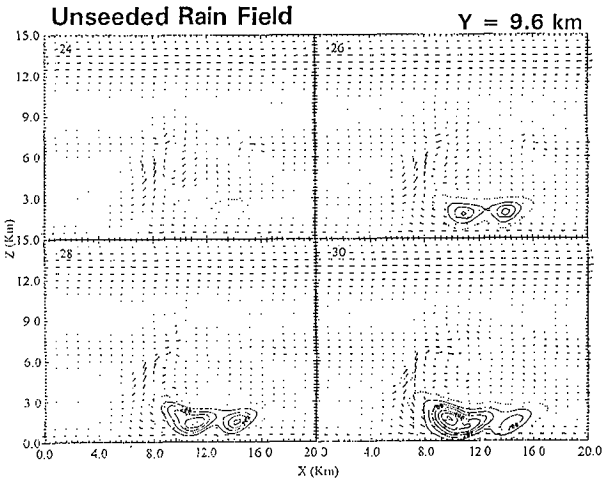

Fig. 9: X-Z cross sections of the rain field at y = 9.6 km from 24 to 30 min for the unseeded case. The contour interval is 0.1g kg^{-1} in all panels. The arrows show the wind in the X-Z plane.

ground by 30 min. The maximum mixing ratio at this time is around 1.0 g kg^{-1}.

Figure 10 shows horizontal cross sections of the rain field at the surface from 30 to 36 min. At 30 min, two rain cores are clearly defined. These two cores merge by 34 min and continue to intensify until 36 min. The rain core to the northwest is the dominant surface rainfall producer of the simulation. The maximum rain mixing ratio of 1.15 g kg^{-1} is recorded at this time. After 36 min, the values decrease slightly until the end of the period of consideration (44 min).

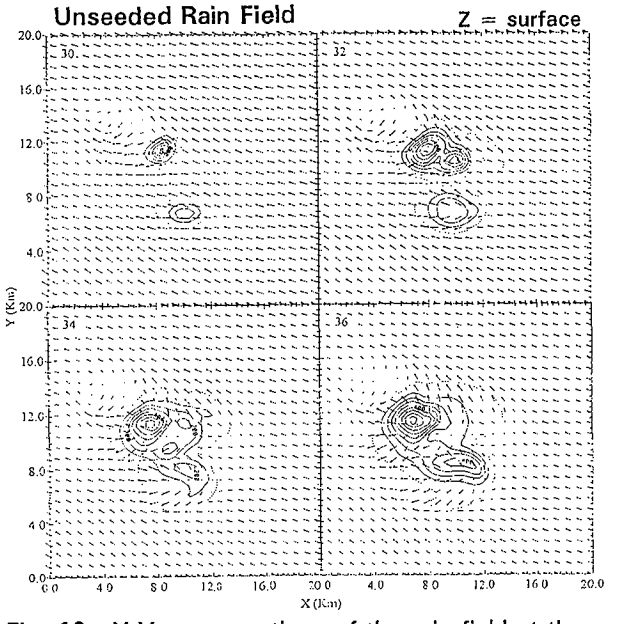

Fig. 10: X-Y cross sections of the rain field at the model surface from 30 to 36 min for the unseeded case. The contour interval is 0.1 g kg^{-1} in all panels. The arrows show the wind in the X-Y plane.

3.7 Development of the Seeded Rain Field

At 22 min, the first significant amounts of rain are indicated in the seeded case. The maximum rain mixing ratio at this time is 0.12 g kg^{-1}. Figure 11 shows X-Z cross sections of the rain field from 24 to 30 min for the seeded case. At 24 min, two rain cores are clearly defined and appear to be much stronger than those shown in Fig. 9 for the unseeded case. Both rain cores develop until 26 min. By 28 min, the left (western) rain core continues to grow while the right (eastern) rain core has begun to dissipate. Both rain cores reach the ground at this time with a maximum rain mixing ratio of 1.0 g kg^{-1}. The maximum rain mixing ratio for the seeded case is 1.2 g kg^{-1} at 30 min. Similar to the unseeded case, the formation of these two cores in the seeded rain field is the result of the graupel/hail melting process which shows up in Fig. 8 at 24 min. The maximum value slowly decreases after 30 min until the end of the period of consideration at 44 min.

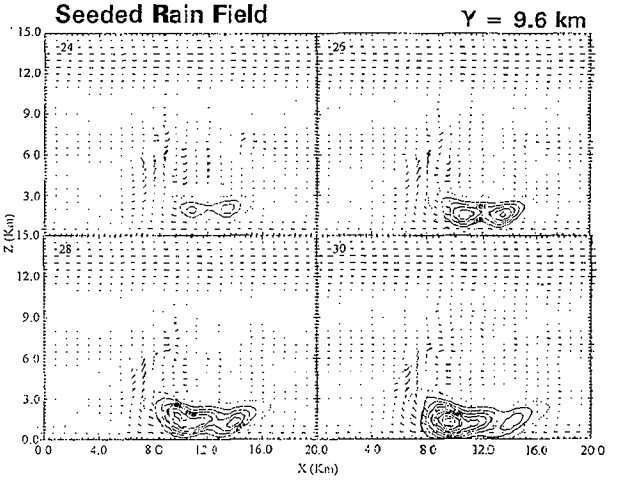

Fig. 11: X-Z cross sections of the rain field at y = 9.6 km from 24 to 30 min for the seeded case. The contour interval is 0.1 g kg^{-1} in all panels. The arrows show the wind in the X-Z plane.

Figure 12 shows X-Y cross sections of the rain field at the model surface from 30 to 36 min. At 30 min, two rain cores are clearly defined. They are much stronger than those seen in the unseeded case (Fig. 10) at the same time. The two cores merge by 32 min and grow stronger until 34 min. By 36 min, the southern portion begins to dissipate while the northern part remains fairly strong.

4. ADDITIONAL RESULTS AND GENERAL DISCUSSION

The discussion from the previous section has shown that there is a slight seeding effect in

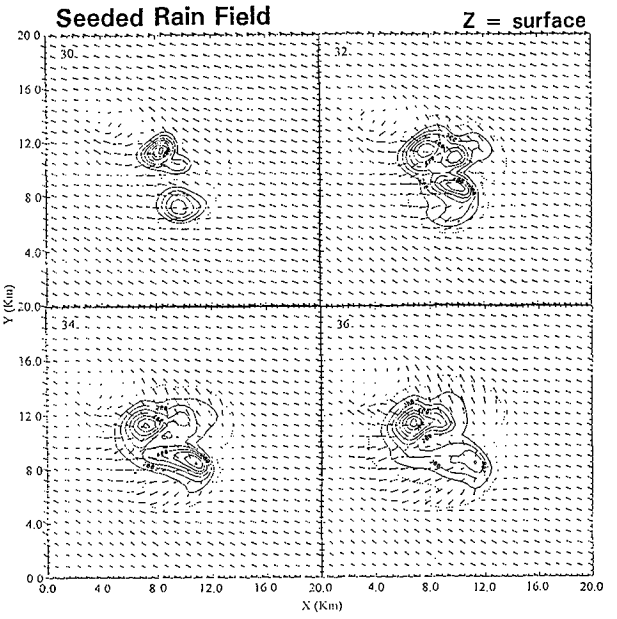

Fig. 12: X-Y cross sections of the rain field at the model surface from 30 to 36 min for the seeded case. The contour interval is 0.1 g kg^{-1} in all panels. The arrows show the wind in the X-Y plane.

the three-dimensional model results. Precipitation formation in the seeded case occurs 2 min earlier than in the unseeded case. In this section, the seeded and unseeded cases will be compared in greater detail.

Figure 13a,b illustrates the time evolution of the maximum cloud ice and snow amounts, respectively, for the two cases. Cloud ice in the seeded case shows up 2 min earlier and in larger amounts than in the unseeded case. This is a direct effect of the seeding agent. The two cases indicate the same cloud ice maximum amounts by 18 min. This occurs near the level of complete glaciation (-35°C) in the northeast quadrant. Between 20 and 30 min, the unseeded case has slightly larger maximum amounts of cloud ice than the seeded case. This is because most of the AgI has been used up by this time and the newer turret on the northwest side occurs too late for a direct seeding effect. After 30 min, the maximum cloud ice amounts in both cases slowly decrease. In terms of domain totals, the seeded case indicates an increased amount of cloud ice (5 to 10%) compared to the unseeded case after 26 min.

Figure 13b shows the time evolution of maximum amounts of snow for both cases. As expected, the snow field in the seeded case shows up 2 min earlier and in greater amounts than the unseeded case at the early stage. This is associated with the earlier formation of cloud ice shown in Fig. 13a. The two cases have almost the same maximum snow amount at 18 min, and both reach their respective highest maximum values at 24 min. There is a steady decrease after 24 min in both cases, as much of the snow is transformed into graupel. In terms of domain totals, the unseeded case indicates approximately 5% more snow than the seeded case after 24 min.

The time evolution of the maximum graupel/hail and rain mixing ratios for the two cases are illustrated in Fig. 14a,b. As was the case for cloud ice and snow, graupel/hail in the seeded case shows up 2 min earlier than in the unseeded case. The seeded case reaches its highest maximum value at 24 min, while the unseeded case does not peak until 2 min later. During this period, the maximum values remain larger in the seeded case. The rapid decrease after 26 min is due to the fallout and melting of the graupel/hail. The formation of rain in this simulation is primarily due to the melting of graupel/hail. In terms of domain totals, the seeded case indicates up to 15 KT more graupel/hail than the unseeded case from 20 to 24 min. This is equivalent to a 100% increase at 20 min, decreasing to +15% at 24 min. Both cases display steady decreases and similar values between 27 and 38 min.

Figure 14b shows that the rain field develops 2 min earlier and in larger mass concentration after 30 min in the seeded case. The rain develops later in the unseeded case, and is stronger at the later stages. In terms of domain totals, the seeded case indicates more rain (by as much as 7 KT, or +100%) out to 31 min. The values are nearly equal at 32 min, and the unseeded case indicates about 10% more rain thereafter.

Surface accumulations of rain and hail were calculated at coarse time resolution from data on the history files. These estimates indicate peak rainfall depth increased by about 5% (for values in the range of 2 mm) for the seeded case. Total rainfall was increased by over 20% in the seeded case (29 KT vs. 24 KT for the unseeded case). Hail amounts were much smaller but indicated decreases of 40% or more in the seeded case.

Figure 15 shows the time evolution of the maximum vertical velocity for the seeded and unseeded cases. This figure illustrates the single cell nature of the primary updraft which reaches its maximum value at 18 min. The decrease after 18 min is due to the loading of graupel/hail and rain. There is no evidence of a dynamic seeding effect. The secondary cell indicated in the later stages (after 36 min) is associated with new growth to the northwest of the original cell. It is of little significance to the discussion of seeding effects.

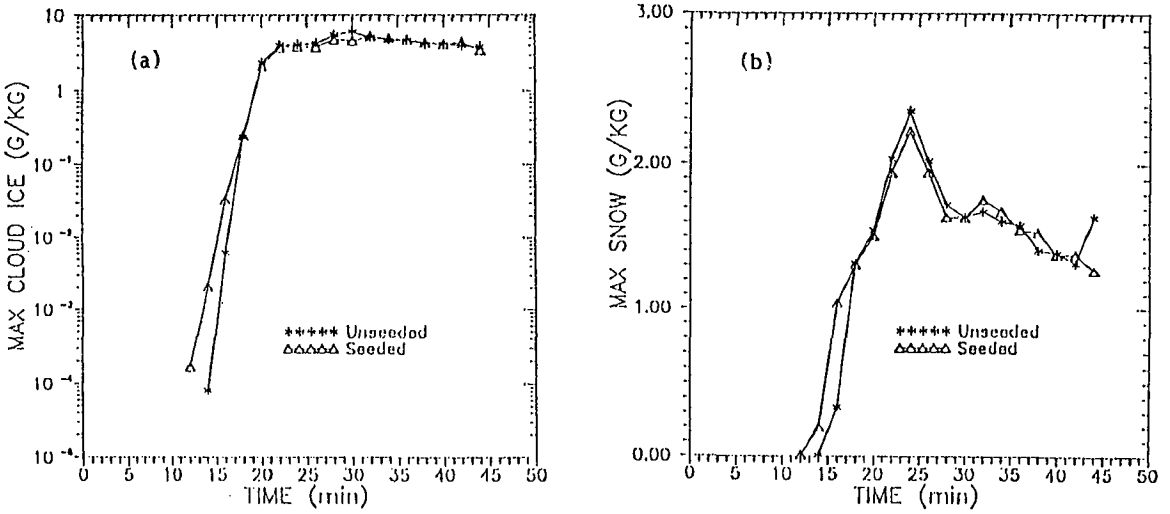

Fig. 13: (a) Time evolution of the maximum mixing ratio of cloud ice for the unseeded and seeded 3D cases. (b) Time evolution of the maximum mixing ratio of snow for the unseeded and seeded 3D cases.

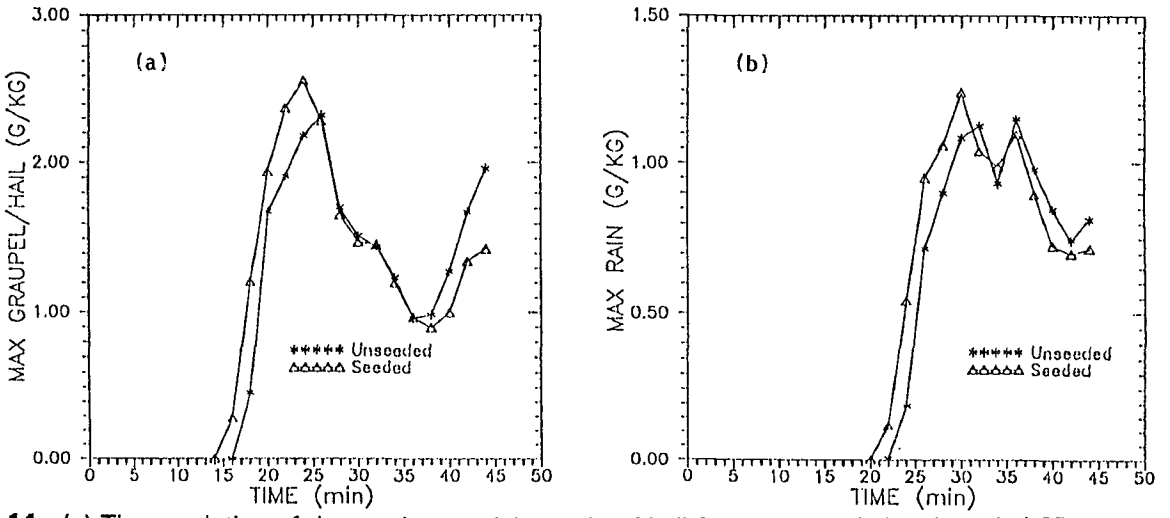

Fig. 14: (a) Time evolution of the maximum mixing ratio of hail for the unseeded and seeded 3D cases. (b) Time evolution for the maximum mixing ratio of rain for the unseeded and seeded 3D case.

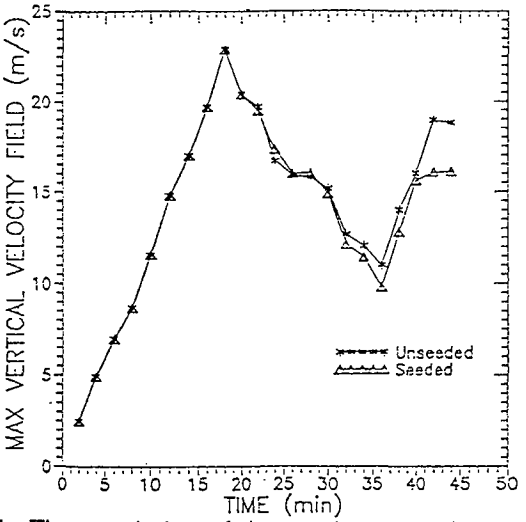

Fig. 15: Time evolution of the maximum vertical velocity for the unseeded and seeded 3D cases.

5. CONCLUSIONS

These results of cloud seeding simulations in a 3D cloud model are consistent with some of our earlier work using 2D cloud models. The earlier ice initiation caused by the seeding agent is crucial to the overall seeding effect in the model cloud, leading to increased precipitation. In this case, both seeded and unseeded model clouds develop very similarly with respect to their dynamics; not so with respect to their microphysics.

It is typical for virtually all of the AgI to be activated in 2D simulations. Seeding material transported through the sides or top of the cloud in the 2D model then tends to be drawn back into the cloud as it descends to lower levels. For the 3D seeded case in this study, 10% of the AgI remains unactivated, caught in a dead zone of virtually no net transport to the southeast of the cloud around 4 km AGL. This may be due to the less than optimal placement of the seeding agent in the three-dimensional seeded case.

It is premature at this time to make any general, sweeping conclusions about the usefulness of 2D or 3D cloud seeding results. Just because a model is 2D does not invalidate results. Just because a model is 3D does not mean that it is right. The plausibility of results from both 2D and 3D looks reasonable and supports observational results in many cases; but they both could be wrong. In addition, keep in mind that the results reported above are for one 3D cloud case only. Further work is necessary to compare 2D, 3D, and observational work to determine the usefulness and appropriateness of the models in predicting cloud seeding results.

Acknowledgments. The research was sponsored by the National Science Foundation under Grant No. ATM-9206919. Support for this computing research was provided by the National Center for Atmospheric Research, in Boulder, Colorado. The National Center for Atmospheric Research is operated by the University Corporation for Atmospheric Research and is sponsored by the National Science Foundation.

We also thank Mrs. Joie Robinson for her assistance in preparing this manuscript.

REFERENCES

Aleksić, N. M., R. D. Farley and H. D. Orville, 1989: A numerical cloud model study of the Hallet-Mossop ice multiplication process in strong convection. *Atmos. Res.*, **23**, 1-30.

Clark, T. L., 1977: A small scale numerical model using a terrain following coordinate system. *J. Comput. Phys.*, **24**, 186-215.

Clark, T. L., 1979: Numerical simulations with a three-dimensional cloud model: Lateral boundary condition experiments and multi-cellular severe storm simulations. *J. Atmos. Sci.*, **36**, 2191-2215.

Clark, T. L., 1982: Cloud modeling in three spatial dimensions, Chapter 10 in *Hailstorms of the Central High Plains*. **Vol. I**, The National Hail Research Experiment. Charles A. Knight and Patrick Squires, eds., Colorado Associated Univ. Press, Boulder, CO. 282 pp.

Clark, T. L., and R. D. Farley, 1984: Severe downslope windstorm calculations in two and three spatial dimensions using anelastic interactive grid nesting: A possible mechanism for gustiness. *J. Atmos. Sci.*, **41**, 329-350.

Dye, J. E., J. J. Jones, N. P. Winn, T. A. Cerni, B. Gardiner, D. Lamb, R. L. Pitter, J. Hallett, and C. P. R. Saunders, 1986: Early electrification and precipitation development in a small, isolated Montana cumulonimbus. *J. Geophys. Res.*, **91**, 1231-1247.

Farley, R. D., 1987: Numerical modeling of hailstorms and hailstone growth. Part III: Simulation of an Alberta hailstorm - natural and seeded cases. *J. Appl. Meteor.*, **26**, 789-812.

Farley, R. D., P. E. Price, H. D. Orville and J. H. Hirsch, 1989: On the numerical simulation of graupel/hail initiation via the riming of snow in bulk water microphysical cloud models. *J. Appl. Meteor.*, **28**, 1128-1131.

Farley, R. D., S. Wang and H. D. Orville, 1992: A comparision of 3D model results with observations for an isolated CCOPE thunderstorm. *J. Meteorol. Atmos. Phys.*, **49**, 187-207.

Helsdon, J. H., Jr., and R. D. Farley, 1987: A numerical modeling study of a Montana thunderstorm: Part I. Model results versus observations involving non-electrical aspects. *J. Geophys. Res.*, **92**, 5645-5659.

Hsie, E-Y., R. D. Farley and H. D. Orville, 1980: Numerical simulation of ice-phase convective cloud seeding. *J. Appl. Meteor.*, **19**, 950-977.

Kessler, E., 1969: On the distribution and continuity of water substance in atmospheric circulations. *Meteor. Monogr.*, **10**, No. 32. 84 pp.

Kopp, F. J., H. D. Orville, R. D. Farley and J. H. Hirsch, 1983: Numerical simulation of dry ice cloud seeding experiments. *J. Climate Appl. Meteor.*, **22**, 1542-1556.

Lilly, D. K., 1962: On the numerical simulation of buoyant convection. *Tellus*, **14**, 148-172.

Lin, Y-L., R. D. Farley and H. D. Orville, 1983: Bulk parameterization of the snow field in a cloud model. *J. Climate. Appl. Meteor.*, **22**, 1065-1092.

Nguyen, Phuong, 1993: Modeling of cloud seeding effects in one-, two-, and three-dimensional cloud models. M.S. Thesis, Dept. of Meteorology, S.D. School of Mines and Technology, Rapid City, SD. 140 pp.

Ogura, Y., and N. A. Phillips, 1962: Scale analysis of deep and shallow convection in the atmosphere. *J. Atmos. Sci.*, **19**, 173-179.

Orville, H. D., and J-M. Chen, 1982: Effects of cloud seeding, latent heat of fusion and condensate loading on cloud dynamics and precipitation evolution: A numerical study. *J. Atmos. Sci.*, **39**, 2807-2827.

Orville, H. D., R. D. Farley and J. H. Hirsch, 1984: Some surprising results from simulated seeding of stratiform-type clouds. *J. Climate Appl. Meteor.*, **23**, 1585-1600.

Smagorinsky, J., 1963: General circulation experiments with the primitive equations: 1. The basic experiment. *Mon. Wea. Rev.*, **91**, 99-164.

COMPARISON OF CLOUD TOWER AND UPDRAFT RADII WITH THEIR INTERNAL TEMPERATURE EXCESSES RELATIVE TO THEIR ENVIRONMENTS

William L. Woodley[1], Eyal Amitai[2], and Daniel Rosenfeld[2]

[1] Woodley Weather Consultants, Littleton, Colorado
[2] Dept. of Atmospheric Sciences, Hebrew University of Jerusalem, Jerusalem, Israel

Abstract. Measurements of in-cloud temperature using reverse-flow thermometry were made in and around vigorous Thai supercooled convective clouds on 10 days in April and May 1993. Cloud vs. environment temperature differences were derived from these data and the differences were correlated with cloud and updraft radii at the level (6.5 km) of cloud penetration. This was done as a function of whether the clouds were isolated, growing in a group of comparably-sized clouds, or growing as "feeders" to cumulonimbus clouds. Positive correlations were noted in all instances, ranging from a minimum of 0.11 to a maximum of 0.48. The correlations were greatest for the comparisons of the temperature differences with updraft breadth. It was noted further that, for a given tower size or updraft width, the temperature differences were largest for clouds growing as feeders to cumulonimbus clouds. The implications of these findings to the design and evaluation of cloud seeding experiments are discussed.

This work was conducted under a contract with the Bureau of Reclamation as part of a program sponsored by the U.S. Agency for International Development to upgrade Thailand's weather modification capability.

1.0 INTRODUCTION

This paper is an outgrowth of continuing scientific discussions that the authors have had with a number of their colleagues. It is the contention of the authors that the life prognosis for a particular convective cloud depends in large part on where it lives and on its ancestry and that, in designing a convective cloud seeding experiment, one must take these factors into account. They argue further that, if one wants to detect the effect of seeding, it is best to select those clouds in which natural forcing is not so dominant that it overwhelms the expected signal from seeding. The seeded clouds may well become large and develop their own forcing. It is best, however, not to begin the seeding experiment with that process already well underway. Not everyone accepts these views.

As to a cloud's place of residence, Rosenfeld and Gagin (1989) have shown that, other factors being equal, clouds living in isolation produce about one-third the rain volume of those growing in clusters. As to ancestry, it is the authors' observation that relatively small convective clouds growing as feeders to gigantic parents are more likely to resemble those parents at maturity than a comparably-sized convective cloud growing in isolation some distance away, when it reaches maturity.

While working in Thailand on the Applied Atmospheric Resources Research Program (AARRP) (Woodley et al., 1994; Rosenfeld et al., 1994), the question arose whether simple measurements within a cloud might reveal differences that are related to a cloud's ancestry and place of residence. In earlier work, Woodley and Kreasuwun (1992) had used Thai cloud physics measurements to show a relationship between the visual appearances of Thai supercooled convective clouds and their maximum cloud liquid water contents. There was reason to hope, therefore, that meaningful science might come out of the current investigation, despite the relative simplicity of the Thai cloud physics platform.

Because clouds thrive on buoyancy (e.g., Simpson and Wiggert, 1969;1971), which is proportional to the difference between the internal cloud virtual temperature and that in its near environment, there was reason to start with the in-cloud temperature measurements. Positive differences (i.e., the temperature of the cloud exceeds that of its near environment) represent positive buoyancy and negative differences represent negative buoyancy. All clouds go through a natural cycle of growth and decay, having positive buoyancy during the growth phase and negative buoyancy during their decay phase. Other factors being equal, the larger the buoyancy, the larger the cloud will grow and the longer it will last.

One of the factors that inhibits cloud buoyancy, in addition to the water and ice load that the cloud tower is carrying, is the entrainment of drier air into the cloud circulation. This forces the cloud to evaporate some of its liquid water to

saturate the entrained air. In doing so, the in-cloud air is cooled and buoyancy is decreased. It would seem intuitively obvious, therefore, that the larger the cloud the more protected its internal core should be from the deleterious effects of entrainment and subsequent evaporative cooling. If this is so, one would expect a positive correlation between the size of a cloud tower and/or the breadth of its internal updraft and the temperature excess that the cloud enjoys over its environment, while it is in its active growth phase. One might also expect the nature of the relationship to be a partial function of cloud ancestry and place of residence. These uncertainties are the focus of this paper.

This research was conducted under a contract with the Bureau of Reclamation as part of a program sponsored by the U.S. Agency for International Development to upgrade Thailand's weather modification capability.

2.0 INSTRUMENTATION AND DATA

An Aero Commander 690B aircraft was provided to Thailand's AARRP effort under lease from Thai Flying Service. This turbo-prop aircraft was equipped with an airborne data acquisition and seeding system and served as the cloud physics platform and seeder for the program. In addition to standard avionics and flight instrumentation, the Aero Commander was equipped with the following: a Johnson-Williams-type liquid water content meter manufactured by Cloud Technology, Inc., a thermo-electric dew point hygrometer, a reverse flow thermometer, a Ball variometer and a satellite-based (GPS) navigation system that permits location of the aircraft to within 100 m. A forward-looking nose video camera was mounted in the cockpit and provided a continuous view of cloud conditions during flight through the extreme right side of the windshield. The liquid water hot wire and the Ball variometer were configured to measure water contents and draft speeds up to 6.0 gm/m^3 and 10 m/sec (2,000 ft/min), respectively. No Thai cloud had cloud water contents exceeding 6.0 gm/m^3 --- the largest was nearly 4.0 gm/m^3. Many Thai clouds did, however, have drafts exceeding 10 m/sec, particularly during pre-monsoon conditions.

Beginning on 15 April and continuing through June 6, 1993, flights of the Aero Commander aircraft were made at about 6.5 km MSL through visually-suitable clouds at temperatures ranging between -7 and -10°C, in order to access their internal characteristics. Most clouds were quite vigorous and appeared to contain primarily supercooled water. None of the cloud towers had been seeded prior to cloud penetration. At issue for this study were estimates of temperature, draft sign, breadth and strength and the diameter of the tower at penetration altitude.

Data from 10 flight days were subject to analysis: April 15, 18, 20, 21, 22, 23, 25, 29, May 4, 7, 8, and 9. Following each flight, the recorded data were processed to provide the times and locations of each cloud, the ambient temperature and dew point and the internal cloud temperatures, drafts and water contents. Pass times were converted to pass distances by multiplying by the aircraft true airspeed. In those instances when the aircraft passed through the center of the cloud bubble top --- determined from viewing the video tape from the aircraft nose camera --- the pass distance corresponds to a cloud diameter.

3.0 ANALYSIS PROCEDURES

Three assumptions and seven steps were necessary in relating cloud tower radii and updraft breadths to their internal temperature excesses relative to their environment:

Assumptions:

1. The clouds were penetrated in the prime of their lives such that one could expect to measure the maximum cloud-environment temperature excesses existent at the flight level,

2. The cloud vs. environment temperature difference can be estimated by taking the difference between the maximum measured in-cloud temperature and the average environmental temperature in the 60 sec prior to cloud penetration,

3. Cloud radius can be estimated by multiplying the time to traverse the tower by the aircraft true airspeed (in m/sec) and dividing by two.

Steps:

1. The cloud penetration data were analyzed to obtain cloud and environmental temperatures. Only those clouds whose maximum internal temperature exceeded the maximum environmental temperature in the 60 sec prior to cloud penetration were retained in the sample. Those that were eliminated were in their dying phase and would not satisfy Assumption 1.

2. The cloud vs. environment temperature difference was estimated according to Assumption 2. In instances when the aircraft either ascended or descended due to cloud drafts from a baseline flight pressure during a particular cloud pass, the temperatures were corrected back to the baseline pressure using moist adiabatic ascent or descent.

3. The video tapes from the aircraft nose camera were viewed to determine whether the aircraft penetrated near the center of the bubble/vortical cloud top. Only those clouds that were penetrated near their centers were retained in the sample.

4. Cloud radius was estimated as in Assumption 3.

5. Each cloud remaining in the sample was classified from the video tape as either growing alone (i.e., isolated), or growing in a group of similarly-sized towers, or growing as a "feeder" tower to or in association with a pre-existing cumulonimbus.

6. A scatter-graph was constructed and the correlation calculated, relating each cloud radius to its maximum cloud vs. environment temperature excess.

7. Upon the completion of step 6, a scatter-graph was constructed and correlation was calculated, relating updraft radius to the maximum cloud vs. environment temperature excess.

4.0 RESULTS

The results for step 6 are provided in Figure 1 in which the cloud classification (isolated, group or cumulonimbus) for each of the 81 data points is indicated. Despite the scatter, there appears to be a weak relationship between cloud tower size and the temperature excess that it enjoys relative to its environment. The linear correlation coefficients for cloud categories of isolated, group and Cb are 0.40, 0.35 and 0.11, respectively. Although each category does not explain much of the variance, linear best-fits were derived for each. Note that for a given radius the in-cloud temperature excess is a function of where the cloud is growing. For example, isolated clouds having a particular top radius have a smaller temperature excess than those of same size growing as feeders to Cbs. The most plausible explanation is that isolated clouds are more adversely affected by entrainment than those growing as a family or as a part of a Cb complex.

Although the results are physically reasonable, the point scatter of Figure 1 does not allow for much confidence in them. This scatter is likely due to at least the following factors: 1) not all clouds were penetrated in the prime of their lives, and 2) errors in radius estimation may have been made due either to inclusion or exclusion of extraneous cloud material as part of the subject cloud and/or to passage of the aircraft above the true cloud radius.

The next step (step 7) to refine the relationship further was to relate the in-cloud temperature excess to the portion of a given cloud pass that contained updraft. The steps 1 through 6 were repeated with the exception of step 4. In its place was substituted an estimate of the pass length in km that contained updraft. Division by 2 provided a crude estimate of updraft radius.

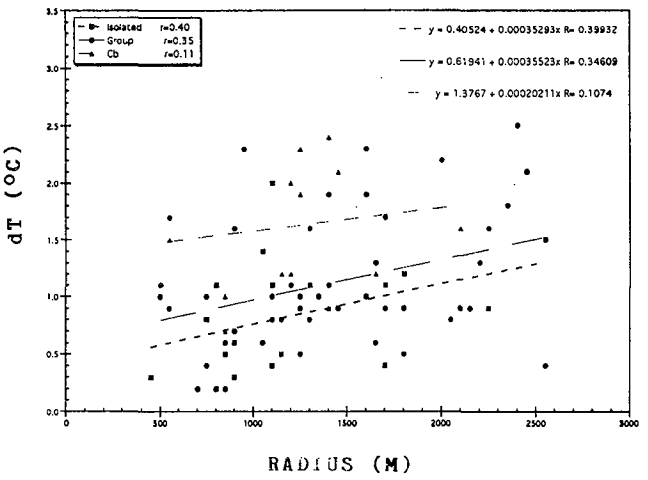

Figure 1. Scatter plot of cloud-top radius vs. the difference in temperature between maximum internal cloud temperature and the mean environmental temperature in the 60 sec prior to cloud penetration. The plot is stratified as a function of where the subject cloud was growing (i.e., isolated, within a group or in association with a cumulonimbus cloud). The linear best-fit lines and correlations are shown.

In some instances, this approach produced very different radius measurements from the original approach, especially when the cloud was large but inactive and without much updraft. In very active clouds, however, the updraft radius and the visual cloud-radius were nearly the same.

A new plot relating updraft radius to in-cloud temperature excess is provided in Figure 2. The scatter of the 81 data points is still great, but the correlations have improved to 0.45, 0.47 and 0.48 for the isolated group and Cb categories. The impressions gained from step 6 are reinforced in step 7. For a given category, the larger the updraft radius the larger the cloud vs. environment temperature excess. Further, the in-cloud excess is greater for a given cloud, if it is a part of Cb complex than it is if it is growing isolated from other clouds. These results are not surprising. Clouds thrive when growing in association with other clouds and they struggle if forced to fight for life alone.

5.0 DISCUSSION

This study has accomplished two things. First, it has demonstrated that there is indeed a positive relationship between the breadth of a cloud tower and its internal temperature excess relative to its environment. Second, it has established the importance of considering the "heredity" of a cloud in predicting its future. A cloud growing by itself without any family will have a harder time surviving in its hostile environment than a cloud that is growing within a large family, especially if some of those family members are very large.

Although this is intuitively obvious to some scientists, others argue that a cloud's familial history is of no importance in predicting its future. In their view, cloud towers of the same size, shape and internal structure at a given time can be compared over their lifetimes, regardless of their initial family circumstance. Such thinking is wrong, and it will create havoc when designing and evaluating an experiment that is focused on convective clouds.

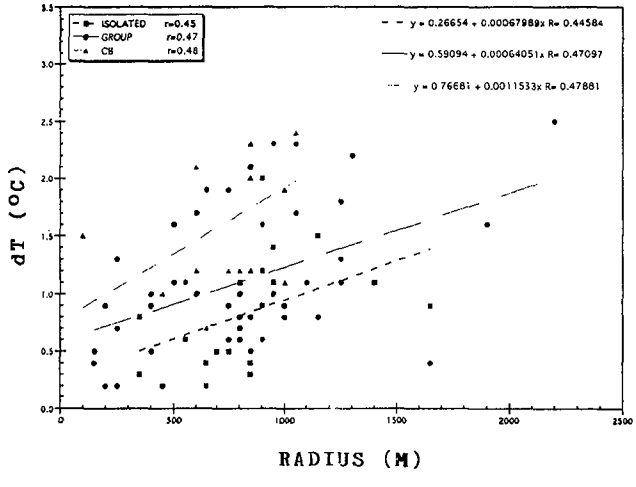

Figure 2. Scatter plot of the radius of the internal cloud-top updraft vs. the difference in temperature between maximum internal cloud temperature and the mean environmental temperature in the 60 sec prior to cloud penetration. The plot is stratified as a function of where the subject cloud was growing (i.e., isolated, within a group or in association with a cumulonimbus cloud). The linear best-fit lines and correlations are shown.

It is recommended, therefore, that a convective cloud seeding experiment be designed to ensure that clouds of comparable family history be selected for treatment and compared subsequently. If this is not possible, it is important that the clouds be partitioned after-the-fact as a function of their ancestry. Orphan clouds should be compared to orphan clouds and those that began in association with enormous extended cloud families should be compared only to other clouds with similar beginnings. Otherwise cloud ancestry will confound any attempt to get at the effect of seeding intervention.

6.0 REFERENCES

Rosenfeld, D., and A. Gagin, 1989: Factors governing the total rainfall yield from continental convective clouds. J. Appl. Meteor., 28, 1015-1030.

Rosenfeld, D., W.L. Woodley, B. Silverman, C. Hartzell, W. Khantiyanan, W. Sukarnjanaset, P. Sudhikoses, and R. Nirel, 1994: Testing of dynamic cold-cloud seeding concepts in Thailand. Part II: Results of analyses. J. Wea. Mod., 26.

Simpson, J., and V. Wiggert, 1969: Models of precipitating cumulus towers. Mon. Wea. Rev., 97, 471-489.

Simpson, J., and V. Wiggert, 1971: 1968 Florida cumulus seeding experiment: Numerical model results. Mon. Wea. Rev., 99, 87-118.

Woodley, W.L., and J. Kreasuwun, 1992: Relationship between the visual appearances of Thai supercooled convective clouds and their maximum cloud liquid water contents. J. Wea. Mod., 24, 89-97.

Woodley, W.L., D. Rosenfeld, B. Silverman, C. Hartzell, W. Khantiyanan, W. Sukarnjanaset, P. Sudhikoses, and R. Nirel, 1994: Testing of dynamic cold-cloud seeding concepts in Thailand. Part I: Experimental design and its implementation. J. Wea. Mod., 26.